CREEP FAILURE OF ALUMINIUM ALLOYS

AT HIGH TEMPERATURES

ALEXANDER McLURE B.Sc.

Thesis submitted for the Degree of Doctor of
Philosophy to the Faculty of Engineering,
The University of Glasgow

Dept. of Mechanical Engineering,
(Mechanics and Mechanisms),
The University of Glasgow,
GLASGOW, W.2.

December
1971

ACKNOWLEDGEMENTS

The Author wishes to thank Professor J.D. Robson, Rankine Professor of Engineering, University of Glasgow, for the provision of laboratory facilities; Professor P. Hancock, formerly Senior Lecturer in Mechanical Engineering, University of Glasgow, and now Professor of Engineering Metallurgy, Cranfield Institute of Technology, for his help and guidance with the project; Mr. R. Fletcher, Lecturer in Mechanical Engineering, University of Glasgow, for his help and guidance with the project and assistance with photography; other members of staff, both academic and technical, and research students of the Dept. of Mechanical Engineering who gave their assistance; Mr. D.M. Gill for his assistance with graphs and diagrams; the Science Research Council for their financial assistance; and his wife, Joan, for typing the manuscript.

CONTENTS

INDEX OF TABLES AND FIGURES

CHAPTER I

INTRODUCTION

1.1 Intercrystalline Creep Failure

The fracture of polycrystalline metals may occur in two ways. When the fracture path passes through the crystals or grains, the separation is said to be transcrystalline or transgranular. When the fracture path follows the boundaries between differently orientated crystals, the separation is said to be intercrystalline or intergranular. The majority of polycrystalline metals and alloys, when subjected to certain conditions of stress at temperatures greater than 0.5 Tm (Tm – melting temperature), display the inter-crystalline mode of failure. In general, this type of fracture occurs under creep conditions when the applied stress system produces low strain rates and long rupture lives. Low ductility, as measured by elongation and reduction of area at fracture, characterises the failure. The results of extensive research (reviewed in section 1.3) have established that the failure is initiated by the nucleation and subsequent growth of sub-microscopic fissures in the grain boundaries.

Although the intercrystalline nature of the failure was realised early in the twentieth century, it was only after the Second World War that progress was made in advancing theories to explain the phenomenon. A considerable portion of the research effort has been directed towards the determination of the mechanisms of nucleation and growth of the grain boundary discontinuities. While this approach has the best chance of producing high strength, high temperature alloys not subject to sudden cavitation failure, the engineer has to use the available materials of today in the

construction of components encountering creep conditions. Although it is necessary to obtain better creep resisting alloys, information is also required on the effects of internal discontinuities in the alloys which are currently used. The question arises as to whether the appearance of holes in the material constitutes failure. Since polycrystalline metals and alloys already contain holes of atomic dimensions, by way of crystal imperfections and grain intersections, the relative size of the internal hole will feature prominently in the answer to the above question.

Metals and alloys, when tested under conditions of stress and temperature which produce intergranular failure, do not always exhibit grain boundary cracks behind the fracture surface. It is assumed, in such a case, that a single crack, once nucleated, propagates rapidly across the load bearing area and causes sudden failure. The engineer, therefore, is concerned with the effect of stress concentrations generated by the presence of the internal discontinuity. The size, shape, and number of intergranular discontinuities have been found to vary with strain rate (eg. Gittins and Williams 1967), with stress (eg. Nemy and Rhines 1959), and with combinations of stress and temperature (eg. McLean 1956 – 57). In addition, the ductility of metals and alloys exhibiting intercrystalline failure varies with the parameters stress, strain rate and temperature (eg. Greenwood et al. 1954), thus indicating that the effect of a stress concentration also depends on those parameters.

Consider, for example, the situation where a metal component is subjected to periods of creep at a high temperature at a small stress and then subsequently subjected to periods at a lower temperature at a larger stress. Discontinuities developed in the grain boundaries at the high temperature, but having little effect under those conditions, might produce catastrophic failure at the lower temperature. In situations where the applied stresses are known to be uniaxial, the engineer may be able to predict possible component life using creep rupture data, if available, for

the material. However, the use of the uniaxial data for the prediction of creep behaviour under multiaxial conditions would be inadmissable since the growth of intergranular discontinuities is affected by the stress system — eg. Hull and Rimmer 1959, Ratcliffe and Greenwood 1965. Therefore, uniaxial and multiaxial creep properties may not be equivalent. The lack of suitable multiaxial stress creep data forces designers to make use of the available uniaxial data and not all are aware of the dangers inherent in the substitution.

1.2 Objectives of the Research

The main objective of this research was to determine the effects that intergranular discontinuities have on the creep properties of a metal or alloy under different conditions of stress and temperature and under different stress systems. It is hoped that guidance to engineers using cavitation prone alloys would be given by providing answers to the problems, concerning stress concentrations and multiaxial stress systems, raised in the previous section.

The first step in the investigation was to develop a method of producing samples of a material with a controlled amount of intergranular discontinuities. The creep properties of this material, at a high creep temperature (very much greater than 0.5 Tm) and at a low creep temperature (about 0.5 Tm), would be compared with those of the untreated material. Comparison of creep properties between the two temperatures, under uniaxial conditions, would be carried out using rupture life or minimum creep rate as the correlating parameter. Comparison of the effects of discontinuities under uniaxial and multiaxial stress systems, at the same temperature, would be made at similar values of 'effective' stress, since that is the most common link, used by engineers, to correlate behaviour under different stress systems.

Although many qualitative and quantitative theories have been proposed for the mechanisms of nucleation and growth of cavities, experimental evidence is not conclusive in all cases. During the development of a method for producing a cavitated material, and during the creep testing of that material, more information regarding nucleation and growth is likely to accumulate. Attempts will be made to correlate the new data with the work of previous researchers. However, it is not the objective of this research to formulate any new theories regarding the nucleation and growth of grain boundary discontinuities, but, if evidence of a previously unreported mechanism is found, it will be recorded. The effect of environment on the nucleation and growth of cracks is of

importance to the engineer and this topic will be studied.

Before selecting a material for the project and suitable methods of testing, it was advisable to study the work of previous researchers on the effect of cracks on the creep properties. It was also necessary to become acquainted with the theories of nucleation and growth in order to understand the nature of the discontinuities. This latter condition was essential if correlation with previous work was to take place. Hence, the next section describes relevant previous studies.

1.3 Relevant Previous Studies

1.3.1 The Nucleation and Growth of Intergranular Discontinuities

In the past fifteen years there have been many reviews (McLean 1957, Davies and Dennison 1958, Grant 1959, Gifkins 1959, Gifkins 1963, Garofalo 1965, McLean 1966) describing the state of knowledge on intergranular fracture at their time of writing. More recently, Tapin (1970) has produced a short review of cavitation with emphasis on ductility. On the whole, these reviews have been impartial and have related satisfactorily the evolution of the various theories of nucleation and growth. The present author will not provide another exhaustive review, but will briefly record the more important points which have arisen. Recent research on the problem has tended to provide more information on existing theories, supplementing qualitative explanations with quantitative results.

Creep, under conditions of low stress and high temperature (greater than 0.5 Tm), favours the formation of grain boundary discontinuities. The discontinuities have been found to occur as two distinct types. At temperatures in the region of half the melting point and relatively high stresses, the predominant mechanism of failure is that of triple point cracking. Wedge shaped cracks open up at the junction of three or four grains and propagate under the action of the applied stress to cause failure. At temperatures nearer the melting point and much lower stresses a 'cavitation' mechanism of fracture is dominant. In this case, small voids are nucleated at intervals along the boundaries and these grow, with the help of the applied stress, to link up and cause complete failure. The appearance and extent of intergranular cracks are strongly affected by grain boundary migration (Chang and Grant 1953, Chen and Machlin 1960) and by environment (Intrater and Machlin 1959, Scaife and James 1968). However, the effect of the latter is related to the control it exerts on grain boundary migration (Chen and Machlin 1960). The effect of environment is reviewed in a subsequent chapter.

The conditions of stress and temperature which favour the formation of intergranular discontinuities are also those which favour grain boundary sliding. It is now generally agreed that some degree of grain boundary sliding is necessary for the nucleation of both triple point wedges and grain boundary cavities, but its role in the growth mechanism is still uncertain.

A triple point crack may be nucleated when grain boundary shear produces a stress concentration at the junction of three grains. In the absence of grain boundary migration or intergranular deformation to relieve the stress concentration, a wedge shaped crack may open up to provide compatibility for continued deformation. Although this mechanism was first proposed by Zener (1948), Grant and his associates pioneered the study of triple point cracks with surface observations on Aluminium and its alloys (Servi and Grant 1951b, Chang and Grant 1952, 1953). The criticism of their work is that processes on the surface may not be representative of processes in the interior of a polycrystalline aggregate. Hence, much effort has gone into comparing the extent of grain boundary sliding in the interior with that occurring at the surface.

Since Rachinger's observation (1952) that γ (ratio of elongation due to sliding to total elongation) could be as high as 0.87 in the interior while only 0.20 at the surface, there has been a steady flow of results on the same topic. Rachinger used a grain counting technique which was subsequently criticised by others (eg. McLean 1957) on the basis that grain boundary migration would tend to round off grains in the interior. Rachinger, however, provided further evidence to confirm his results (1959). Other researchers (Ishida et al. 1965) using an internal marker technique, as well as the grain shape method, showed the latter to give larger and more variable values of γ. Stevens (1966) reviewed the values of γ obtained by different researchers and came to the conclusion that the discrepancy lay in the incorrect equations that the majority had used. However, high

values of γ, in the absence of large-scale boundary migration, do seem unlikely. As Gibbs (1967) pointed out, grain boundary sliding can provide only two independent strain components (in the plane of the boundary) in localised regions. Other intragranular deformation processes are necessary to provide the three additional independent strain components for compatible deformation under constant volume conditions, (von Mises 1928).

The mechanism of growth of the triple point crack from nucleus to a critical propagating length is still a matter of some conjecture. The difficulty lies in the discrepancy between experimental results and the values predicted by the theory. Recently, Williams (1969) has proposed a model for wedge crack growth based on the assumption that the opening displacement at the crack tip is the resultant of a component due to sliding in the grain boundary and a component due to the stress concentration across the tip of the crack. Complete failure occurs when the crack opening displacement reaches a critical size and propagation across the load bearing area takes place.

The mechanisms of nucleation and growth of grain boundary cavities have involved more speculation than those of triple point cracks. Greenwood (1954), observing that cavities formed mainly on boundaries transverse to the applied stress axis, suggested that nucleation occurred by the agglomeration of sufficient numbers of vacant lattice sites to form a stable hole. However, Machlin (1956) showed that the vacancy supersaturations necessary for homogeneous nucleation of cavities were very much larger than those likely to occur. Gifkins (1956) postulated that cavities could be nucleated on sliding grain boundaries where intragranular slip had produced jogs in the boundary. Chen and Machlin (1956) had concurrently come to a similar conclusion that jogs were favourable nucleation sites.

The mechanism of growth of a cavity has produced two opposing camps. On one side the view is held that growth

occurs mainly by diffusion of vacancies from the grain boundary (Hull and Rimmer 1959, Ratcliffe and Greenwood 1965, Gittins 1967). On the other side, the view is held that grain boundary sliding plays a much greater part than any diffusion mechanism, (Davies et al. 1968, Davies and Williams 1969). Spark (1969) has proposed a mechanism of growth which reconciles the two opposing views. He postulates that, whereas the volume increase may be primarily due to stress-induced grain boundary diffusion, the increase of area of cavitated grain boundary may be determined primarily by sliding.

Although the diffusion theory of growth applies quite well to pure metals, it has been found, however, that the measured growth rate of cavities is significantly decreased in more highly alloyed materials in much the same way as the creep rate (McLean 1956 – 57). To explain this observation Ishida and McLean (1967) proposed that dislocations in the grain boundary nucleated and aided the growth of cavities when they became bowed round particles in the boundary. Grain boundary sliding at 'non-wetting' inclusions or at second-phase particles where adhesion with the matrix has been overcome by the deformation process (Harris 1965, Greenwood and Harris 1965) also seems a probable nucleation mode. Further growth may then occur by diffusion and/or continued grain boundary sliding.

Several other theories of cavity nucleation have not found universal acceptance because of insufficient evidence. The proposed mechanism of a cavity opening at a grain/sub-grain boundary intersection by sliding, (Presland and Hutchinson 1963) suffers from the possibility that the sub-boundary migrated to the cavity after nucleation. The assumption that small cavities already exist in the material before creep conditions are imposed, rather begs the question of nucleation. Condensation of dissolved gas molecules seems more likely to be a stabilising mechanism for a cavity than a nucleating mechanism.

Until the advent of high accuracy density measuring techniques, there was considerable speculation as to when in the creep life, intergranular discontinuities first begin to nucleate. The density measurements of Boettner and Robertson (1961) on copper and Ratcliffe and Greenwood (1965) on magnesium have shown that nucleation begins in the primary stage of the creep curve. Continuous nucleation of cavities throughout the creep life seems probable and research workers have used this concept to explain the observed variation of density with strain and time (Greenwood 1963, Ratcliffe and Greenwood 1965), and to formulate quantitative theories of cavity growth (Speight and Harris 1967, Greenwood 1969, Woodford 1969a, 1969b). Gittins (1967), using optical microscopy, showed that cavities nucleated in copper at a rate such that the total number present was proportional to $(\text{time})^{0.5}$. However, Evans and Waddington (1969) used Gittins' results to show that the observed increase in number of cavities with increasing strain (and time) could be due to the limit of optical detection. They support the view that all cavities are nucleated during the early stages of the creep life and the apparent increase in number is due to their growth to a detectable size. The concept of continuous nucleation, therefore, still raises some dissenting voices.

The conclusion to be drawn from this review of nucleation and growth is that, although grain boundary sliding has been established as a prerequisite for crack nucleation, the mechanism or mechanisms of growth are still unresolved. Nucleation by more than one mode with grain boundary sliding seems probable. The case for growth by vacancy diffusion is as convincing as that for growth by sliding. The truth probably lies in the compromise suggested by Spark (1969). Whenever possible in the present research comparison will be made with previous work in an attempt to resolve some of the speculation.

1.3.2 Effect of Grain Boundary Discontinuities on Creep Properties

Few previous research workers have attempted to examine the effect of similar amounts of internal discontinuities under different conditions of stress and temperature. Some workers, for example, Nield and Quarrell (1957), Chen and Machlin (1957) and Kramer and Machlin (1959), retested high temperature uniaxial creep specimens at lower temperatures and their results are reviewed in a subsequent paragraph. The previously mentioned work of Hull and Rimmer (1959) and Ratcliffe and Greenwood (1965) showed the effect of a multiaxial stress system on the growth of intergranular discontinuities. On applying a hydrostatic pressure to a magnesium test piece being strained by a uniaxial tensile stress, Ratcliffe and Greenwood observed that, although plastic deformation continued, there was no continued growth of intergranular discontinuities (when the hydrostatic pressure equalled the tensile stress). This result indicates that the same quantity of intergranular discontinuities can have widely different effects on the mechanical properties of a material when the stress system is altered.

Nield and Quarrell (1957) compared the room temperature ductilities of specimens of an Aluminium – Manganese alloy deformed at creep temperatures under constant load and constant strain rate conditions. Their objective was to determine the time at which cracks first appeared and the stage of development at which they could propagate easily through the specimen. They observed a fall in room temperature ductility as the creep elongation of the specimens increased. A sudden fall was noted for specimens deformed to the tertiary stage of the creep curve. These results provide some indication of the effects under different conditions. Chen and Machlin (1957) using α – brass, and later Kramer and Machlin (1959) using commercially pure nickel, performed similar experiments. The latter found that at lower temperatures (– 196 deg.C.) the ductility of nickel decreased linearly with an increase in prior high temperature (920 deg.C.) creep strain. With all three materials, the fall

in low temperature ductility was ascribed to the formation of grain boundary cracks. The decrease of ductility with increasing creep elongation was explained by the growth of cracks to a critical propagating length before complete failure would take place. One wonders if the same decreases in ductility would have been observed if the low temperature tests had been conducted at a creep temperature.

Nemy and Rhines (1959), while investigating possible reasons for the tertiary stage of the creep curve, retested, at the same stress and temperature, specimens of an Aluminium-Magnesium alloy crept to various stages of the tertiary creep curve. They found that, in general, minimum creep rates were higher in the retested specimens and the strain/time curve went into tertiary much earlier. The variation was found to depend on both stress and temperature. At most stresses, but not all, the behaviour could be linked with the formation of intercrystalline cracks. An obvious extension to their work would be to retest the crept specimens at another temperature and stress.

1.4 Material and Method

1.4.1 Choice of Material

To study the effects of intergranular discontinuities on creep properties under different conditions of stress and temperature, it was necessary to find a material which would :

a) exhibit intercrystalline cracking;
b) have a large amount of data on its creep properties for comparison and information;
c) be easy to work with so that the maximum number of tests could be made in the shortest time.

The material chosen was commercial purity Aluminium (99.0 + pct). There are references in the literature reporting its intercrystalline failure (Hanson and Wheeler 1931, Servi and Grant 1951a, McKeown et al. 1954, Nield and Quarrell 1956–57, Nemy and Rhines 1959), and creep data on Aluminium in general is extensive. High purity Aluminium (99.99 + pct) does not exhibit intercrystalline failure but always draws down to a thin neck under tensile stresses and fails in a trans-crystalline manner, (Servi and Grant 1951a). The addition of small amounts of impurities to the pure metal apparently produces a highly complex alloy and the difference in properties is due to the large effect that small amounts of impurities have on grain boundary migration in Aluminium.

The batch of Aluminium used in the present research conformed to B.S. 1476 E1C and had silicon as the main impurity. The chemical analysis is shown in Table 1.1. The material was obtained in the form of 1 in. diameter extruded bar.

Table 1.1

Element	Weight (pct)
Silicon	0.30
Iron	0.07
Zinc	0.015
Magnesium	0.013
Chrominium	0.01
Copper	0.006
Manganese	0.003
Nickel	0.003
Aluminium	balance

Is it an alloy?

1.4.2 Choice of Method

The preparation of Aluminium test pieces with intergranular discontinuities could have been achieved by three methods of mechanical testing, viz. constant load creep, constant stress creep and constant strain rate. To produce a repeatable amount of cavitation the test piece would have to be deformed to a pre-determined strain or for a pre-determined time. Although strain and time in a creep test may be considered as dependent variables, the scatter found in repeated tests under certain conditions of stress and temperature does not always substantiate this view. Rather than performing two sets of creep tests to determine whether strain or time (or neither?) was the parameter which produced repeatable amounts of intercrystalline cracking, constant strain rate testing was chosen as the method of preparation, since strain then becomes proportional to time, and only one set of tests needs to be carried out.

Although stress in the constant strain rate test varies with strain (and time), a variation would also have occurred

in a constant load creep test. Similarly, nominally constant stress creep tests would have had a stress variation, since the formation of holes would have reduced the load bearing area. Constant stress creep machines can only cope with the uniform thinning of the gauge length according to the constant volume criterion of plastic deformation. For this reason, the uniaxial creep testing of the cavitated and virgin materials was carried out at constant load.

Commercially pure Aluminium is not a structural material used by engineers where creep strength is important. In the present research it was being used, principally, as a testing medium and, therefore, test temperatures close to reality were not essential. Preparation of creep test pieces with intergranular discontinuities was carried out at a temperature of 500 deg.C. Uniaxial and multiaxial creep tests were performed at temperatures of 250 deg.C. (0.56 Tm) and 500 deg.C. (0.83 Tm). Testing at these extremes of temperature would show up differences in behaviour to intercrystalline discontinuities, if they exist.

Essential for the success of the project was the ability to measure accurately the amount of intercrystalline cracking which a test piece had undergone. Metallography was necessary to demonstrate that intergranular cavitation and triple point cracking had taken place, and it was thought that this method would also be capable of assessing the extent of intercrystalline cracking. In practice, metallography proved to be unsuitable for the latter purpose and another method had to be found. Mention was made in a previous section of the measurement of density change as a means of following the growth of cavities. This technique was adopted in the present work and provided a simpler and more accurate method of measuring cavitation than metallography.

1.4.3 Creep Testing under Multiaxial Stress Conditions

One of the objectives of this research was to compare the effects of intergranular discontinuities on the creep

properties of a metal or alloy under a uniaxial stress system with those under a multiaxial stress system. Apart from the experimental difficulties of applying a known multiaxial stress system to a test piece of the material and measuring the resulting strains, there also exists the problem of finding an adequate basis for comparison of the data with that from uniaxial stress creep tests. The multiaxial stress system chosen was the simple biaxial tensile stress system of the thin-wall tube under internal pressure. For a closed-end tube of internal diameter D, wall thickness t, under internal pressure P, the principal stress system set up in the wall consists of an axial tensile stress σ_L $(= \frac{PD}{4t})$, a tangential or hoop, tensile stress σ_θ $(= \frac{PD}{2t})$, and a radial stress σ_r. The radial stress σ_r varies from zero at the outside surface to a compressive stress equal to the internal pressure at the inside surface; and for a thin-wall tube it may be considered negligible. The axial and hoop stresses remain in the constant ratio of 1:2 as the tube deforms, since both depend only on the term $\frac{PD}{t}$.

In the analysis of the plastic flow of metals under multiaxial stress conditions, the criterion adopted for the onset of yielding is usually the Mises invariant or the Tresca yield condition. For a system of principal stresses σ_1, σ_2 and σ_3 in an isotropic material, the Mises criterion states that yielding will occur when the effective stress $\bar{\sigma}$ defined by,

$$\bar{\sigma} = \sqrt{\frac{1}{2}\left[(\sigma_1 - \sigma_2)^2 + (\sigma_2 - \sigma_3)^2 + (\sigma_3 - \sigma_1)^2\right]} \qquad (1.1)$$

reaches the yield stress (σ_y) of the material in uniaxial tension. In the Tresca yield condition, plastic flow occurs when the maximum principal shear stress in the multiaxial system reaches the maximum shear stress at the yield point in uniaxial tension:-

$$\frac{\sigma_1 - \sigma_2}{2}, \quad \frac{\sigma_2 - \sigma_3}{2}, \quad \frac{\sigma_3 - \sigma_1}{2} = \frac{\sigma_y}{2} \qquad (1.2)$$

These two yield criteria may also be used to describe plastic flow behaviour under multiaxial creep conditions and, of the two, the Mises invariant has been found, in general, to give better agreement with experiments (Finnie and Heller 1959). The numerical factor in equation 1.1 was chosen such that, for a uniaxial stress σ_1, the equation reduces to $\bar{\sigma} = \sigma_1$. In the present research, the Mises invariant, as described in equation 1.1, was used to relate the biaxial stress system of the thin-wall tube to the uniaxial case. Substituting $\sigma_1 = \sigma_\vartheta = \frac{PD}{2t}$, $\sigma_2 = \sigma_L = \frac{PD}{4t}$ and $\sigma_r = 0$ in equation 1.1 yields,

$$\bar{\sigma} = \frac{\sqrt{3}}{4} \frac{PD}{t} \tag{1.3}$$

Corresponding to the definition of an effective stress $\bar{\sigma}$ for plastic flow, an effective plastic strain increment $\delta\bar{\varepsilon}$ may be defined to correlate the principal plastic strain increments $\delta\varepsilon_1$, $\delta\varepsilon_2$ and $\delta\varepsilon_3$:-

$$\delta\bar{\varepsilon} = \sqrt{\frac{2}{9}\left[(\delta\varepsilon_1 - \delta\varepsilon_2)^2 + (\delta\varepsilon_2 - \delta\varepsilon_3)^2 + (\delta\varepsilon_3 - \delta\varepsilon_1)^2\right]} \tag{1.4}$$

As before, the numerical factor was chosen such that, for the uniaxial strain increment $\delta\varepsilon_1$, equation 1.4 reduces to $\delta\bar{\varepsilon} = \delta\varepsilon_1$. Plastic strain increments must be used since the state of plastic strain depends on the previous stress/strain history of the material as well as the current stress state. It has been assumed in the present analysis that the elastic strains are negligible.

Using the analysis of Finnie and Heller (1959) for a system of principal stresses σ_1, σ_2 and σ_3, in an isotropic material in which the principal axes of strain do not rotate, the corresponding principal plastic strain increments $\delta\varepsilon_1$, $\delta\varepsilon_2$ and $\delta\varepsilon_3$, may be expressed by,

$$\delta\varepsilon_1 = \frac{\delta\bar{\varepsilon}}{\bar{\sigma}}\left[\sigma_1 - \frac{1}{2}(\sigma_2 + \sigma_3)\right]$$

$$\delta\varepsilon_2 = \frac{\delta\bar{\varepsilon}}{\bar{\sigma}}\left[\sigma_2 - \tfrac{1}{2}(\sigma_3 + \sigma_1)\right] \qquad (1.6)$$

$$\delta\varepsilon_3 = \frac{\delta\bar{\varepsilon}}{\bar{\sigma}}\left[\sigma_3 - \tfrac{1}{2}(\sigma_1 + \sigma_2)\right]$$

If the stresses are applied and remain in constant ratio, it follows from equations 1.6 that the strain increments also remain in constant ratio. Therefore, equations 1.6 may be integrated to yield the total plastic strains ε_1, ε_2 and ε_3 :-

$$\varepsilon_1 = \frac{\bar{\varepsilon}}{\bar{\sigma}}\left[\sigma_1 - \tfrac{1}{2}(\sigma_2 + \sigma_3)\right]$$

$$\varepsilon_2 = \frac{\bar{\varepsilon}}{\bar{\sigma}}\left[\sigma_2 - \tfrac{1}{2}(\sigma_3 + \sigma_1)\right] \qquad (1.7)$$

$$\varepsilon_3 = \frac{\bar{\varepsilon}}{\bar{\sigma}}\left[\sigma_3 - \tfrac{1}{2}(\sigma_1 + \sigma_2)\right]$$

where $\bar{\varepsilon}$ is the effective plastic strain and from equation 1.4,

$$\bar{\varepsilon} = \sqrt{\frac{2}{9}\left[(\varepsilon_1 - \varepsilon_2)^2 + (\varepsilon_2 - \varepsilon_3)^2 + (\varepsilon_3 - \varepsilon_1)^2\right]} \qquad (1.8)$$

For the thin-wall tube under internal pressure, the stress ratios remain constant and equations 1.7 may be applied. Substituting, $\sigma_1 = \sigma_\vartheta = \frac{PD}{2t}$, $\sigma_2 = \sigma_L = \frac{PD}{4t}$, $\sigma_3 = \sigma_r = 0$, and $\bar{\sigma} = \frac{\sqrt{3}}{4}\frac{PD}{t}$ in equations 1.7, produces for the plastic strains ε_ϑ $(= \varepsilon_1)$, ε_L $(= \varepsilon_2)$ and ε_r $(= \varepsilon_3)$,

$$\varepsilon_\vartheta = \frac{\sqrt{3}}{2}\bar{\varepsilon}$$

$$\varepsilon_L = 0 \qquad (1.9)$$

$$\varepsilon_r = -\frac{\sqrt{3}}{2}\bar{\varepsilon}$$

Thus, in the thin-wall tube under internal pressure, there is no change in axial length and the hoop and radial strains are equal and opposite. Since the hoop strain is equivalent to the fractional change in diameter $(\frac{\delta D}{D})$, the monitoring of the change in diameter produces the measure of the effective plastic strain $\bar{\varepsilon}$, that is,

$$\bar{\varepsilon} = \frac{2}{\sqrt{3}} \frac{\delta D}{D} \quad (1.10)$$

Using equations 1.3 and 1.10, an effective stress/effective strain curve may be constructed for the material when tested under the biaxial tensile stress conditions of the thin-wall tube under internal pressure. Since, by definition, effective stress and effective strain reduce to the uniaxial stress and uniaxial strain, respectively, under uniaxial conditions, the $\bar{\sigma}/\bar{\varepsilon}$ curve should be equivalent to the uniaxial stress/strain curve for the material under the same conditions of temperature and strain rate. Further, under creep conditions, the effective strain/time curve for the material, when tested as a thin-wall tube under a constant effective stress (~~constant internal pressure~~), should be the same as the uniaxial strain/time curve, when the magnitudes of the uniaxial and effective stresses are the same. Although, by definition, effective stress and effective strain reduce, in the uniaxial case, to uniaxial stress and uniaxial strain, respectively, the equivalence in the curves described above is clearly dependent on the ability of the concepts of effective stress and effective strain to provide an adequate link between material behaviour under a uniaxial stress system and under a multi-axial stress system. The evidence, as cited by Finnie and Heller, indicates that, when deformation of the metal or alloy is mainly by a shear process within the grains, the Mises invariant is adequate and, therefore, may be used to describe plastic flow in metals at ordinary temperatures. However, under high temperature (greater than 0.5 Tm) creep conditions, intergranular discontinuities have been found to develop (section 1.3) and their behaviour under a multiaxial

stress system has been shown to be different from that under a uniaxial system. For example, Hull and Rimmer (1959) on copper and Ratcliffe and Greenwood (1965) on magnesium, showed that application of a hydrostatic pressure to a creep specimen, while tested under a uniaxial tensile stress, suppressed the development of intergranular discontinuities. The rupture life and the ductility, as measured by elongation and reduction of area at fracture, were both increased by the superposition of the hydrostatic pressure. Hence, although effective stress and effective strain may be adequate links between uniaxial and multiaxial behaviour in the early stages of creep when intergranular discontinuities are too small to significantly affect the overall deformation process, the two concepts should be unable to correlate data of the later stages of creep.

Stress rupture testing of thin-wall tubes, such as by Kooistra et al. (1952) on steel and Sticha (1969) on Cr/Mo steels, has indicated that the maximum principal stress (the hoop stress) controls the rupture behaviour. The work of Kennedy et al. (1959) on the creep of Inconel tubes under internal pressure and additional axial load also supports the maximum principal tensile stress criterion of rupture. This research also supports the use of Mises criterion for correlating creep rates in the early stages of the test. However, evidence that use of the maximum principal tensile stress criterion does not correlate uniaxial and multiaxial rupture data was presented by Slocombe and Benyon (1963). In stress rupture tests on Nimonic 90 tubes under internal pressure at temperatures of 650 deg.C. and 750 deg.C., they found rupture life in tubular tests to be much less than in uniaxial tensile creep tests when compared at the same values of hoop and uniaxial stresses. Finnie and Heller (1959), cite evidence for the use of the Mises criterion in determining rupture behaviour as well as evidence to support the use of the maximum principal tensile stress criterion. The present author agrees with their conclusion that there may be no simple criterion for adequately predicting rupture life under multi-axial stress from uniaxial data.

In the present research, creep tests will be carried out on thin-wall tubes of commercially pure aluminium under internal pressure and, as well as rupture life, the tangential creep strain will be measured during the tests by monitoring the change in diameter. The tubes will be manufactured from the same batch of material used to produce the uniaxial creep test pieces and, hence, direct comparison of creep properties between the two stress systems will be possible. The tube tests will be performed at internal pressures which produce effective stresses in the tube wall equal to the uniaxial tensile stresses used in the tensile creep tests. Comparison of resulting strains produced by the two stress systems will be carried out using the concept of effective strain. The results of these tests will show the effect that intergranular discontinuities have on the use of effective stress and effective strain in relating multiaxial and uniaxial creep behaviours. The tube tests will be performed at the same temperatures as the uniaxial creep tests, viz. 250 deg.C. and 500 deg.C.

Uniaxial creep tests on specimens containing known, controlled amounts of intergranular discontinuities have been planned to compare the effects of the same quantity of discontinuities under different stress and temperature conditions. A similar procedure will be attempted under the biaxial stress conditions of tubes under internal pressure. In this way, a picture may be built up of the effects of the same quantity of discontinuities in a material under two different stress systems at a high creep temperature (much greater than 0.5 Tm) and at a lower creep temperature (about 0.5 Tm).

CHAPTER II

TENSILE TESTING

2.1 Introduction

To study the effects of intergranular discontinuities on the creep properties of Aluminium, it was necessary to develop a method of producing creep test pieces with a controlled amount of grain boundary cavities and/or triple point cracks. As explained in the introductory chapter, this (objective) could have been achieved by straining under high temperature creep conditions for a pre-determined time or to a pre-determined strain. Since there was doubt as to which of the two would provide the more repeatable results, constant strain rate testing, combining the two variables, was selected as the method of preparing creep test pieces.

To show that intercrystalline cracking was possible in the batch of commercially pure aluminium obtained, a test piece was slowly elongated at a constant strain rate and a temperature of 500 deg.C. by approximately 20 pct. On sectioning and polishing this test piece, a large number of intergranular cracks were observed. Consequently, a series of tensile tests was planned at a range of strain rates and a temperature of 500 deg.C. By varying the amount of strain received by different specimens at a particular strain rate, analysis by metallography or otherwise would determine the strain rate and range of strains to be used for the preparation of creep test pieces.

Tensile tests were also performed at a temperature of 250 deg.C. to investigate the fracture behaviour of commercially pure aluminium at a lower temperature. Since

250 deg.C. was also one of the planned creep testing temperatures, information on tensile strength and elongation to fracture at this temperature would be helpful in the planning of future creep tests. The same (sentiments) also apply to tensile and creep tests at a temperature of 500 deg.C.

2.2 Experimental Procedure

2.2.1 Testing Equipment

The tensile tests were performed on a 'Hounsfield' Tensometer equipped with an automatic load and extension recorder. Heating of the specimen to the test temperature was accomplished by means of a tube furnace manufactured by Wild-Barfield Ltd. and designed for use with the 'Hounsfield' Tensometer. Temperature control of the furnace was achieved using a Silicon Controlled Rectifier type of proportional temperature controller. This instrument known as a 'Sirect' uses a Platinum Resistance thermometer as the sensing element. The thermometer was placed inside the furnace tube against the wall. This position gave the most precise temperature control. The manufacturer of the 'Sirect' states that, under average conditions, temperature control to $\pm$ 0.2 deg.C. may reasonably be expected at all temperature levels.

2.2.2 Strain Rates

To ensure a constant crosshead speed, a motor driven unit was used in conjunction with the tensometer. With the aid of additional pulleys and gear boxes, four different crosshead speeds were obtained. The nominally constant specimen strain rates were 0.1, 1, 10 and 100 pct per hour. These strain rates cannot be regarded as constant throughout the test. The crosshead movement of the tensometer has to account for the beam deflection(measuring load) and other deformations in the machine as well as the specimen extension.

Hamstad and Gillis (1966) have shown that, for most conventional tensile testing machines regarded as 'hard', the actual specimen strain rate can vary from initial to yield point values by a factor of approximately 20 or more, depending on the relative stiffnesses of specimen and machine. In the present work, calculations showed that the specimen strain rate during elastic deformation was about 100 times less than the nominal strain rate based on crosshead speed. The

'Hounsfield' Tensometer is a 'soft' machine.

When the ultimate load is reached, the crosshead speed becomes equal to the specimen extension rate. In the Aluminium specimens tested, all, except at the slowest strain rate, attained the ultimate load by 1.4 pct strain and the load dropped slowly for a considerable strain thereafter. The variation of initial strain rate was ignored as all specimens were strained by more than 1.4 pct. The problem appeared again when calculating Strain Rate Sensitivity values and this is discussed later.

2.2.3 Test Piece Design and Strain Measurement

The major factors influencing the design of the test piece were: the low strength of the material at 500 deg.C., the limited length of constant temperature along the furnace tube and the desirability of adhering to B.S. 3688 : Part 1 : 1963. The last objective was to facilitate comparison, if necessary, with the work of other researchers. Test pieces of circular cross-section were chosen because of their ease of manufacture. Threaded grips were selected as the most suitable method of applying load to the test piece. Pull rods of heat-resisting steel were used to connect test piece grips with the 'button head' chucks of the Tensometer. Various designs of test piece were tried until that shown in Figure 2.1 proved to be the best compromise on the above factors. This test piece had a cross-sectional area of 0.1 square inch (64.5 mm^2) and a parallel length of 1.75 in. (44.45 mm.)

The rotation of the recording drum of the Tensometer provides an accurate measurement of crosshead movement. Test piece extension can be calculated from that measurement by subtracting the components due to beam deflection and machine deformation. However, the resulting value of extension includes the contribution of the transition radius of the test piece. To obtain a more accurate measure of extension, three pairs of divider points were marked on the parallel

length of the test piece at 120 deg. intervals round the circumference before testing. Each pair of divider points marked a gauge length of 1.40 in. (35.55 mm.). The distance between a pair of gauge marks was measured to ± 0.05 mm. using a microscope equipped with measuring table and Vernier Scale. The measurement was made before and after tensile straining. Appendix 2.1 shows that accuracy of strain measurement was ± 0.3 pct for strains less than 30 pct and ± 0.5 pct for strains 30 to 100 pct.

2.2.4 Temperature Measurement

Alumel/Chromel thermocouples were used to measure specimen temperature. In the first few tests, three thermo-couples, one at each end and one at the mid-point, were secured to the gauge length and their output monitored on a slidewire potentiometer with an accuracy of ± 0.1 deg.C. Temperature distribution along the gauge length was found to be better than ± 1 deg.C. In subsequent tests only one thermocouple was used and this was attached at the mid-point of the gauge length. This action was deemed valid because the setting up procedure was the same for each test. Through-out the heating and straining periods temperature was continuously recorded on a 'Kent' Chart Instrument. This temperature/time recorder indicated temperature with a resolution of ± 1 deg.C.

2.2.5 Test Details

Before assembly, each test piece was thoroughly washed in alcohol to remove all traces of dirt and oil. The gauge diameter was measured to ± 0.001 mm. with a micrometer at six points along the gauge length. The average of the six readings was used later to calculate stress. The thermocouple was securely attached by wire at the mid-point, making sure that the thermocouple bead was in contact with the gauge length surface. Test piece, grips and pull rods were then assembled in the tube furnace on the tensometer. The open ends of the tube were plugged with 'Triton Kaowool Ceramic

Fibre'.

Heating of the specimen to temperature took approximately 30 minutes with less than 2 deg.C. overshoot. Test pieces were held at temperature for $1\frac{1}{4}$ hours before straining commenced. At the end of the straining period, the load was released and the test piece allowed to cool. The strained gauge length was then measured as were the reduced diameters at the six points. The test piece was then ready for metallographic or other examination.

Although accuracy in measuring the stress applied to the test piece was not essential for the preparation of creep test pieces with intergranular cavities, an estimate of the error in the measured values of maximum stress was calculated. The error in measured load depended on which tensometer spring beam was used in the tensile test. For the slowest strain rate and 500 deg.C., a 16 lbf. beam was used and accuracy here was estimated to be $\pm$ 0.5 lbf. At the three faster strain rates, beams of 62.5 lbf. and 125 lbf. were used and accuracy rose to $\pm$ 0.1 lbf. Although gauge diameter could be measured to $\pm$ 0.001 mm., the diameter was found to vary by as much as $\pm$ 0.025 mm. along the gauge length. At 250 deg.C., beams of 1120 lbf. and 2240 lbf. were used and their accuracy was estimated to be $\pm$ 1 lbf. Therefore, although stress at 0.1 pct/h and 500 deg.C. was measured with an accuracy of $\pm$ 5.6 pct, the accuracy rose to about $\pm$ 0.7 pct at all other combinations of strain rate and temperature. These values are calculated in Appendix 2.1.

2.3 Stress/Strain Curves

The load/extension curves from the automatic recorder had to be corrected for beam deflection, machine deformation and irrelevant specimen deformations before they could be used to produce stress/strain curves. The necessary adjustment to extension was obtained by performing the tensile test in the same manner as described previously, but using a test piece of 1 in. diameter. The extension on the gauge length of the 1 in. diameter specimen could be regarded as negligible. The load/extension curve for the large diameter specimen was then subtracted from the original to produce an accurate load/extension curve for the smaller test piece.

Figures 2.2 and 2.3 show engineering stress to base engineering strain, for the four strain rates of interest, at 250 deg.C. and 500 deg.C. respectively. These curves have several interesting features apart from the obvious conclusion that the material is strain rate sensitive at both temperatures.

At both test temperatures, the stress/strain curve reaches a maximum stress after a relatively small amount of strain and a large amount of elongation occurs subsequently with a continuously decreasing load, until finally localised necking and fracture take place. The localised necking did not occur until large strains had been achieved. At 500 deg.C. and the slowest strain rate (0.1 pct/h) necking only occurred in the fractured specimen. At the higher strain rates at this temperature, detectable necking occurred after 15 – 20 pct strain. Only a few test pieces were strained at the lower temperature but similar trends were observed. Slight necking in this case occurred after about 5 pct strain.

This behaviour has also been observed in other materials by Guard et al. (1954) and Nádai and Manjoine (1941). Guard et al. suggest recovery under stress, such as found by Wood and Suiter (1951) in aluminium, as one possible explanation. As the phenomenon did not appear to be directly related to

the present project, the matter was not pursued further.

The stress/strain curves at 500 deg.C. and the two slowest strain rates had another interesting feature. At 1 pct/h and approximately 17 pct strain and at 0.1 pct/h and approximately 30 pct strain, the stress began to decrease at a slower rate than it had been doing since the ultimate. In fact, the engineering stress became almost constant while the test piece continued to elongate. In one test at 1 pct/h, this behaviour continued until a strain of 55 pct, when pulling was stopped. The gauge length was still parallel, although reduced in diameter. Later, it will be shown that large amounts of intergranular cracking were observed at these two strain rates. The behaviour does seem to be connected with intergranular cracking.

2.4 Metallography

While the tensile testing programme continued, a suitable polishing and etching technique was developed for the material. As well as demonstrating the presence of intergranular cavitation in strained specimens, it also showed the structure of the 'as received' bar and the effect of heating alone. At first it was hoped that metallography would also be a method of measuring the amount of cavitation, but it soon became apparent that it was too time-consuming and inaccurate.

2.4.1 Polishing and Etching

Sections of the Aluminium were mounted in perspex and successively ground on 220, 320, 400 and 600 grade silicon carbide papers, over which water slowly flowed. Mounted sections were then polished by diamond paste on a rotating disc of 'Selvyt' cloth. The final polish was $\frac{1}{4}$ micron diamond paste and this was found to produce a virtually scratch free surface, suitable for microscopic examination. Under the microscope, specimens which had cavitated could be clearly distinguished, although many of the holes and cracks were 'flowed over'. Etching was necessary to remove the flowed layer.

Etching of the Aluminium, in order to clearly distinguish the grain boundaries, proved to be more difficult than was at first thought. Many of the standard chemical etches were tried as well as electrolytic etches. Even an ion etching technique was used, but this only gave good results on un-mounted 1 in. diameter sections of the 'as received' bar. A room temperature solution of 1 gramme caustic soda per 100 ml. water was found to give the most acceptable etched structure. Etching times were rather long, taking 15 to 20 minutes, depending on the history of the specimen. The reaction of the caustic soda solution with the sections of specimens heated or strained at 250 deg.C. differed from the reaction with those strained at 500 deg.C.

With the former, the grains were darkened and the boundaries only lightly etched in some cases and completely untouched in others. The behaviour appeared to be due to the precipitation of impurities on heating at 250 deg.C. Specimens heated to 500 deg. C. and furnace cooled over a period of 5 to 6 hours also showed the effect. Later, it will be shown that cavities could still be detected under these conditions with specimens tested under creep conditions of low stress and a temperature of 250 deg.C.

2.4.2 Results

In addition to the 'as received' bar, two samples of the material, which had been annealed for 1 hour and 2 hours, respectively, at a temperature of 500 deg.C., were also sectioned, polished and etched. It was found that short periods of annealing had no apparent effect on the grain structure. Comparison of sections of the 'as received' bar perpendicular to the extrusion axis and parallel to that axis showed the grain structure to be equiaxed. Figures 2.4 to 2.7 are photographs of sections of the 'as received' and heat treated materials, parallel to the extrusion axis (vertical in the photographs). Three different magnifications have been used to facilitate comparison with subsequent micrographs presented in the thesis.

Figures 2.6 and 2.7 demonstrate that, in addition to numerous grain boundary particles available as cavity nucleation sites, there also appear to be a number of stable cavities already present in the 'as received' material. Although it is possible that the etch has dislodged large impurity particles in the grain boundaries, the formation of cavities during the hot extrusion of the original bar seems more likely.

Optical examination of etched sections of test pieces strained at a temperature of 500 deg.C. showed that intercrystalline discontinuities occurred at all four strain rates. The amount of discontinuities increased with increasing

strain for each strain rate and, at any particular strain, the amount of cracking was greater for the two slower strain rates (0.1 and 1 pct/h) than for the two faster strain rates (10 and 100 pct/h). Figures 2.8 to 2.11 and Figures 4.3 and 4.5 are photographs of etched sections of the material after straining at 500 deg.C. in air. The stress axis in these photographs, as in all other photographs of uniaxial specimens, is vertical.

In general, the etch tended to round off the sharp outlines of the cracks and to increase their size. Hence, it soon became clear that metallography was not going to provide a simple means of measuring the amount of intergranular cracking. The measurement of total crack volume in the test piece by density change was, therefore, developed before completion of the tensile testing programme. The tensile tests at 250 deg.C. were carried out after the density balance had been put into operation. Since density measurements indicated almost negligible cavitation in test pieces strained at 250 deg.C., no time was wasted in metallography of these specimens. However, some specimens, tested under creep conditions at 250 deg.C., did show a significant density change and intercrystalline cracks in these specimens are described later.

At the two slower strain rates and 500 deg.C., intercrystalline cracking begins with the formation of cavities at points along the grain boundaries (Figures 2.8 and 2.11). At 1 pct/h there are also a few triple point wedge cracks. The cavities and wedges grow until they coalesce to form 'wavy' cracks covering two or three boundaries. Figures 4.3 and 4.5 illustrate the size of the cracks after 10 pct strain. However, the material was able to accommodate strains of about 50 pct before separation into two parts took place. During this deformation, the internal cracks grew continuously in size. Evidently, plastic deformation, around the tips of the cracks, was sufficient to prevent stress concentrations from causing rapid propagation of the cracks and sudden failure. Cavities occurred only on those boundaries which

appeared to be perpendicular or almost perpendicular to the stress axis. Consequently, the 'wavy' cracks were also perpendicular to the stress axis.

At the two faster strain rates and 500 deg.C., the dominant mechanism of cracking is that due to the formation of triple point wedges (Figures 2.9 and 2.10). However, a few cavities still occur at points along the grain boundaries. Figure 2.9 shows that the wedges tend to grow only along those boundaries orientated at a small angle to the stress axis. The presence of this type of discontinuity indicates that grain boundary sliding has taken place. Direct evidence of sliding can be seen in Figure 2.10. The vertical striation, at the right hand side, is offset as it traverses the grain boundaries. With the upper boundary, the offset is distinct and a triple point crack has resulted at the left hand end of this boundary. With the lower boundary, the offset appears as a bend in the striation. In this case, grain boundary migration has occurred to relieve the stress concentration on the triple point and a wedge crack has not appeared.

2.4.3 Conclusions

The above observations are consistent with those of other research workers on a variety of materials and, therefore, do not make any new contribution to the state of knowledge on intergranular fracture. They show that the mechanism of fracture can change from one of cavitation to one of triple point cracking over a small range of strain rates at the same temperature. Metallography has achieved its object in demonstrating, qualitatively, the size, shape and number of intercrystalline cracks, but has failed to provide a simple means of describing them quantitatively.

2.5 Fracture at Constant Strain Rate

Figures 2.12 and 2.13 show the effects of strain rate and temperature on the mode of fracture of commercially pure aluminium. The test conditions are presented in Table 2.1 along with the variation of ductility as measured by elongation and reduction of area at fracture.

Table 2.1

Temperature deg.C.	Strain Rate pct/h	Strain pct	Reduction of Area pct
500	0.1	51.9	48.6
500	1	36.4a	53.2a
500	10	44.9	69.6
500	100	61.8b	83.3b
250	1	10.7	26.5
250	10	17.3	32.5
20	10	29.1	84.2

Notes a Another test at this strain rate and temperature was strained to 54.6 pct elongation without rupture. The gauge length thinned uniformly by only 26.5 pct.

b This test piece was stopped before rupture took place.

In Figure 2.12, the fracture at room temperature is the typical ductile 'cup and cone' failure. At 250 deg.C., the fracture surfaces are typically intergranular and Table 2.1 shows that ductility was lowest at this temperature. Figure 2.13 illustrates the change in behaviour as the strain rate increases from 0.1 to 100 pct/h, at a temperature of 500 deg. C. At the slowest rate, little localised necking has taken place and the fracture surface indicates an intergranular type of failure. As the strain rate is increased, localised necking becomes more pronounced, but the fracture surface

retains the intergranular characteristic. However, the results of Table 2.1 show that, although intergranular cracks develop in the test piece at 500 deg.C., the material is able to cope with their effects and continues the deformation process to large strains.

The differing behaviours at 250 deg.C. and 500 deg.C. are quite startling. Grain boundary cavities and triple point cracks have been shown to develop at a temperature of 500 deg.C. Presumably, this process also occurs at 250 deg.C. However, while at 500 deg.C. the cavities and cracks are unable to cause fracture, as is evidenced by their continued growth, those formed at 250 deg.C. have a more damaging effect since sudden failure occurs with much lower ductility. These results show quite clearly that cavities and cracks can have widely differing effects under different conditions of stress and temperature.

2.6 Summary and Conclusions

Constant strain rate tensile tests were performed on commercially pure aluminium at temperatures of 250 deg.C. and 500 deg.C. and strain rates of 0.1, 1, 10 and 100 pct/h. Metallography demonstrated that intergranular discontinuities developed in the material when strained at 500 deg.C. The amount of discontinuities increased with increasing strain for a particular strain rate and decreased with increasing strain rate for a particular strain. For slow strain rates the discontinuities originated mainly as cavities at points along grain boundaries and for high strain rates as wedge cracks at triple points. Metallography was, however, unsuitable for quantitative estimation of the amount of intergranular discontinuities. Measurement of density change was considered to be a better method and the procedure is described in the next chapter. Comparison of fractured test pieces, elongations to fracture and reductions of area at fracture surfaces for tests at 250 deg.C. and 500 deg.C., indicated that catastrophic failure results from the formation of intergranular discontinuities at 250 deg.C. At the higher temperature of 500 deg.C., however, the discontinuities do not appear to hinder continued deformation.

APPENDIX 2.1

1) Error in Measurement of Strain by reference marks

$$\text{Strain, } \varepsilon = \frac{L - Lo}{Lo}$$

where Lo is original gauge length = 35.55 $\pm$ 0.05 mm, and L is strained gauge length (measured also to $\pm$ 0.05 mm).

Taking natural logarithms of both sides of above equation,

$$\ln \varepsilon = \ln (L - Lo) - \ln Lo$$

and differentiating,

$$\frac{\partial \varepsilon}{\varepsilon} = \frac{\partial (L - Lo)}{L - Lo} - \frac{\partial Lo}{Lo}$$

Partial differentials may be replaced by small increments denoted by prefix δ,

$$\frac{\delta \varepsilon}{\varepsilon} = \frac{\delta (L - Lo)}{L - Lo} - \frac{\delta Lo}{Lo}$$

This equation may be used to calculate the error $\delta\varepsilon$ in ε caused by the errors δL in L and δLo in Lo. Maximising errors,

$$\frac{\delta \varepsilon}{\varepsilon} = \frac{\delta L + \delta Lo}{L - Lo} + \frac{\delta Lo}{Lo}$$

and $$\delta \varepsilon = \frac{\delta L + \delta Lo}{Lo} + \varepsilon \frac{\delta Lo}{Lo}$$

Hence, $$\delta \varepsilon = 0.003 + 0.0014\ \varepsilon$$

For strains less than 0.3, error in measured strain is $\pm$ 0.003 and for strains 0.3 to 1, error in measured strain is $\pm$ 0.005.

2) Error in Measurement of Stress

$$\text{Stress, } \sigma = \frac{4P}{\pi D^2} ,$$

where P is the measured value of load and D is the measured value of test piece diameter.

Applying the same analysis as in 1) leads to,

$$\frac{\delta\sigma}{\sigma} = \frac{\delta P}{P} + 2\frac{\delta D}{D}$$

and, hence, this equation may be used to calculate the error $\delta\sigma$ in σ due to the errors δP in P and δD in D.

Diameter of test piece = 9.070 mm and $\delta D = \pm 0.025$ mm.

Hence, from above equation,

$$\frac{\delta\sigma}{\sigma} = \frac{\delta P}{P} + 0.00555$$

For tests at 500 deg.C. and 0.1 pct/h,

Maximum Stress = 0.87 N/mm^2 = 125.9 lbf/in^2

Maximum Load = 10.0 ± 0.5 lbf.

Hence, $\frac{\delta\sigma}{\sigma} = \pm 5.6$ pct.

For tests at 500 deg.C. and 1, 10, and 100 pct/h, maximum loads were, approximately, 30.0 ± 0.1 lbf, 50.0 ± 0.1 lbf, and 70.0 ± 0.1 lbf, respectively.

For tests at 250 deg.C. and 0.1, 1, 10 and 100 pct/h, maximum loads were, approximately, 657 ± 1 lbf, 893 ± 1 lbf, 1112 ± 1 lbf, and 1273 ± 1 lbf, respectively. Substitution of these values into the above equation for $\frac{\delta\sigma}{\sigma}$ leads to the solution that error in measured value of maximum stress was ± 0.7 pct.

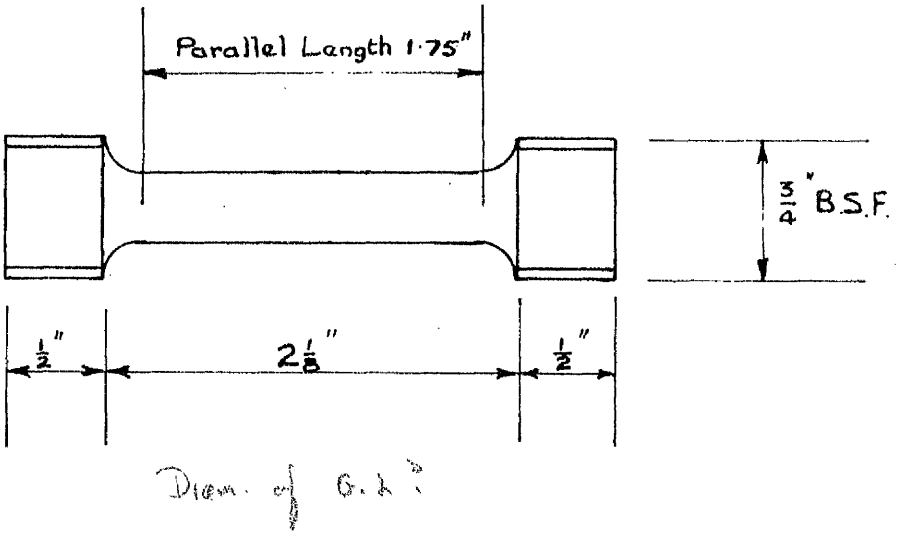

Figure 2.1 Tensile Test Piece

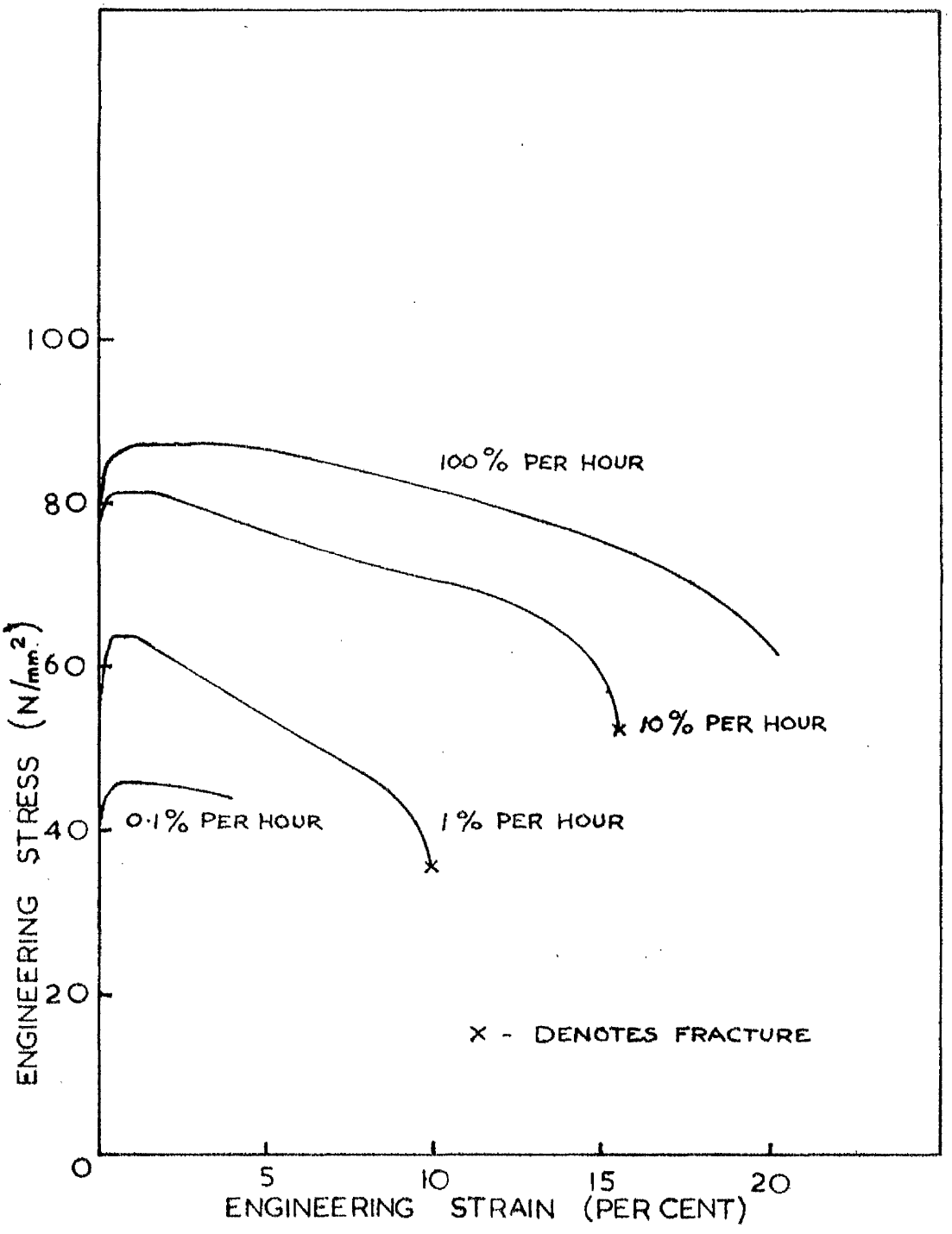

Figure 2.2 250 deg.C.; constant strain rate tensile tests; engineering stress against engineering strain

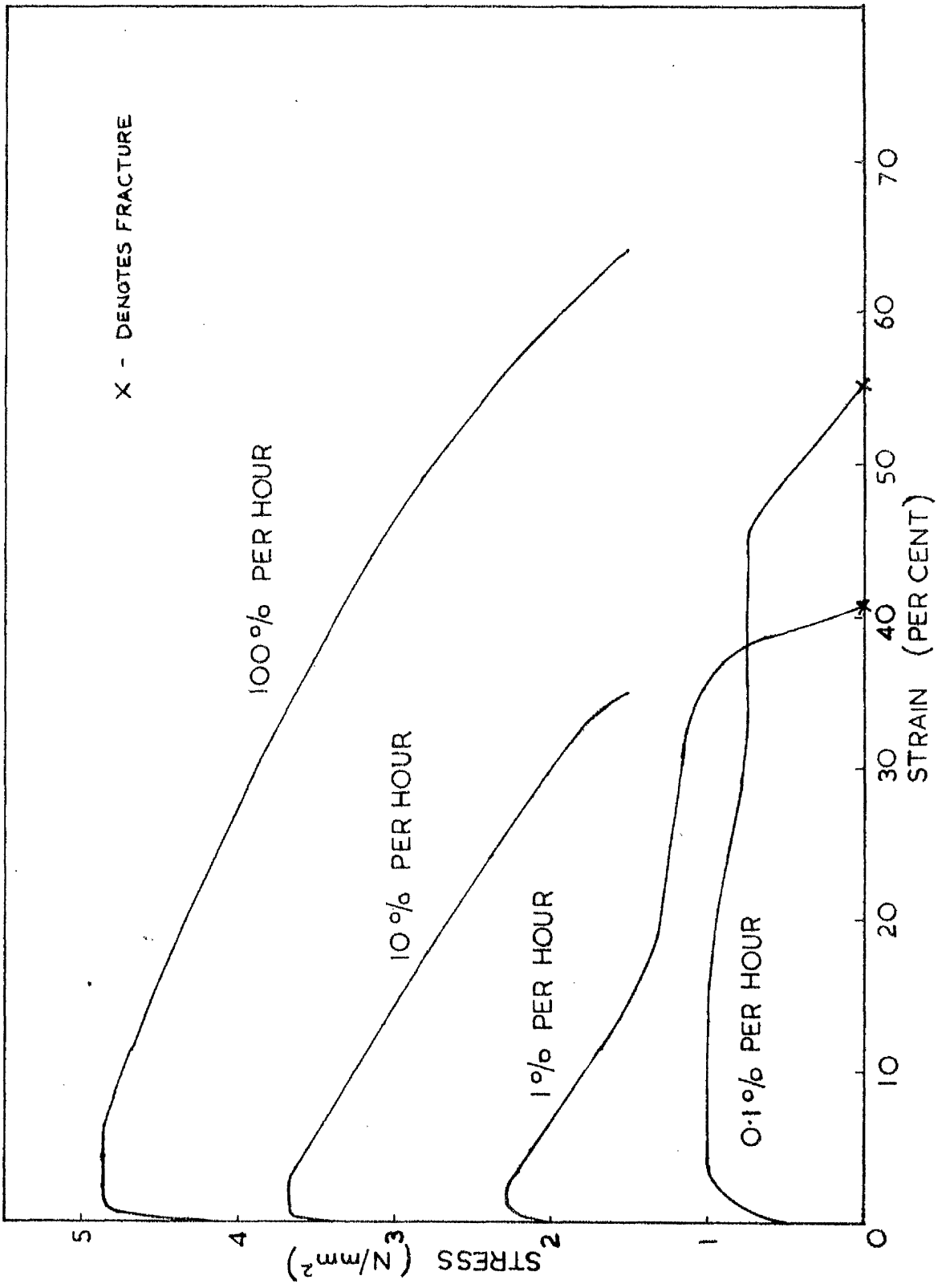

Figure 2.3 500 deg.C.; constant strain rate tensile tests; engineering stress against engineering strain

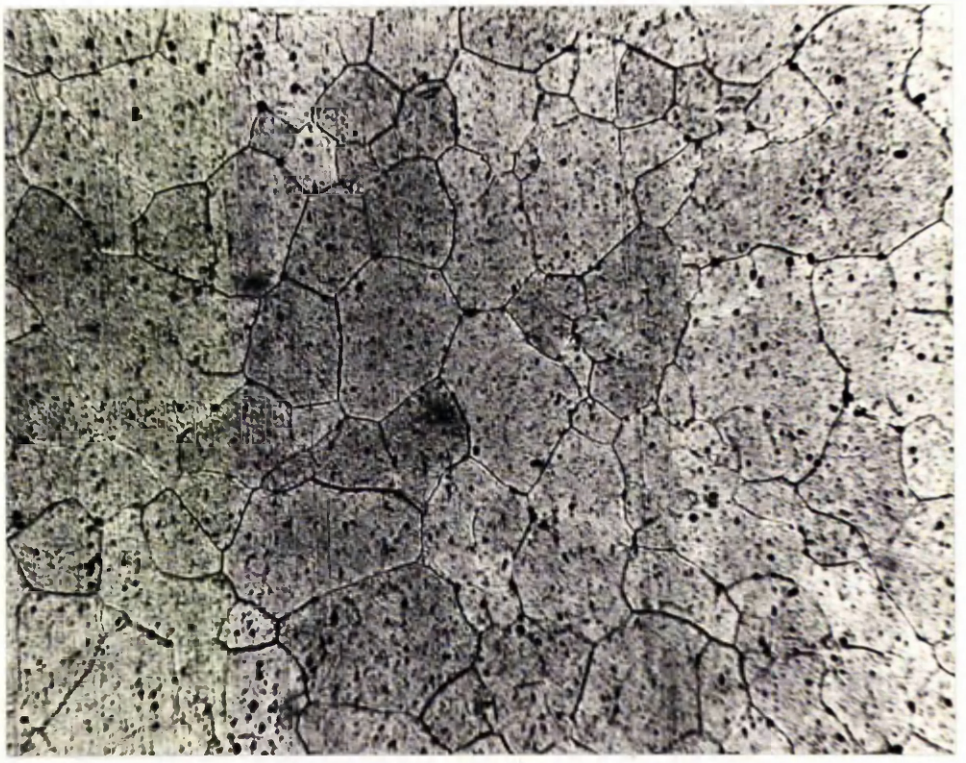

Figure 2.4 'As received' material, annealed for 2 hours at 500 deg.C. Axis of bar is vertical in plane of micrograph. Magn. 125X.

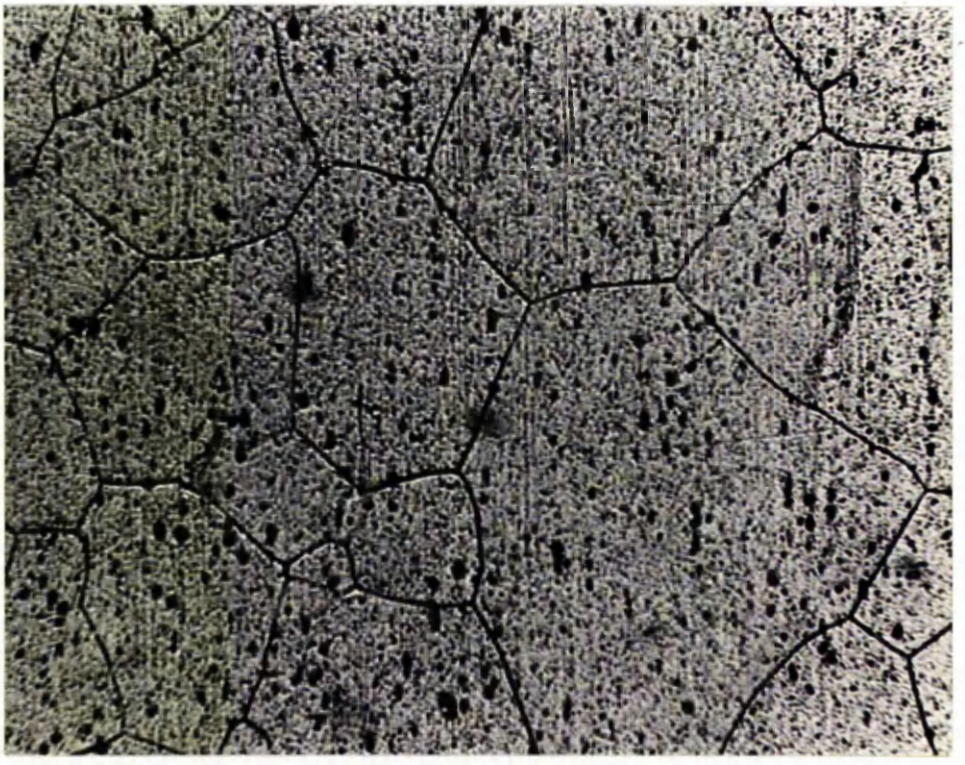

Figure 2.5 'As received' material. Axis of bar is vertical in plane of micrograph. Magn. 250X.

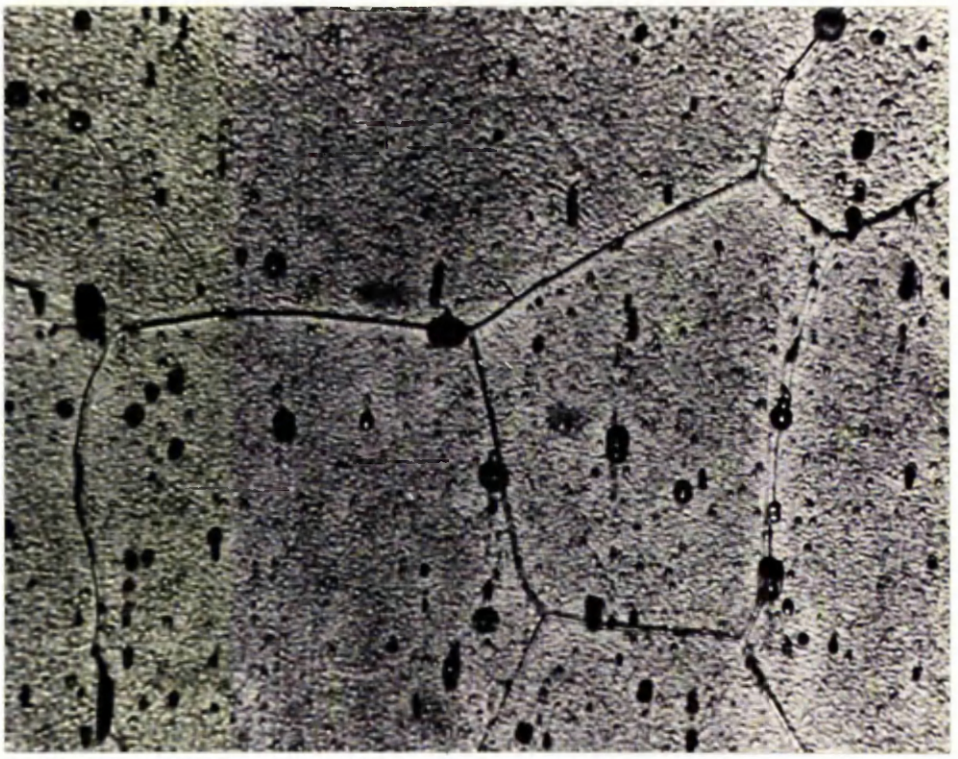

Figure 2.6 'As received' material. Axis of bar is vertical in plane of micrograph. Magn. 630X.

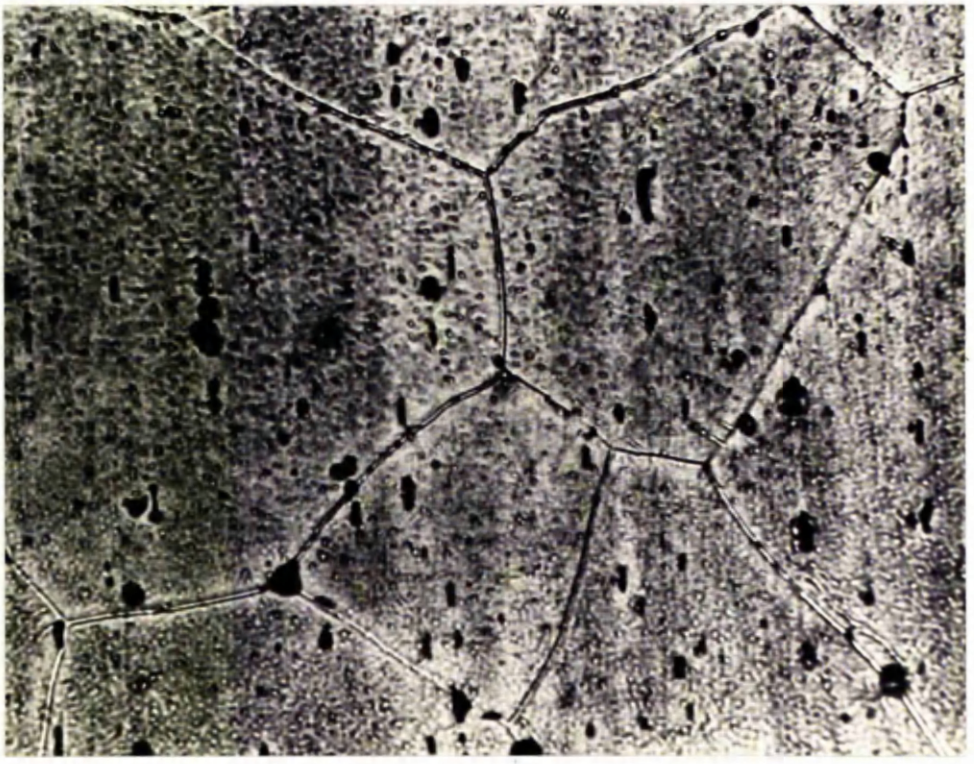

Figure 2.7 'As received' material, annealed for 1 hour at 500 deg. C. Axis of bar is vertical in plane of micrograph. Magn. 630X.

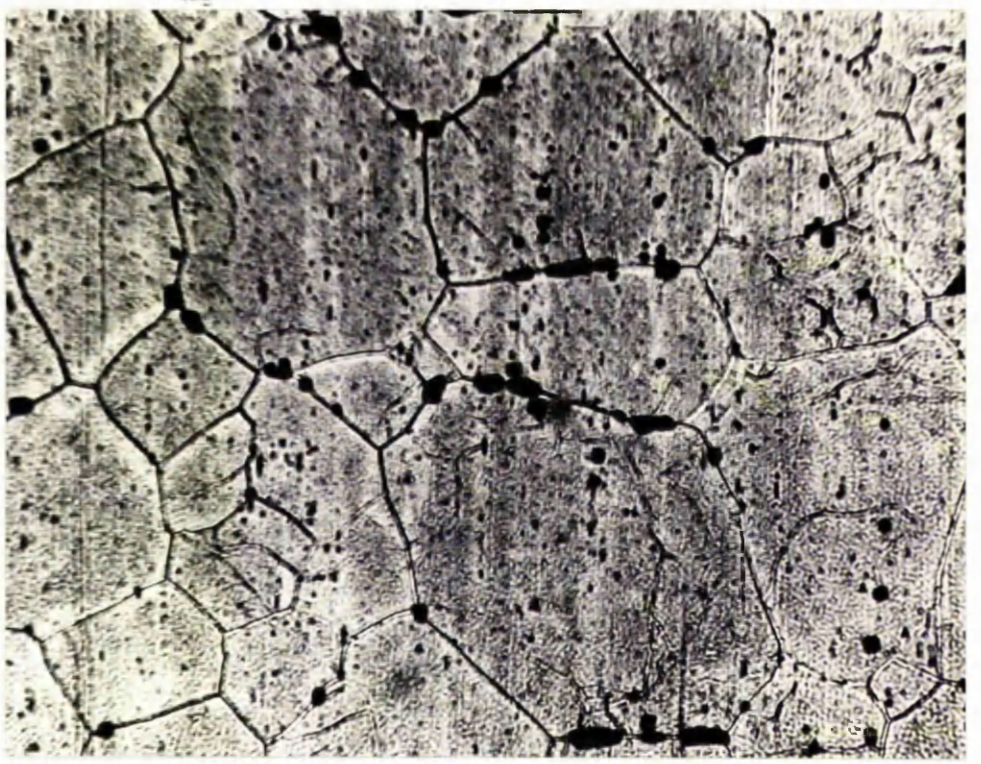

Figure 2.8 500 deg.C., 1 pct/h to 1.8 pct strain and 0.264 pct density decrease. Stress axis vertical. Magn. 250X.

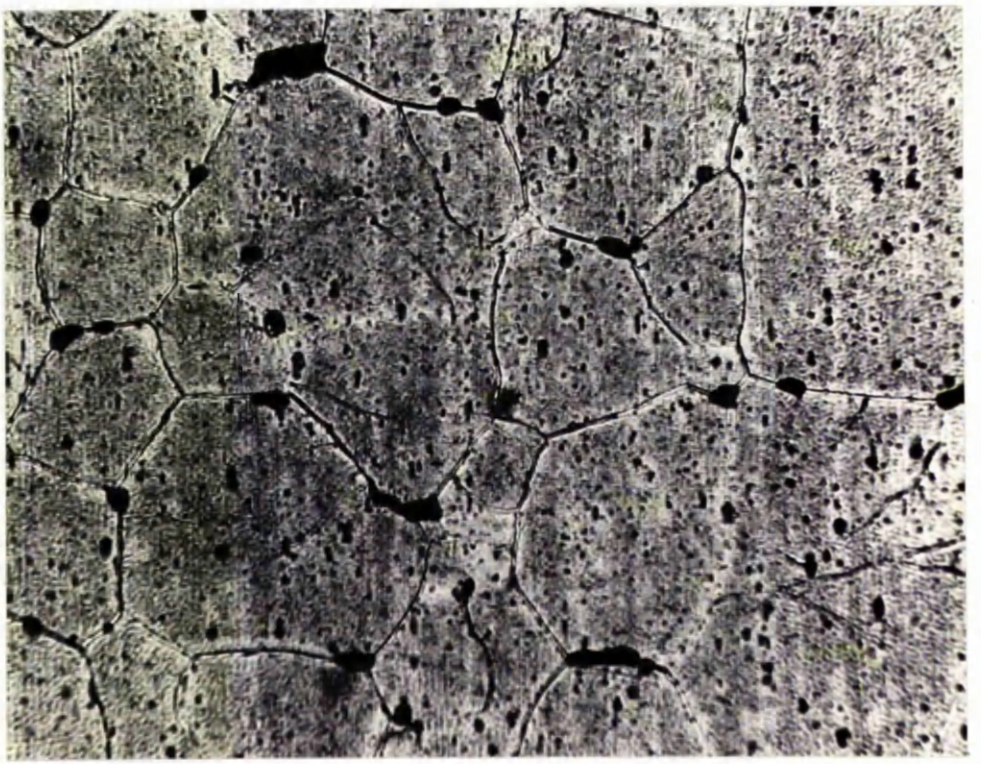

Figure 2.9 500 deg.C., 10 pct/h to 7.6 pct strain and 0.287 pct density decrease. Stress axis vertical. Magn. 250X.

Figure 2.10 500 deg.C., 100 pct/h to 7.5 pct strain and 0.089 pct density decrease. Stress axis vertical. Magn. 250X.

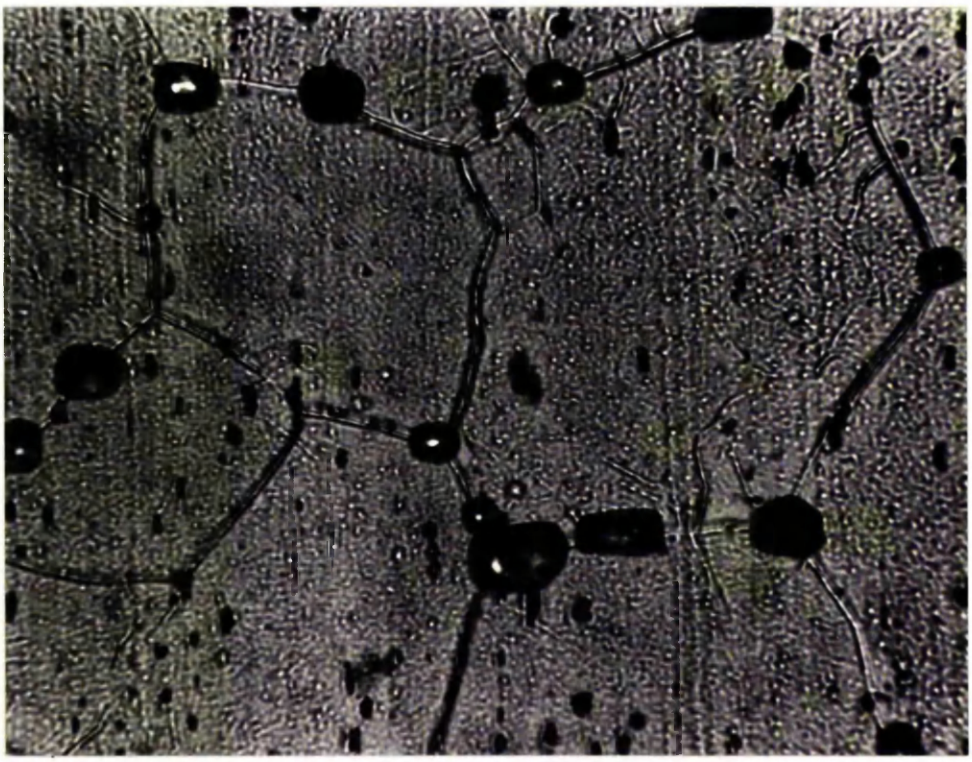

Figure 2.11 500 deg.C., 1 pct/h to 0.8 pct strain and 0.171 pct density decrease. Stress axis vertical. Magn. 630X.

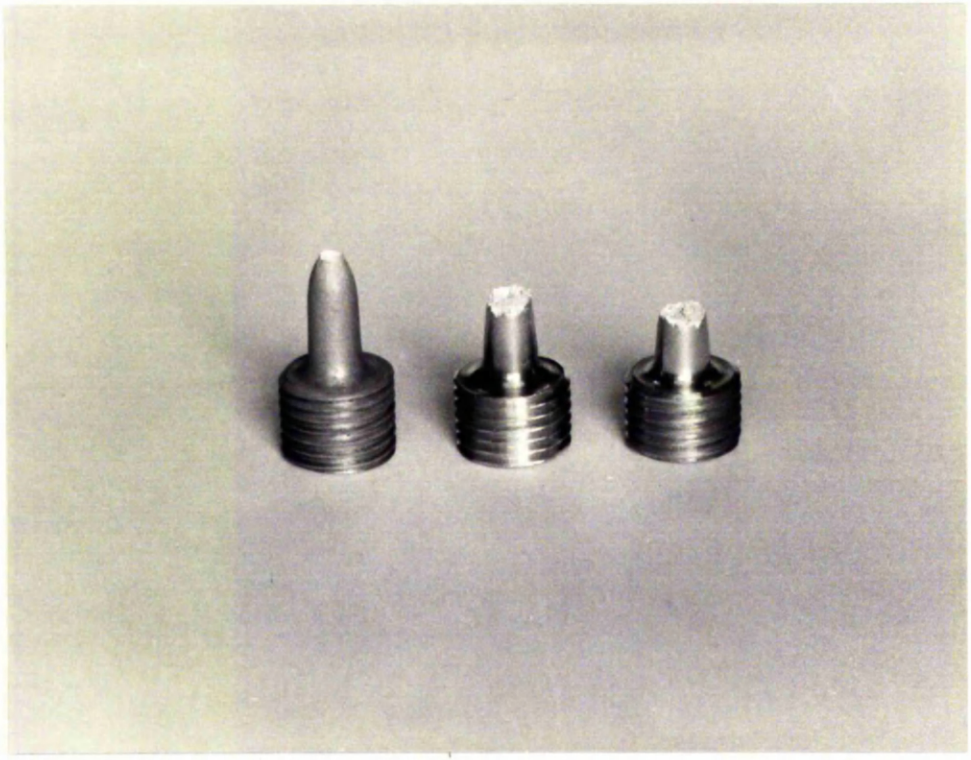

Figure 2.12 Fracture profiles : 20 deg.C. and 10 pct/h (left), 250 deg.C. and 10 pct/h (middle), 250 deg.C. and 1 pct/h (right).

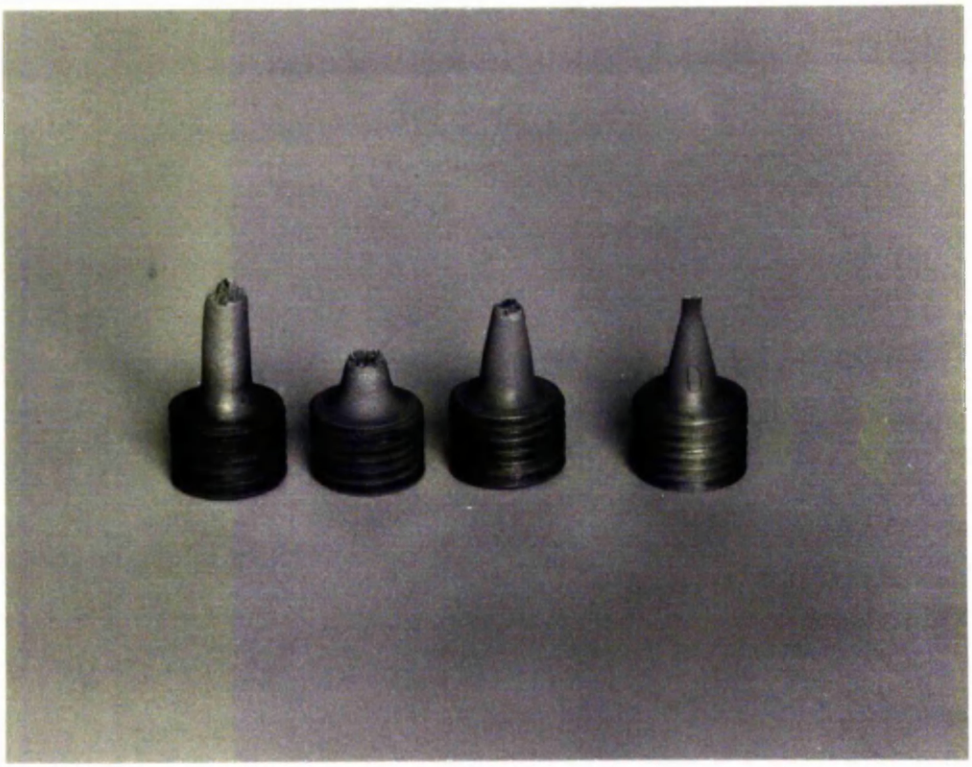

Figure 2.13 Fracture profiles : 500 deg.C. and, from left to right, 0.1, 1, 10 and 100 pct/h.

CHAPTER III

TENSILE DENSITY CHANGES

3.1 Introduction

In the previous chapter it was shown that, although metallography was able to demonstrate the size, shape and position of intergranular discontinuities in commercially pure aluminium, which had been slowly strained at high temperature, it was unsuitable for the accurate measurement of the total volume of cracking in a specimen. A simpler and more accurate method was thought to be the measurement of the associated change in density of the material. The measurement of this density change, by means of a hydrostatic weighing technique, is now a well established method of studying the growth of intergranular discontinuities. In addition to the straightforward measurement of density change by the difference in the absolute densities of virgin and cavitated material, differential weighing techniques have also been developed, providing greater accuracy in measuring small density changes (Bell, 1958; Ratcliffe, 1965).

Available in Glasgow University Engineering Department was a hydrostatic density balance. This apparatus (shown in Figure 3.1) was similar in design to the one constructed by Bell. Although the balance was suitable for measuring density changes by a differential weighing technique, the absolute method was found more convenient to use. By this method, the variation of the density decrease due to intergranular cracking with strain, strain rate and temperature was determined for commercially pure aluminium. An absolute

measure of total crack volume per unit weight is obtained on dividing the fractional density decrease by the density of the strained specimen :—

$$\text{Total crack volume/unit weight} = \frac{\rho_o - \rho_1}{\rho_o \rho_1} \qquad (3.1)$$

where ρ_o was the original density of the material and ρ_1 is the density of the strained material.

3.2 The Hydrostatic Density Balance

3.2.1 Derivation of Operating Equation : Absolute Method

This derivation for the density of a solid body, using Archimedes Principle, was extracted from Bell (1958).

Let M be the mass of the specimen,

V be the volume of the specimen at temperature t,

ρ be the density of the specimen at temperature t,

d be the density of the liquid at temperature t,

α be the density of the weights used,

β_1 be the density of the air when the specimen is weighed in air,

β_2 be the density of the air at the time the specimen is weighed in liquid,

W^β be the weight in air of the specimen,

W^d be the weight in liquid of the specimen.

The equations of equilibrium are :

In air
$$M - V\beta_1 = W^\beta \left(1 - \frac{\beta_1}{\alpha}\right) \qquad (3.2)$$

In liquid
$$M - Vd = W^d \left(1 - \frac{\beta_2}{\alpha}\right) \qquad (3.3)$$

If these weighings are made in quick succession, the air density may be assumed constant and we may write β for β_1 and β_2. Therefore,

$$M - V\beta = W^\beta \left(1 - \frac{\beta}{\alpha}\right)$$

$$M - Vd = W^d \left(1 - \frac{\beta}{\alpha}\right)$$

whence

$$\rho = \frac{M}{V} = \frac{W^{\sigma}{}_{d} - W^{d}{}_{\sigma}}{W^{\sigma} - W^{d}} \qquad (3.4)$$

The correction to the equilibrium equations for the effect of air buoyancy is necessary if high accuracy is to be achieved.

In the above derivation of equation 3.4, the volume of the specimen, when weighed in air, was assumed to be equal to the volume of the specimen when weighed in liquid. This is only true when the air and liquid temperatures are the same. In practice, the air and liquid temperatures may differ by a few deg.C. The discrepancy may be ignored if the density and volume of the specimen are referred to the liquid temperature, as was done in the derivation of equation 3.4. Then, the effect of the slight discrepancy in specimen volume when weighed in air becomes negligible since, in the equilibrium equation, it is multiplied by σ, and σ is much smaller than d. However, the temperature difference between air and liquid which can be tolerated, depends on the intended accuracy of measurement.

3.2.2 The Balance

The main features of the apparatus have been described elsewhere (Bell, 1958). Briefly, it consists of a modified two pan analytical balance situated on a vibration free mounting. Two additional weighing pans are suspended in the working liquid by 0.002in. diameter 'Nichrome' wire, attached to hooks on the undersides of the original pans. Since the analytical balance is equipped with air dampers, the lower pans have to be of wire mesh construction to prevent overdamping while weighing in liquid. To eliminate the effects of draughts and dust, the analytical balance is enclosed in a perspex box and the suspension wires are enclosed in perspex tubes.

Increased resolution of the weight of a specimen was achieved by using an optical pointer. A plane mirror (10 mm. diameter), mounted in line with the axis of the pivot of the beam, reflected the image of a projector lamp filament on to a screen, 4 metres distant. On the screen, an image movement of 1 mm. from the zero position represented an increase or decrease of 0.1 mg. in weight. The weight of a specimen was resolved to $\pm$ 0.05 mg.

The two lower pans of the balance are submerged in the working liquid contained in the arms, A and B, of the copper inner vessel, shown in Figure 3.2. The inner vessel is situated in a temperature controlled water bath, capable of maintaining temperature to $\pm$ 0.01 deg.C. In practice, temperature control of the working liquid in the inner vessel was also $\pm$ 0.01 deg.C. Measurement of working liquid temperature was achieved with a mercury in glass thermometer, placed in limb H of the inner vessel. Stirring of the working liquid was effected by way of a pulsating air pressure supplied by a small pump (J). Details of this method of stirring appear in the paper by Bell.

Distilled tap water was used as the working liquid. Other recommended liquids, such as diethyl phthallate and acetylene tetrabromide were not used because satisfactory results were achieved using water. In addition, both of the recommended liquids have unpleasant physical properties and one of them, acetylene tetrabromide, is denser than aluminium, which would have made weighings in that liquid (rather) difficult.

3.2.3 Experimental Procedure

Since the temperature controlled baths were allowed to run continuously, with both stirring systems in operation, no time was lost in waiting for them to reach a steady temperature. The gauge lengths, removed from the strained test pieces, were thoroughly washed in water and alcohol and

then allowed to dry in air. For the weighings of the specimen in air, the lower pans were not suspended from the undersides of the original pans. The balance was then poised and the zero position of the image on the screen was recorded. The balance was un-poised and then repoised to check the zero position. The specimen was placed on one pan, and, when sufficient weights had been added to the other pan to bring the image on the screen back to the zero position, the air temperature and pressure, as well as the weights, were recorded. The procedure was repeated with the specimen on the other pan to reduce zero position errors of the balance. The average of the two weighings was taken as the weight of the specimen in air.

After weighing in air, specimens were placed in the inner water bath and allowed 20 minutes to attain the slightly higher temperature (2-3 deg.C.) of the working liquid. The lower pans were then suspended from the undersides of the original pans and the weighing procedure was repeated for the specimen in water. In addition to air temperature and pressure, water temperature was also recorded for each weighing. While the balance was poised, the inner and outer vessel stirring systems were switched off to reduce disturbance due to vibration.

3.2.4 Calculation of Results and Error Estimation

The density of the specimen at the water temperature was calculated with the aid of equation 3.4. The weights, W^{β} and W^{d}, were the average of the dual weighings and had an accuracy of $\pm$ 0.05 mg. The Handbook of Physics and Chemistry (1963 Edition) was used to provide the density of water and an equation to compute the density of air. The effect of the partial water vapour pressure in the atmosphere was considered to be negligible. The equation used to compute values of air density was,

$$\text{Air density, } \rho^{\beta(a)} = \frac{0.001293\ P}{(1 + 0.00367t)\ 76} \quad g/cc$$

where P is the air pressure in cms. Hg. and t is the air temperature in deg.C. The value of specimen density obtained, corresponding to the water temperature, was then adjusted to 20 deg.C. using the volume coefficient of expansion of aluminium, 72 x 10^{-6} per deg.C.

Error Estimation

From equation 3.4,

$$D = \frac{W^{\beta}_{d} - W^{d}_{\beta}}{W^{\beta} - W^{d}} = (1 - \frac{W^{d}_{\beta}}{W^{\beta}_{d}}) \div \frac{W^{\beta} - W^{d}}{W^{\beta}_{d}}$$

Taking natural logarithms of both sides of equation,

$$\ln D = \ln (1 - \frac{W^{d}_{\beta}}{W^{\beta}_{d}}) - \ln (\frac{W^{\beta} - W^{d}}{W^{\beta}_{d}})$$

Since $d \gg \beta$,

$$(1 - \frac{W^{d}_{\beta}}{W^{\beta}_{d}}) \simeq 1 \quad \text{and} \quad \ln (1 - \frac{W^{d}_{\beta}}{W^{\beta}_{d}}) \simeq 0$$

Therefore,

$$\ln D = - \ln (W^{\beta} - W^{d}) + \ln W^{\beta} + \ln d$$

Putting the logarithms in differential form,

$$\frac{\delta D}{D} = - \frac{\delta (W^{\beta} - W^{d})}{W^{\beta} - W^{d}} + \frac{\delta W^{\beta}}{W^{\beta}} + \frac{\delta d}{d}$$

where prefix δ denotes error in measured quantity.

Maximising errors,

$$\frac{\delta D}{D} = \frac{\delta W^{\beta} + \delta W^{d}}{W^{\beta} - W^{d}} + \frac{\delta W^{\beta}}{W^{\beta}} + \frac{\delta d}{d}$$

Now, $\delta W^{\beta} = \delta W^{d} = \pm 0.00005$ g.,

δ (water temperature) $= \pm 0.01$ deg.C. and, therefore,

$\delta d = \pm 0.000003$ g/cc.

The aluminium specimens weighed approximately 6 g. in air and 4 g. in water. Therefore,

$$\frac{\delta D}{D} = \frac{0.00010}{2} + \frac{0.00005}{6} + \frac{0.000003}{1} = \underline{0.00006}$$

The density of aluminium is 2.70 g/cc and, hence,

$$\delta D = \pm (0.00006 \times 2.70)$$

$$= \underline{\pm 0.0002 \text{ g/cc}}$$

A specimen of the 'as received' material, which had its density measured six times, was found to yield the value 2.6978 g/cc four times, and the values 2.6977 g/cc once and 2.6980 g/cc once. Hence, accuracy of measurement was taken as $\pm$ 0.0002 g/cc for a 6 g. specimen, in agreement with the Error Estimation. Nine random samples of the 'as received' material, including the one above, then had their densities measured. The results are presented in Table 3 1.

Table 3.1

Density (g/cc)	2.6975	2.6976	2.6977	2.6978	2.6979	2.6980
No. of measured values at the above density	1	1	2	3	1	1

From the results of Table 3.1, it was concluded that the 'as received' material had a density of 2.6978 g/cc and, that variation from this value for different samples of the material, was within the accuracy of the method of measurement. Therefore, measurement of density change by the difference in the absolute values of the densities of the 'as received' and tested materials was accurate to $\pm$ 0.0004 g/cc or $\pm$ 0.015 pct.

3.3 Strain-Dependence of Density Changes

3.3.1 Preliminary Experiments

Before investigating the density changes caused by slow straining at high temperature, it was necessary to determine the effect on the material of annealing at the high temperature. A specimen heated for 168 hours at a temperature of 250 deg.C. showed (negligible (< 0.0004 g/cc) change in density from that of the 'as received' material. However, a specimen, heated at a temperature of 500 deg.C. for several time periods, showed an increase of density for each successive period. A maximum density of approximately 0.06 pct greater than that of the 'as received' material was attained after 200 hours and this value was maintained for longer periods of annealing at 500 deg.C. On sectioning, polishing and etching the specimen, extensive grain growth was found to have occurred, there being only two or three grains across the 0.357 in. diameter of the specimen. The increase in density was, therefore, caused by the elimination of grain boundaries through grain growth. Initially, the sintering out of the few cavities, observed during metallography of the 'as received' material, would also contribute to the density increase.

3.3.2 Results from Tests at 500 deg.C.

The variation of fractional density decrease with strain for commercially pure aluminium, elongated at constant strain rate at a temperature of 500 deg.C., is shown in Figure 3.3. The experimental points represent the fractional density decreases in the strained gauge lengths of different test pieces, with the original value of density taken to be 2.6978 ± 0.0002 g/cc. Although the fractional density decrease must be divided by the density of the strained gauge length to produce total crack volume/unit weight (Section 3.1), the fractional density decrease may be taken as representing the total crack volume/unit weight for 'small' density decreases. 'Small' is defined by the

relative magnitudes of density decrease and accuracy of measurement. In the present research, accuracy of density decrease measurement was $\pm$ 0.0004 g/cc or $\pm$ 0.015 pct. Therefore, density decreases of less than 2 pct could be assumed to accurately represent the total crack volume/unit weight. The effect of the discrepancy on fractional density decreases greater than 2 pct is shown for the 1 pct/h curve in Figure 3.3. The curve, marked 'A' in Figure 3.3, was obtained as follows :

From equation 3.1,

$$\text{Total crack volume/unit weight} = \frac{\rho_o - \rho_1}{\rho_o \rho_1}$$

Let $\frac{\rho_o - \rho_1}{\rho_o} = x$, then $\rho_1 = \rho_o (1 - x)$

Hence,

$$\text{Total crack volume/unit weight} = \frac{x}{\rho_o (1 - x)} \qquad (3.5)$$

Curve 'A' in Figure 3.3 represents the plot of $\frac{x}{1 - x}$ against strain, and is, therefore, proportional to total crack volume/unit weight since ρ_o is constant. It was concluded that fractional density decrease could be taken as a good approximation for total crack volume/unit weight for values greater than 2 pct. Subsequently in this Thesis, fractional density decrease has been taken as representing total crack volume/unit weight. Since fractional density decrease will always be calculated from the standard value of 2.6978 $\pm$ 0.0002 g/cc, the density decrease, itself, may represent the fractional density decrease.

Figure 3.3 shows that fractional density decrease and, therefore, total crack volume/unit weight, increase continuously with strain for each of the four strain rates. Extrapolation of each curve back to the origin, indicates

that internal discontinuities develop from the beginning of plastic deformation. Although the strain recorded for each experimental point was the permanent strain, this value may also be regarded as that of the plastic strain if the effects of hysterisis in the stress/strain curve may be neglected. The plots of fractional density decrease against strain can be approximated to straight lines over much of their length. Therefore, total crack volume/unit weight appears to be proportional to strain for commercially pure aluminium deformed under constant strain rate conditions at a temperature of 500 deg.C. Since strain is proportional to time under those conditions, total crack volume/unit weight may also be regarded as proportional to time. However, the proportionality between strain and time was not observed in the present tests because of the 'softness' of the tensile testing machine. The crosshead movement of the machine has to account for the deflection of the spring beam, measuring load, as well as the extension of the test piece. Therefore, time of test was always greater than the value of strain/strain rate. This variation in the actual strain rate experienced by the gauge length of the test piece was mentioned in section 2.2.2 of Tensile Testing. It was concluded that, due to the shape of the stress/strain curve for commercially pure aluminium at high temperature, the effect of the variation in strain rate could be ignored for most values of strain. It was pointed out, however, that, in gauge lengths strained by less than 1.4 pct, the effect of the slight variation in strain rate may not be ignored. This is illustrated in Figure 3.3 by the experimental point at 0.8 pct strain in the 1 pct/h curve. The larger density decrease observed is consistent with the gauge length having experienced a slower strain rate.

Figure 3.3 shows that, for the same strain, the fractional density decrease or volume of intergranular cracking increases with decrease of strain rate from 100 Pct/h to 1 pct/h. This behaviour was to be expected since, as the strain rate decreased, more time became available for the growth of grain boundary cavities by a diffusion process.

Greenwood et al. (1954) observed an increase of intergranular cavitation in α-brass, copper and magnesium as the strain rate was lowered, in tensile tests at constant temperature. However, as shown by Figure 3.3, this trend was not continued in commercially pure aluminium for the strain rate less than 1 pct/h ie. 0.1 pct/h. For that strain rate, the density decrease against strain plot lies between the 1 pct/h and 10 pct/h curves. These results suggest that there exists a particular strain rate for which the volume of intergranular cracking is a maximum. Some further tensile tests were carried out on the material at strain rates between 0.1 and 10 pct/h, to determine the value of the strain rate for which maximum intergranular cracking occurred. The test pieces were strained by approximately 25 pct and then had their changes in density measured. The results have been plotted in Figure 3.4 and the extrapolated values for the four original strain rates have also been included. A maximum decrease in density was observed for a strain rate of 0.7 pct/h. Hence, in commercially pure aluminium, deformed at constant strain rate and a temperature of 500 deg.C., the amount of intergranular cracking was a maximum at 0.7 pct/h. For strain rates larger or smaller than this value, the total volume of intergranular discontinuities was less for the same strain.

The observation of a maximum amount of cracking for a particular strain rate was also observed in an aluminium/magnesium alloy by Nield and Quarrell (1957). In constant strain rate tests at temperatures of 260 deg.C. and 300 deg.C., minimum values of reduction of area at fracture were found to occur at a strain rate between 1 and 10 pct/h. Metallography confirmed that the increased ductility at slow strain rates was consistent with a decrease in the extent of intergranular cracking. In addition, they observed large-scale grain boundary migration in the sections of specimens strained at the slow rates. Since extensive grain growth has already been found in a specimen of commercially pure aluminium annealed at a temperature of 500 deg.C. for over 200 hours, it must be concluded that grain boundary migration was, at

least, one factor causing the observed behaviour in the present material.

The influence of boundary migration on intergranular cavitation may be twofold. Firstly, the ability of grain boundary migration to relieve stress concentrations caused by barriers to boundary sliding will reduce the total number of cavity nuclei produced. Secondly, since boundary migration is a diffusion process, it will assist the tendency of a cavity of sub-critical size to sinter up under the action of surface tension forces. Hence, the stress-directed flow of vacancies attempting to stabilise the cavity of sub-critical size, has also to overcome the annihilating effect of boundary migration. This competition between boundary migration and the growth mechanism may be expected to continue if the cavities reach a stable size. However, stable cavities tend to sinter out under zero stress conditions even in the absence of boundary migration. Since zero stress may be considered as the limiting case of low stress, the vacancy diffusion flux, causing sintering at zero stress, may also be expected to compete with stress-directed diffusion of vacancies causing growth. Therefore, as the strain rate or stress decreases and the flux of vacancies due to stress-directed diffusion also decreases, the combined effects of grain boundary migration and the vacancy flux, tending to sinter cavities, may be sufficient to slow down the rate of cavity growth. At very low stresses, the combined effects may be able to prevent cavity growth completely. To show that these effects may be responsible for the observed behaviour of commercially pure aluminium, annealing experiments were carried out on specimens containing small amounts of cavities. The results are described in section 3.4.

3.3.3 Results from Tests at 250 deg.C.

Density changes measured on gauge lengths of the few test pieces strained at a temperature of 250 deg.C. are presented in Table 3.2.

Table 3.2

Specimen No.	Strain Rate pct/h	Strain pct	Density Decrease ±0.015pct	Comments
77	0.1	3.5	0.011	No Necking
80	1	4.8	0	No Necking
78	1	10.7	0.045	Fracture Test
74	10	17.3	0.063	Fracture Test
73	100	19.9	0.115	Localised Necking

Examination of Table 3.2 shows that density decreases were only associated with the gauge lengths of fractured and necked test pieces. If discontinuities developed in the material before necking occurs, they were apparently too small to be detected by the present method of density change measurement. In section 2.5 the fracture surfaces of specimens 74 and 78 were shown to be typical of inter-crystalline failure. The small density decreases recorded in their gauge lengths (minus the fracture surfaces) confirms the suggestion that the development of intergranular discontinuities caused failure. Also, it is noteworthy that only a small total volume of intergranular discontinuities was necessary to cause complete failure.

3.3.4 Preparation of Creep Test Pieces

The main purpose of the tensile testing programme was to obtain a method of preparing creep test pieces with a controlled amount of intergranular discontinuities. Tensile testing of commercially pure aluminium at a temperature of

500 deg.C. has been shown able to achieve this objective, when used in conjunction with accurate density measurements. Creep test pieces, with specific amounts of intergranular discontinuities, were to be strained under constant load conditions at high and low creep temperatures and the results compared with tests on the crack-free material. Therefore, it was necessary to keep deformation of the material to a minimum during the preparation of the test pieces with intergranular discontinuities. Tensile straining at a strain rate of 1 pct/h was chosen to prepare the creep test pieces. As shown by Figures 3.3 and 3.4, this strain rate produces nearly the maximum amount of discontinuities for a given strain and without the complications of grain boundary migration found at strain rates less than 0.7 pct/h.

In the preparation of creep test pieces, the following procedure would be adopted. Straining would be carried out at a rate of 1 pct/h for a pre-determined time so as to produce the required strain. Reference to Figure 3.3 would determine the density decrease for that strain and, therefore, the total volume of intergranular discontinuities in the specimen. Test pieces would be strained by less than 15 pct to avoid the complications of necking and this would also permit the assumption of a uniform distribution of discontinuities throughout the gauge length. Then, by measuring the cross-sectional area after the preparation, it should be possible to estimate the loss in material cross-section due to cracks. The prepared specimens would be strained by different amounts so as to produce different sizes and shapes of intergranular discontinuities.

3.4 Annealing Experiments

3.4.1 Introduction

In section 3.3.2 it was noted that the volume of intergranular discontinuities in commercially pure aluminium, when tested under constant strain rate conditions at a temperature of 500 deg.C., depended on strain rate in an unexpected way. The annealing experiments, reported in this section, were designed to show that the unexpectedly small amount of intergranular cracking observed at low strain rates could be due to the tendency of cavities to sinter at low stresses – by grain boundary migration or otherwise. Specimens containing small amounts of grain boundary cavities were annealed at a temperature of 500 deg.C. and by studying the variation of density with annealing time, it was expected that useful information on the above problem would be provided. Previous research on a variety of cavitated materials has shown that annealing under conditions of zero stress causes sintering of cavities in a manner consistent with grain boundary diffusion, eg. Gittins and Williams (1969), Alexander and Balluffi (1957), Evans and Walker (1970) and Beeré and Greenwood (1971). Although a reduction of the total volume of the discontinuities was expected in aluminium by annealing, the variation of this reduction with time was important in determining the effects of sintering.

3.4.2 Procedure

The specimens used in the experiments were the gauge lengths of test pieces strained at a temperature of 500 deg.C. to produce a small amount of intergranular discontinuities. The specimens were annealed in a muffle-type electric furnace at a temperature of 500 deg.C. Temperature control was estimated to be better than $\pm$ 5 deg.C. The specimens were removed from the furnace at regular intervals, air cooled and then had their absolute densities measured as described previously. Density decrease from the

standard value of 2.6978 g/cc was again measured to ± 0.0004 g/cc or ± 0.015 pct.

3.4.3 Results — Density Changes

Figures 3.5 and 3.6 show the variation of density decrease and, therefore, volume of intergranular discontinuities with annealing time, for five specimens having different initial amounts of intergranular discontinuities. Curves 46 and 67 are of specimens derived from test pieces strained at 100 pct/h and 10 pct/h, respectively. Curves 64, 65 and 62 are of specimens derived from test pieces strained at 1 pct/h. An idea of the type and extent of intergranular discontinuities in specimens 64 and 65, before annealing took place, is given by Figures 2.8 and 4.5, respectively. Specimens 46 and 67 would have proportionally more triple point cracks to grain boundary cavities than specimens 64, 65 and 62, since 46 and 67 were strained at higher strain rates.

The curves in Figures 3.5 and 3.6 show that the total volume of intergranular discontinuites continuously decreases with annealing time. The rate of decrease or sintering, rapid at first, also decreases with annealing time. The initial rate of sintering increases with decreasing initial volume of intergranular cracking. In specimen 64 complete sintering of cavities was achieved after 160 hours at 500 deg.C. In specimen 46 the annihilation took longer — 1000 hours. Complete sintering in specimens 67, 65 and 62 was not achieved within the annealing time available. However, extrapolation of curves 65 and 67 suggests that complete sintering would take place in these specimens after 2000 — 3000 hours.

3.4.4 Results — Metallography

Three of the specimens, 64, 65 and 62, were sectioned, polished and etched after completion of the

annealing tests. In the section of specimen 64, no cavities were observed and extensive grain growth was found to have occurred. Since the specimen had been annealed for a further 450 hours after complete sintering of the grain boundary cavities, a grain size of 2 – 3 grains across the 0.357 in. diameter of the specimen had been produced. The same type of grain growth has already been noted after annealing the 'as received' material for over 200 hours (section 3.3.1). As with the annealed 'as received' sample, specimen 64 also reached a maximum density of 0.06 pct greater than that of the 'as received' material.

Sections of specimens 62 and 65 after annealing are shown in Figures 3.7 and 3.8, respectively. Comparison of Figure 3.8 with what specimen 65 would have looked like before annealing, ie. Figure 4.5, shows that, as well as greatly reducing the number of intergranular cracks, the sintering process has blunted the sharp outlines of the cracks. A similar conclusion is reached for the effects of sintering on specimen 62, as shown in Figure 3.7. In both specimens, grain growth has occurred. However, the remaining cracks have had a restraining effect on the grain boundaries, thus preventing the formation of the very large grain size observed in specimen 64.

3.4.5 Discussion

Comparison of the density decrease/time curves with the results of Gittins and Williams (1969) on high purity copper, Evans and Walker (1970) on stainless steel, and Beeré and Greenwood (1971) on magnesium and tough-pitch copper, demonstrates that the behaviour of commercially pure aluminium, containing grain boundary discontinuities, is similar to that of the above materials when it is annealed at 500 deg.C. Initially, the rate of sintering is large but soon diminishes to an almost constant value. In specimen 64 the cavities completely sintered out before a constant ~~rate~~ density was achieved. Evans and Walker concluded that gas stabilisation was responsible for the decreasing sintering rate in

stainless steel. In magnesium and tough-pitch copper, Beere and Greenwood suggest that it is caused by the closure of small cavities, resulting in a rapid decrease in the total number of cavities remaining. The latter explanation seems to fit the results on Aluminium better. In specimens 46 and 64, the cavities completely sintered and gas stabilisation, presumably, would not have allowed that to happen. In specimens 62 and 65, as shown by Figures 3.7 and 3.8, there have been reductions in the number of cracks in both specimens.

The explanation that the decreasing rate of sintering with time is caused by the sintering out completely of small cavities, also provides an explanation of the observation that the initial rate of sintering increases with decreasing initial volume of cracking. With increase of total volume of intergranular cracking, the proportion of small cavities to large cavities decreases, since not only have the small cavities grown, but many of them have coalesced to form large cracks (see Figures 2.8 and 4.5). Hence, the variation of sintering rate with time in specimen 62 was small, since the specimen contained many large cracks and only a few small cavities, before annealing commenced.

The results of the annealing tests have shown that intergranular cracks may be reduced in volume by the sintering process. Since the results compare favourably with those of other workers, it can be inferred that the sintering process in commercially pure aluminium at 500 deg.C. is similar to that found in the compared materials, ie. one of grain boundary diffusion. The sintering process was accompanied by extensive grain growth which the cavities and cracks tended to restrain. Thus, it can be expected that grain boundary migration will try to eliminate cavities in order to promote grain growth. Therefore, in tensile tests at slow strain rates, the sintering process, aided by grain boundary migration, may be capable of reducing the rate of intergranular crack growth. Hence, the unexpectedly small amounts of intergranular discontinuities found in the

material at strain rates less than 0.7 pct/h appear to be caused by the above effects. Later, a similar effect will be described in constant load uniaxial creep tests at a temperature of 500 deg.C. and low values of stress.

3.4.6 Conclusions

Annealing experiments on specimens of commercially pure aluminium, with different amounts of intergranular discontinuities, produced sintering curves similar to the results of previous workers. The volume of intergranular cracking and the rate of sintering both decreased continuously with time. The variation in the rate of sintering also depended on the proportion of large to small cavities or cracks in the material. Specimens with small initial volumes of cracks and, therefore, a large proportion of small cavities, showed a large variation of sintering rate. Extensive grain growth accompanied the sintering of cracks. In specimens, where the cavities sintered completely, the grain growth was unrestricted, but in other specimens, the remaining cracks restrained grain growth. It was concluded that the sintering process, aided by grain boundary migration, was capable of producing the unexpectedly small amounts of intergranular cracking in commercially pure aluminium, when strained at a temperature of 500 deg.C. and strain rates less than 0.7 pct/h.

3.5 Summary and Conclusions

The density decrease in strained test pieces of commercially pure aluminium due to intergranular discontinuities has been measured by a hydrostatic weighing technique with an accuracy of $\pm$ 0.015 pct. Using this technique, the variation of the amount of intergranular discontinuities in the strained material with strain, strain rate and temperature was observed. At a temperature of 250 deg.C., density changes detected the presence of only a small amount of discontinuities. At the higher temperature of 500 deg.C., the growth of intergranular discontinuities was extensive, confirming the observations of metallography. Density decrease and, therefore, total crack volume/unit weight were found to increase with increasing strain (and time) for each of the four strain rates considered (0.1, 1, 10 and 100 pct/h). Nucleation and growth of discontinuities appeared to start with the deformation process and growth was such that, for most of the density decrease/strain curve, a linear relationship was observed.

Density measurements showed that a maximum amount of intergranular cracking occurred in commercially pure aluminium when strained at a rate of 0.7 pct/h and a temperature of 500 deg.C. The unexpectedly small amounts of cracking, observed at strain rates less than 0.7 pct/h, were shown, by annealing experiments on cavitated material, to be caused by sintering of cavities at low stresses, aided by grain boundary migration. The sintering/time curves obtained were in agreement with the results of previous workers and it may be concluded, therefore, that the process of sintering in commercially pure aluminium was one of grain boundary diffusion.

A strain rate of 1 pct/h at a temperature of 500 deg.C. was chosen for the preparation of creep test pieces with controlled amounts of intergranular discontinuities. The next stage in the project was to determine the creep

properties of the 'as received' material, to obtain suitable stresses for showing the effects of intergranular discontinuities under different conditions of stress and temperature. Before describing those tests, the effect of environment on intergranular cracking will be discussed. Also, the use of Rate Sensitivity calculations in predicting creep behaviour will also be discussed.

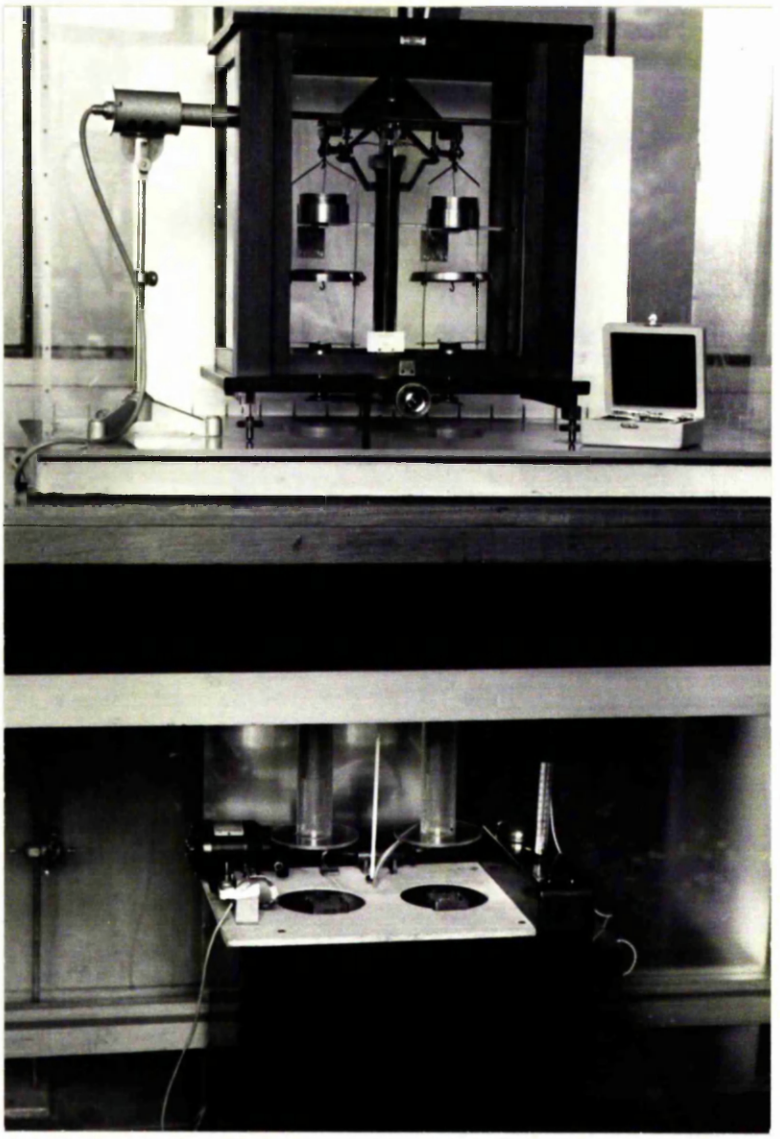

Figure 3.1 The Hydrostatic Density Balance

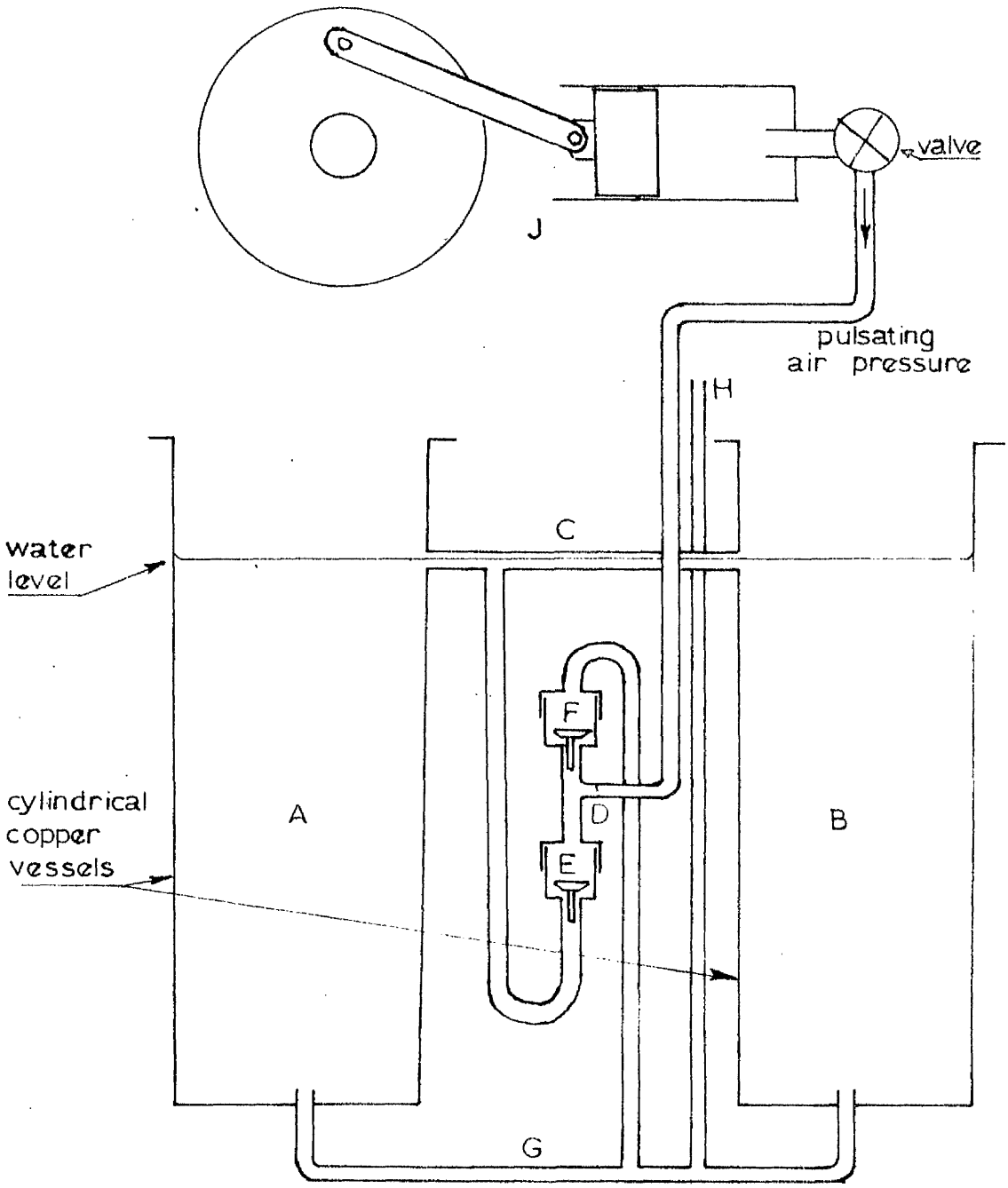

Figure 3.2 Inner Vessel of Hydrostatic Density Balance showing stirring system

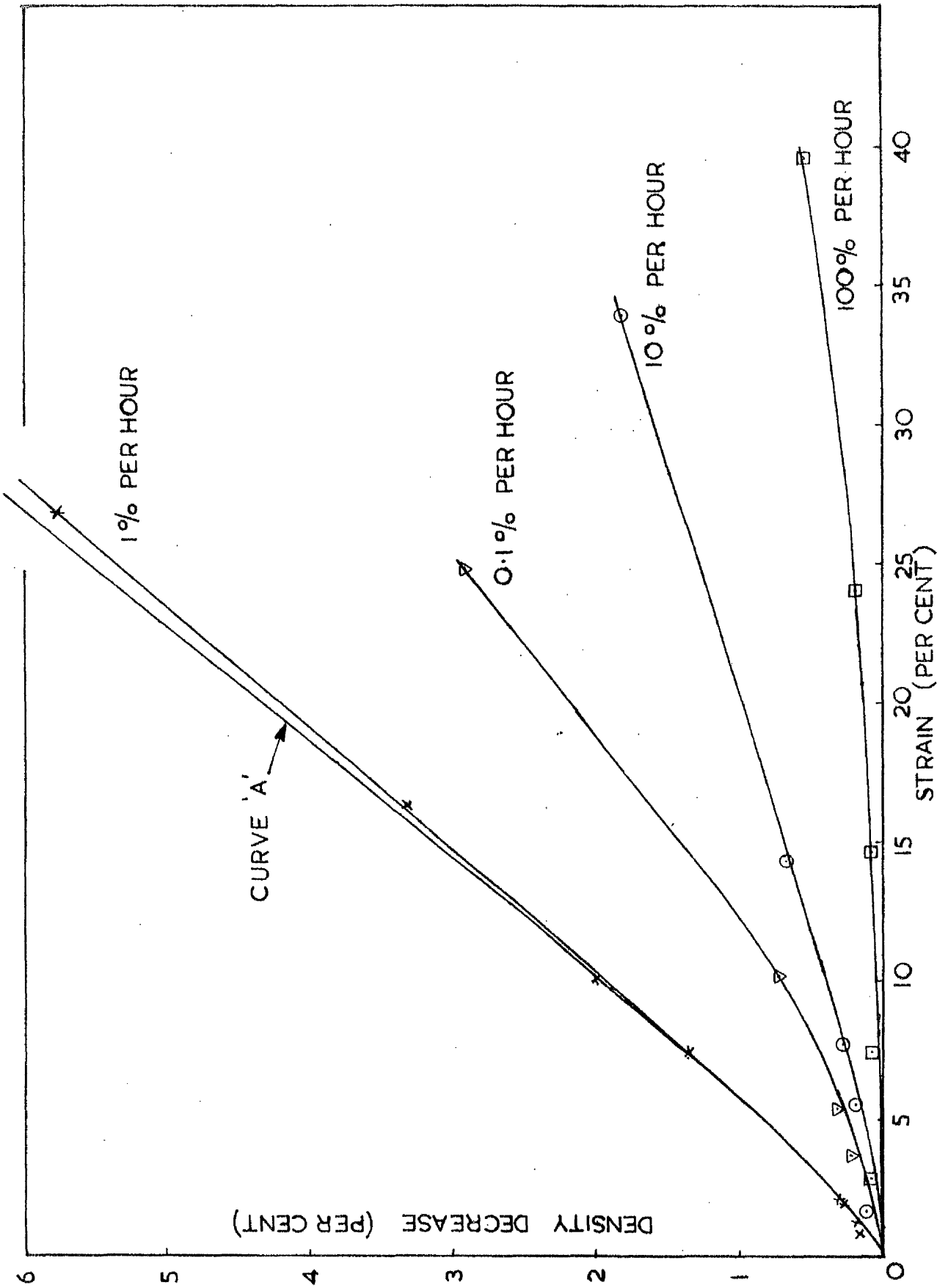

Figure 3.3 500 deg.C.; constant strain rate tensile tests; fractional density decrease against strain

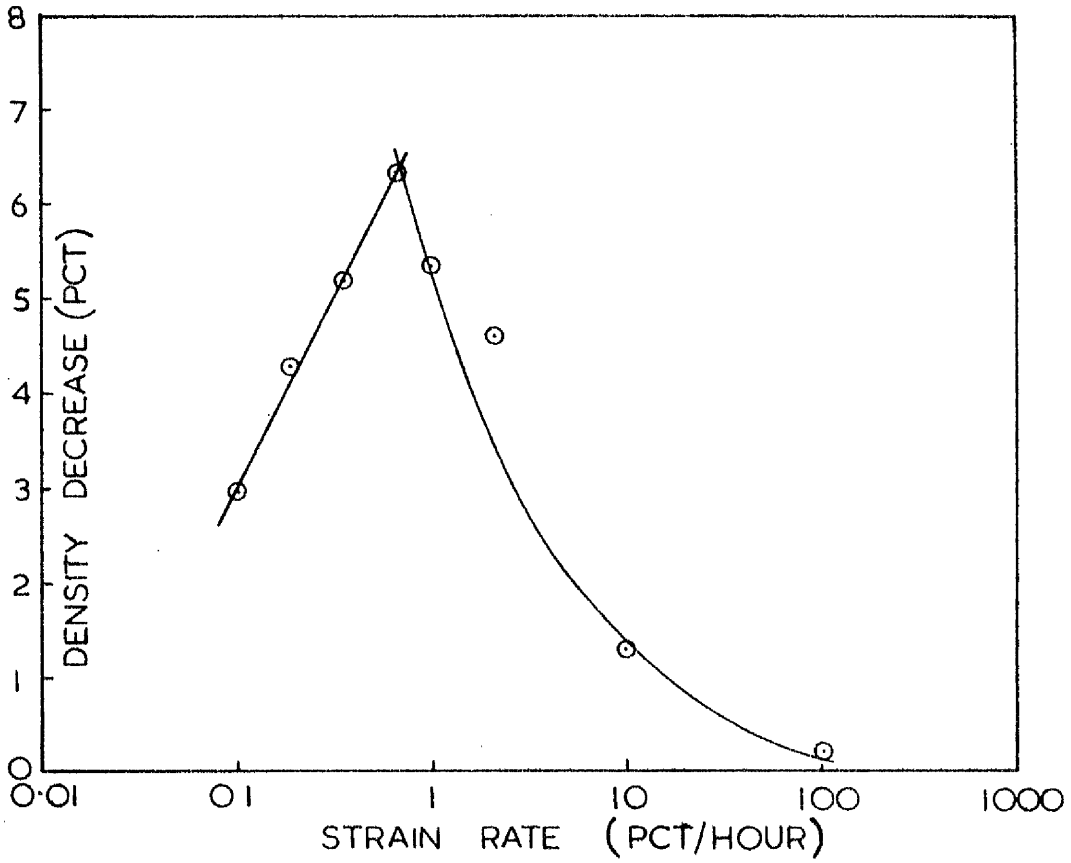

Figure 3.4 500 deg.C.; constant strain rate tensile tests; fractional density decrease against $\log_{10}$ (strain rate) at 25 pct strain

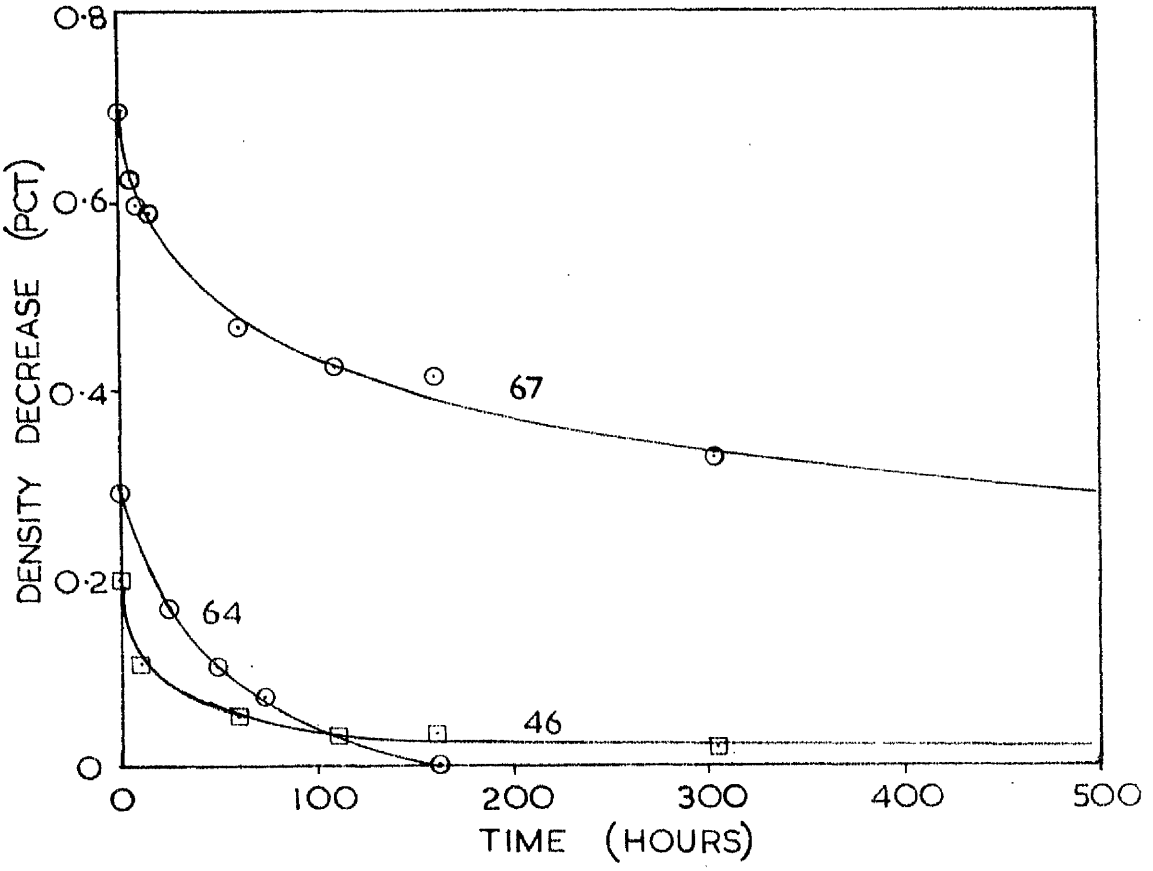

Figure 3.5 Annealing/Sintering Experiments at 500 deg.C.; fractional density decrease from 2.6978 g/cc against annealing time

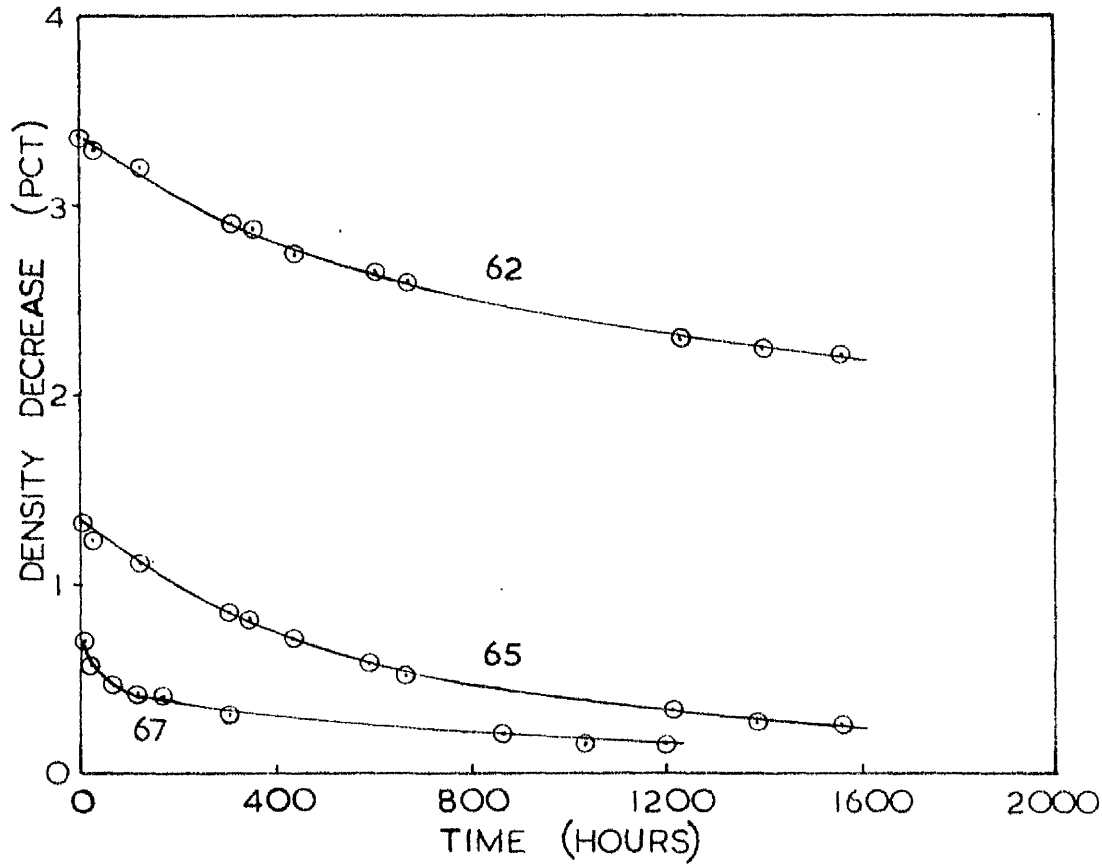

Figure 3.6 Annealing/Sintering Experiments at 500 deg.C.; fractional density decrease from 2.6978 g/cc against annealing time

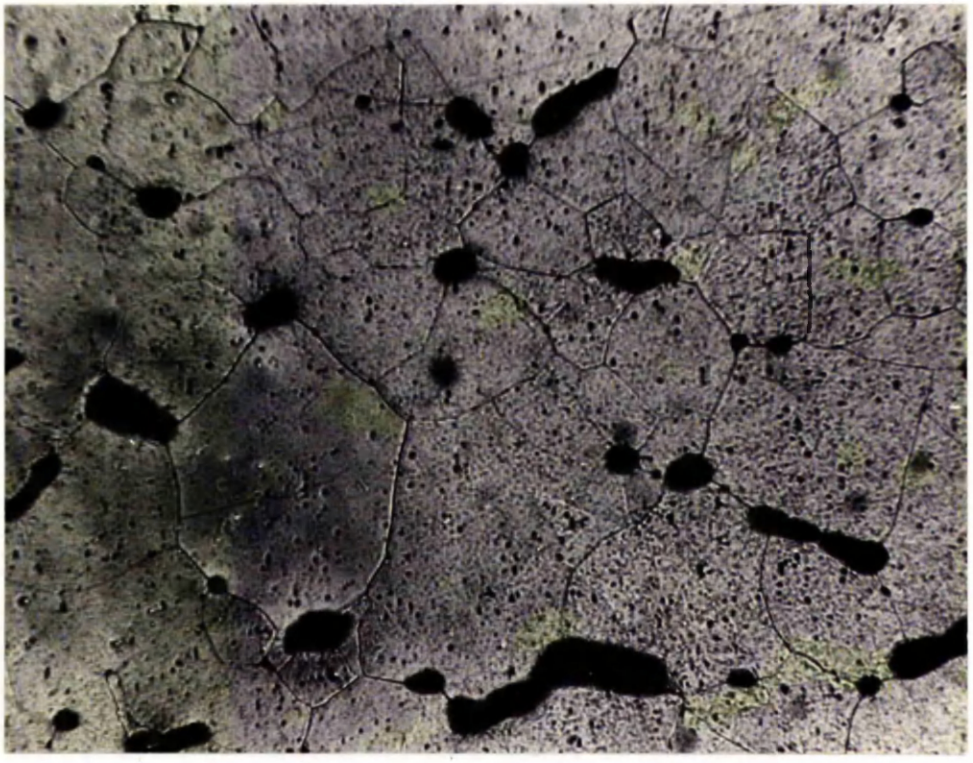

Figure 3.7 Specimen 62 after annealing for 1570 hours at 500 deg.C. Original stress axis vertical. Magn. 125X.

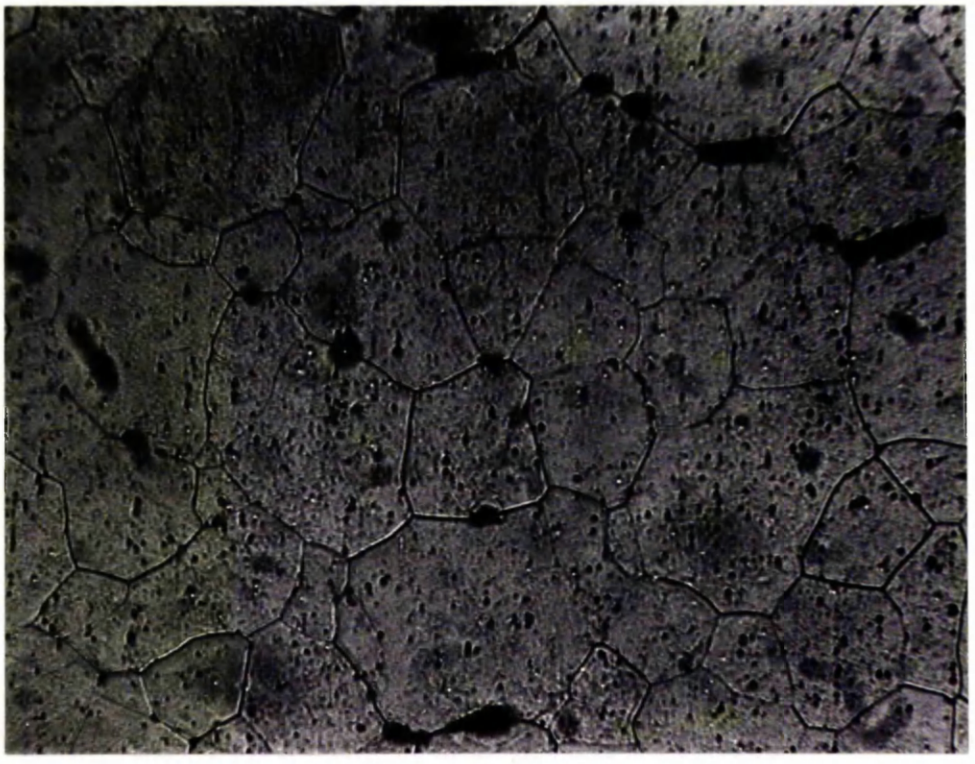

Figure 3.8 Specimen 65 after annealing for 1500 hours at 500 deg.C. Original stress axis vertical. Magn. 125X.

CHAPTER IV

EFFECT OF ENVIRONMENT

4.1 Introduction

Engineers and designers have always to consider carefully the effect that environment may have on the material chosen for a component. Corrosion due to oxidation is a problem in metals and alloys subjected to high temperatures. When the component is also subjected to stress, the effect that oxidation may have on intercrystalline failure is also important. Intergranular fracture is influenced by the diffusion of oxygen along the grain boundaries as well as the segregation of impurity and parent metal oxides at the boundaries. Hence, the effect that environment has on intercrystalline failure appears to be due to the control it exerts over grain boundary structure, sliding and migration (Garofalo, 1965 p. 232).

The effect that environmental oxygen has on intercrystalline failure varies with the metal or alloy considered. The nucleation and growth of cavities in copper is greatly influenced by small traces of oxygen in the test atmosphere. Thus, oxygen free high conductivity (OFHC) copper shows increasing elongation to fracture as the temperature increases from 350 to 750 deg.C., when strained in high vacuum (5×10^{-4} mm. Hg.), (Chen and Machlin, 1960). In a slightly lower vacuum ($10^{-2} - 10^{-3}$ mm. Hg.), OFHC copper showed decreasing elongation to fracture as the temperature similarly increased (Greenwood et al. 1954). Chen and Machlin attribute the latter behaviour to the large effect of the small partial pressure of oxygen on grain boundary

migration, slowing the rate of migration sufficiently to allow intergranular cavities to nucleate and grow. Bleakney (1952) and Boettner and Robertson (1961) also found that small amounts of oxygen had a large effect on the inter-crystalline failure of copper.

In a more practical high temperature material, 18/8 0.8 pct niobium stabilised stainless steel, Scaife and James (1968) illustrated the effect of environmental oxygen on the extent of intergranular cavitation. Specimens tested in air were more prone to cavitation than those tested in vacuum under the same conditions of temperature and load. They attributed the greater amount of cavitation in air specimens to the decrease in activation energy for grain boundary sliding brought about by gaseous diffusion. Hence, nucleation and growth of cavities by sliding became easier.

In contrast to copper, aluminium of high purity appears to be insensitive to the presence of oxygen in the test atmosphere. High purity aluminium (99.99+ pct) does not exhibit intercrystalline cracking and always fails in a ductile fashion. This occurs in both air (Servi and Grant, 1951a) and in vacuum (Bleakney, 1952). This absence of intercrystalline cracking in high purity aluminium is attributed to the ease of grain boundary migration. Stress concentrations due to boundary sliding are relieved by migration before cavities or triple point cracks can nucleate. Traces of residual oxygen and the presence of oxygen in the test atmosphere do not seem to affect the rate of migration. However, high purity aluminium with 0.7 wt. pct of oxide deliberately added, exhibited intercrystalline cracking when strained in air at a temperature of 450 deg.C. (Beghi, Geel and Piatti, 1970). Oxide particles in the grain boundaries slowed the rate of migration and hence allowed triple point wedges and cavities to nucleate and grow. The presence of particles in the boundaries may also have provided additional nucleation sites. Hence, oxygen in the form of aluminium oxide, can hinder grain boundary migration and can favour intercrystalline cracking in aluminium, if present in the

form of large particles. In high purity Aluminium, without oxide particles, either oxygen does not proceed further than the thin layer of stable surface oxide or, if it does, it is in a form which does not hinder boundary migration or favour intercrystalline cracking.

Traces of impurity elements, as well as oxygen in the form of Aluminium Oxide, are sufficient to transform the ductile behaviour of aluminium, at creep stresses and temperatures, to one of intercrystalline failure (Servi and Grant, 1951a, Wilms, 1954). As before, the impurity particles hinder grain boundary migration thus allowing the nucleation and growth of triple point wedge cracks and grain boundary cavities. Although it has been shown that atmosphere has no effect on the creep behaviour of high purity aluminium (Bleakney, 1952), it does not necessarily follow that it should have no effect on the creep behaviour of commercially pure aluminium. The latter is a highly complex alloy due to the presence of impurities and, under high temperature creep conditions, develops intergranular discontinuities. The question arises as to the method by which environmental oxygen might influence the extent of intergranular cavitation in commercially pure aluminium. However, it is firstly necessary to demonstrate that atmosphere does have an effect on the extent of intergranular cavitation.

If environmental oxygen does influence intergranular cavitation in commercially pure aluminium, then a simple way to demonstrate such an effect would be to test samples of the material in air and in an inert atmosphere under creep conditions. Comparison of the extent of intercrystalline cracking in corresponding test pieces would resolve the speculation. The variation of density change (and hence total crack volume) with strain and strain rate for tensile tests in air at a temperature of 500 deg.C. has already been described. After suitable modifications, it was possible to use the tensile testing equipment for constant strain rate

testing in a gaseous environment other than air. Hence, a series of tests in argon were planned at corresponding strain rates to those performed in air. As with the air specimens, the extent of intercrystalline cracking would be measured by means of the change in density and by metallography.

4.2 Tensile Testing in Argon

The equipment used for constant strain rate testing in air has already been described. For tensile straining in argon the test piece and grips were enclosed in a cylindrical chamber as shown in Figure 4.1. The chamber was a stainless steel tube fitted with water cooled brass end caps. The water cooling was necessary to preserve the rubber 'O' rings used as seals between pull rods and holes in the brass end caps, and the rubber gasket between brass cap and stainless steel tube. Without a test piece in position, a force of approximately 0.5 lbf. (2.31 N) was necessary to move the pull rod through the 'O' ring. In tests at the slowest strain rate (0.1 pct/h), this meant that maximum load was underestimated by 5 pct. At the higher strain rates of 1, 10 and 100 pct/h, maximum loads were underestimated by 1.5 pct, 1 pct and 0.7 pct, respectively. These errors were allowed for in the subsequent calculations of stress.

The position of the sensing element of the temperature controller had to be moved from inside the furnace tube to outside the winding. This was necessary to accommodate the argon chamber. Temperature control was not noticeably affected. Thermocouple wires passed through rubber plugs in one of the end caps. The assembly of test piece and thermocouples was the same as in air tests.

After assembly of the test piece, high purity argon gas (less than 5 P.P.M. impurity) was introduced to the chamber through an opening at one end and was exhausted into water via an outlet at the other end. The flow rate was adjusted to give an argon pressure in the chamber slightly in excess of atmospheric. Two hours were allowed before heating was started. As a further precaution, tantalum sheet was placed on the floor of the chamber as an oxygen 'getter'. After straining was completed, the argon flow was continued during cooling to prevent oxidation of the test piece.

Tensile tests were performed in argon at a temperature of 500 deg. C. and strain rates of 0.1, 1, 10 and 100 pct/h to strains comparable with those of specimens tested in air. Gauge lengths of strained test pieces had their densities measured in the hydrostatic density balance. Hence, the density change from that of the unstrained material provided a measurement of total void volume in the gauge length.

4.3 Comparison of Behaviour in Air and Argon

Only a limited number of tests were carried out in argon but the few that were show clearly a difference in behaviour from that in air. Figure 4.2 depicts the variation of density change with strain as continuous curves for air tests and individual points for argon tests. At each of the four strain rates, the total volume of intergranular discontinuities was less in argon than in air for the same strain. The difference was greater the slower the strain rate. As a check, a test piece was strained at 1 pct/h and 500 deg.C. to 17.3 pct strain using the argon chamber, but with the gas inlet and outlet ports open to the air. The gauge length of this test piece had a density decrease of 4.62 pct, a result which lies above the 1 pct/h air curve. The conclusion was that the difference in behaviour between air and argon was real.

The load/extension curves for air and argon test pieces were similar in shape with the values of the maximum tensile stress in argon falling within the range of values of those tested in air. However, the rate of decrease of load after the maximum was slower in argon than in air.

At the slowest strain rate (0.1 pct/h) the two argon test pieces showed negligible change in density. On sectioning, polishing and etching one of the specimens, the negligible change was confirmed by the absence of internal discontinuities. Figures 4.3 and 4.4 are micrographs of an air specimen and an argon specimen, respectively, strained at 0.1 pct/h to similar strains. Intercrystalline cracking is absent in the argon specimen but occurs extensively in the air specimen. However, the argon specimen did have a small number of large, isolated grain-boundary holes. The density change due to these holes had been too small for the density balance to record. Comparison of Figures 4.3 and 4.4 with micrographs of the 'as received' and heat treated materials (Figures 2.4 – 2.7) shows that grain growth has

taken place in both air and argon specimens. However, the proportion of large to small grains seems to be greater in the argon specimen.

Figures 4.5 and 4.6 illustrate the extent of intercrystalline cracking in an air and an argon specimen, respectively, strained by similar amounts at 1 pct/h. Again, the extent of intercrystalline cracking was less in the argon specimen. In the air specimen, the cavities have coalesced to form 'wavy' cracks, while in the argon specimen most of the cavities and triple point cracks can be identified individually. As with the slower strain rate, some grain growth has taken place in both specimens, but the resulting grain structures are similar.

Similar, though less obvious, differences were noted in micrographs of specimens strained at 10 and 100 pct/h. Both in air and in argon, at these two strain rates, the predominant fracture mechanism was that of triple point cracking. At 1 pct/h, as shown by Figure 4.6, grain boundary cavities as well as triple point cracks were observed. Figure 4.7 shows a selection of triple point cracks in an argon specimen strained at 10 pct/h and Figure 4.7 shows a triple point crack in an argon specimen strained at 100 pct/h. The etch has tended to round off the sharp points of the cracks and, in addition, has probably enlarged them.

4.4 Discussion

The results of tensile tests in air and in argon have shown that the presence of oxygen in the test atmosphere accelerates the intergranular fracture process. At a stage in the deformation of an argon test piece, when the triple point wedges and grain boundary cavities were individually identifiable, the wedges and cavities in a corresponding air specimen had coalesced to form 'wavy' cracks, stretching along two or three grain boundaries. Also, the influence of oxygen on the extent of intercrystalline cracking increased as the applied strain rate decreased. Although these results have shown that oxygen in the test atmosphere increases the extent of intergranular cracking, they have not indicated the method by which this influence was exerted. Evidence of grain boundary migration in both air and argon test pieces was obtained by metallography. Comparison of Figures 4.3 and 4.4 showed that grain growth in argon was greater than in air. Hence, it appears that the restraint of oxygen on grain boundary migration was responsible for the larger amount of intercrystalline cracking in the specimens strained in air. A possible means by which oxygen could be absorbed by the aluminium creep specimen might be via the intergranular discontinuities themselves. The discontinuities might form continuous paths along grain boundaries for the absorption of oxygen.

Since test atmosphere has been shown to influence the extent of intercrystalline cracking in commercially pure aluminium, one would expect to find more cracks close to the surface of an air specimen than in the centre of that specimen. Metallographic examination of air specimens, at all strain rates, showed the distribution of cracks to be uniform across the diameter of each specimen. This observation is surprising in view of the evidence of other research workers who have observed a surface effect. Boettner and Robertson (1961) observed one in copper and Scaife and James (1968) one in stainless steel. Nemy and Rhines (1959)

observed an increase in cavitation close to the surface of an Aluminium – 2.6 pct Magnesium alloy test piece stopped early in the tertiary stage of the creep curve. At the same temperature (400 deg.C.), but a lower stress, the fissures occurred uniformly throughout the entire cross-section. Hence, a surface effect may not always be observed.

It was noted in section 4.3 that, although the maximum tensile strengths of the test material in air and argon were similar, the rate of decrease of load after the maximum was less in argon than in air. A possible explanation of this behaviour is that cavity formation and growth before the maximum was so small that it did not affect the strength of the material. After the maximum, however, the slower development of intergranular discontinuities in the argon test piece showed up as an increase in strength over the air test piece for corresponding strains.

Scaife and James (1968) found that stainless steel tested under creep conditions exhibited lower minimum creep rates and longer secondary creep periods in vacuum than in air. They attributed this observation to the greater amount of intercrystalline cracking found in air specimens. Their results, along with the present work on Aluminium, suggest that enhanced creep resistance may be obtained in some cavitation prone materials by coating their surfaces to prevent absorption of oxygen, either as oxide or gas.

4.5 Conclusions

The presence of oxygen in the test atmosphere accelerates the intergranular fracture process in commercially pure aluminium at creep stresses and temperatures. The effect was thought to be caused by the influence of oxygen on the rate of grain boundary migration in the metal. The absence of a surface effect, expected in cases where environment has an influence, was noted. It was pointed out that, although the influence of oxygen on intercrystalline cracking in commercially pure aluminium was established by the tensile tests, no indication of the method by which the oxygen was absorbed was obtained.

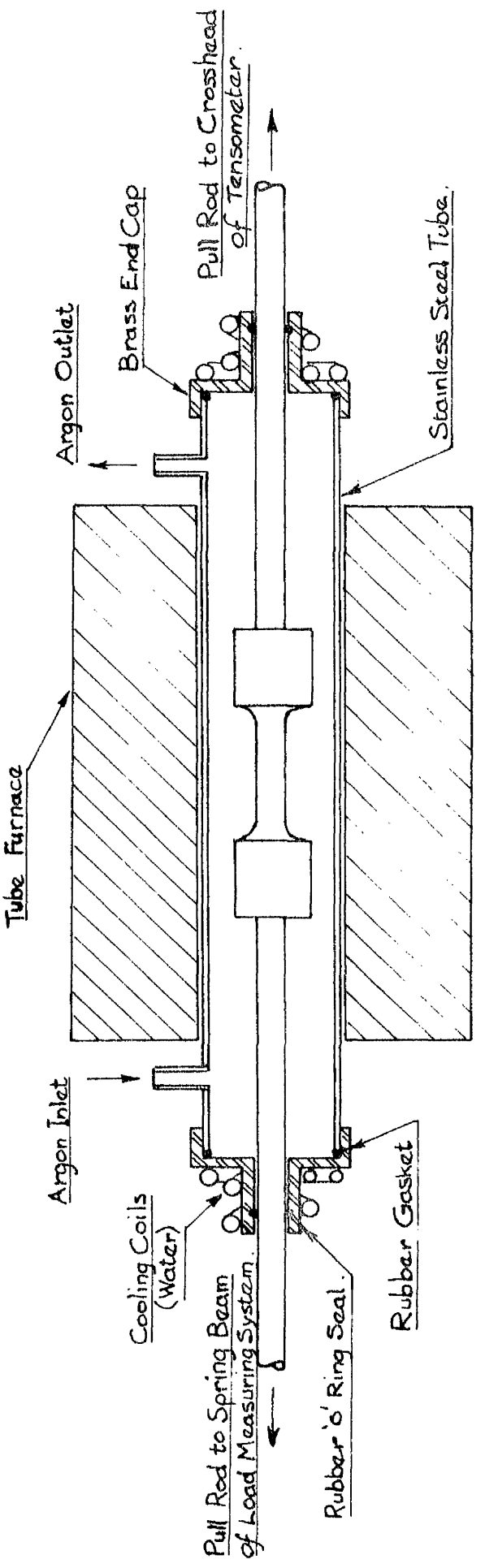

Figure 4.1 System for Tensile Testing in an Argon Atmosphere at High Temperature

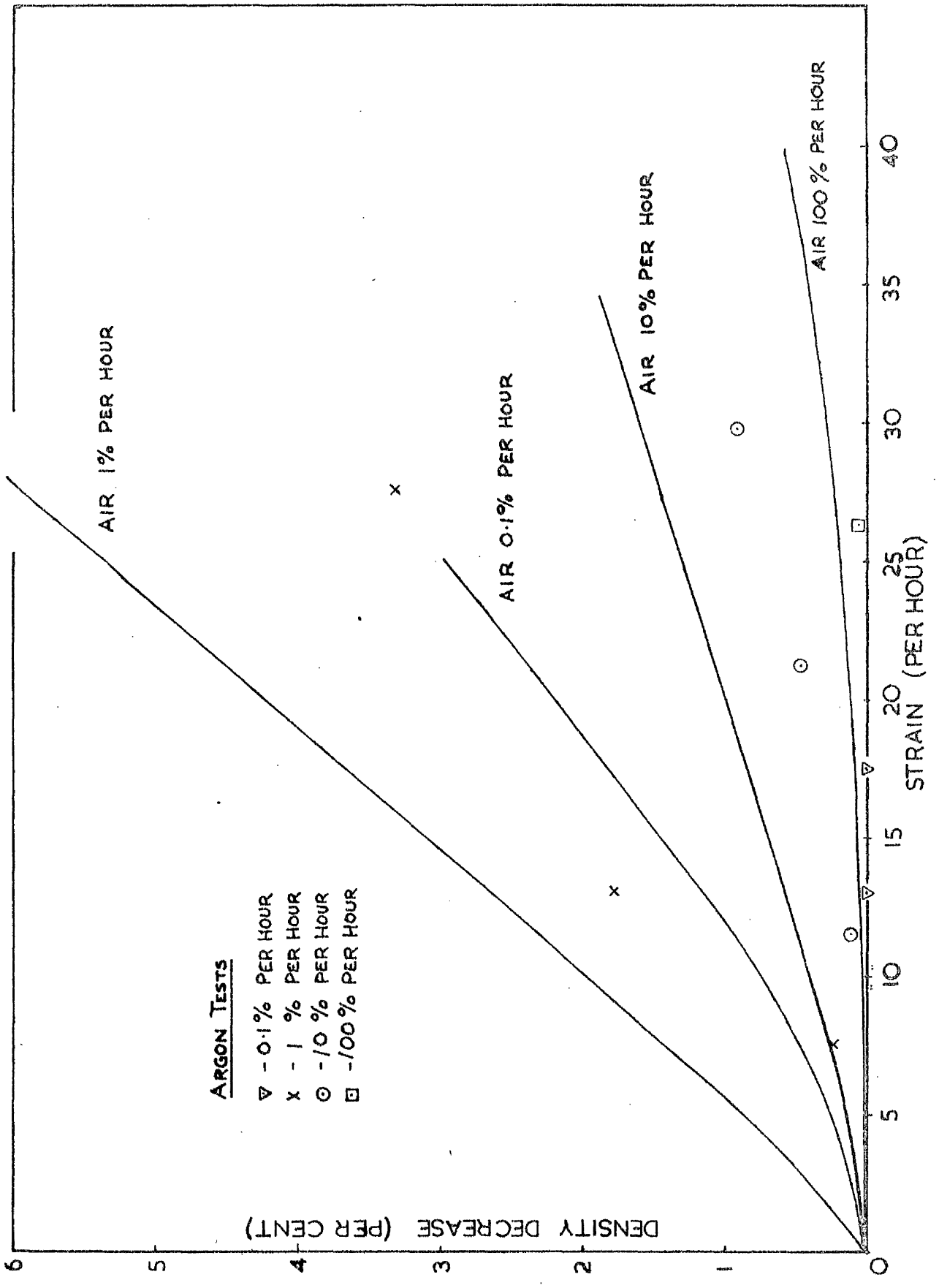

Figure 4.2 500 deg.C.; constant strain rate tensile tests; comparison of density decreases in argon and in air with respect to strain

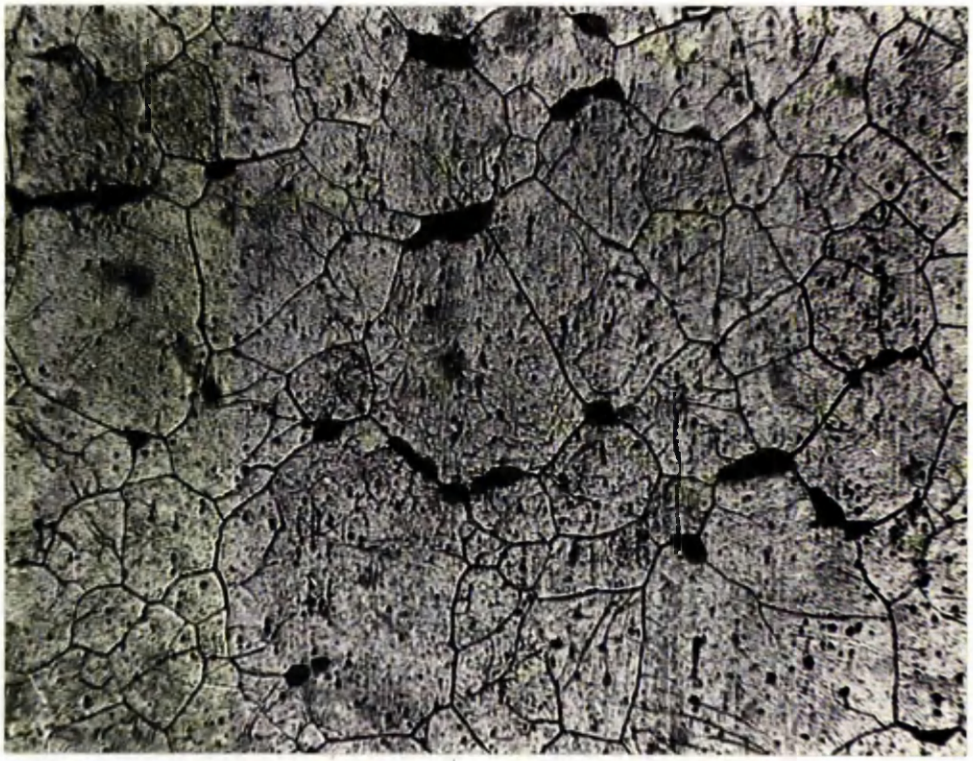

Figure 4.3 Air, 500 deg.C., 0.1 pct/h to 10 pct strain and 0.712 pct density decrease. Stress axis vertical. Magn. 125X.

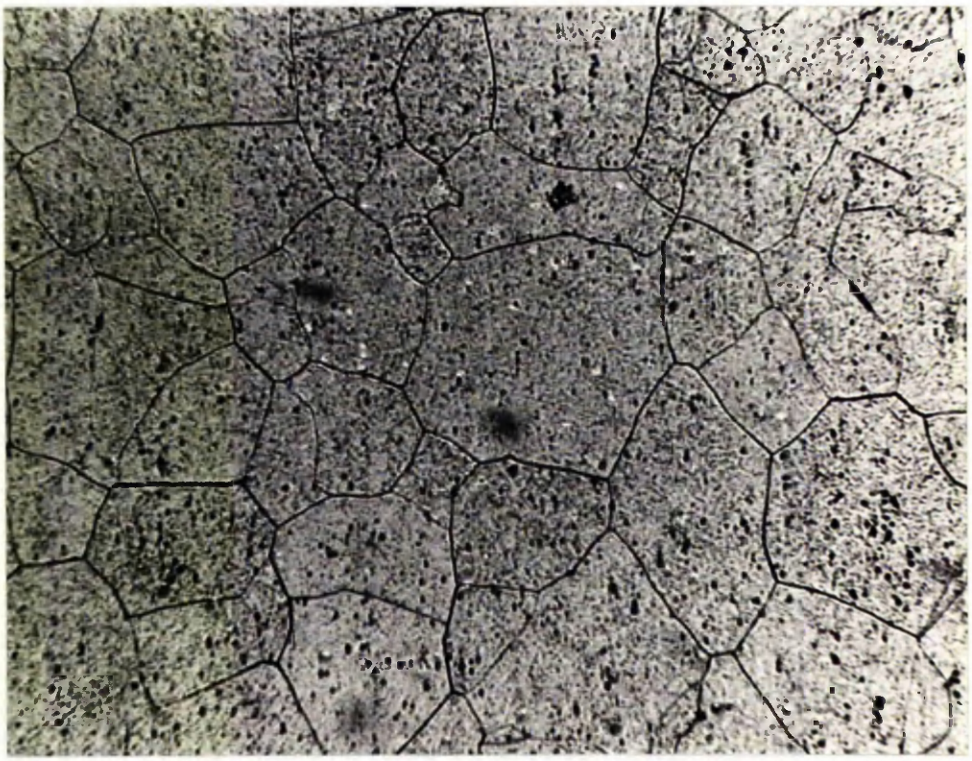

Figure 4.4 Argon, 500 deg.C., 0.1 pct/h to 13.1 pct strain, zero density change. Stress axis vertical. Magn. 125X.

Figure 4.5 Air, 500 deg.C., 1 pct/h to 9.9 pct strain and 1.995 pct density decrease. Stress axis vertical. Magn. 125X.

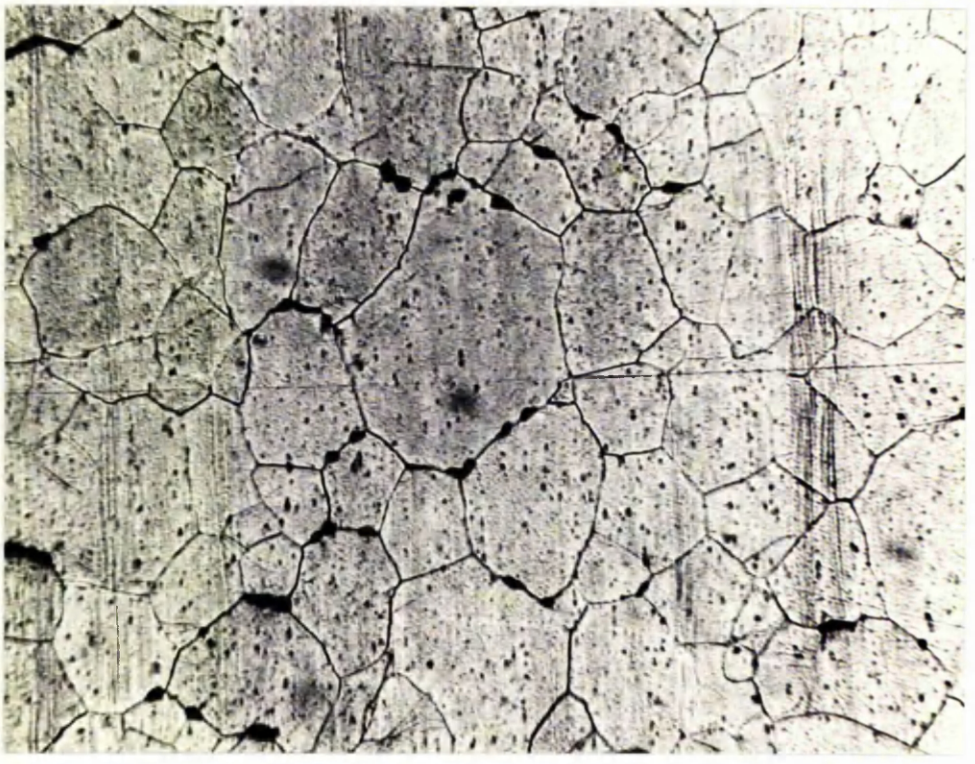

Figure 4.6 Argon, 500 deg.C., 1 pct/h to 7.6 pct strain and 0.263 pct density decrease. Stress axis vertical. Magn. 125X.

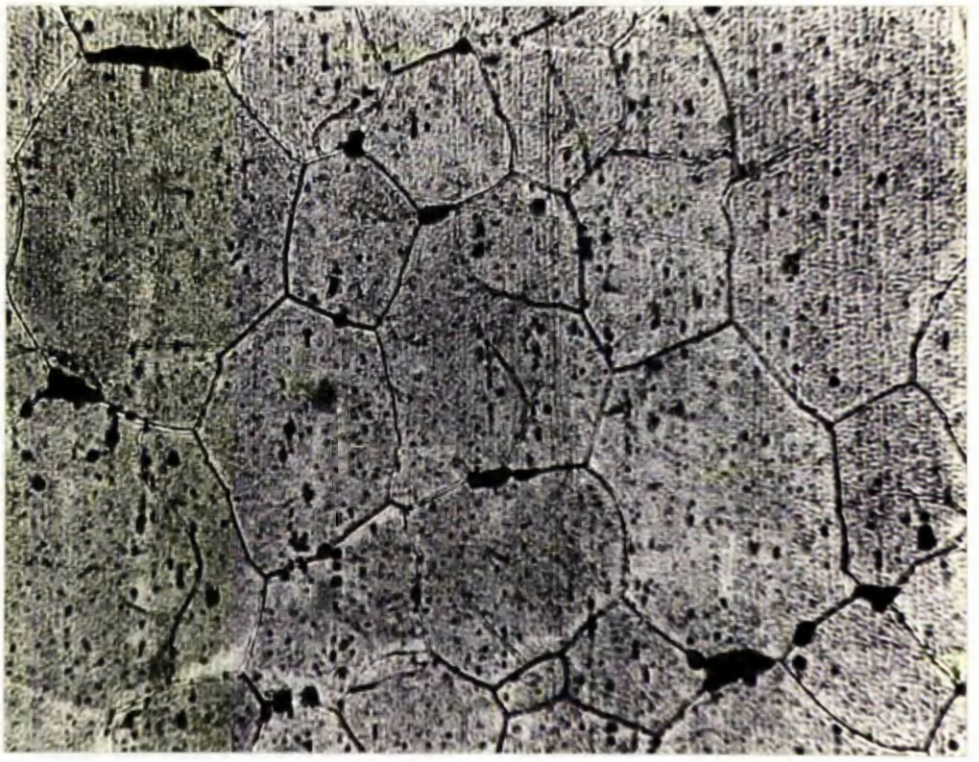

Figure 4.7 Argon, 500 deg.C., 10 pct/h to 11.6 pct strain and 0.134 pct density decrease. Stress axis vertical. Magn. 250X.

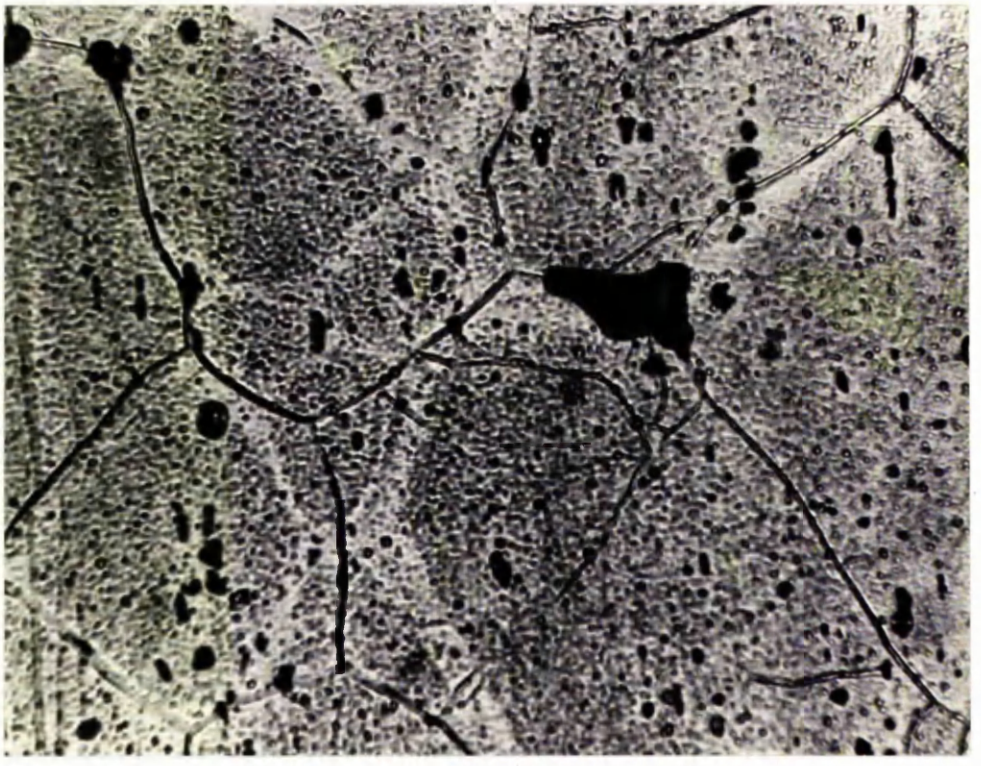

Figure 4.8 Argon, 500 deg.C., 100 pct/h to 26.3 pct strain and 0.067 pct density decrease. Stress axis vertical. Magn. 630X.

CHAPTER V

RATE SENSITIVITY : PART I

5.1 Introduction

After the Tensile Testing programme was sufficiently well advanced to show that the method could produce samples of commercially pure aluminium with intergranular discontinuities, the programme of uniaxial creep testing was started. Before commencing with the designing and building of the testing equipment, it was essential to obtain some idea of the range of stresses to be employed. The values of the maximum stresses, observed in the constant strain rate tensile tests on the material, were taken as giving suitable guidance in that respect. It was further expected that the tensile data might be of some use in predicting creep rates in the planned tests. Weertman (1956) showed this to be possible for high purity aluminium (99.996 pct) at temperatures from 150 deg.C. to 550 deg.C. In constant strain rate tensile tests, he observed the following relationship between the maximum stress, strain rate and temperature:-

$$\text{strain rate} = A/T\ (\text{stress})^{4.4} \exp(-Q/RT) \qquad (5.1)$$

where A is a constant, R is the gas constant, T is the absolute temperature, and Q is the activation energy. He further observed that the steady-state creep rates from the constant stress creep tests of Servi and Grant (1951a), also on high purity aluminium, satisfied the above equation. Hence, in this case, at least, minimum creep rates were predictable from constant strain rate tensile data. In the present tests on commercially pure aluminium, the strain rates (0.1 - 100 pct/h) and the temperatures (250 deg.C. and 500 deg.C.) were

of the same order as those employed in the tests of Weertman. It was expected, therefore, that by using the values of maximum stress measured in constant strain rate tensile tests as the applied creep stresses, the resulting minimum creep rates would be similar to the strain rates employed in the tensile tests. Since, in the tensile tests, the maximum engineering stress occurred at low values of engineering strain (less than 2 pct), the values of stress, strain, and strain rate could be regarded as also representing the true values of those parameters. A larger discrepancy between predicted and experimental values of minimum creep rate would result from the use of constant load rather than constant stress during the creep test. The discrepancy would decrease, however, with decrease of strain at which the minimum creep rate occurred.

The work of Weertman on aluminium is only one example of the research aimed at correlating creep and tensile behaviour. The interchange of creep and tensile behaviour is often considered in the form of rate sensitivity — the sensitivity to stress of the minimum creep rate and the sensitivity to strain rate of the maximum tensile stress. An equation, relating strain rate and stress in the manner of equation 5.1, arises from the experimentally observed linear relation (at constant temperatures) between the logarithms of strain rate and stress. The gradient of the linear plot is the stress exponent (n) of equation 5.1, and may be used as a measure of rate sensitivity. That is,

$$\text{Rate sensitivity, } n = \frac{d(\log_{10} \dot{\varepsilon})}{d(\log_{10} \sigma)} \qquad (5.2)$$

The validity of applying equation 5.2 to creep and tensile data in order to obtain a correlation has been discussed by Lubahn and Felgar (1961). They point out that the value of n may only be the same for creep and tensile data when those data apply to the material in the same metallurgical condition. Hence, rate sensitivity values must be compared at the same values of plastic strain, so that the effects of strain

hardening may not influence the result. Although Weertman referred his values of maximum stress, in constant strain rate tensile tests, to a strain of 0.4, there is no indication in the paper of Servi and Grant that any or all of their values of minimum creep rate were observed at a creep strain of 0.4.

Even the precaution of calculating rate sensitivity values at the same plastic strain, in sets of creep and tensile curves, may not be sufficient to ensure a reasonable comparison between the respective values of n, since other metallurgical processes (recovery, recrystallisation, grain growth) may take place in different ways in the two types of test. To alleviate the effect on rate sensitivity of possible metallurgical differences between strain/time curves at different stresses or stress/strain curves at different strain rates, Lubahn and Felgar recommended the use of a sudden stress change or a sudden strain rate change during a single creep or tensile test, respectively. The observed change in creep rate or tensile stress should then be the result of the stress or strain rate change alone, since metallurgical processes would only proceed at a finite rate. The equivalence of creep and tensile rate sensitivity values, at the same plastic strain, should then depend only on the deformation process being the same in the two types of test.

Equation 5.1 was the form, approximating behaviour at low stresses, of a more complex equation relating steady state creep rate $\dot{\varepsilon}$, applied stress σ, and temperature T, derived by Weertman (1955) from a dislocation model:-

$$\dot{\varepsilon} = A\,\sigma^{1.11} \sinh (B\,\sigma^{1.78}/RT) \exp (-Q/RT) \qquad (5.3)$$

where A and B are constants and Q is the activation energy of self-diffusion. For the batch of high purity aluminium previously considered, the upper limit of 'low stress' was approximately 20 N/mm^2. Equation 5.3 was derived by Weertman from theoretical considerations. Similar equations relating $\dot{\varepsilon}$, σ and T have been derived empirically from the curve fitting of experimental creep results. For example, Garofalo

(1963) found the following relation to fit experimental results on copper, aluminium, an Al – 3.1 pct Mg alloy, and an austenitic stainless steel, over wide ranges of stress and temperature:–

$$\dot{\varepsilon} = A^1 (\sinh \alpha\sigma)^n, \text{ temperature constant} \qquad (5.4)$$

where A^1, α and n are constants. Equations relating steady state or minimum creep rates are important from an engineering point of view, since they allow extrapolation of existing data to stress and temperature conditions where no data are available. The more accurately the equation fits the existing experimental results, the better the prediction of behaviour which might be expected. However, a compromise has to be maintained between the greater complexity of equations giving greater accuracy and the resulting higher costs and increased time involved in employing those equations. Hence, the basis of most design formulae, used by engineers in creep calculations for practical purposes, tends to be the simplest relation between minimum creep rate and stress. The relation most often used (Hult 1966 p. 24, Finnie and Heller 1959 p. 116) is the Power Creep Law,

$$\frac{\dot{\varepsilon}}{\dot{\varepsilon}_o} = A \left(\frac{\sigma}{\sigma_o}\right)^n, \text{ temperature constant} \qquad (5.5)$$

where A is a constant depending on structure and temperature, n is a constant, and $\dot{\varepsilon}_o$ and σ_o are reference minimum creep rate and reference stress, respectively. The latter two parameters have been excluded from equations 5.1 to 5.4 for the sake of brevity. However, they are necessary for dimensional homogeneity, when the units of measurement applicable to the above equations are not clearly stated.

The validity of equation 5.5 (like that of equation 5.1) relies on the experimental observation that the logarithm of minimum creep rate and applied stress produce a linear plot of gradient n. The Power Creep Law, then, should really only be

employed within the range of stress and temperature where experimental data have shown n to be constant. Even within those ranges, the ability of the equation to represent creep data depends on the scatter in experimental results. Frequently, however, the experimental data available to a designer are sparse and contain large amounts of scatter. The accurate determination of the creep exponent, n, becomes impossible and large errors can result. In general, plots of log minimum creep rate against log stress have been found to produce an increasing gradient with increasing stress, after some particular value of stress – for example, Garofalo (1963). In the higher stress range, it has been found that stress and log minimum creep rate produce a linear relation (Sherby et al. 1954, Garofalo 1963). Hence, at high stress levels, minimum creep rate and stress may be correlated by,

$$\frac{\dot{\varepsilon}}{\dot{\varepsilon}_o} = A^1 \exp\left(B \frac{\sigma}{\sigma_o}\right), \text{ temperature constant} \qquad (5.6)$$

where A^1 is a constant depending on temperature and structure, B is a constant, and $\dot{\varepsilon}_o$ and σ_o are, as previously, reference values of minimum creep rate and stress. The hyperbolic sine function (equations 5.3 and 5.4) may, therefore, be used to represent behaviour over the entire stress range since, for high stresses, it approximates to the form of equation 5.6, and, at low stresses, to that of equation 5.5. The Power Creep Law, however, is easier to deal with mathematically and it can be expected that designers will still continue to use correlations of the form shown in equation 5.5.

The present results of constant strain rate tensile tests and constant load creep tests on the same batch of commercially pure aluminium at temperatures of 250 deg.C. and 500 deg.C., provide an opportunity of,

1) Comparing creep and tensile data to determine if the latter is capable of predicting the former.
2) Examining the range of validity of the Power Creep Law.
3) Illustrating the possible consequences of using the Power Creep Law outwith its range of validity (if such a range is found).

As previously mentioned, possible errors due to the use of a constant engineering strain rate and engineering stress in tensile tests could be neglected since the maximum stress occurred at small values of strain. The errors, due to the use of constant load, rather than constant stress, in the creep tests, could also be regarded as minimal, since, as shown in the following Chapter, minimum creep rates were achieved at low values of strain. In section 2.2.2 of Tensile Testing, mention was made of the influence of the testing machine on the actual specimen strain rate during the strain hardening region of the stress/strain curve. In this first part of Rate Sensitivity, only values of maximum stress were used and, therefore, the strain rates were taken as the nominal engineering strain rates. However, in Rate Sensitivity : Part II, the variation in the applied strain rate did have to be considered.

The interpretation of results had to bear in mind that the material has already been shown to be metallurgically unstable under the tensile testing conditions described in Chapter II. Grain growth was found to have occurred in specimens strained slowly at 500 deg.C. Another important factor to be considered was the possible influence on results of the intergranular discontinuities which have been observed to develop in the material in tensile tests. This was, in fact, the main objective of the present research – the determination of the effect of intergranular discontinuities on the creep properties of commercially pure aluminium – and it may not be possible to segregate the effect of discontinuities until the tests described in Chapter IX have been completed.

The objectives 1), 2) and 3), listed above, require the uniaxial creep data of Chapter VI, and, hence, discussion of those items must wait until Chapter VII. In the next section of the present Chapter, the tensile data from Chapter II will be discussed with respect to its possible use in predicting creep behaviour.

5.2 Prediction of Creep Behaviour from Tensile Data

In Figures 5.1 and 5.2, the maximum stresses recorded in constant strain rate tensile tests on commercially pure aluminium, at temperatures of 250 deg.C. and 500 deg.C., respectively, have been plotted against strain rate on a logarithmic basis. For the purpose of preparing test pieces with intergranular discontinuities, tensile tests were performed at strain rates of 0.1, 1, 10 and 100 pct/h and the results of these tests have been described in Chapters II and III. The data from these tests, as shown in Figures 5.1 and 5.2, indicated a non-linear relation between the logarithms of maximum stress and strain rate. Further tests were carried out at strain rates of 1000 and 10000 pct/h, in the same manner previously described for tests at the slower rates, to determine if the observed trends in the original data continued to higher stresses and strain rates. Instead of assuming each strain rate to be the nominally constant value calculated from tensometer motor drive and pulley gears, the actual crosshead speed for each test was calculated from the rotation of the automatic recording drum, and the actual engineering strain rate from that. As shown in Figures 5.1 and 5.2, variation of strain rate from test to test was small and all values were close to the planned rates.

Although few tests were performed at the lower temperature of 250 deg.C., the results, presented in Figure 5.1, indicate that the gradient of the log(maximum stress) against log(strain rate) plot continuously decreases from 0.1 to 10000 pct/h. Therefore, rate sensitivity (n), as defined by equation 5.2, continuously increases over the same range of strain rate. Although the possible influence of metallurgical instability on these results cannot be completely ruled out, any effect at the four highest strain rates must be minimal since maximum stresses at these rates were achieved in less than 30 minutes. Similarly, density measurements failed to detect a significant amount of intergranular discontinuities, but it would be unwise to state that this rules out discontinuities completely as the cause of the behaviour. The

variation of n with log maximum stress has been plotted in Figure 5.3. This graph must be interpreted with some caution since it was derived from the measurement of the gradient of the curve in Figure 5.1. A relatively small change in the shape of that curve produces a relatively large change in the value of the gradient, which is itself difficult to measure accurately. With the foregoing reservation in mind, the plot of Figure 5.3, however, does illustrate the rapid increase which occurred in the value of n over the stress range of 45 to 110 N/mm^2. Figure 5.3 shows that n tends to a value of about 6 for stresses below 45 N/mm^2 and rises rapidly to about 57 with increase of stress to 110 N/mm^2.

The results, presented in Figures 5.1 and 5.3, have shown that maximum stress and strain rate in tensile tests on commercially pure aluminium at a temperature of 250 deg.C., cannot be correlated by the Power Creep Law, expressed in equation 5.5, with a constant value of n. However, since Figure 5.1 indicated a continuous function between log maximum stress and log strain rate, it should still be possible to predict creep rates from that plot, although with less accuracy due to the uncertainty in the curve. This assumed interchange of tensile and creep data has also indicated that the creep rate should become more stress sensitive as the stress increases. Therefore, it may be expected that scatter in the strain/time curves of creep tests will increase as the stress increases. This latter factor will be important in the search for a stress at 250 deg.C. which produces low scatter creep data.

The results at the higher temperature of 500 deg.C. (Figure 5.2) showed the same trend as at the lower temperature of 250 deg.C., for the four original strain rates of 0.1, 1, 10 and 100 pct/h. Figure 5.4 illustrates the increase of rate sensitivity (n) with stress from 2.6 at approximately 1 N/mm^2 to 12.4 at approximately 5 N/mm^2. The increase, though less dramatic than at 250 deg.C., again indicates that the Power Creep Law, with n constant, does not apply to the tensile data over the stress range 1 – 5 N/mm^2 at 500 deg.C.

Prediction of creep rates, although still possible, is made difficult by the broad scatter band of results indicated in Figure 5.2. This assumed interchange of tensile and creep data again indicates that scatter in the strain/time curves of creep tests may be expected to increase with increase of stress, since the sensitivity of strain rate to stress has been shown to increase with increase of stress from 1 to 5 N/mm^2.

The additional tensile tests, performed at strain rates of 1000 and 10000 pct/h, did not confirm the trend in behaviour established by the slower rates. Consideration of the results for the three strain rates, 100, 1000 and 10000 pct/h, indicated a linear relation between the logarithms of maximum stress and strain rate, with a value of 5.45 for n. At large stresses and strain rates, the material was stronger than predicted by the results of smaller stresses and strain rates. Why there should be a discontinuity in the log maximum stress/log strain rate plot at 100 pct/h is not clear. As for tests at 250 deg.C., the influence of metallurgical instability can be regarded as minimal for the four largest strain rates. However, significant amounts of intergranular discontinuities were found by density measurements and metallography at small strains in specimens strained at 1 pct/h and 500 deg.C. Density measurements also showed that the amount of intergranular discontinuities decreased with increasing strain rate and at 100 pct/h the density measurements indicated that the amount was very small. It is possible, therefore, that the discontinuity in the curve of Figure 5.2 denotes the point at which intergranular discontinuities stop influencing the deformation process.

5.3 Summary and Conclusions

Logarithmic plots of maximum stress against strain rate, from tensile tests on commercially pure aluminium at temperatures of 250 deg.C. and 500 deg.C., have been presented. Owing to the non-linear nature of the plots, creep behaviour may only be predicted within the range of stresses covered by the curves. Evidence of the validity of these predictions will be obtained by the constant load creep tests, described in the next chapter, and discussion of that evidence will take place in Chapter VII. However, assuming that the interchange of data is possible, the results indicate that the exponent (n) of stress in the Power Creep Law (equation 5.5) increases with increase of stress, and, hence, scatter in strain/time curves of the proposed creep tests may also be expected to increase with stress. Again, the evidence for or against this behaviour will be obtained in the next chapter.

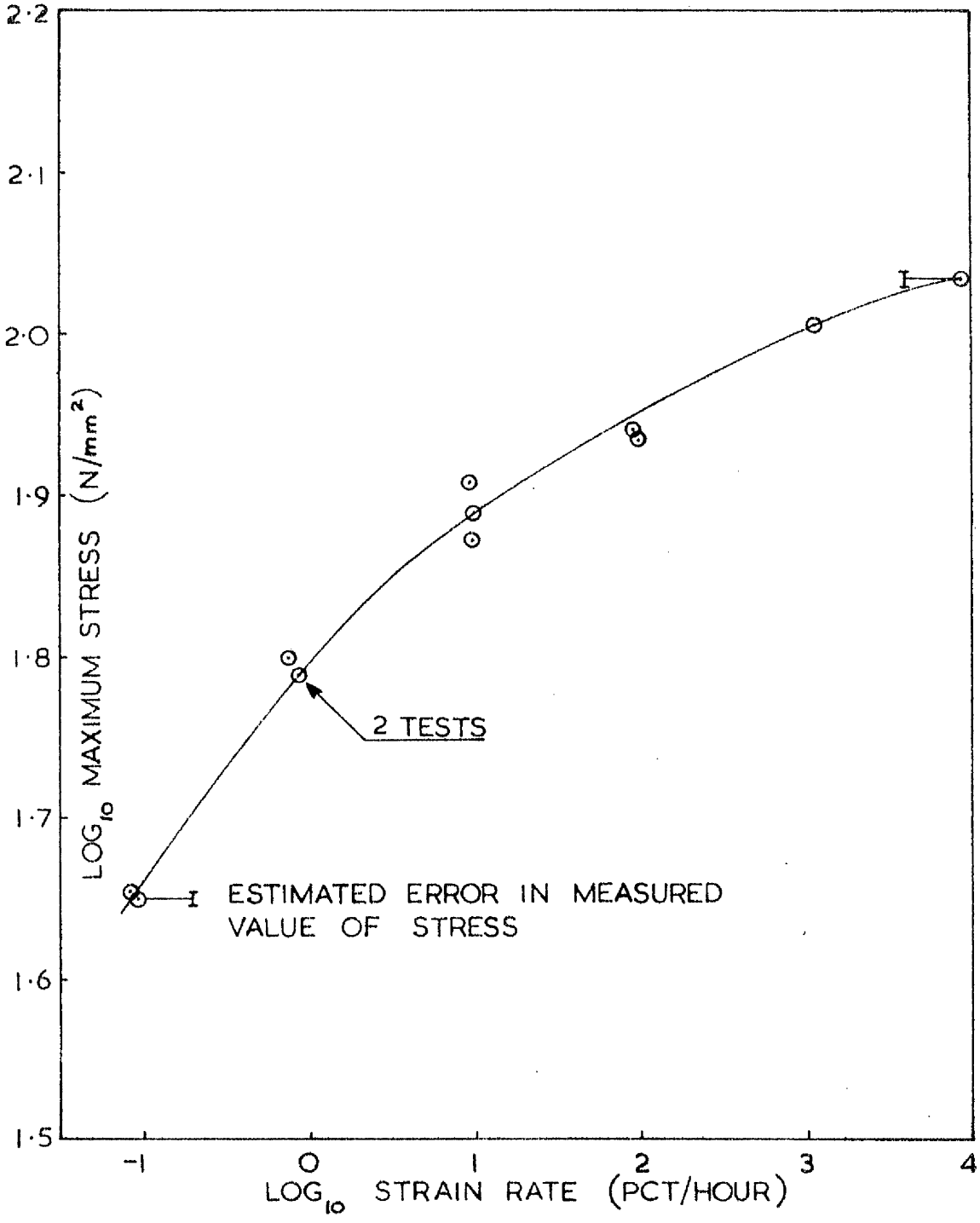

Figure 5.1 250 deg.C.; constant strain rate tensile tests; $\log_{10}$ (maximum stress) against $\log_{10}$ (strain rate) at 1.4 pct strain

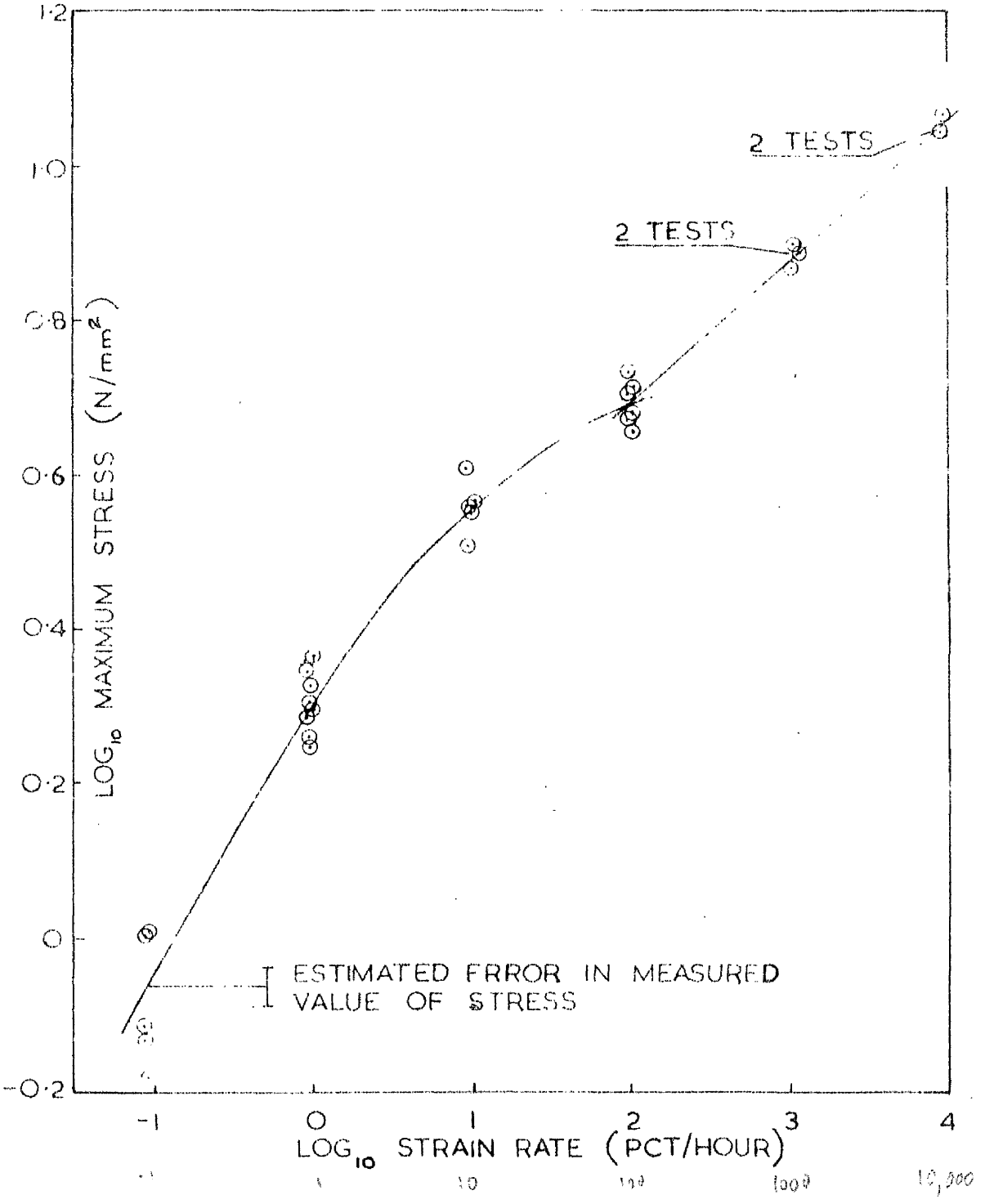

Figure 5.2 500 deg.C.; constant strain rate tensile tests; $\log_{10}$ (maximum stress) against $\log_{10}$ (strain rate) at 1.4 pct strain

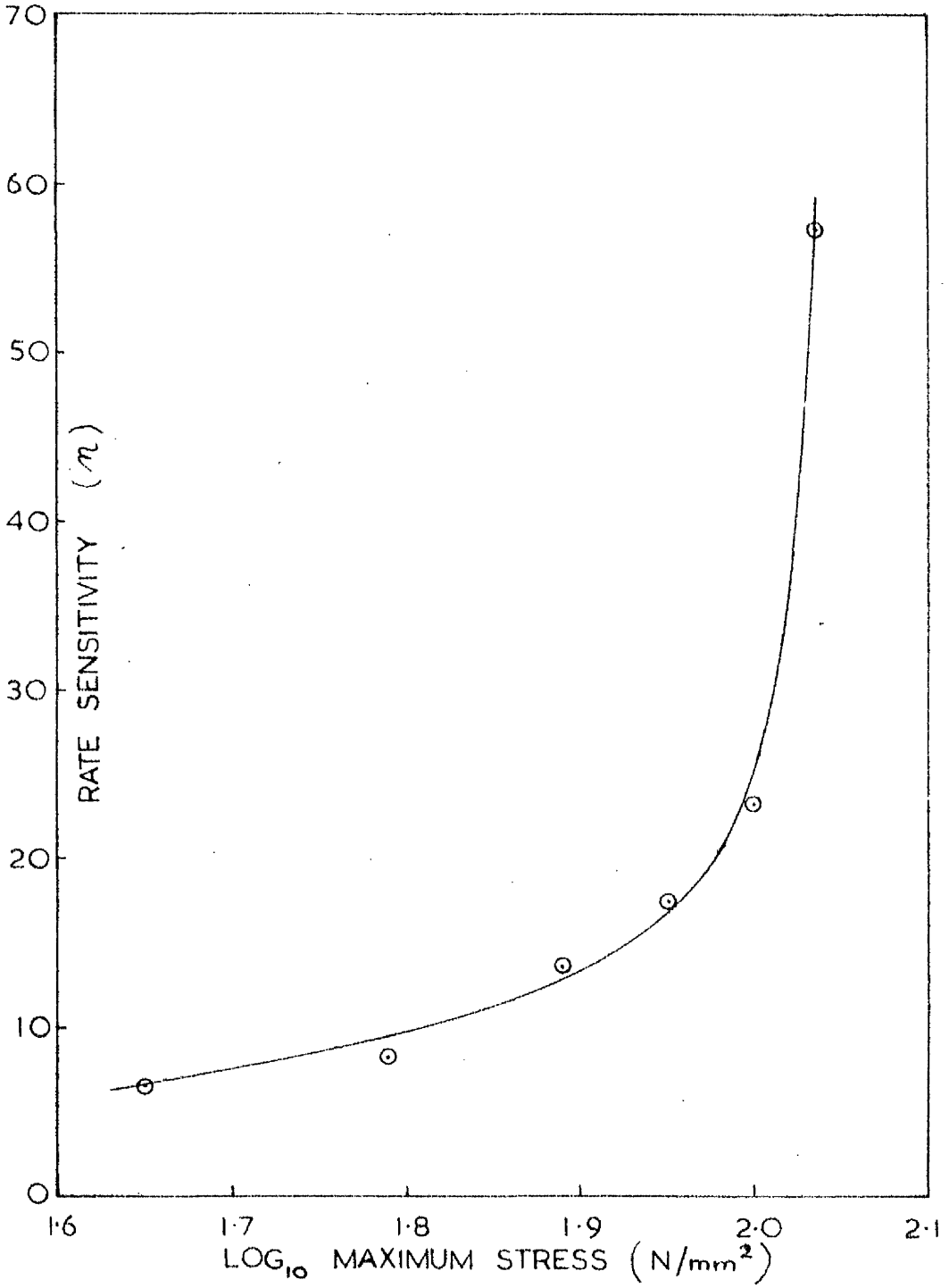

Figure 5.3 250 deg.C.; constant strain rate tensile tests; rate sensitivity (n) against $\log_{10}$ (maximum stress)

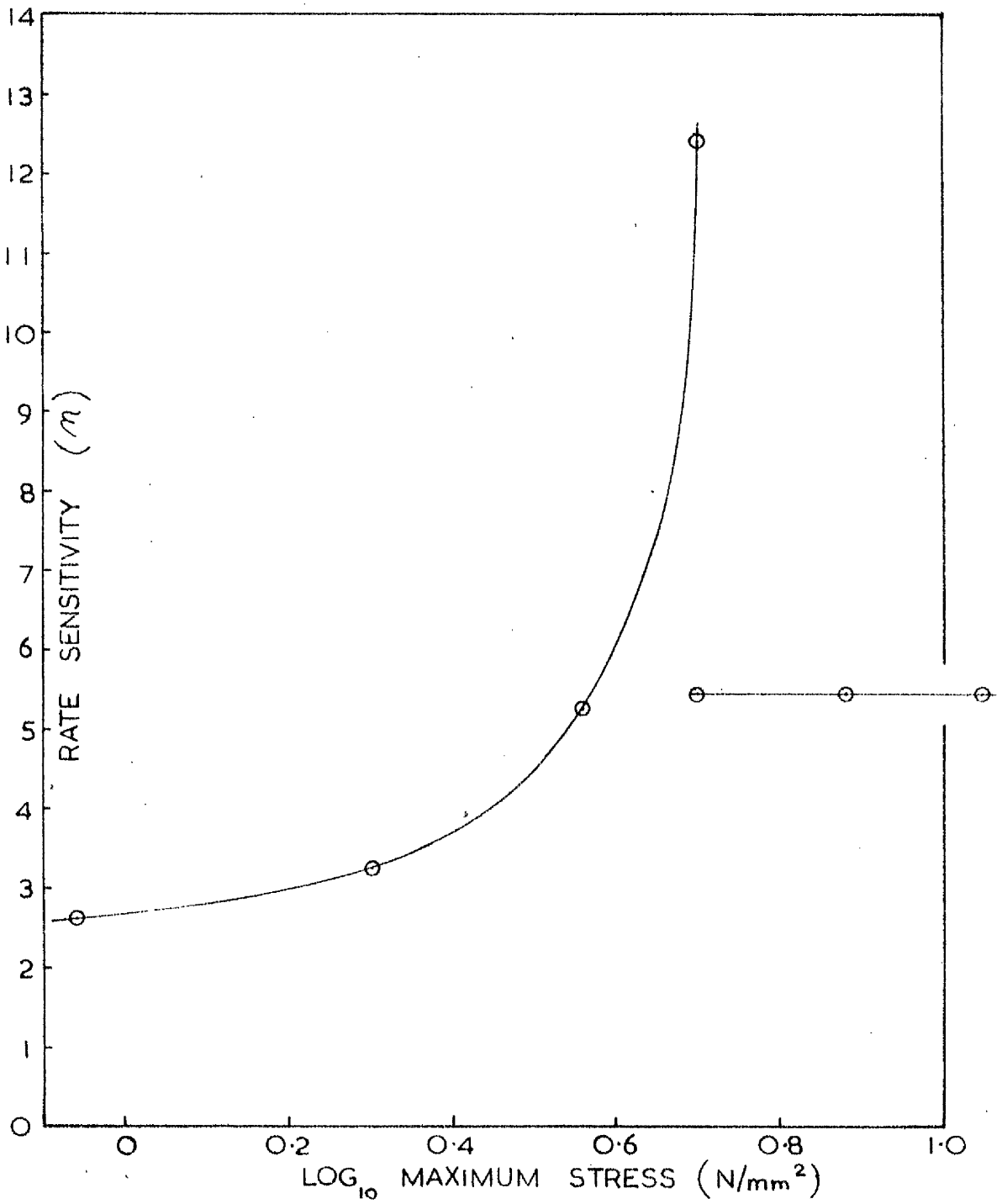

Figure 5.4 500 deg.C.; constant strain rate tensile tests; rate sensitivity (n) against $\log_{10}$ (maximum stress)

CHAPTER VI

UNIAXIAL CREEP TESTING

6.1 Introduction

Chapters II and III described a method of producing test pieces with a known, controlled amount of intergranular discontinuities. To study the effect of these discontinuities on the creep properties of the test pieces at 250 deg.C. and 500 deg.C., comparison would be made between their strain/time curves and those of test pieces without intergranular discontinuities. The comparison would become easier with decrease of scatter in the strain/time curves. The main purpose of the work described in this chapter, therefore, was to find a stress at 250 deg.C. and a stress at 500 deg.C. for which scatter in the strain/time curves was least. The results of Chapter V indicated that the sensitivity of the minimum creep rate should increase with increase of applied stress and, therefore, scatter in the strain/time curve should decrease with decreasing applied stress. However, although low minimum creep rates were suitable for the study, a compromise would have to be made to obtain practical testing times.

Chapter V discussed the possible interchange of tensile and creep data. To show if an interchange of data was possible for the present material, it was suggested that creep tests should be carried out at the maximum stresses recorded in the tensile tests at 250 deg.C. and 500 deg.C. Since no other guide was available to assist in the choice of creep stresses, it was decided to use the maximum stresses for the first series of tests. The creep testing equipment was designed to suit those testing conditions. If the above

stresses proved unsuitable, tests at other stresses would be performed.

In addition to obtaining stresses producing low scatter strain/time curves and data for strain rate sensitivity calculations, information on the growth of intergranular discontinuities during creep of commercially pure aluminium would be obtained by measuring the density decrease in strained specimens. The results of these measurements and a comparison with those obtained from constant strain rate tensile tests will be reported in Chapter VIII.

6.2 Creep Testing Equipment

As well as the creep machine itself, suitable test pieces, grips, pull rods, extensometry and furnaces also had to be designed to meet the requirements of the testing conditions. The design of these items was largely dictated by the dimensions of the test piece. To maintain continuity with Tensile Testing, a cylindrical test piece of 0.1 in^2 cross-sectional area was chosen for the creep tests. The guage length was 1.80 in. and the test piece conformed to B.S. 3688. In this section, creep machine and furnace will be described, and in section 6.3, test piece, grips, pull rods and extensometry.

6.2.1 Creep Machine

The creep machine was designed to accommodate loads of up to 1 ton and a cylindrical furnace 16in. length by 8in. diameter. The machine was of the lever loading type, with a lever ratio of 10 : 1, and incorporated design features of both 'Mand' and 'Dennison' creep machines, in use at Glasgow University Engineering Department. Attention was paid to achieving easy access to the test piece during setting up of the creep test.

Figure 6.1 shows the creep machine in diagrammatic form. The upper and lower ball joints (C) allow transmission of load to the pull rods without bending moments and hence keep the stress system uniaxial. The capstan arrangement (E) facilitates levelling of loading beam when required. The universal joint (F) prevents loading eccentricities on the load pan (G) being transmitted to the beam by any inaccuracies in the knife edge (B) and its saddle (H). Figure 6.2 shows the creep machine with the furnace in the raised position and a screw grip test piece set up with thermocouples and extensometry. Two machines were built in order to minimise testing time, one machine for each temperature.

Constant stress creep machines were considered to be

unsuitable for the project because of their use of the constant volume criterion of plastic deformation. The development of internal discontinuities in the material during testing invalidates the calculation. However, accurate knowledge of the size and distribution of the discontinuities could be used to modify a constant stress creep machine to allow for the above effect.

6.2.2 Furnace Design and Temperature Control

In the design of the furnace, data presented by Laubitz (1959) were used in an attempt to obtain as large a constant temperature zone as possible with a small furnace. The furnace, which was 16in. long by 8in. overall diameter, had a heated length of 12in. The tube had a bore of $2\frac{9}{16}$in. and was of 'Purox' Alumina. The single winding was resistance wound using 'Nichrome V' wire, the winding density varying according to the formula of Laubitz. 'Kaowool' ceramic fibre was used as insulation, being contained by aluminium alloy sheeting and asbestos end plates, the latter also acting as a means of support for the furnace tube.

As in tensile tests, temperature was controlled by a silicon rectifier type of proportional temperature controller. The temperature sensing element of the controller, a platinum resistance thermometer, was positioned against the inside of the furnace tube wall. Alumel/Chromel thermocouples were used to measure temperature. Their millivolt outputs were continuously monitored on a Chart Recorder with a resolution of $\pm$ 1 deg.C. Measurement of temperature to $\pm$ 0.1 deg.C. was obtained with a slidewire potentiometer.

6.3 Test Piece and Extensometry Design

6.3.1 Choice of Test Piece

The main objective of the creep testing programme was to determine stresses at 250 deg.C. and 500 deg.C. which produced low scatter strain/time curves. Penny and Leckie (1968) have demonstrated that scatter in creep curves can largely be accounted for by bending of the test piece due to misalignment or initially bent pull rods. They suggest the use of universal joints (Penny et al. 1966) between test piece and pull rods, as a remedy. Consequently, it appeared reasonable to incorporate this idea in the current project. A conventional screw grip test piece was also developed in case difficulties were encountered with the universal joint test piece.

To obtain an accurate measurement of strain during a test, the extension of a gauge length, marked on the test piece would be measured directly. This was to be carried out by means of collars clamped round protusions marking the gauge length. The differential movement of the collars would be recorded outside the furnace with linear displacement transducers. The test pieces and grips were designed to accommodate this system of extensometry.

6.3.2 Test Pieces and Grips

Figure 6.3 shows the universal joint test piece with the screw grip test piece alongside. Figures 6.4 and 6.5 provide details of the dimensions of the two test pieces. The protusions marking the gauge length of 1.80in. (45.70mm.) were of square cross-section for attachment of extensometry (see section 6.6.3). The universal joint test piece was connected to the upper and lower pull rods by way of universal blocks. Figure 6.6 shows the assembly of the test piece with the views of the upper block in section. Load was transmitted from pull rod to block, and from block to test piece, through load bearing pins, the axes of which are shown in the

diagram. In the original design of Penny et al. (1966), load was transferred to the test piece by collars gripping the plane faces around the holes of the test piece as well as by the load bearing pins. This was found unnecessary in the present project since no distortion of the hole in the test piece was observed due to the action of the load bearing pin. The pull rods, universal blocks and load bearing pins were all machined from heat resisting steel.

The assembly of screw grip test piece and pull rods was shown in Figure 6.2. For this test piece, a seating was machined into one end of the pull rod to accommodate the $\frac{3}{4}$in. B.S.F. screw grip. As before, pull rods were of heat resisting steel.

6.3.3 Strain Measurement

The method of measuring the extension of the test piece gauge length is illustrated in Figures 6.6 and 6.7. Although in Figure 6.6 the assembly is shown for a universal joint test piece, the same set-up was suitable for use with a screw grip test piece (see Figure 6.2). In Figure 6.6, the upper and lower extensometry collars both consist of two identical halves (details of which are shown in Figure 6.8) which are clamped round the protusions marking the gauge length. A square section was chosen for the protusion because of the softness of the material. During machining of the test piece and during assembly of the creep test, this shape of section would provide sufficient strength to prevent damage. Two screws were used to fasten together the two parts of each collar with sufficient pressure to hold the extensometry in position without causing undue stress on the test piece.

The differential movement of the collars (and, therefore, the extension of the gauge length) was transmitted by legs (Figure 6.6) of rectangular cross-section to a position below the furnace where it was measured by the system shown in Figure 6.7 Two pairs of legs were used to provide two

readings of extension. The average of the two readings would be more accurate than either reading by itself. Rubber bands were used to hold both pairs of legs in position, steel rollers being used as spacers between outer and inner legs, and between inner legs and flats machined on the pull rod. The rollers also permitted easy relative movement of the legs. The inside legs, attached to the lower collar (Figure 6.6), both had a capacitance type, linear displacement transducer attached to their lower ends (Figure 6.7). Similarly, the outside legs, attached to the upper collar, both had micrometer heads attached at their lower ends. The relative displacement of transducer body and core (held in contact with the anvil face of the micrometer by a spring) follows the differential movement of the legs. Although the range of movement of the core is only 0.5in., the effective measuring range was increased to 1in. by the 0.5in. range of the micrometer head.

The output signals of the displacement transducers were measured and recorded by a system supplied by Rank Precision Industries Ltd. The Indicator Unit of this system provides a visual digital display of transducer position with a resolution of 0.0002 mm. A Programme Scanner linked to the Indicator Unit controls the recording of the visual reading on paper tape at pre-determined time intervals. An additional facility of the system is that it can average the readings of two transducers. Using this system, an accurate record of specimen extension with time was obtained automatically. Although the system had a resolution of 0.0002 mm., the accuracy of measurement was assumed to be $\pm$ 0.001 mm.

6.4 Experimental Procedure

Similar procedures were involved in the assembly of tests using either type of specimen. The differences will be pointed out in the description. Before assembly of the test, the specimen was washed thoroughly in alcohol and dried in air. The gauge diameter was measured with a micrometer at seven points along the length and the average reading used to determine the required load. As a check on extension, three pairs of divider points, each pair 1.80in. (45.70 mm.) apart, were inscribed at 120 deg. intervals round the top faces of the protusions marking the gauge length. Their distance apart was measured with a microscope and vernier scale, as described in Tensile Testing. As shown in Appendix 6.1, measurement of strain by this method was accurate to $\pm$ 0.2 pct for strains up to 50 pct and $\pm$ 0.3 pct for strains 50 – 150 pct. Measurement of strain during the creep test by transducers was more accurate – $\pm$ 0.01 pct for strains up to 10 pct and $\pm$ 0.1 pct for strains 10 – 100 pct.

The balance weights on the beam of the creep machine were adjusted so that the beam maintained a level position with no weight on the load pan and the upper pull rod, test piece and upper extensometry attached. The test piece and both pull rods were then set up in the machine with a small weight on the load pan to maintain alignment. With the screw grip test piece, alignment depended on the accuracy of the threads in both pull rod and test piece. With the universal joint test piece, alignment depended not only on machining accuracy but also on accurate positioning of the test piece on the load bearing pin. This was achieved with a 'feeler' gauge. The assembled test piece was shown in Figure 6.6.

The next stage in the procedure was the attachment of extensometry collars and legs. The collars were positioned so that the legs were aligned with the flat parallel faces of the pull rod. The three thermocouples were then secured by wire to the gauge length, one at each end and one at the mid-point. The displacement transducers were then locked in

position, making sure that their axes of displacement were parallel with the axis of the pull rod. The furnace was lowered over the assembly and the open ends plugged with 'Kaowool' ceramic fibre, to reduce heat loss. The lever loading beam was then supported in position so that the test piece experienced negligible load.

Heating of the test piece to temperature took $1\frac{1}{4}$ hours and a further $1\frac{1}{4}$ hours were allowed for stabilisation of the temperature. In a preliminary test, the vertical position of the furnace was varied until the temperature recorded by the thermocouple at the mid-point of the gauge length was a maximum. The temperatures recorded by the other two thermocouples were then less than 0.5 deg.C. below the maximum temperature. Temperature controller was then adjusted so that the average of the three readings was equal to the required test temperature of 250 deg.C. or 500 deg.C. During a creep test, temperature was controlled with an accuracy of $\pm$ 0.5 deg.C. The error in temperature contributing to scatter in the strain/time curves was considered to be $\pm$ 1 deg.C. In Chapter VII, it will be shown that the estimated error in creep rate, due to this error in temperature, was $\pm$ 6 pct at 250 deg.C. and $\pm$ 3 pct at 500 deg.C.

The load was applied to the test piece by lowering the load pan at a constant rate with an electric actuator. In this device, a spindle supporting the load pan moves at a constant linear rate through the action of a D.C. electric motor. The weights used on the load pan had different accuracies. For the combinations of weights used in tests at 250 deg.C., the error was of the order $\pm$ 0.1 N producing an error in applied load of $\pm$ 1 N (lever arm ratio 10:1). At 500 deg.C. the error in applied load was of the order $\pm$ 0.5 N. The estimated errors in the applied stresses, due to the errors in applied loads and test piece diameters, have been calculated and tabulated in Appendix 6.1. Apart from the two smallest creep stresses at 500 deg.C., the error in applied stress was in the range $\pm$ (0.5 – 1) pct. The calculation of the expected error in minimum creep rate, due

to this error in applied stress, depends on the function chosen to relate minimum creep rate and stress. The calculation has, therefore, been left until section 7.3 of Rate Sensitivity : Part II.

Creep tests, which were not taken to fracture, were stopped by firstly, switching off furnace current, secondly, removing the applied load by supporting the lever beam and thirdly, raising the furnace above the test piece. The test piece cooled in air to room temperature in approximately 2 hours. Cooling under load was not used because, at high stresses, significant amounts of creep strain would have occurred during cooling. After removing the test piece from the grips, the extensions of the three gauge lengths marked by the divider points were measured and compared with that recorded by the transducer system. The gauge diameter was again measured at seven points along the gauge length.

Creep testing procedure for the two smallest stresses at 500 deg.C. was different from the above. For a stress of 0.61 N/mm^2, the lever loading beam was fixed in position, and the load applied to the test piece consisted of the weight of the lower pull rod, that portion of the extensometry clamped to the lower gauge mark and those parts of the lower ball joint of the creep machine connected to the pull rod. The parts of the creep machine ball joint were disconnected for the load necessary to produce a stress of 0.35 N/mm^2. For these two stresses, accuracy of applied load was $\pm$ 0.5 N.

6.5 Comparison of Screw Grip and Universal Joint Test Pieces

To compare the performance of the two types of test piece, four tests (two with each type) were carried out at 250 deg.C. and at that stress which was the maximum stress in tensile tests at 10 pct/h, namely 76.65 N/mm^2., (11,120 lbf/in^2.). Four corresponding tests were carried out at 500 deg.C. and 3.65 N/mm^2., (530 lbf/in^2.). The strain/time curves for these tests are shown in Figures 6.9 and 6.10. The curves at 250 deg.C., shown in Figure 6.9, were all taken to failure. At this temperature there are no features which distinguish one type of test piece from another. It was concluded that, at 250 deg.C., there was no advantage in using the more elaborate test piece. At the higher temperature of 500 deg.C., because of the very large extensions, only one of the tests was taken to rupture. From the curves, shown in Figure 6.10, it was again concluded that no advantage lay in using the universal joint test piece.

Difficulties were encountered in the use of the universal joint test piece at 500 deg.C. The aluminium tended to weld itself to the load bearing pin, so that easy removal of the specimen from the universal block was impossible. Because of oxidation, all parts of the assembly had to be cleaned with emery paper after each test. At 250 deg.C. no problems were encountered and setting up and removal of test piece were as convenient as with a screw grip specimen. Preparation of creep test pieces with a controlled amount of intergranular discontinuities would have been difficult with the universal joint test piece. After straining at a temperature of 500 deg.C., the material was very soft and re-machining was impossible. Hence, preparation of test pieces with intergranular discontinuities by the proposed method of constant strain rate testing at 500 deg.C. would have to take place with the test piece in its final form. Due to the size of the universal blocks, straining in the original Tensile Testing equipment was not possible. The designing and building of additional tensile testing equipment seemed unjustified, since it had been shown that screw grip test pieces were

capable of carrying out the tests. Hence, the project was continued using screw grip test pieces.

About this time, it was realised that there were large differences in the creep properties of the material, when tested at 250 deg.C., in the 'as received' and annealed conditions. To study the effect of holes on the creep curve at 250 deg.C., comparison would have to be made with creep curves of the material which had been annealed at 500 deg.C. However, a series of tensile tests had been completed at 250 deg.C., which gave information on Strain Rate Sensitivity. The decision was made to do a series of creep tests at 250 deg.C. on the 'as received' material, to complete the Rate Sensitivity results and to use these creep tests in choosing a suitable stress for the study of the effect of holes. Additional creep tests would then be performed at that stress to check the low scatter criterion. For these tests, it was decided to utilise the Universal Joint Test Piece, although, in the planned tests on the annealed 'as received' material, screw grip test pieces would be used.

Although the Universal Joint Test Piece was not found to make a significant difference to the limited number of comparative tests on aluminium, the idea should not be discarded. Penny et al. (1966) showed the design to substantially reduce bending in test pieces. It is possible that the tests performed on aluminium did not have a significant amount of bending to be corrected. There was not sufficient time to perform more comparative tests or to try and improve the design, and so the investigation was not continued. Screw grip test pieces had shown themselves capable of producing reasonable results and would have to be used in future tests for the study of the effect of intergranular discontinuities on the creep properties.

6.6 Uniaxial Creep Curves

6.6.1 High Temperature : 500 deg.C.

Representative log. strain/log. time curves are shown in Figure 6.11 for the seven stresses used in creep tests at 500 deg.C. Stresses 4.99, 3.65, 2.26 and 0.87 N/mm^2. were the maximum stresses recorded in constant strain rate tensile tests on the material at 500 deg.C. and strain rates of 100, 10, 1 and 0.1 pct/h, respectively. Additional tests at stresses of 1.38, 0.61 and 0.35 N/mm^2 were performed to obtain further information on Rate Sensitivity (Chapter VII) and the growth of intergranular discontinuities (Chapter VIII) as well as for the original purpose of obtaining low scatter strain/time curves.

The scatter in the strain/time curves was found to be least at a stress of 1.38 N/mm^2. As the applied stress was increased or decreased from that value, the scatter tended to increase. Figure 6.12 shows the strain/time curves at 1.38 N/mm^2 for six tests at that stress. Comparison of these curves with those at a stress of 3.65 N/mm^2, shown in Figure 6.13, illustrates the increase of scatter with increase of applied stress. Figures 8.3 to 8.6 in Uniaxial Creep Density Changes also demonstrate the trend, although only a few tests have been plotted in each figure. Figure 7.2 of Rate Sensitivity : Part 2, as well as showing the increase of scatter in minimum creep rates with increase of stress, also shows the increase of scatter in minimum creep rates with decrease of stress. Again, for the few curves plotted, Figures 8.1, 8.2 and 8.3 confirm the trend. The increase of scatter as the applied stress was increased was predicted by the tensile data in Chapter V. With increase of applied strain rate in tensile tests at 500 deg.C., the sensitivity of the recorded stress to strain rate decreased. Conversely, it would be expected that the sensitivity of the strain rate to stress would increase as the applied stress is increased in a creep test.

The increase in scatter for stresses less than 1.38

N/mm^2 is more difficult to explain, since, by the reasoning of the previous paragraph, the creep rate should be less stress sensitive. One probable factor influencing the scatter was the uncertainty in the value of the applied stress. Restraints, caused by extensometry and thermocouples, which were insignificant at high stresses, would become important at low stresses. However, practical tests to measure these restraints showed them to be negligible. Metallurgical factors, such as grain boundary migration, may also have contributed to the scatter.

A primary stage in the creep curve and a significant instantaneous extension on loading were only observed at the two highest stresses (4.99 N/mm^2 and 3.65 N/mm^2). In addition, a linear secondary stage of creep was difficult to identify in many of the curves. In fact, it could be argued that the minimum creep rate was merely a point of inflexion on the strain/time curve which, by suitable choice of scales, could be made to resemble a linear region. The point of inflexion occurred, in general, at strains less than 1 pct. Since localised necking was only observed at stresses of 2.26 N/mm^2 and over, the rapidly increasing creep rate could not be explained by that factor. Even at these higher stresses, localised necking did not occur until strains greater than 20 pct.

In the absence of localised necking, an increasing creep rate occurs in constant load tests due to thinning of the gauge length according to the constant volume criterion of plastic deformation. Using that criterion and the Power Law for Minimum Creep Rate, calculations were performed to determine if thinning was solely responsible for the increasing creep rate. (See Appendix 6.2) The results showed that the creep rate should reach twice the minimum value at strains of 7 pct to 32 pct for reasonable values of index n. In the present series of tests, creep rates doubled by approximately 2 pct strain except for the highest stress (4.99 N/mm^2) and some curves at the second highest stress (3.65 N/mm^2). These results show that there are additional factors causing the

rapidly increasing creep rate. Later, it will be shown that rapid growth of intergranular discontinuities occurred during creep at stresses less than 3.65 N/mm^2. It is concluded that the development of these discontinuities was a major factor influencing the behaviour of the creep rate. At the two highest stresses, the creep rate doubled at strains of the right order for the effect to have been caused by thinning of the gauge length.

6.6.2 Low Temperature : 250 deg.C.

Representative log strain/log time curves are shown in Figure 6.14 for the six stresses used in creep tests at 250 deg.C. Stresses 76.65, 61.50 and 45.35 N/mm^2 were the maximum stresses recorded in constant strain rate tensile tests on the material at 250 deg.C. and strain rates of 10, 1 and 0.1 pct/h, respectively. It was found necessary to perform tests at the three lower stresses of 27.60, 17.91 and 10.00 N/mm^2, firstly, because of the large scatter in strain/time curves at the first three stresses and secondly, to obtain additional data for rate sensitivity calculations.

As for creep tests at 500 deg.C., it was observed that, scatter in the strain/time curves of tests at 250 deg.C., increased with increase of applied stress. The strain/time curves shown in Figures 6.15 to 6.18 verify this observation. Only two creep tests were performed at the lower stress of 17.91 N/mm^2 and only one at 10.00 N/mm^2. Therefore, it is impossible to say, from these three tests, that the low scatter trend would continue. However, the errors produced at 500 deg.C. and low stresses by uncertainty in the value of applied stress, by restraints due to thermocouples and extensometry and by metallurgical changes in the material, should be much less severe at 250 deg.C., where loads were very much larger. Hence, it was concluded that the low scatter curves would continue to lower stresses at 250 deg. C. Figure 7.1 of Rate Sensitivity : Part 2 confirms the trend by illustrating the increase in scatter of minimum creep rates with increase of applied stress from 27.60 to 76.65 N/mm^2. Again, as with creep tests at 500 deg.C., tensile

testing predicted the increase of scatter in creep tests at 250 deg.C.

At each of the six stresses, a significant instantaneous extension on loading was recorded. The strain/time curves at the three highest stresses (45.35, 61.50 and 76.65 N/mm^2) had well defined primary regions. The secondary region could be regarded as a point of inflexion in the curves before the tertiary stage. At 27.60 N/mm^2 the curve showed no primary region, but there was a well defined secondary region. The tertiary stage of the curve at this stress did not appear until a strain of 1 pct had been attained. At higher stresses, the creep rate rapidly increased in a manner already described for tests at 500 deg.C. The same analysis, however, for thinning of the gauge length was more difficult to apply, since the minimum creep rate is more stress sensitive at 250 deg.C. (This is shown in the next Chapter). Also, there were insufficient tests to assess accurately the strain at which localised necking began.

6.6.3 Choice of Stresses for Studying Effect of Intergranular Cracks

To study the effect of the same amount of intergranular discontinuities on the creep properties of commercially pure aluminium under different conditions of stress and temperature, it was necessary to use rupture life or minimum creep rate as a basis for comparison. In the practical situation, one of the great difficulties presented by intercrystalline cracking is its ability to produce premature failure under conditions producing low values of creep rate when otherwise long rupture lives and large elongations might be expected. Hence, the above study should be conducted at low values of minimum creep rate. In addition, comparison of the creep properties of the cracked and virgin materials will only give conclusive results when the stress employed produces low scatter strain/time curves. A stress of 1.38 N/mm^2 has been shown to produce strain/time

curves with least scatter for a temperature of 500 deg.C. (Figure 6.12). The minimum creep rate under those conditions was 0.156 pct/h and rupture life approximately 50 hours for the virgin material. A stress of 27.60 N/mm^2 has been shown to provide low scatter strain/time curves at a temperature of 250 deg.C. (Figure 6.15). Under those conditions, the minimum creep rate was 0.0023 pct/h and a strain of 2.85 pct was achieved in 1000 hours. Although these two stresses satisfy the essential condition of low scatter in strain/time curves at the two temperatures, they bear no similarity to each other in terms of rupture life or minimum creep rate.

The constant strain rate tensile and constant load creep tests described so far have all been performed on the 'as received' material. The effects of different heat treatments prior to testing were not considered. However, in the proposed method of preparation of cracked test pieces, the material will be strained at a temperature of 500 deg.C. It was necessary, therefore, to show the effect of heating alone on the creep properties. A creep test piece was heated at a temperature of 500 deg.C. for 24 hours and was then allowed to air cool (tensile straining of creep test pieces would take less than 24 hours). The strain/time curve of this test piece at 500 deg.C. and 1.38 N/mm^2 shows that the heat treatment has had no effect, (curve 73 in Figure 6.12). However, the repetition of this test at 250 deg.C. and 27.60 N/mm^2 produced a strain/time curve with a much greater minimum creep rate than that of similar tests on the 'as received' material. Consequently, a series of creep tests were performed at this stress and temperature on the heat-treated aluminium. Different periods of heating at 500 deg.C. were employed to show if time had any effect. The strain/time curves are presented in Figure 6.19 and the time periods of the heating at 500 deg.C. were:

Curve No.	70	89	75	72	74
Time (hours)	1	1	12	24	24

Figure 6.19 shows that scatter in the strain/time curves of

the heat-treated material is low and that different periods of heating of 1 – 24 hours have no effect. Since test pieces in constant strain rate tensile tests are soaked at 500 deg.C. for $1\frac{1}{4}$ hours before straining, creep test pieces which are pre-strained at that temperature to produce intergranular discontinuities, will also be in the above heat-treated condition. Hence, comparison of creep properties may only take place between the cracked material and the virgin material which has been heat-treated at 500 deg.C. for 1 – 24 hours.

The stress and temperature conditions selected for the study of the effect of intergranular cracks on creep properties were :-

1) 27.60 N/mm^2 and 250 deg.C., where the annealed material has a minimum creep rate of 0.005 pct/h and a rupture life of approximately 300 hours, and
2) 1.38 N/mm^2 and 500 deg.C., where the annealed material has a minimum creep rate of 0.156 pct/h and a rupture life of approximately 50 hours.

The rupture lives of 1) and 2) are in the ratio 6 : 1 and the minimum creep rates 1 : 30. When comparing the relative effects of intergranular discontinuities under the above conditions, these ratios must be kept in mind.

6.7 Fracture Behaviour

6.7.1 High Temperature Fracture : 500 deg.C.

Three tests were allowed to continue until fracture occurred. These were at stresses of 1.38 N/mm^2, 2.26 N/mm^2 znd 3.65 N/mm^2. The strain/time curves for the three tests are shown in Figures 9.5, 10.6, and 6.10 respectively. Figure 6.20 is a photograph comparing the profiles of the fracture surfaces and illustrates the rapid change in nature of the failure over a small stress range. Table 6.1 presents the creep rupture data:—

Table 6.1

Stress N/mm^2	Rupture Life h	Strain at Fracture pct	Reduction of Area at Fracture pct
3.65	1.17	77.5	99.3
2.26	8.40	51.0	59.0
1.38	53.50	85.5	47.7

Figure 6.20 shows the high stress fracture to be typically ductile with the gauge diameter necking to a point before final failure. Density measurements, (described later), showed that the growth of intercrystalline discontinuities at this stress was almost negligible until the onset of localised necking. The fractures at the two lower stresses indicate an intercrystalline mode of failure and, indeed, density measurements (Chapter VIII) at these two stresses produced evidence of the rapid growth of internal discontinuities. The appearance of cracks on the gauge surface of the specimen, fractured at the lowest stress (1.38 N/mm^2), occurred along the whole gauge length, but were more prominent around the fracture surface. In this specimen, the amount of localised necking in the fracture area was negligible.

An interesting feature of these fracture tests was the

large elongation at the lowest stress. Although internal discontinuities were developing rapidly throughout the creep life, the effect on the material was not catastrophic. The results infer that stress concentrations due to intercrystalline cracks at high temperatures in Aluminium have little effect on the creep properties. However, it has already been surmised in the previous section (6.6) that formation of cavities is one factor causing the rapidly increasing creep rate observed. The point is that the cavities do not restrict further deformation of the material and hence cause premature failure. A method of testing this hypothesis would be to creep test specimens with small amounts of cavities already present in the grain boundaries. These tests were performed and are described in a subsequent Chapter.

6.7.2 Low Temperature Fracture : 250 deg.C.

Figure 6.21 shows the fracture surface profiles of three tests that were allowed to continue until failure. The three stresses were 45.35 N/mm^2, 61.50 N/mm^2 and 76.65 N/mm^2, and Figure 6.14 shows their strain/time curves on a double logarithmic plot. The creep rupture data for the tests, which were conducted using the 'as received' material, are presented in Table 6.2.

Table 6.2

Stress N/mm^2	Rupture Life h	Strain at Fracture pct	Reduction of Area at Fracture pct
76.65	0.53	19.0	58.7
61.50	4.02	15.7	52.3
45.35	45.55	13.0	41.8

Comparison with Table 6.1 shows that, although a narrower range of stress was employed at 250 deg.C., the rupture lives had a similar spread to those at the higher temperature. Figure 6.21 demonstrates that the mode of failure at 250 deg.C.

becomes more intergranular in nature as the stress decreases, although the fracture surfaces of all three had the 'honeycomb' appearance of intercrystalline failure. The creep rupture data of Table 6.2 confirm this trend, with lower elongations and reductions of area as the stress decreases. However, whereas the reductions of area at 250 deg.C. and 500 deg.C. are similar, the elongations at 250 deg.C. are much less than those at 500 deg.C. These results confirm the observation in Figure 6.21 that the deformation is mainly confined to regions of localised necking. The inference is that internal discontinuities develop in the neck and sudden failure occurs due to the coalescence of the discontinuities or to the propagation of one particular crack across the gauge diameter. Either way, stress concentrations do seem to have a large effect on the creep properties and this effect becomes more important as the stress and, therefore, strain rate decreases. This latter point suggests that the development of cavities is strongly time dependent.

Further investigation of the possible effect of discontinuities could be achieved by performing a similar series of tests to those already suggested for the study of the effect of holes at 500 deg.C. Test pieces with internal discontinuities already present would be creep tested at 250 deg.C. The above results suggest that the effect at 250 deg.C. will be much greater than that at 500 deg.C. The tests at 250 deg.C. and 500 deg.C. are described later in Chapter IX.

6.8 Summary

Equipment has been developed for creep testing commercially pure aluminium over a wide range of stresses and at temperatures of up to 500 deg.C. From the results of repeated tests at a variety of stresses, two stresses, which produced low scatter strain/time curves and convenient testing periods, were chosen for the study of the effect of holes on the creep curve. These stresses were 1.38 N/mm^2 at 500 deg.C. and 27.60 N/mm^2 at 250 deg.C.

Two methods of applying load to the test piece were investigated. One, the conventional screw grip method, gave satisfactory results at both temperatures of interest. The other, a universal joint between test piece and pull rod, proved difficult to use at high temperatures (500 deg.C.) due to corrosion problems. The results from universal joint specimen tests were no better than those from screw grip tests. However, since only a few comparative tests were carried out, no definite general conclusions about the benefits of the universal joint test piece can be made.

Some interesting conclusions regarding the effect of intercrystalline cracks on the creep curve have been formulated and await further verification. At 500 deg.C., it is postulated that grain boundary cavities, although making intergranular deformation easier and hence creep rate higher, do not have a catastrophic effect on the material, since elongation at fracture was greater at stresses where cavitation did appear than at stresses where it did not. However, at 250 deg.C., the situation is different. At that temperature, holes apparently grow in the regions of localised necking and cause catastrophic failure when they coalesce or when one of them propagates across the width of the test piece.

Slow tensile testing at 500 deg.C. provided a method of preparing creep test pieces with a controlled amount of intercrystalline cracking, measured accurately by density measurements. Now that suitable stresses producing low

scatter creep curves in reasonable times have been obtained, the next stage of the project can begin : creep testing test pieces previously given controlled amounts of intercrystalline discontinuities. However, before going on to describe those tests, more information on Rate Sensitivity and the development of intercrystalline cracks during creep will be presented.

APPENDIX 6.1

Error in Strain Measurement

1) Measurement by average strain on 3 pairs of divider points:

$$\text{Strain, } \varepsilon = \frac{L - Lo}{Lo}$$

where Lo is original gauge length and L is the strained gauge length.

Taking natural logarithms of both sides of above equation,

$$\ln \varepsilon = \ln(L - Lo) - \ln Lo$$

and differentiating,

$$\frac{\partial \varepsilon}{\varepsilon} = \frac{\partial(L - Lo)}{(L - Lo)} - \frac{\partial Lo}{Lo}$$

Partial differentials may be replaced by small increments of the measured quantity with prefix δ denoting a small increment.

$$\frac{\delta \varepsilon}{\varepsilon} = \frac{\delta L - \delta Lo}{L - Lo} - \frac{\delta Lo}{Lo}$$

This equation may then be used to calculate the error $\delta\varepsilon$ in ε arising from the errors δL in L and δLo in Lo. Maximising errors,

$$\frac{\delta \varepsilon}{\varepsilon} = \frac{\delta L + \delta Lo}{L - Lo} + \frac{\delta Lo}{Lo}$$

and

$$\delta \varepsilon = \frac{\delta L + \delta Lo}{Lo} + \varepsilon \frac{\delta Lo}{Lo} \qquad \text{(a)}$$

Original gauge length, Lo = 45.70 $\pm$ 0.05 mm and therefore $\delta Lo = \pm 0.05$ mm = δL.

Hence, from equation (a),

$$\delta \varepsilon = 0.002 + 0.001\, \varepsilon$$

Therefore, for strains less than 0.5, error in strain measurement is $\pm$ 0.002 and for strains 0.5 to 1.5, error is $\pm$ 0.003.

2) Measurement by linear displacement transducers:

$$\text{Strain, } \varepsilon = \frac{\frac{A + B}{2} - \frac{Ao + Bo}{2}}{Lo} = \frac{A + B - Ao - Bo}{2Lo}$$

where Ao and Bo are the original transducer readings ($\pm$ 0.001 mm), A and B are the transducer readings after straining ($\pm$ 0.001 mm) and Lo is the original gauge length (= 45.70 $\pm$0.05 mm).

Applying a similar analysis to that in 1),

$$\delta\varepsilon = \frac{\delta Ao + \delta Bo + \delta A + \delta B}{2Lo} + \varepsilon \frac{\delta Lo}{Lo}$$

and $$\delta\varepsilon = 0.00004 + 0.001\ \varepsilon$$

Therefore, for strains of the order 0.001, error is $\pm$ 0.00005; for strains less than 0.1 error is $\pm$ 0.0001; and for strains 0.1 to 1 error is $\pm$ 0.001.

APPENDIX 6.1

Error in Applied Stress

$$\text{Applied stress, } \sigma = \frac{4P}{\pi d^2} \quad N/mm^2$$

where P is applied load in newtons and d is the test piece diameter in millimeters.

Applying the same analysis as in 1),

$$\frac{\delta\sigma}{\sigma} = \frac{\delta P}{P} + 2\frac{\delta d}{d}$$

where prefix δ denotes error in measured quantity. Specified diameter of test piece was 9.067 mm. (0.357 in.) and actual diameter was found to vary by $\pm$ 0.025 mm. along the gauge length. Therefore, $\delta d = \pm$ 0.025 mm. and,

$$2\frac{\delta d}{d} = 0.0055$$

For creep tests at 250 deg.C., estimated error in weights on load pan = 10g = $\pm$ 0.1 N.

Therefore error in applied load $\delta P = \pm$ 1 N.

For creep tests at 500 deg.C. and stresses 0.87 – 4.99 N/mm^2, estimated error in weights on load pan = $\pm$ 5g = $\pm$ 0.05 N.

Therefore error in applied load $\delta P = \pm$ 0.5 N.

For creep tests at 500 deg.C. and stresses 0.35 and 0.61 N/mm^2, applied load was the dead weight of pull rod, etc., and error in applied load, $\delta P = \pm$ 0.1 N, approximately. However, since the weight of thermocouple cables and transducer cables may have been significant at these low stresses, error in applied load was considered to be $\pm$ 0.5 N.

The estimated errors in applied stress σ have been tabulated below :-

Stress (N/mm^2)	$\frac{\delta\sigma}{\sigma}$	$\delta\sigma$ (N/mm^2)
76.65	0.0057	0.44
61.50	0.0058	0.36
45.35	0.0058	0.26
27.60	0.0061	0.17
17.91	0.0064	0.11
10.00	0.0071	0.07
4.99	0.0071	0.04
3.65	0.0076	0.03
2.26	0.0089	0.02
1.38	0.0111	0.02
0.87	0.0144	0.01
0.61	0.0172	0.01
0.35	0.0276	0.01

APPENDIX 6.2

Increase of Creep Rate due to Thinning of Gauge Length in Constant Load Tests

For this calculation, the Power Creep Law was assumed to approximate behaviour of the creep rate over the small changes in stress encountered as the gauge length thins. This relationship was,

$$\frac{\dot{\varepsilon}}{\dot{\varepsilon}_o} = A \left(\frac{\sigma}{\sigma_o}\right)^n$$

where A is a parameter depending on temperature and structure (both assumed constant), $\dot{\varepsilon}$ is the creep rate and σ is the applied stress, n is a constant, $\dot{\varepsilon}_o$ is the creep rate corresponding to the reference stress σ_o.

Hence,

$$\dot{\varepsilon} = B\,\sigma^n \qquad \text{where } B = \frac{A\dot{\varepsilon}_o}{\sigma_o^n} \quad \text{(constant)}.$$

Therefore, for the one creep curve,

$$\left(\frac{\dot{\varepsilon}_1}{\dot{\varepsilon}_2}\right) = \left(\frac{\sigma_1}{\sigma_2}\right)^n = x \qquad (1)$$

where $\dot{\varepsilon}_2$ is the initial creep rate for initial stress σ_2 (in creep tests at 500 deg.C. there was no primary stage) and $\dot{\varepsilon}_1$ is the creep rate when stress increases to σ_1 as the gauge length thins.

Now, $\sigma_1 = \frac{4P}{\pi d_1^2}$ and $\sigma_2 = \frac{4P}{\pi d_2^2}$, where P is the applied load, d_2 the initial diameter and d_1 the diameter at stress σ_1.

Therefore,

$$\left(\frac{d_2}{d_1}\right) = x^{\frac{1}{2n}}$$

The strain along the gauge length, $\varepsilon_L = -2\,\varepsilon d$, where εd is the strain across the diameter, by the constant volume criterion of plastic deformation. Therefore,

$$\varepsilon_L = -2\,\frac{(d_1 - d_2)}{d_2} = 2\,\frac{(x^{\frac{1}{2n}} - 1)}{x^{\frac{1}{2n}}} \quad \text{by substitution.}$$

Value of ε_L for case in which creep rate doubles ie. x = 2 :-

n	2	4	6	8	10	15	20	25
ε_L (pct)	31.61	16.68	11.48	8.61	7.13	4.87	3.54	2.37

The values of n indicated for creep tests at 500 deg. C. (Figure 7.5) were 2 to 14 and, therefore, creep rate should double in the range 5 – 30 pct strain.

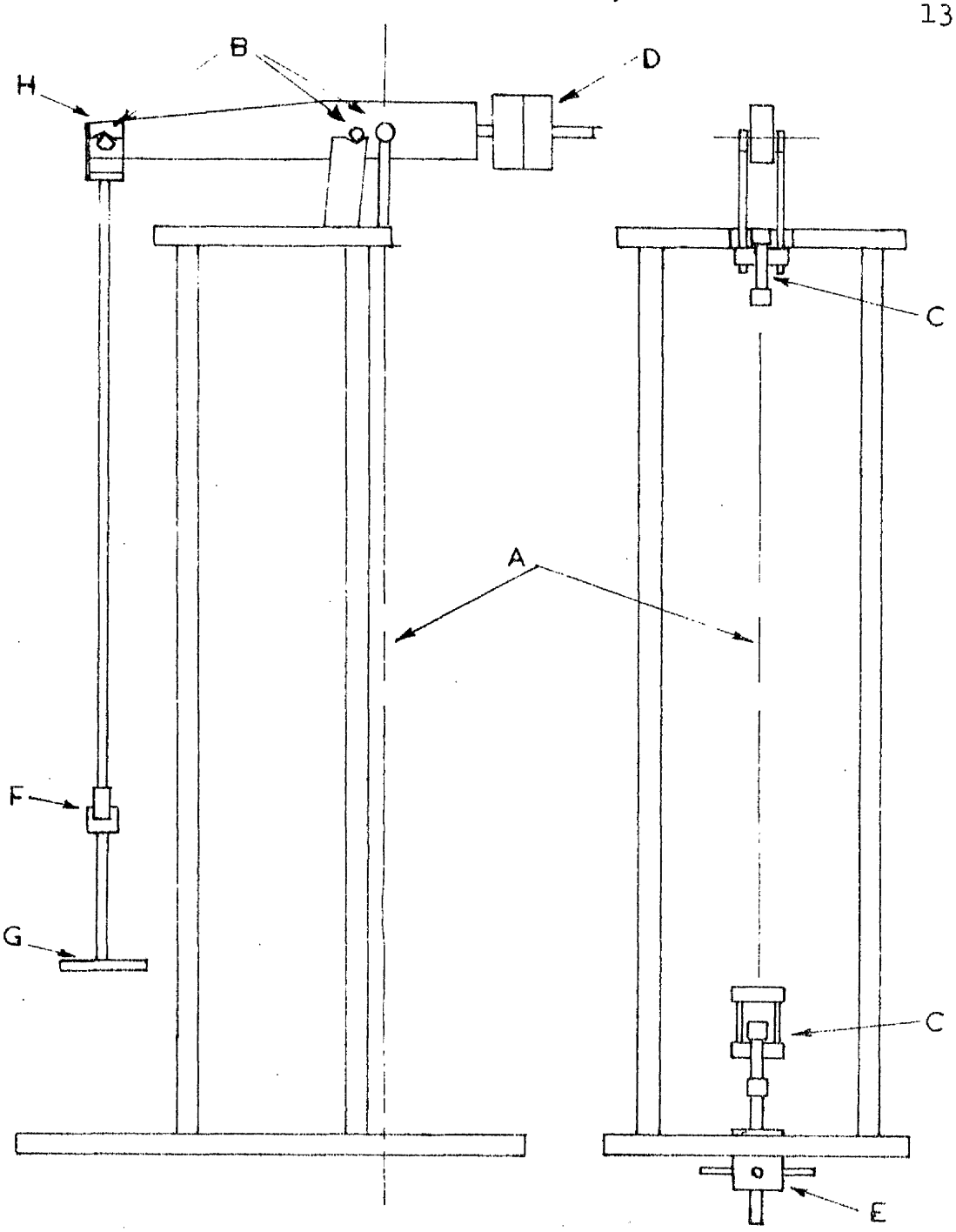

Figure 6.1 Diagram of Uniaxial Creep Machine

A	Axis of Loading	E	Capstan Arrangement
B	Collinear Knife Edges	F	Universal Joint
C	Ball Joints	G	Loading Pan
D	Beam Balance Weights	H	Knife Edge Saddle

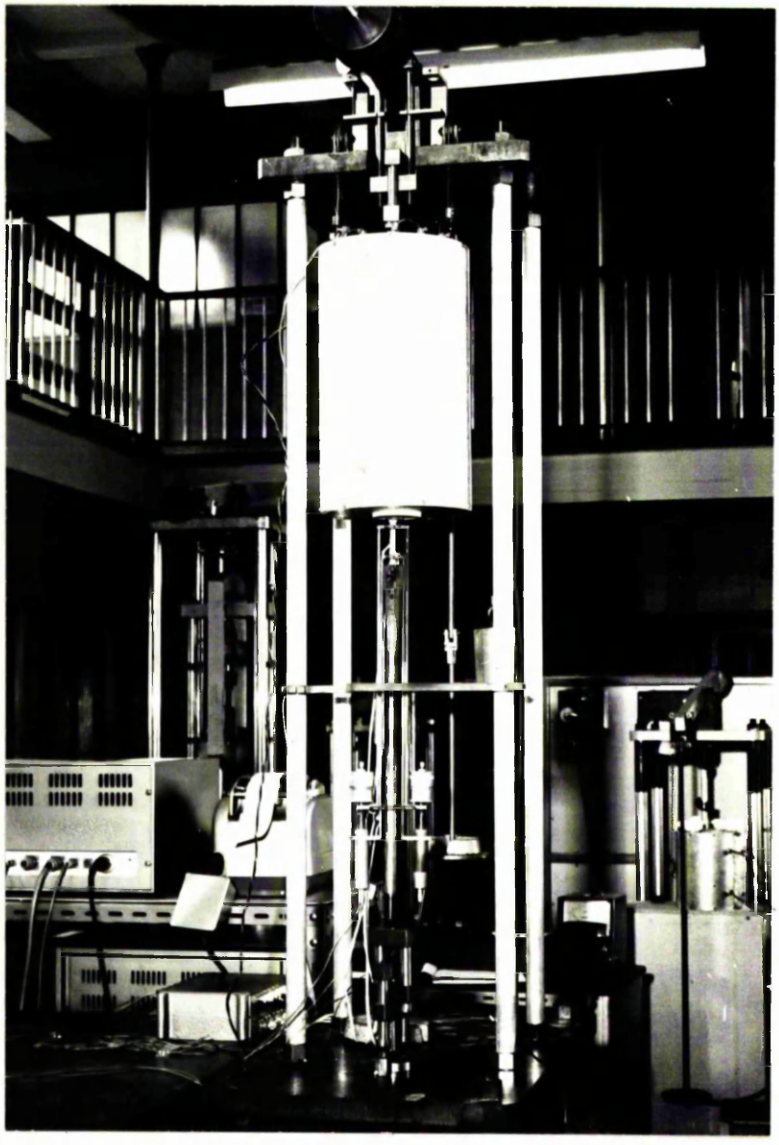

Figure 6.2 Uniaxial Creep Machine with furnace in the raised position. Screw grip test piece set up with pull rods and extensometry.

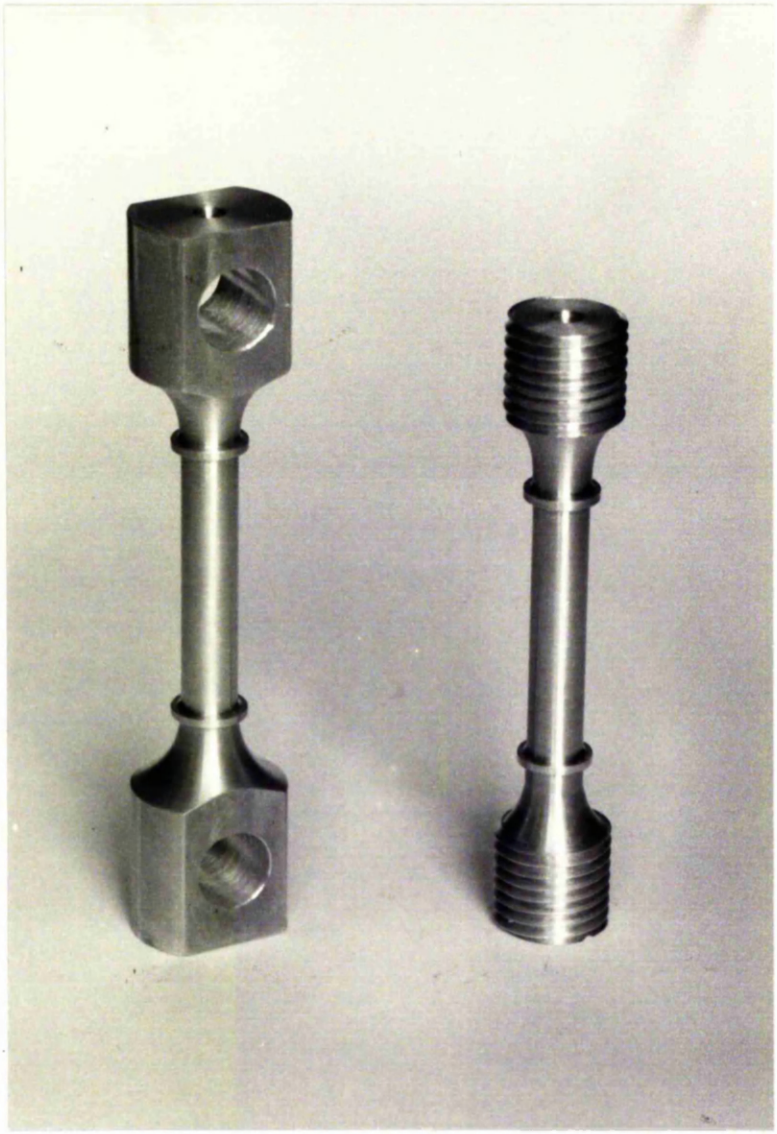

Figure 6.3 Universal Joint Test Piece (left) and Screw Grip Test Piece (right).

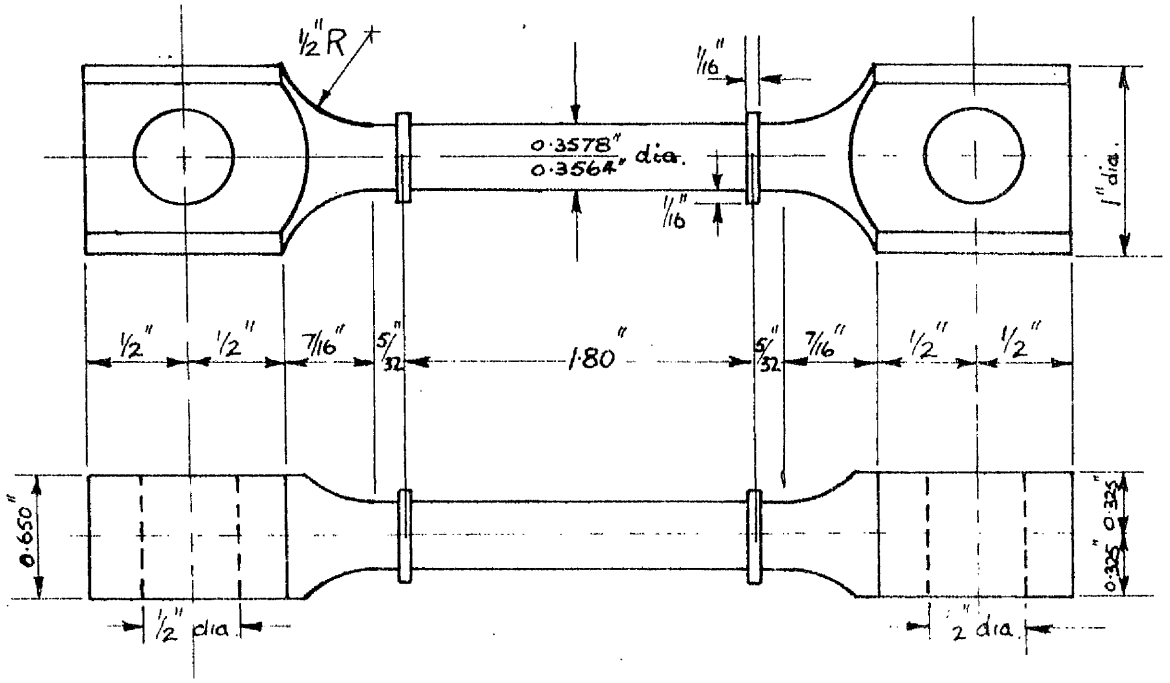

Figure 6.4 Universal-Joint Creep Test Piece

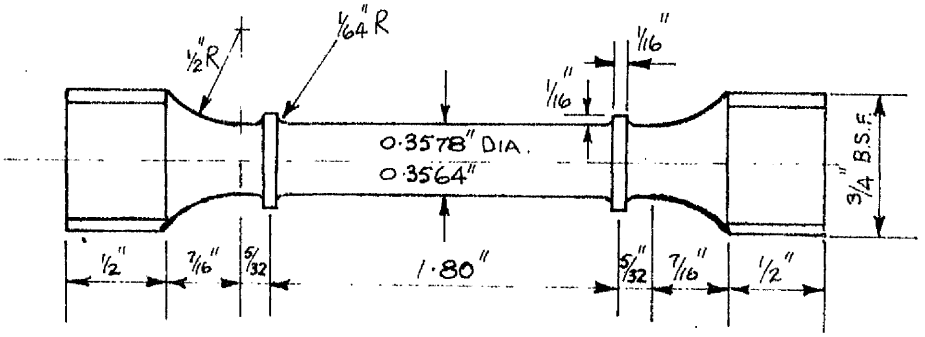

Figure 6.5 Screw-Grip Creep Test Piece

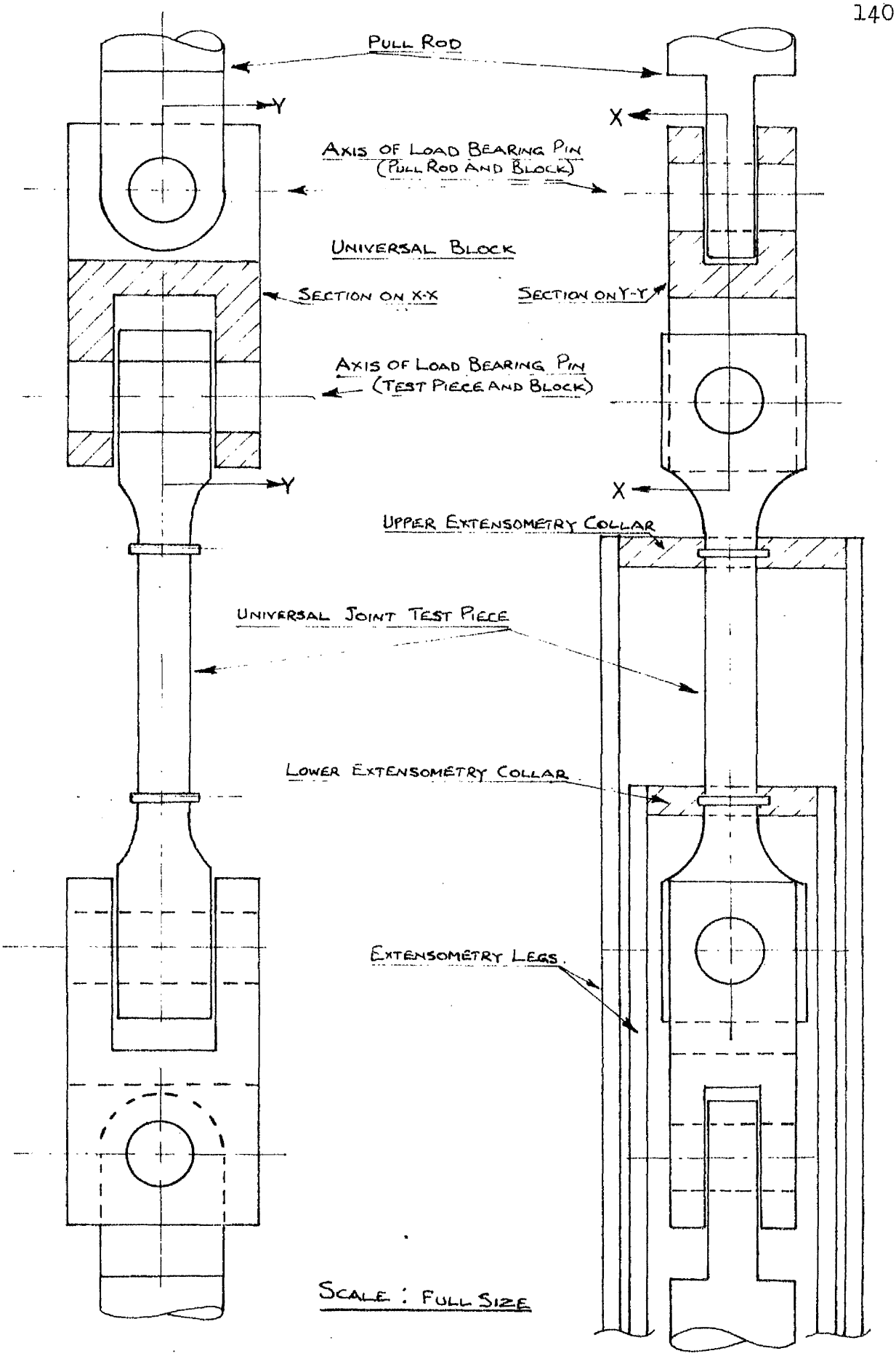

Figure 6.6 Assembly of Test Piece, Grips and Extensometry

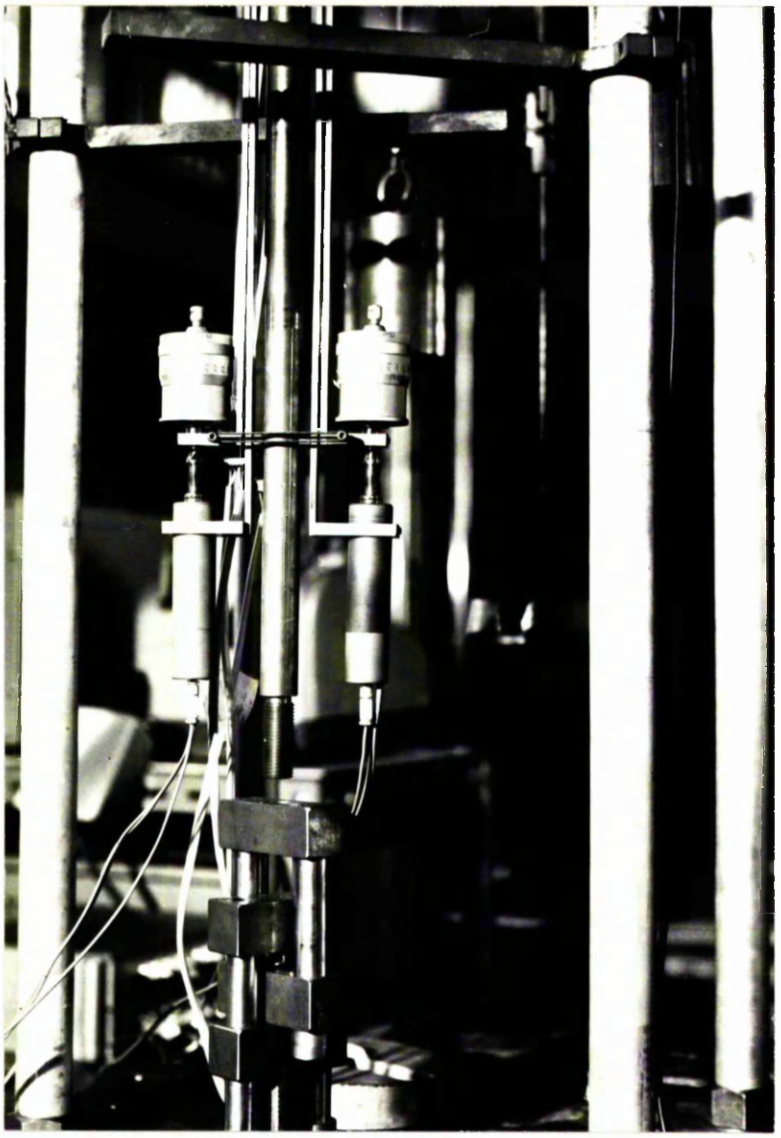

Figure 6.7 Arrangement of linear displacement transducers and micrometer heads, recording differential movement of extensometry legs.

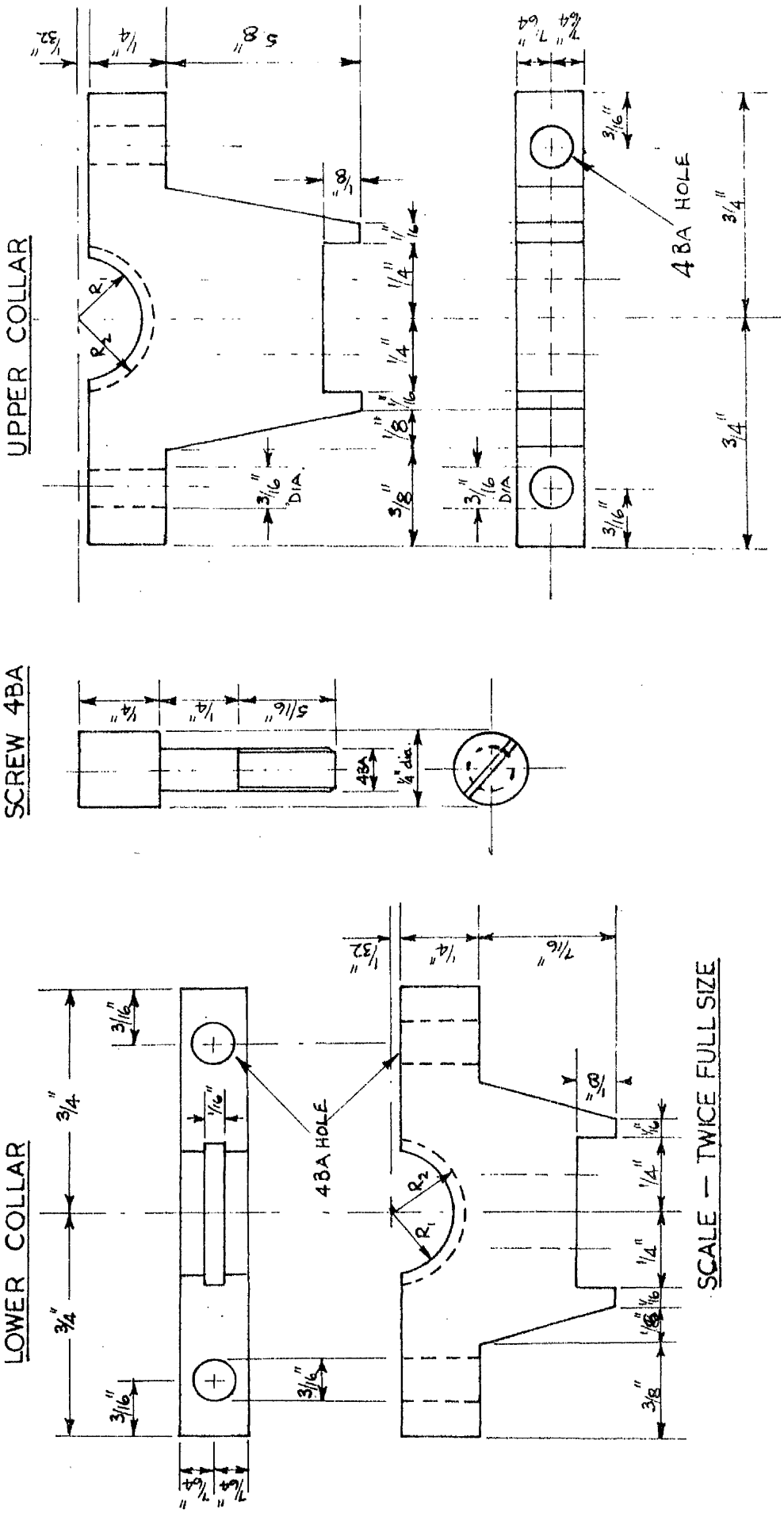

Figure 6.8 Details of Extensometry Collars

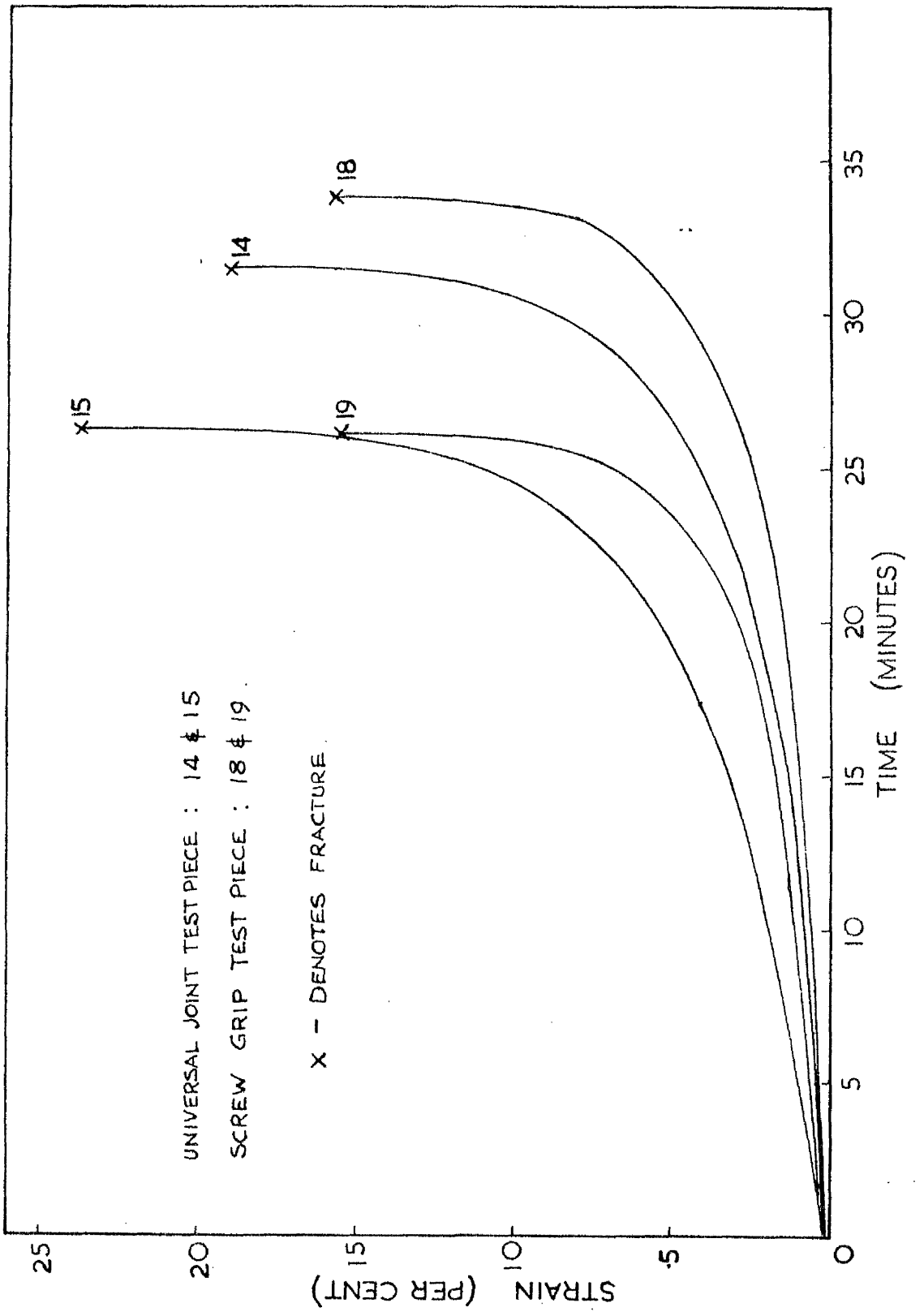

Figure 6.9 Constant load creep tests at 250 deg.C. and 76.65 N/mm^2; comparison of test pieces

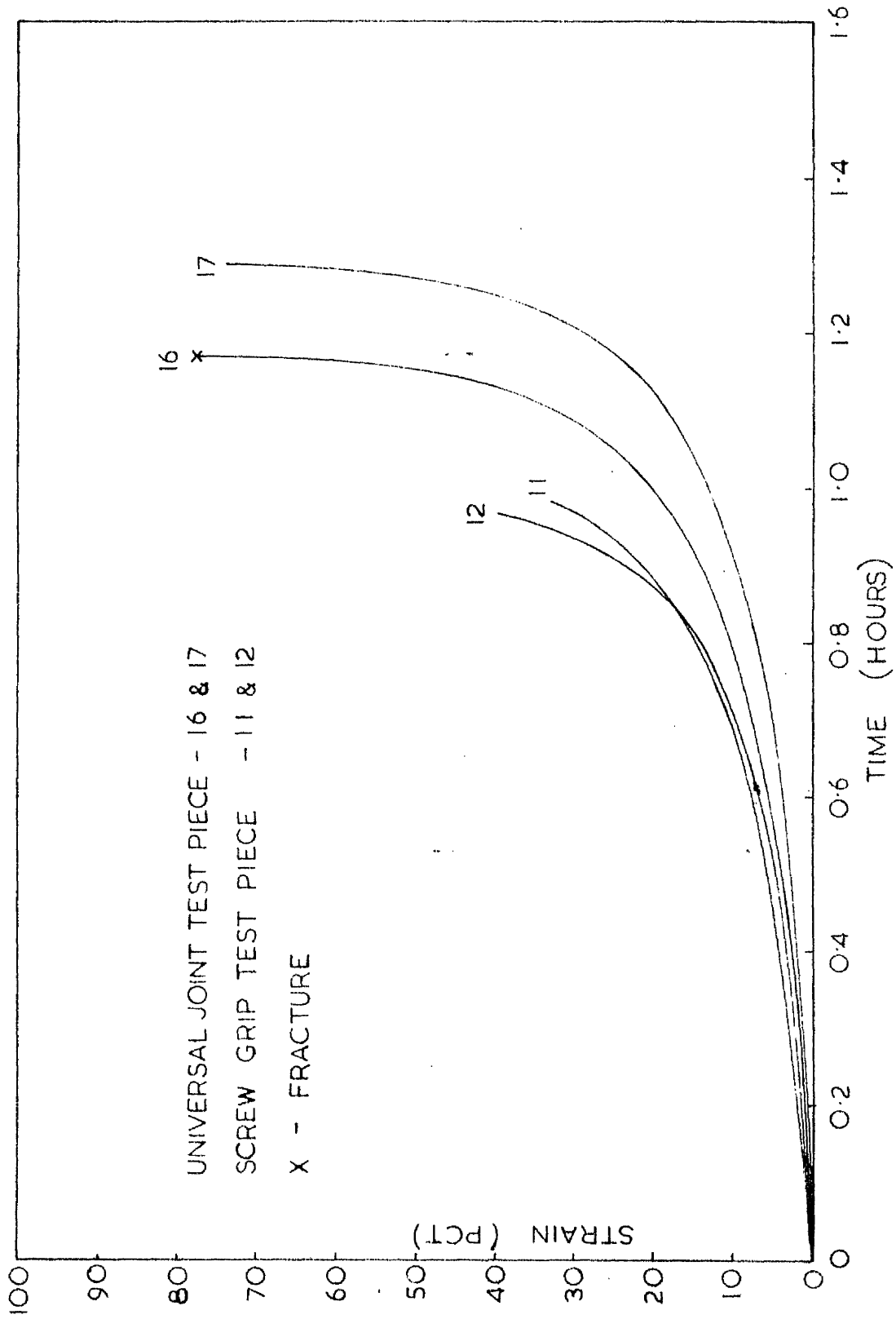

Figure 6.10 Constant load creep tests at 500 deg.C. and 3.65 N/mm^2; comparison of test pieces

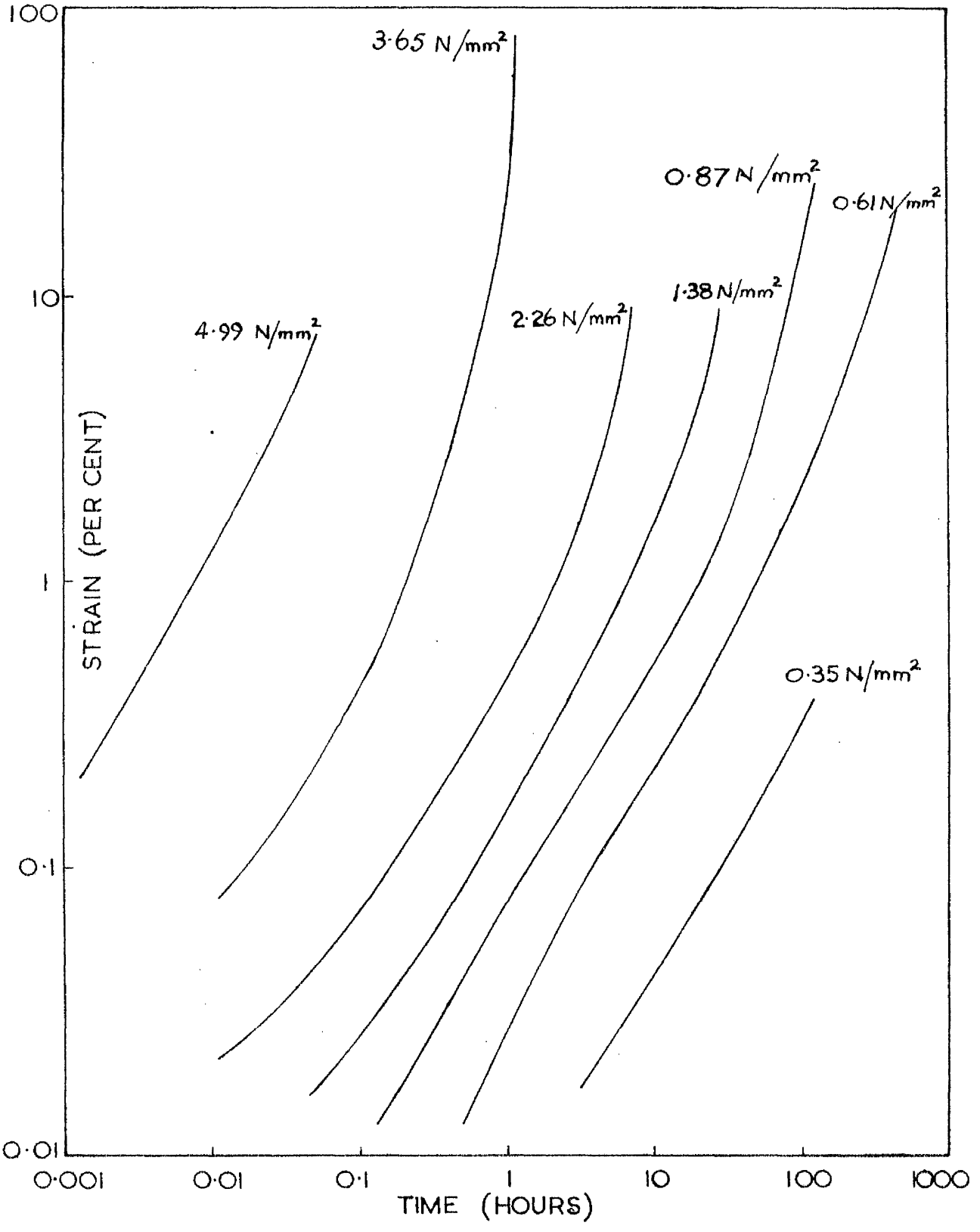

Figure 6.11 Constant load creep tests at 500 deg.C.; $\log_{10}$ (strain) against $\log_{10}$ (time)

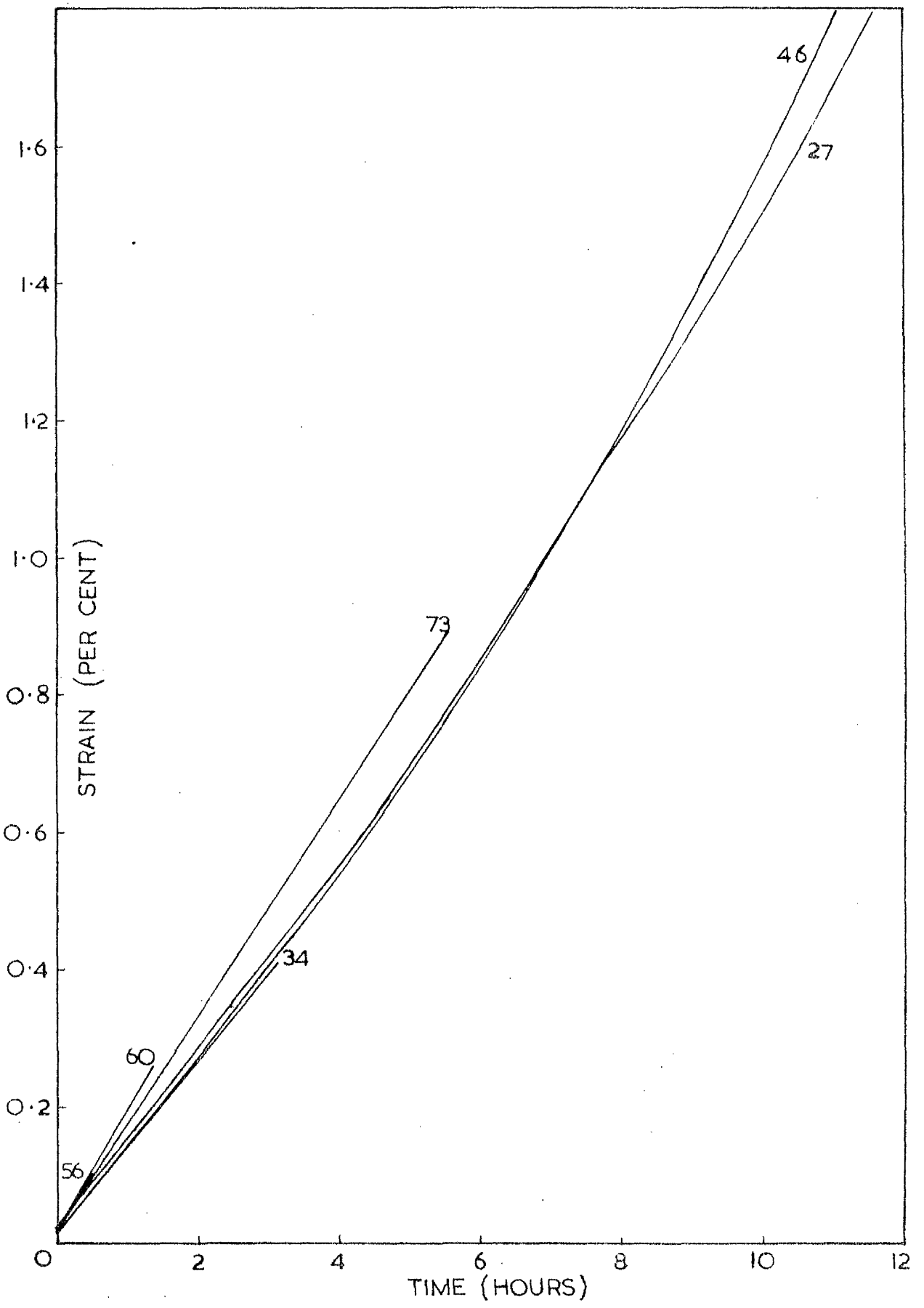

Figure 6.12 Constant load creep tests at 500 deg.C. and 1.38 N/mm^2

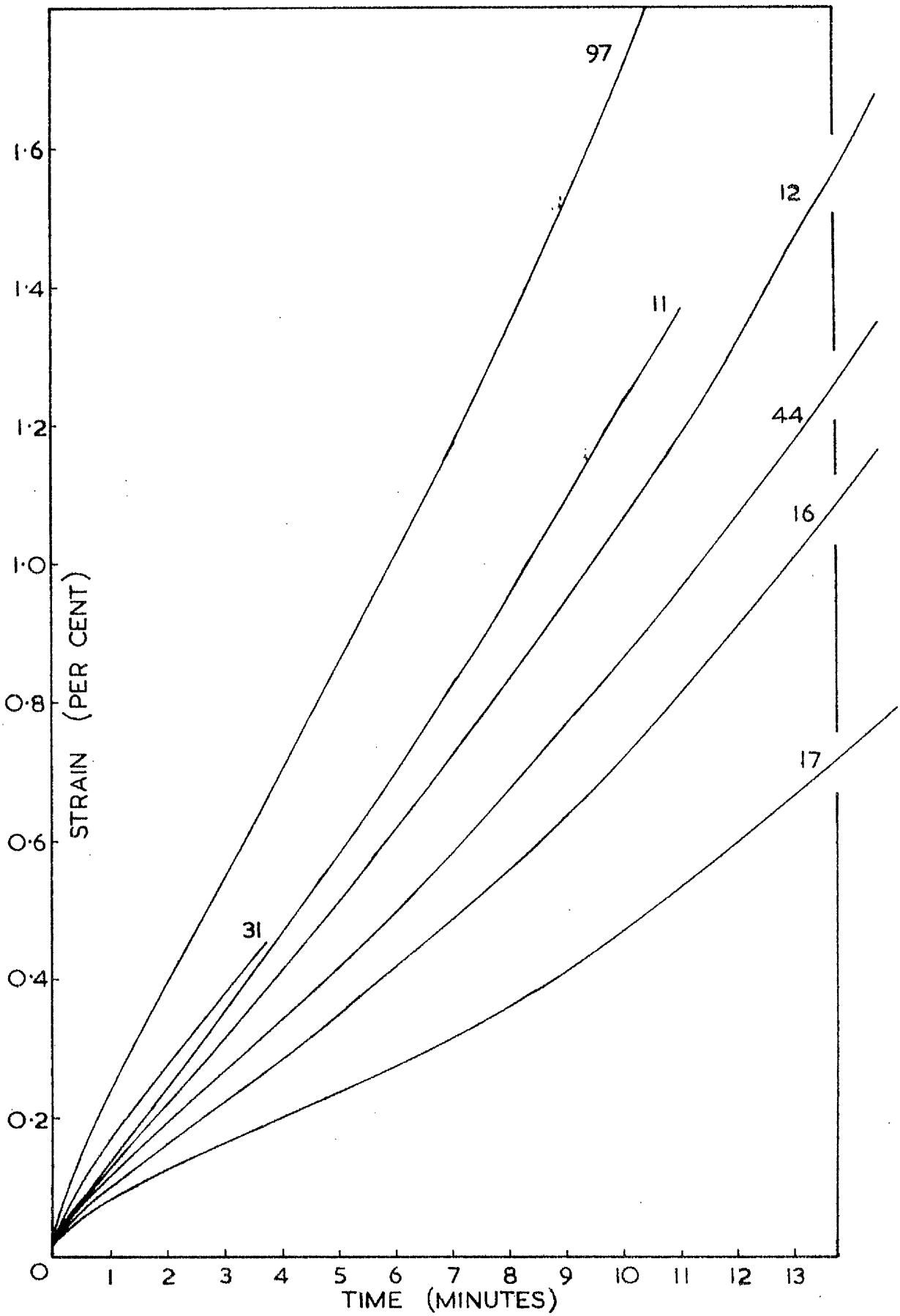

Figure 6.13 Constant load creep tests at 500 deg.C. and 3.65 N/mm^2

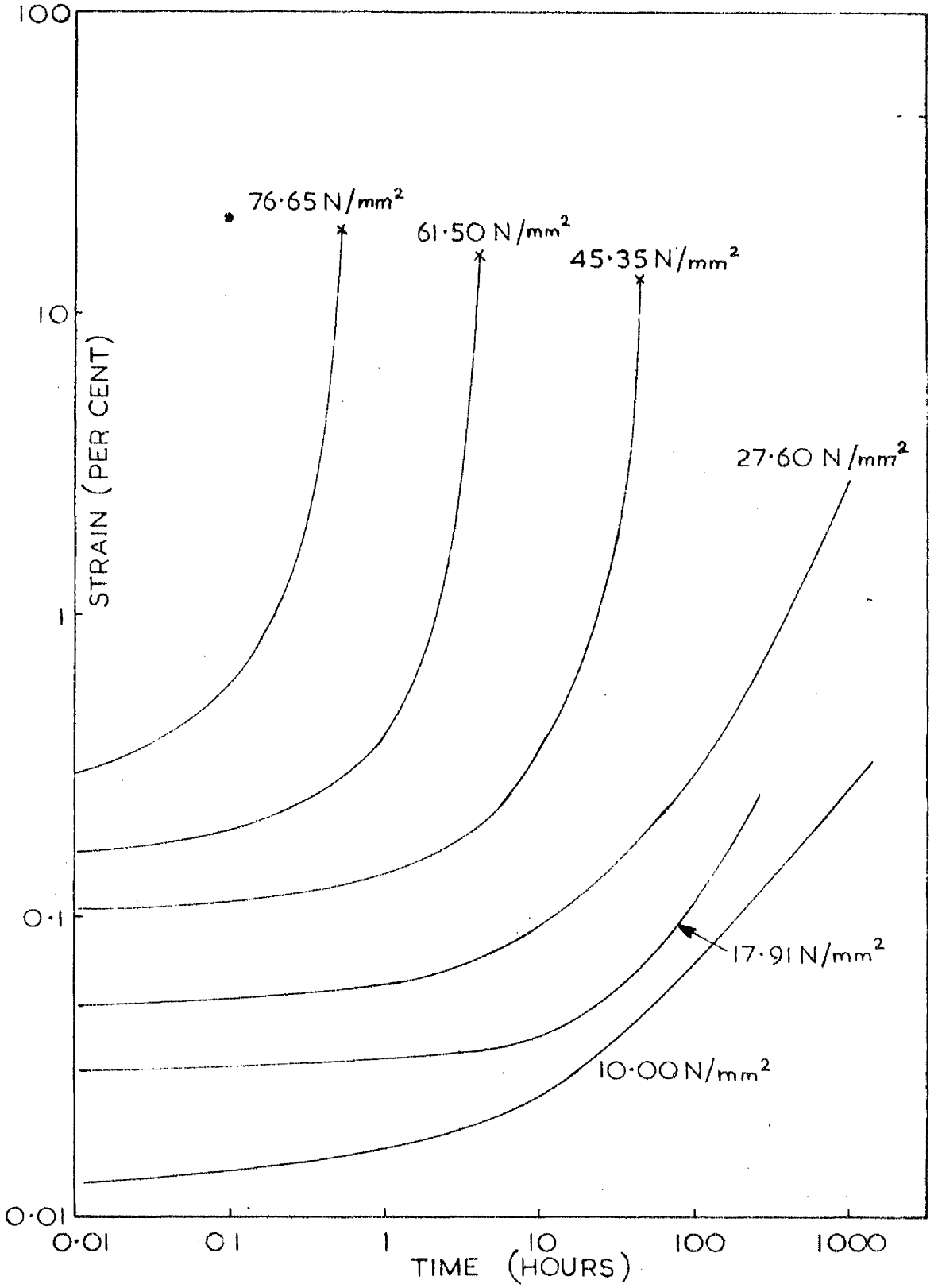

Figure 6.14 Constant load creep tests at 250 deg.C.; $\log_{10}$ (strain) against $\log_{10}$ (time)

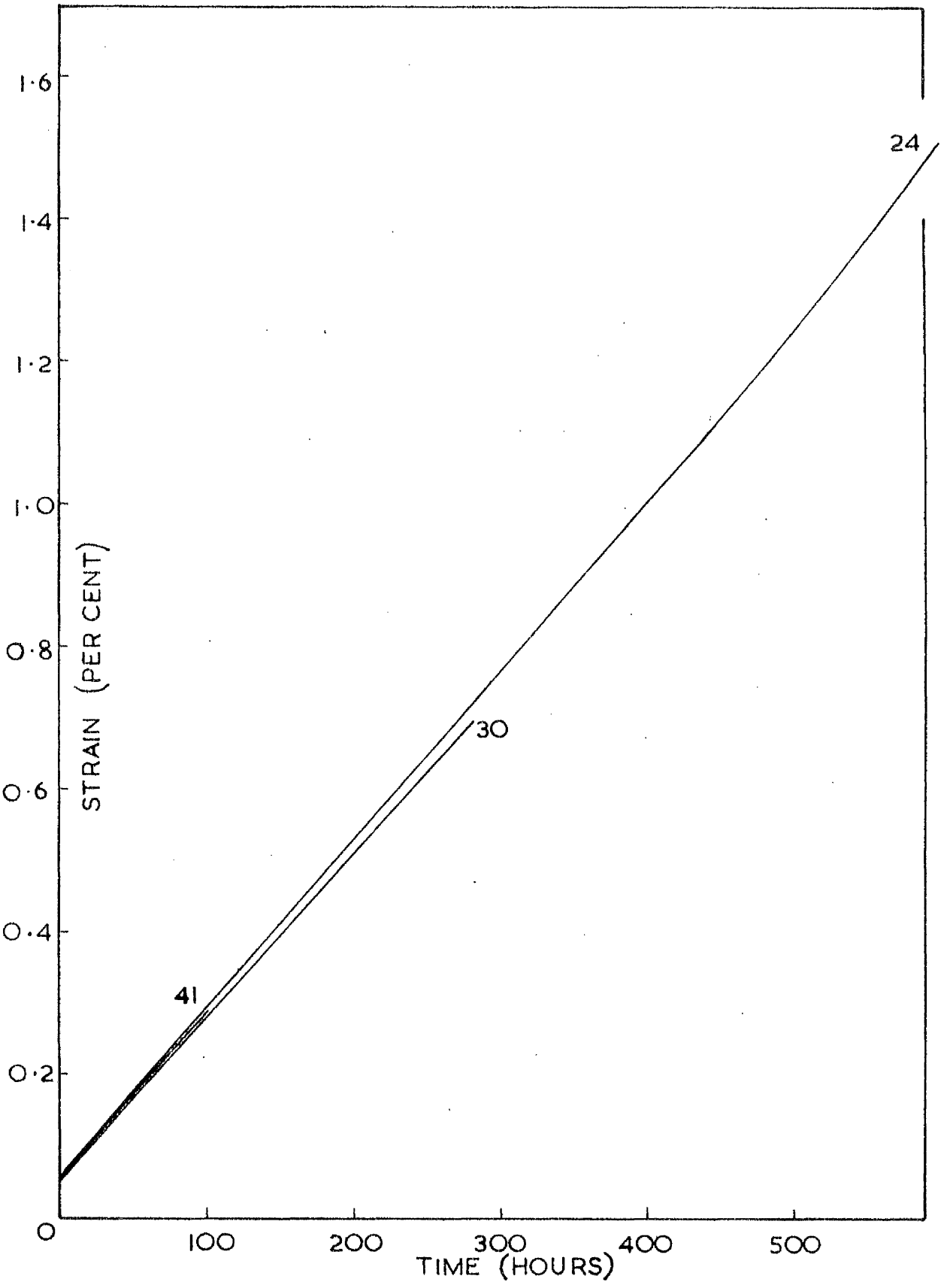

Figure 6.15 Constant load creep tests at 250 deg.C. and 27.60 N/mm^2

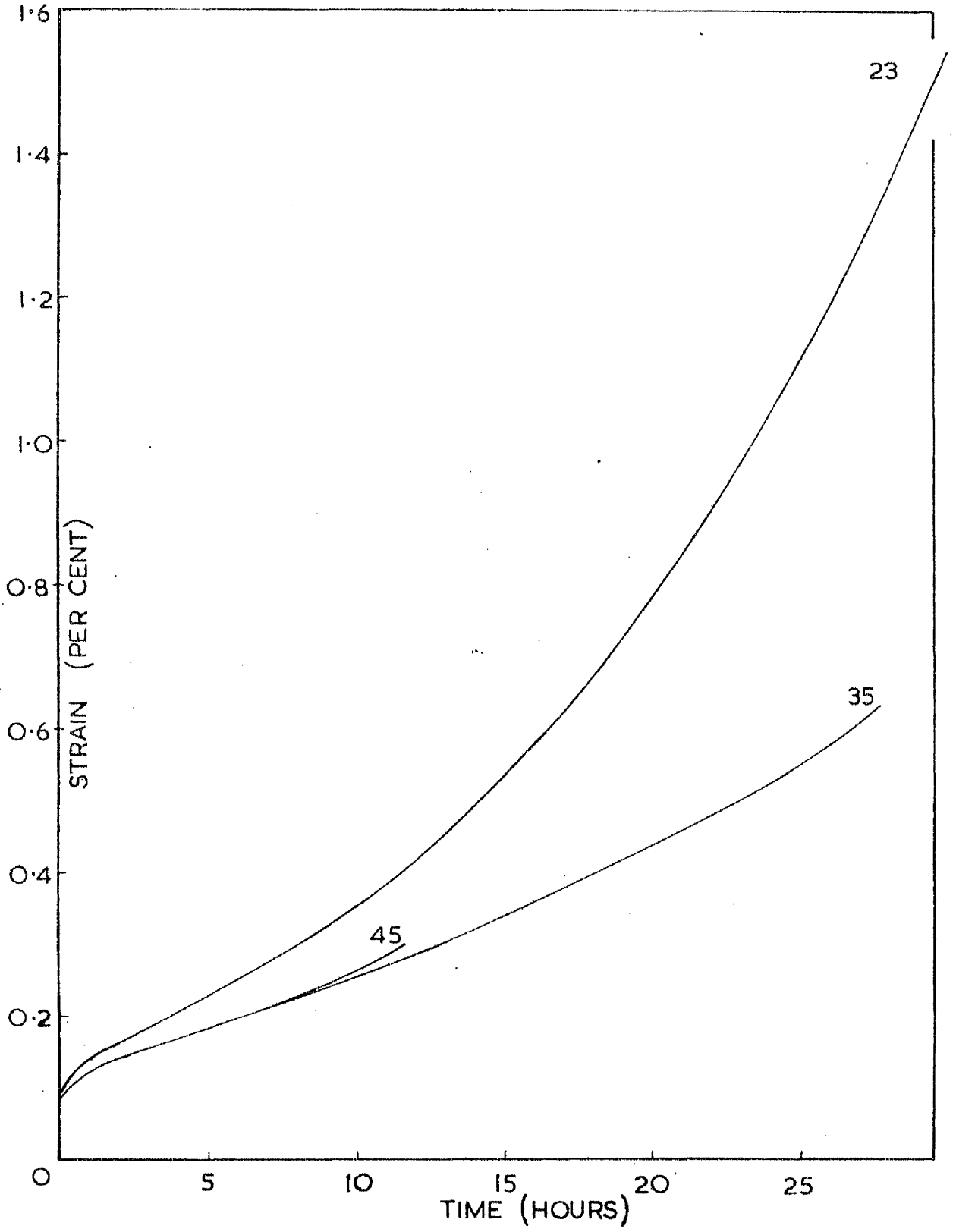

Figure 6.16 Constant load creep tests at 250 deg.C. and 45.35 N/mm^2

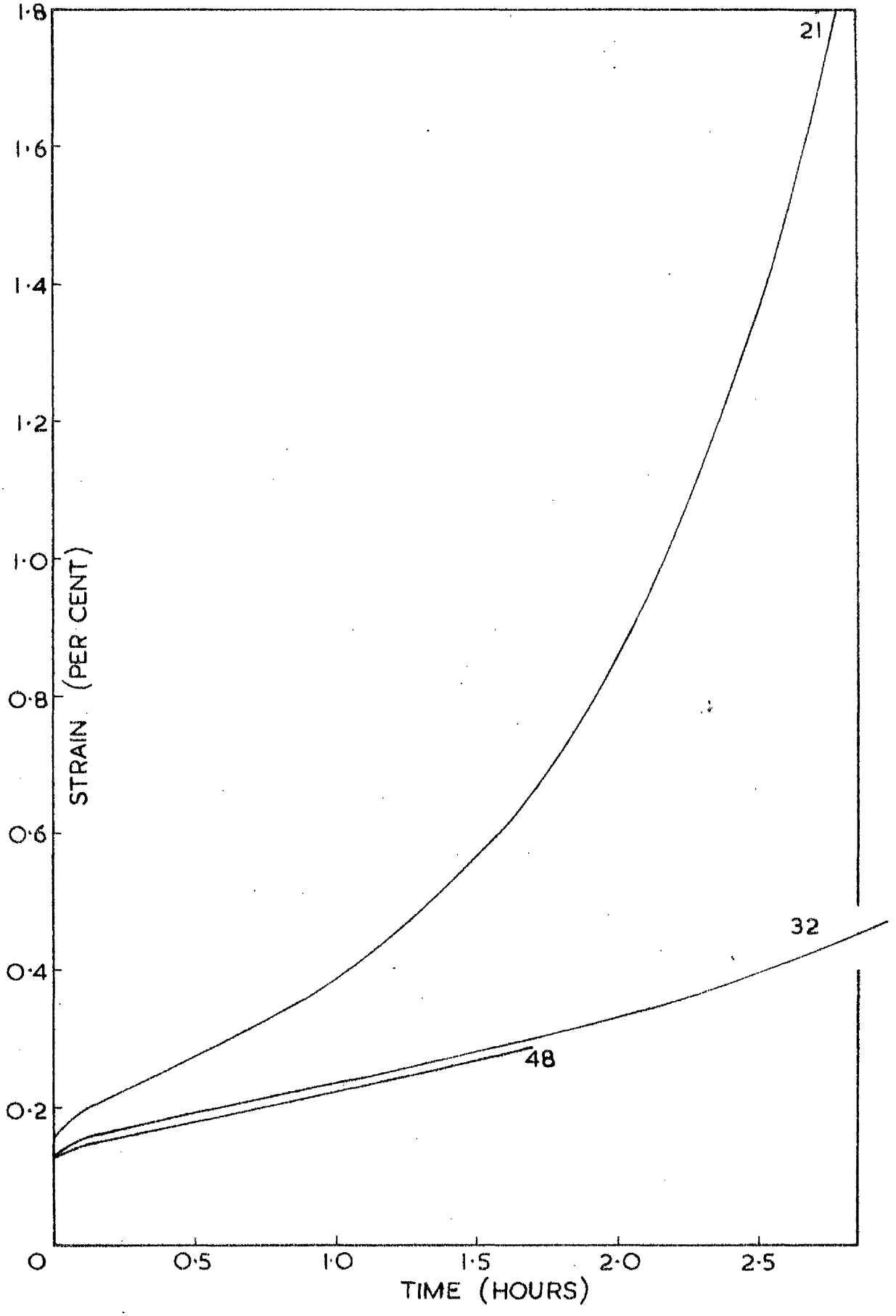

Figure 6.17 Constant load creep tests at 250 deg.C. and 61.50 N/mm^2

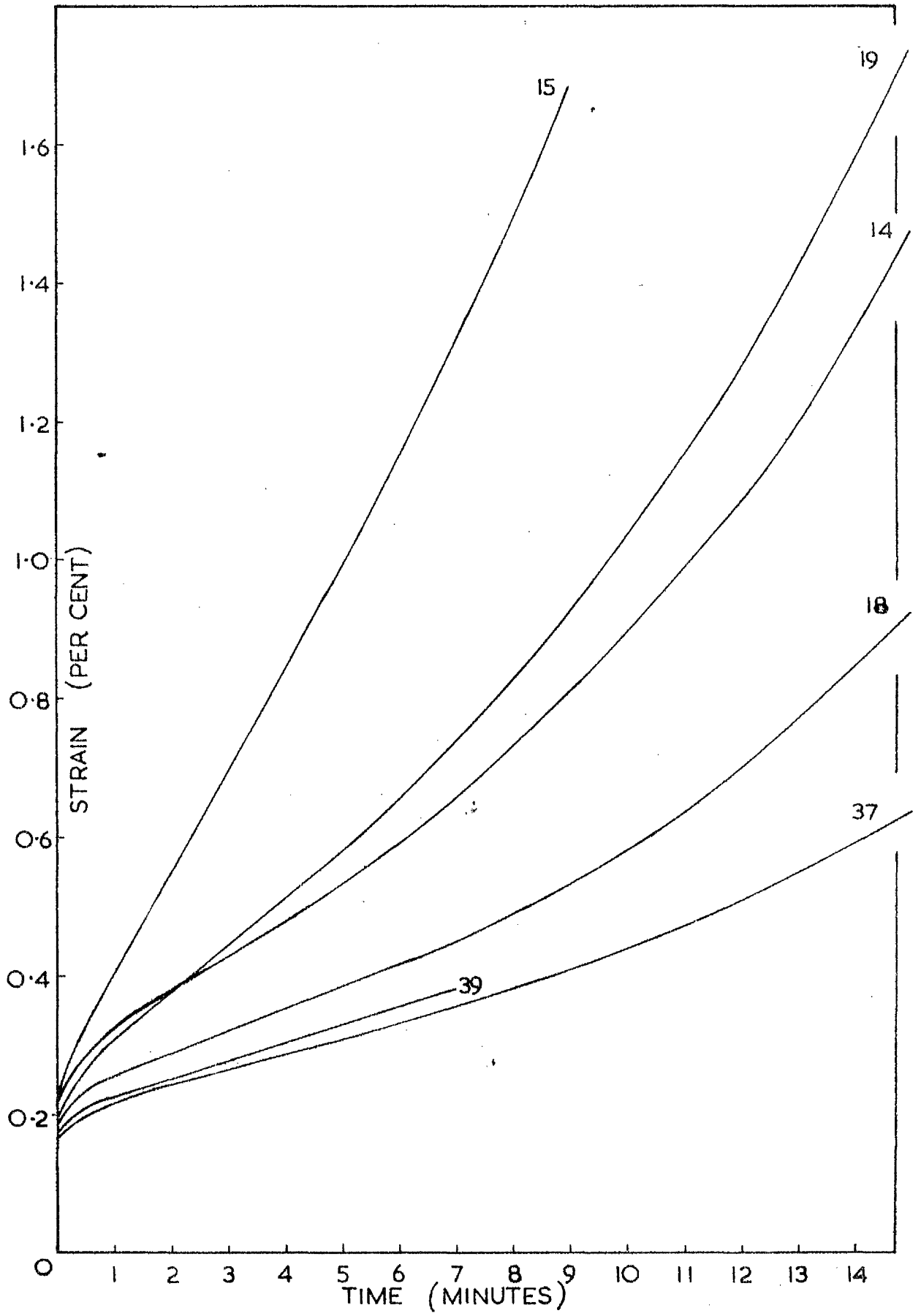

Figure 6.18 Constant load creep tests at 250 deg.C. and 76.65 N/mm^2

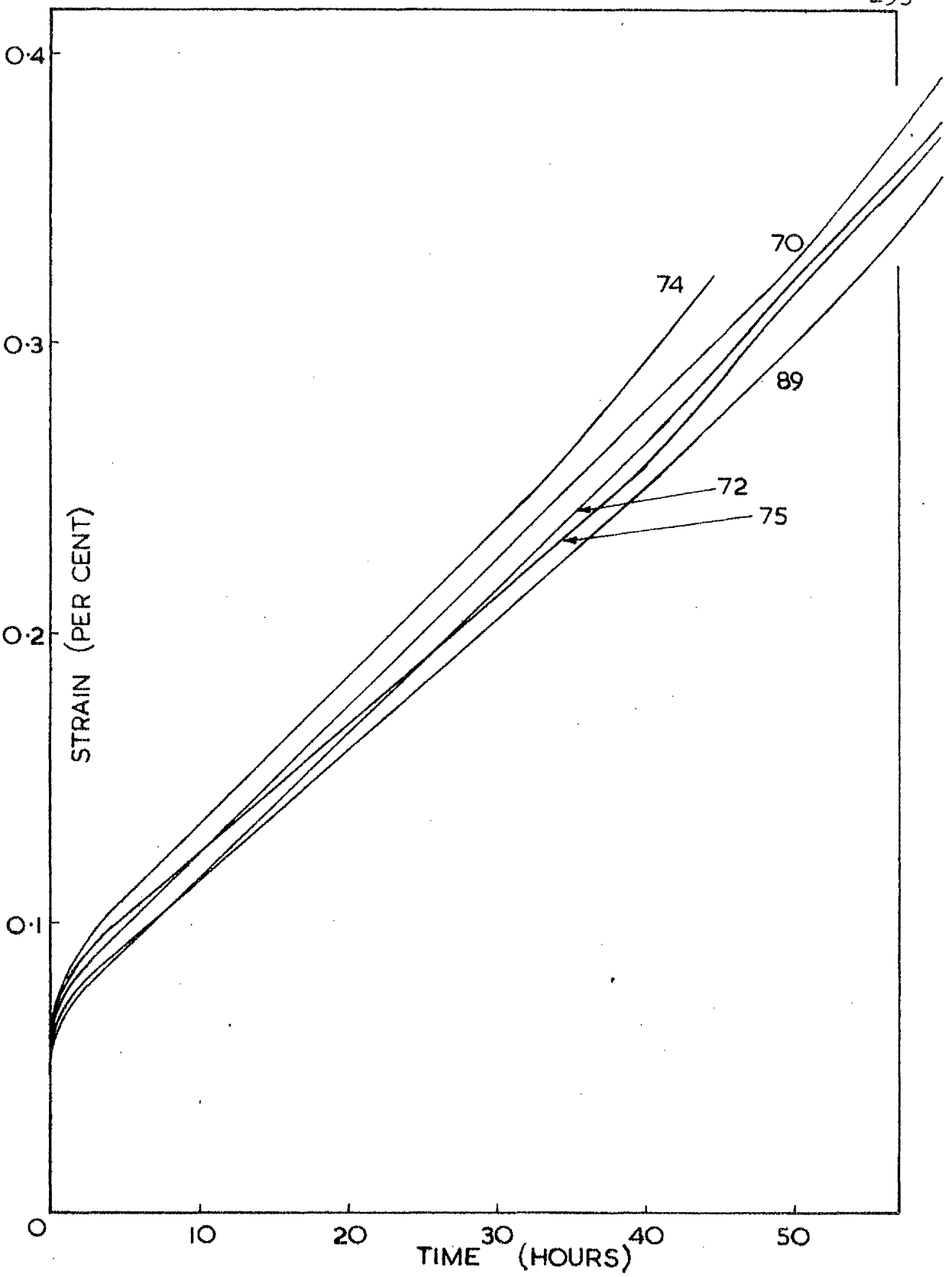

Figure 6.19 Constant load creep tests at 250 deg.C. and 27.60 N/mm^2 on test pieces annealed at 500 deg.C.

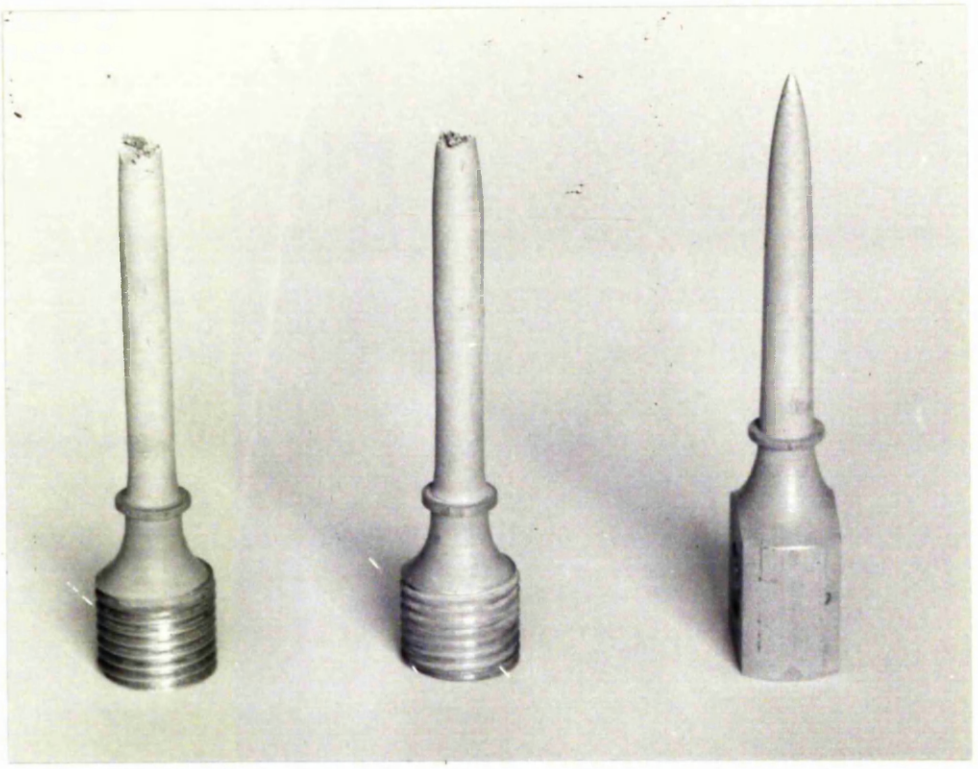

Figure 6.20 Fracture profiles : 500 deg.C. and stresses of 1.38 N/mm^2 (left), 2.26 N/mm^2 (middle) and 3.65 N/mm^2 (right).

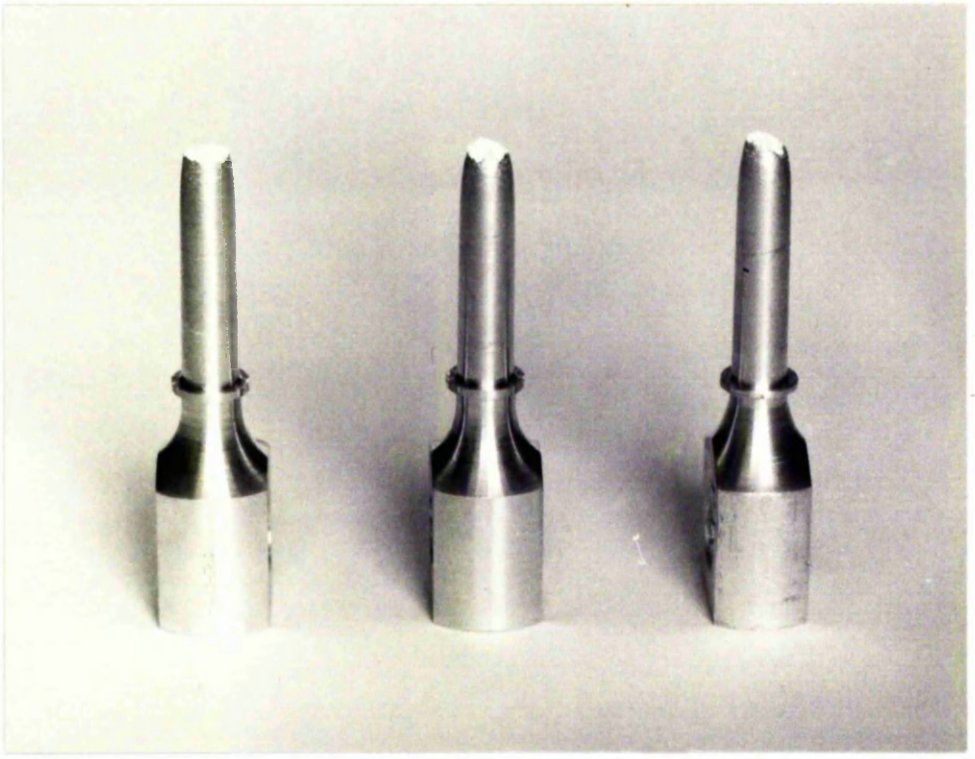

Figure 6.21 Fracture profiles : 250 deg.C. and stresses of 45.35 N/mm^2 (left), 61.50 N/mm^2 (middle) and 76.65 N/mm^2 (right).

CHAPTER VII

RATE SENSITIVITY : PART II

7.1 Introduction

In Chapter V, the possibility of using Tensile Data to predict creep rates was discussed. The results of constant strain rate tensile tests on commercially pure aluminium at temperatures of 250 deg.C. and 500 deg.C. were presented, and predictions of creep behaviour were made. In the present Chapter, those predictions will be compared with the actual behaviour observed in the constant load creep tests, described in Chapter VI. In addition to the comparison of results, the validity of the Power Creep Law (equation 5.6) in relation to the creep results will also be examined and the consequences of using that correlation outwith the experimentally observed range of operation.

The strain/time curves of constant load creep tests, at temperatures of 250 deg.C. and 500 deg.C., were shown in Figures 6.12, 6.13, 6.15, 6.16, 6.17 and 6.18 of the previous chapter (VI). Reference was also made to further strain/time curves presented in Chapter VIII (Figures 8.1 to 8.6). These figures showed that, at a strain of 1.4 pct, the majority of the creep curves were well into a tertiary stage. Since localised necking had not been observed at strains as low as 1.4 pct, it would still have been valid to compare the creep rates at that strain with the tensile data presented in Chapter V. However, one of the objectives of the investigation was to determine the applicability of the Power Creep Law to minimum creep rates, and, in addition, many of the tests were stopped before achieving a strain of 1.4 pct. The minimum creep rate was equal or almost equal to the creep rate at a

strain of 0.3 pct, for most of the curves. Hence, comparison of creep and tensile data took place at a strain of 0.3 pct. The problems of re-measurement of tensile data will be discussed shortly. Before measuring the minimum creep rate at the specified strain, the strain/time curve was plotted to as large a scale as possible in order to ensure the accurate measurement of the gradient of the curve at 0.3 pct.

The re-measurement of tensile data at a strain of 0.3 pct at first presented some problems. The method of obtaining the stress/strain curve for a tensile test from the recorded load/extension curve was described in section 2.3 of Tensile Testing. Representative stress/strain curves were shown in Figures 2.2 and 2.3 for the four original strain rates of 0.1, 1, 10 and 100 pct/h. The stress at a strain of 0.3 pct could be obtained directly from those curves (plotted to a larger scale). Since the stress/strain curve was in the strain hardening region at 0.3 pct strain, the spring beam of the tensometer was still deflecting, and hence, the strain rate experienced by the test piece was less than the rate calculated from the crosshead movement. The actual strain rate was measured in the following manner. From the corrected stress/strain curve, the increment of strain corresponding to a small increment of stress, at 0.3 pct strain, was measured. The time taken to achieve this increment of strain could be calculated by measuring the time taken to achieve the corresponding increment of stress in the original, uncorrected curve, since the correction in that curve was necessary for strain but not stress. The time taken in the uncorrected curve was readily calculated from crosshead speed, recording drum magnification and the rotation of the drum corresponding to the increment of stress. Division of real strain increment by time taken produced the required value of strain rate at 0.3 pct strain. Strain rates at 0.3 pct strain were found to be as much as 50 pct less than the value at the maximum stress.

7.2 Results of Creep and Tensile Tests

In Figures 7.1 and 7.2, minimum creep rate and stress have been plotted on a logarithmic basis for creep tests at temperatures of 250 deg.C. and 500 deg.C., respectively. The corresponding tensile results at 250 deg.C. and 0.3 pct strain have also been plotted in Figure 7.1. For the higher temperature of 500 deg.C., the same comparison has been shown in Figure 7.3. The experimental points have been omitted from that figure for the sake of clarity. The tensile and creep results for 250 deg.C. refer to the material in the 'as received' condition ie. no prior heat treatment. Creep testing at 500 deg.C. was unaffected by prior annealing of the specimen at 500 deg.C. and some results of creep tests on annealed specimens have been included.

The creep results of Figures 7.1 and 7.2 show that, for the stress range employed at each temperature, the relationship between log minimum creep rate and log stress was not linear over the whole of each stress range. A linear relationship was, however, obtained at 250 deg.C. over the stress range 10 – 27.6 N/mm^2 and at 500 deg.C. over the range 0.35 – 1.38 N/mm^2. The gradients of the linear plots were 2.5 and 2.3, respectively. Therefore, under the above conditions of stress, the Power Law Equation (5.5) may be used to correlate minimum creep rates, with n equal to 2.5 for calculations at 250 deg.C., and n equal to 2.3 for calculations at 500 deg.C. For stresses greater than the above limits, the log minimum creep rate/log stress plot shows a rapidly increasing gradient and, hence, the Power Law Equation with n constant is not applicable.

Comparison of creep and tensile data, at both temperatures, can only take place for the range of stress or strain rate in which the tensile and creep results overlap. At the lower temperature of 250 deg.C., this range of stress was 45 – 75 N/mm^2 and the range of strain rate was 0.1 – 10 pct/h. At the higher temperature of 500 deg.C., the corresponding ranges were 0.6 – 4.8 N/mm^2 and 0.03 – 50 pct/h.

Over the respective ranges of stress or strain rate, the log strain rate/log stress curves drawn through the experimental points, were of the same approximate shape with the gradient increasing with increase of stress or strain rate. The agreement between the tensile and creep data, within the respective ranges, became better as the stress or strain rate increased. Also, for any particular stress, the tensile results overestimated the minimum creep rate — an observation which is beneficial from the practical point of view. Therefore for both temperatures within the above ranges of stress or strain rate, tensile data at 0.3 pct strain on commercially pure aluminium may be assumed to reasonably predict minimum creep rates in constant load tests on that material. However, the use of 0.3 pct strain as the reference strain, presumes that the minimum creep rate was already known to occur at that strain. This difficulty can be resolved by comparing the results of Figure 5.1 with those of Figure 7.1, and the results of Figure 5.2 with those of Figure 7.3. In both cases, substitution of tensile data at 1.4 pct strain for tensile data at 0.3 pct strain makes only a small difference to the respective curves, and it can be stated that tensile results at 1.4 pct strain (where maximum stress was reached) also reasonably predicts minimum creep rates, to better than one order of magnitude.

From Figure 5.2, it was noted that logarithms of stress and strain rate were linearly related in tensile tests at 500 deg.C. for the range of strain rate 100 — 10000 pct/h. The results presented in Figure 5.2 were measured at 1.4 pct strain. Figure 7.3 shows the same observation to be true for measurements of stress and strain rate at 0.3 pct strain. It was not possible to determine if the same behaviour was true for creep. Constant load tests with minimum creep rates of approximately 100 pct/h provided an upper limit to the method of creep testing.

The variation of the gradient of the log strain rate/log stress curve with stress has been plotted in Figure 7.4 for creep and tensile results at 250 deg.C., and in Figure

7.5 for the corresponding results at 500 deg.C. The gradient has previously been related to rate sensitivity n (equation 5.2) and to the Power Law Creep exponent n (equation 5.5). The linear segments of the log minimum creep rate/log stress plot produced the constant values of n, previously described. For the stress range, or strain rate range, in which both tensile and creep data have been obtained, the similar shapes of the tensile and creep plots produced similar values of n, for the same value of stress. The approximate curve drawn through these values of n illustrates the rapid increase of that parameter with increase of stress, above that value of stress which has previously been described as denoting the upper limit of applicability of the Power Law Equation. The values of n, obtained by tensile testing at the fastest strain rates of 1000 and 10000 pct/h, confirmed the trends already established in Figures 5.3 and 5.4. At 250 deg.C., n continued to increase rapidly with increase of stress, while at 500 deg. C., the straight line segment of the log strain rate/log stress plot produced a constant value of 6 for n.

The rapid increase in the value of n with increase of stress, for the tensile results of Chapter V, was interpreted as predicting an increase in the sensitivity of the creep rate to the applied stress in creep tests, over the same stress range. It was predicted that the increased sensitivity to stress would show up as an increasing amount of scatter in the strain/time curves as the applied stress was increased. The log minimum creep rate/log stress plots of Figures 7.1 and 7.2 show that the predicted increase of scatter did occur for the stress range in which n was increasing. This increase of scatter has already been noted in section 6.6 of Uniaxial Creep Testing, and Figures 6.12 and 6.13 were presented as illustrating the increase of scatter in strain/time curves with increase of stress at 500 deg.C. and Figures 6.15 to 6.18 the corresponding increase of scatter at 250 deg.C. However, it was also moted that, at the higher temperature of 500 deg.C., an increasing amount of scatter was observed in strain/time curves at low creep stresses. This behaviour is confirmed by Figure 7.2. In the following section, these

variations in the amount of scatter are shown to be a consequence of the variation in the sensitivity of the minimum creep rate to the applied stress.

7.3 Estimation of Error in Minimum Creep Rate

In addition to the error arising from the graphical measurement of the minimum creep rate from the strain/time curve, there also existed an error in the minimum creep rate (via the strain/time curve) due to unavoidable variations in applied stress and test temperature. The latter error was obviously the greater, since the strain/time curves at high stresses had shown a large amount of scatter. Estimation of this error requires an equation relating minimum creep rate, stress and temperature. Although the results have shown that the Power Law Equation, with n constant, was not applicable to the entire range of stress at either of the test temperatures, it is reasonable to use that relation for small changes of stress as long as the appropriate value of n is used for the level of stress considered. This idea arises from the assumption of a continuous function between log strain rate and log stress. Therefore, combining the Power Law for stress with the Arrhenius relationship for the temperature dependence,

$$\left(\frac{\dot{\varepsilon}}{\dot{\varepsilon}_o}\right) = A \left(\frac{\sigma}{\sigma_o}\right)^n \exp\left(-Q/RT\right) \qquad (7.1)$$

where $\dot{\varepsilon}$ is the minimum creep rate (pct/h), σ is the applied stress (N/mm^2), $\dot{\varepsilon}_o$ and σ_o are the reference minimum creep rate and reference stress, respectively, A is a dimensionless parameter depending on structure (assumed constant for the small stress and temperature changes considered), Q is the activation energy for the creep process (cals/mole.), R is the gas constant (= 2 cals/mole.deg.K.), and T is the absolute temperature (deg.K.). ε_o, σ_o and A may be combined in one constant B, such that,

$$\dot{\varepsilon} = B\,\sigma^n \exp\left(-Q/RT\right) \qquad (7.2)$$

Taking natural logarithms of both sides of equation 7.2,

$$\ln \dot{\varepsilon} = \ln B + n \ln \sigma - Q/RT$$

and differentiating,

$$\frac{\partial \dot{\varepsilon}}{\dot{\varepsilon}} = n \frac{\partial \sigma}{\sigma} + \frac{Q}{R} \frac{\partial T}{T^2} \qquad (7.3)$$

The partial differentials of equation 7.3 may be replaced by small increments of the measured quantity and these are denoted by prefix δ.
Hence,

$$\frac{\delta \dot{\varepsilon}}{\dot{\varepsilon}} = n \frac{\delta \sigma}{\sigma} + \frac{Q}{R} \frac{\delta T}{T^2} \qquad (7.4)$$

Equation 7.4 may now be used to calculate the error $\delta\dot{\varepsilon}$ in $\dot{\varepsilon}$ caused by the combined effect of the errors $\delta\sigma$ in σ and δT in T.
Specified temperature (T) = 250 ± 1 deg.C. = 523 ± 1 deg.K.
or = 500 ± 1 deg.C. = 773 ± 1 deg.K.

A value of 33,500 cals/mole was assumed for Q (Garofalo 1965 p. 82).
Therefore,

for tests at 250 deg.C., $\frac{\delta T}{T^2} \frac{Q}{R} = 0.0612$

and for tests at 500 deg.C., $\frac{\delta T}{T^2} \frac{Q}{R} = 0.0280$

The estimated errors in the values of applied stress (σ) were tabulated in Appendix 6.1. Substituting those tabulated results, and the above values of $(\frac{\delta T}{T^2} \frac{Q}{R})$, in equation 7.4, yields the estimated error in minimum creep rates. The value at each stress has been tabulated in Table 7.1. The values of n were taken from Figures 7.4 and 7.5. The values of minimum creep rate ($\dot{\varepsilon}$) were taken from Figures 7.1 and 7.2.

Table 7.1

Stress (N/mm^2)	n	$\frac{\delta\dot{\varepsilon}}{\dot{\varepsilon}}$	$\dot{\varepsilon}$ (pct/h)	$\delta\dot{\varepsilon}$ (pct/h)
76.65	22	0.186	2.0	0.4
61.50	8	0.107	0.13	0.01
45.35	5	0.090	0.016	0.001
✓27.60	2.5	0.076	0.0022	0.0002
17.91	2.5	0.077	0.00077	0.00006
10.00	2.5	0.079	0.00019	0.00001
4.99	14	0.127	85	11
3.65	6.7	0.112	4.2	0.5
2.26	3.0	0.088	0.50	0.04
✓1.38	2.3	0.087	0.14	0.01
0.87	2.3	0.094	0.045	0.004
0.61	2.3	0.101	0.019	0.002
0.35	2.3	0.124	0.0050	0.0006

Table 7.1 illustrates the increase of scatter in the minimum creep rates with increase of stress. However, the scatter bands suggested by the results of Table 7.1 are much less than the experimentally observed scatter of minimum creep rates (Figures 7.1 and 7.2). The experimentally observed increase of scatter at very low stresses at 500 deg. C. is also confirmed by Table 7.1. Again, the relatively large error in the value of the applied stress is one factor causing that scatter. The results of this section show that the increase of scatter with increase of stress is consistent with the idea of an increase in the sensitivity of the minimum creep rate to stress as the stress increases. This increase of stress sensitivity has been described by the increase in the value of the creep exponent n with stress. It is important to realise that the results do not explain why

there should be an increase in the stress sensitivity of the minimum creep rate with increase of stress.

7.4 Stress Dependence of Minimum Creep Rate

The experimental results of the section 7.2 have shown that, for commercially pure aluminium at temperatures of 250 deg.C. and 500 deg.C., there was a range of stress over which the Power Law Equation (5.5), with n constant, could be used to relate minimum creep rate and stress. For creep deformation at 250 deg.C., the range of stress was 10 – 27.6 N/mm^2 with a value of 2.5 for n. For creep deformation at 500 deg. C., the range of stress was 0.35 – 1.38 N/mm^2 with a value of 2.3 for n. The validity of the Power Law, within those stress ranges, was apparently unaffected by the possible influence of metallurgical instability and, as shown in the following chapter, the development of intergranular discontinuities in the material. The similarity in the values of n, obtained under the widely different conditions of stress and temperatures, suggests that the creep exponent is relatively insensitive to temperature. Creep tests at other temperatures are, however, necessary to confirm this suggestion.

Owing to the long testing times involved, creep tests were not conducted at 250 deg.C. for stresses less than 10 N/mm^2, and at 500 deg.C. for stresses less than 0.35 N/mm^2. These stresses, therefore, have been quoted as denoting the lower stress limits of the experimentally verified range of validity of the Power Law Equation. There was no indication, however, that the Power Law did not apply for stresses below those limits. The use of Power Law Equation by designers is based on such observations – that extrapolation is possible to lower stresses where no creep data is available, since data at higher stresses has indicated the validity of the Power Law Equation.

The creep tests performed at stresses greater than those denoting the upper limits to the range of validity of the Power Law Equation, showed the value of the creep exponent, n, to increase rapidly with increase of stress. At 250 deg.C., n increased from 2.5 at 27.6 N/mm^2 to 22 at 76.6 N/mm^2 while, at 500 deg.C., n increased from 2.3 at 1.38 N/mm^2

to 14 at 4.99 N/mm^2. Therefore, extrapolation of creep data, obtained by testing at low stresses, to high stress creep conditions, at the same temperature, is not only invalid but dangerous, if the extrapolation is carried out on the basis of the Power Law Equation. Such extrapolations seriously underestimate the actual rates of creep. The results of tensile tests were in reasonable agreement with the creep results, for the ranges of stress or strain rate, at the respective temperatures, in which the two types of tests overlapped. Since the regions of overlap mainly occurred in the range of stress where n was increasing rapidly, the tensile data were of little use in predicting low stress creep behaviour. The results of very slow strain rate tensile tests at 500 deg.C., however, did venture into the linear range of the log strain rate/log stress plot. Since agreement between tensile and creep data was reasonable in the regions of overlap, it may be assumed that the tensile data give a reasonable indication of creep behaviour at high stresses. Therefore, at 250 deg.C. the creep exponent, n, may be expected to continue increasing with increase of stress above 76.6 N/mm^2. The tensile data indicate a value of 40 for n at 100 N/mm^2 (Figure 7.4). However, at the higher temperature of 500 deg.C., the tensile results indicate a decrease in the value of n to a constant value of 6 for stresses in the range 5 – 10 N/mm^2 (Figure 7.5).

The implications of the foregoing results to creep calculations on components subjected to transient high stresses and temperatures are enormous. For example, under thermal shock conditions high transient stresses may be set up in the component, and, hence, large localised rates of deformation may occur. Unless creep data have been obtained for those high stress conditions, the rates of deformation will be seriously underestimated by the extrapolation of creep data from lower stresses. However, even the knowledge of high stress creep data would not completely solve the problem. Although the value of n was relatively insensitive to temperature within the range of validity of the Power Law Equation, the results have shown that the increase in the value of n with increase of stress was much greater at the

lower temperature of 250 deg.C. than at 500 deg.C. Hence, the effect of the temperature transient, itself, as well as the stress transient it has set up, will influence the resulting rates of deformation. Large localised deformation rates may also occur under constant temperature conditions, if regions of high stress concentration are set up in the component. The stress concentrations may result from design faults, avoidable or unavoidable, and from material discontinuities, such as intergranular cracks.

7.5 Summary and Conclusions

The results of constant strain rate tensile tests and constant load creep tests on commercially pure aluminium at temperatures of 250 deg.C. and 500 deg.C. have shown that minimum creep rates may, with reasonable accuracy, be predicted by tensile data. The results have also shown that minimum creep rates may not be correlated with the applied stresses by the Power Law Equation over the entire stress range. The Power Law Equation was applicable at low stresses with a value of 2.5 for n at 250 deg.C. and a value of 2.3 at 500 deg.C. For stresses greater than 1.38 N/mm^2 at 500 deg.C. and 27.60 N/mm^2 at 250 deg.C., the value of n increased rapidly with stress. This increase in the value of n also appeared as an increase in the scatter of strain/time curves as the applied stress was increased. The results did not, however, explain why there should be an increase in the stress sensitivity of the minimum creep rate with increase of stress. The increase of scatter and the increase in the value of n were the consequence and not the cause of the increase in the stress sensitivity. The results illustrate the dangers involved in extrapolating experimental data outwith the stress or temperature range for which they are known to apply.

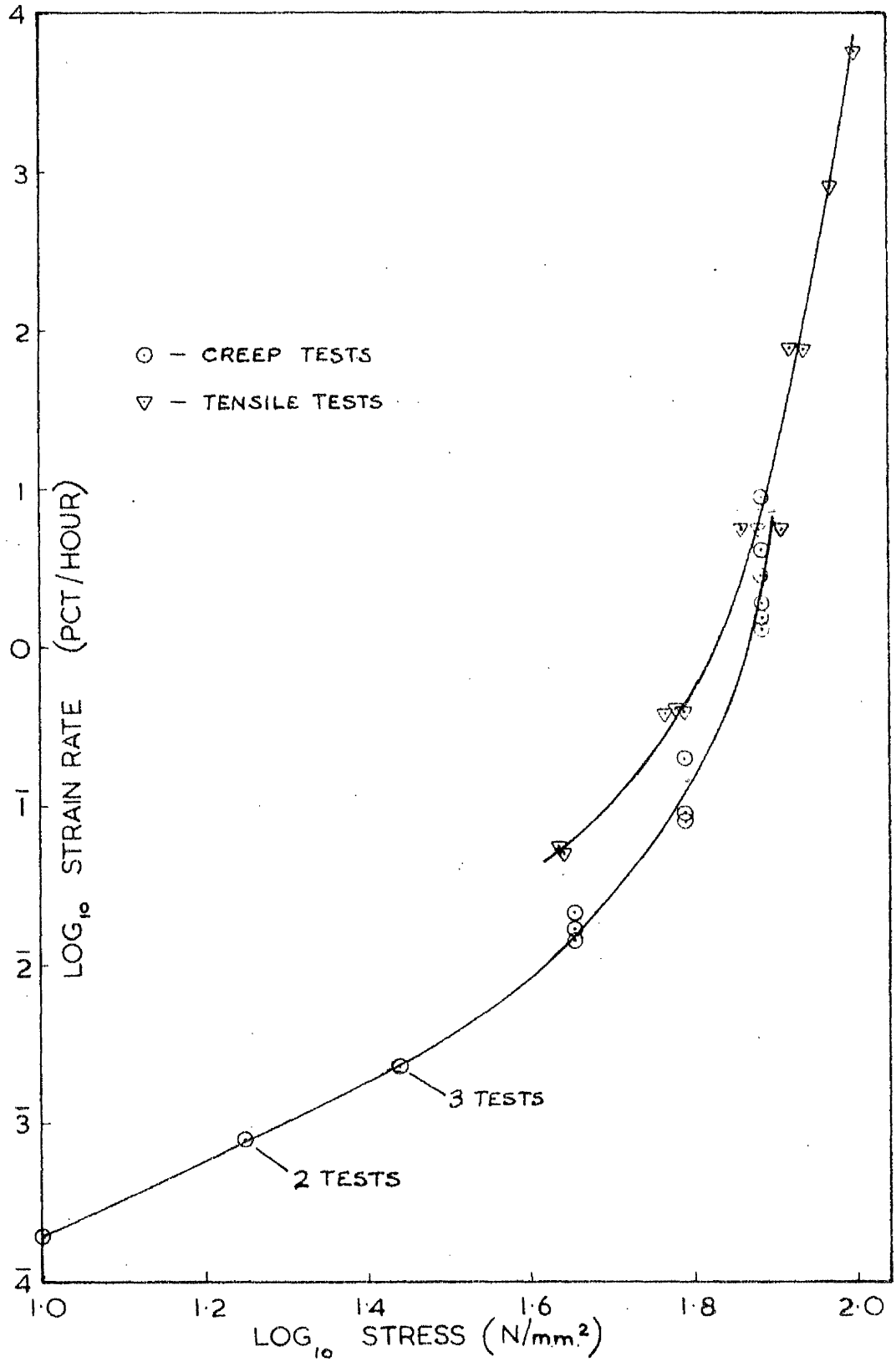

Figure 7.1 Creep and Tensile Tests at 250 deg.C.; $\log_{10}$ (strain rate) against $\log_{10}$ (stress) at 0.3 pct strain

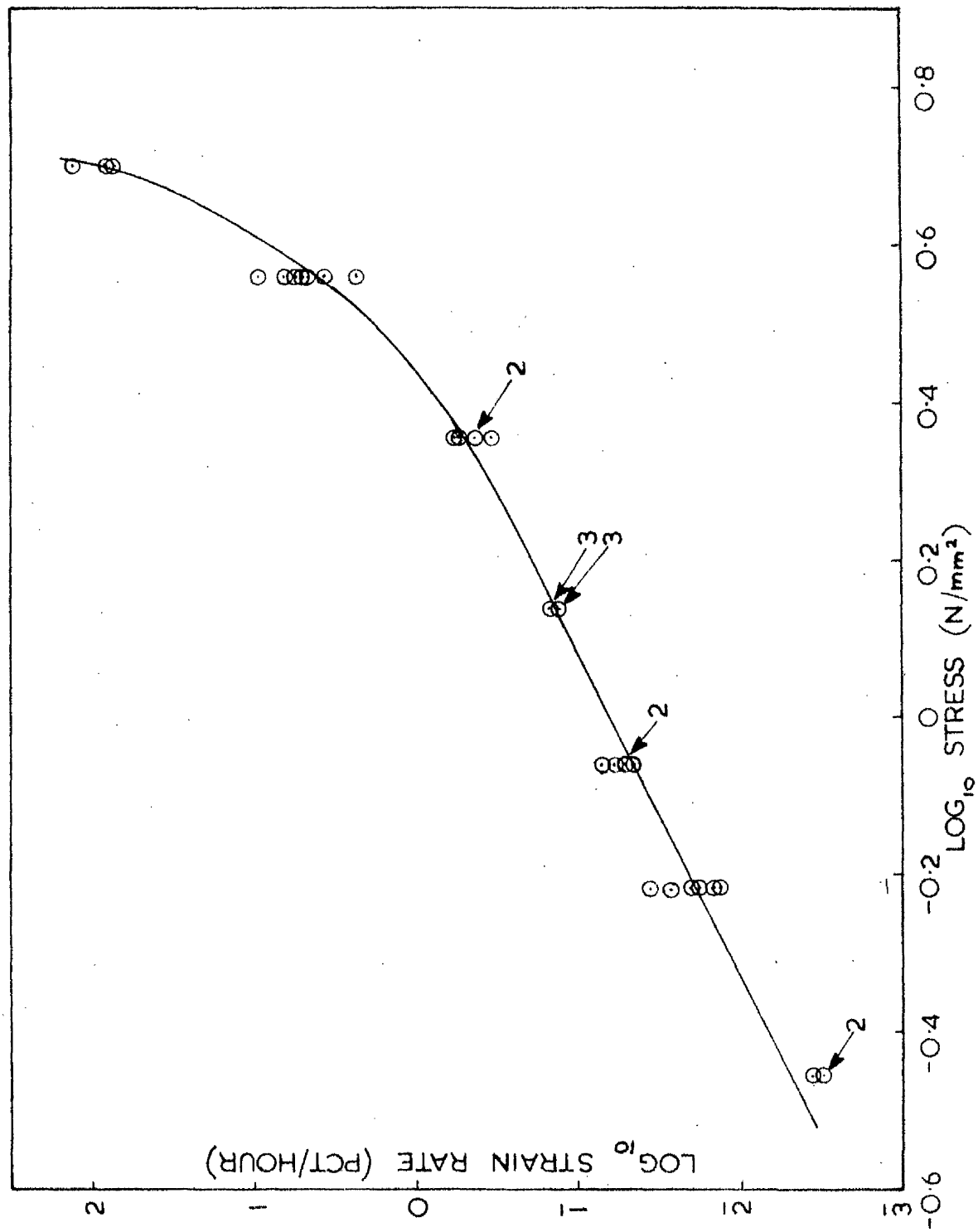

Figure 7.2 Constant load creep tests at 500 deg.C.; $\log_{10}$ (strain rate) against $\log_{10}$ (stress) at 0.3 pct strain

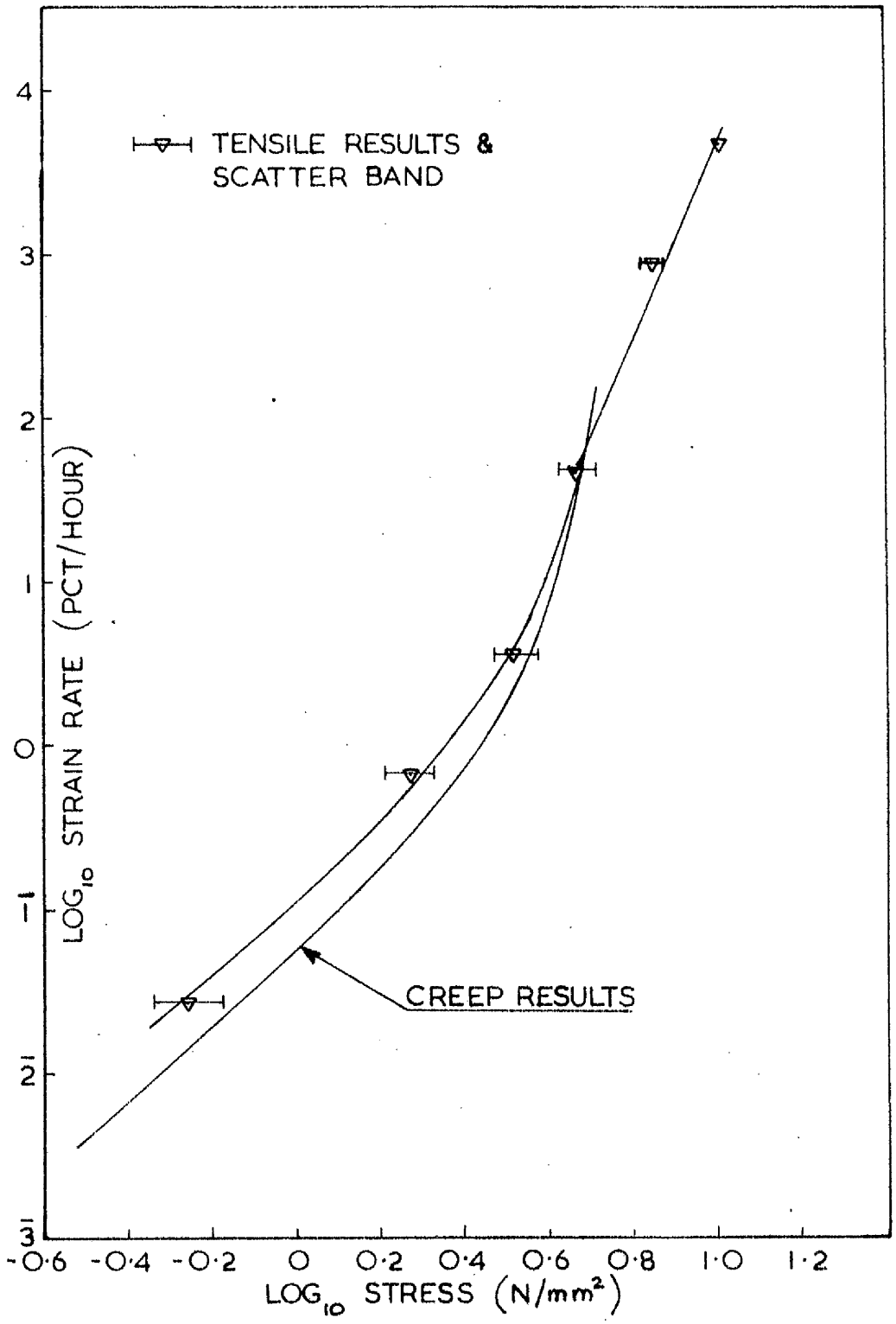

Figure 7.3 Creep and Tensile Tests at 500 deg.C.; $\log_{10}$ (strain rate) against $\log_{10}$ (stress) at 0.3 pct strain

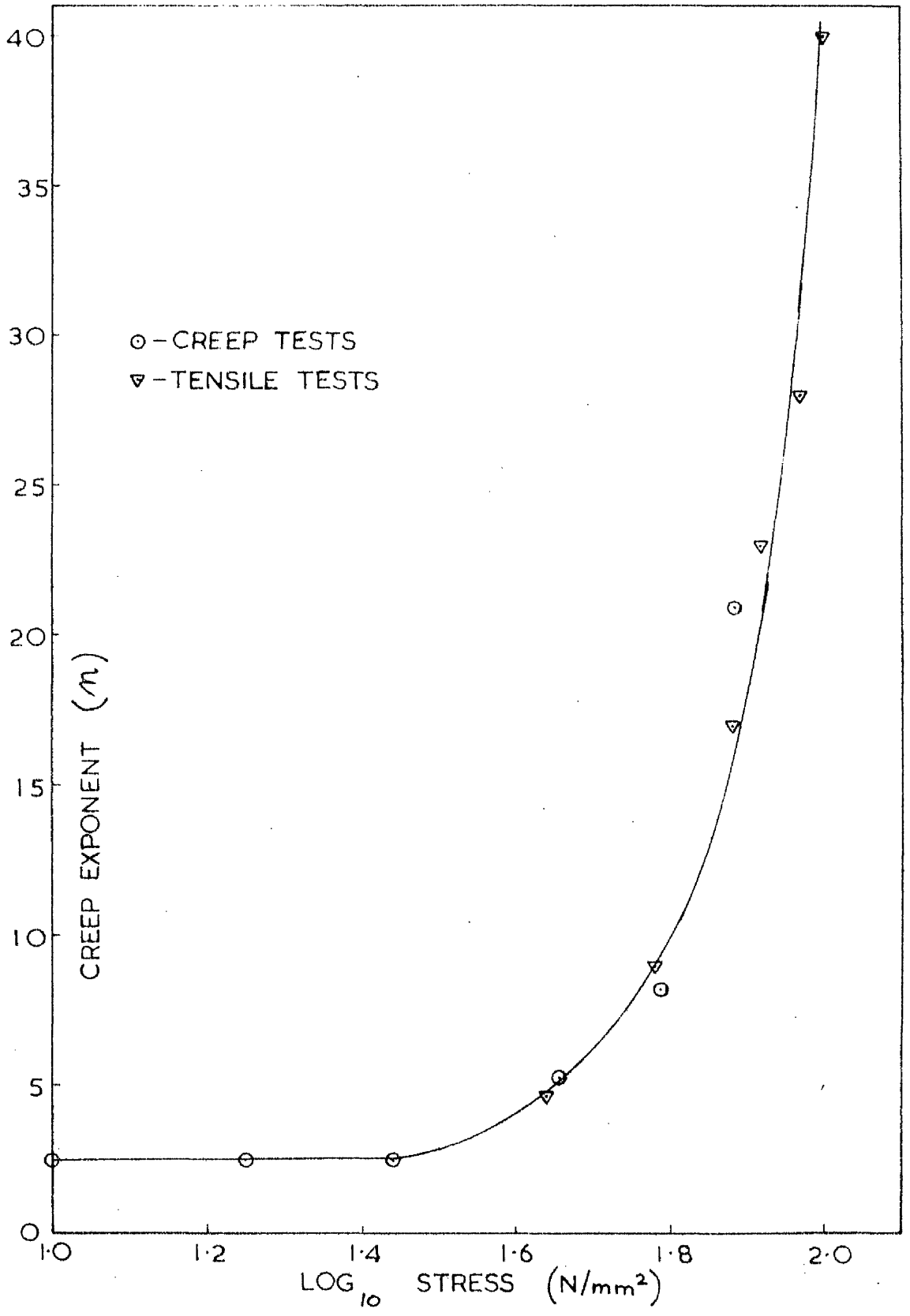

Figure 7.4 Creep and Tensile Tests at 250 deg.C.; creep exponent (n) against $\log_{10}$ (stress) at 0.3 pct strain

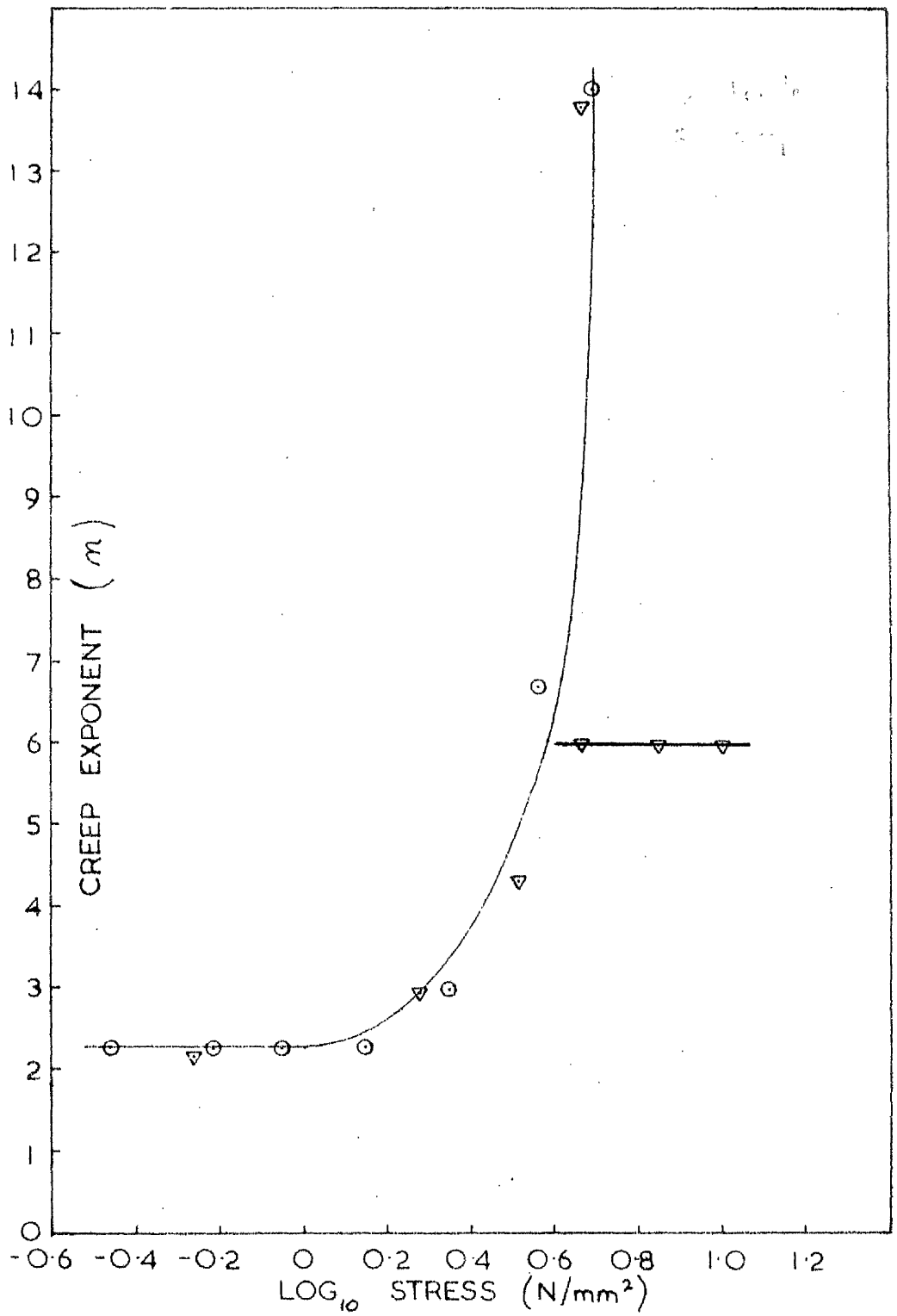

Figure 7.5 Creep and Tensile Tests at 500 deg.C.; creep exponent (n) against $\log_{10}$ (stress) at 0.3 pct strain

CHAPTER VIII

UNIAXIAL CREEP DENSITY CHANGES

8.1 Introduction

The measurement of the density decrease in a material, due to internal discontinuities, by a hydrostatic weighing technique was described in Chapter III. It was pointed out that, although the density decrease could accurately measure the total volume of internal discontinuities, it provided no information on the size, shape and distribution of the discontinuities. However, this drawback has not prevented the method from giving considerable help in the formulation of qualitative and quantitative theories of the growth of intergranular discontinuities. In the present research, measurement of the growth of intergranular discontinuities during creep was necessary in assessing the effects of those discontinuities on the creep properties of commercially pure aluminium. Thus, test pieces, which had been crept under constant load at 250 deg.C. or 500 deg.C., had the density change in their gauge lengths measured. These measurements, combined with metallography, provided more information on the effects of intergranular discontinuities under different conditions of stress and temperature. In addition, comparison could be made with the work of previous researchers and, with this point in mind, the following review was produced.

Density Change and Theory of Rupture

In the first quantitative theory of rupture by intergranular cavitation, Hull and Rimmer (1959) assumed that all the cavities were present as nuclei at time zero, and that failure occurred when the cavities coalesced after growth by

grain boundary diffusion. Their theory leads to total cavity volume (V) being proportional to $(\text{time})^{1.5}$. Apparent verification of the exponent 1.5 was provided by the work of Boettner and Robertson (1961) on copper, when log (density change) was plotted against log (time). However, according to their plot of log (density change) against log (strain), total crack volume should be proportional to $(\text{time})^{3}$ in the secondary creep range (Greenwood, 1963). Greenwood resolved this discrepancy with the Hull and Rimmer theory by combining their equation for the growth of an individual cavity with one expressing the continuous nucleation of cavities. Later, Ratcliffe and Greenwood (1965) showed that, for magnesium, total void volume was proportional to $(\text{time})^{2.5}$ and this was taken as confirmation of the continuous nucleation of cavities.

Speight and Harris (1967) derived an alternative equation for cavity growth to that of Hull and Rimmer. The equation showed that, for both large and small relative void spacings, the Hull and Rimmer formula underestimated the growth rate. Although Gittins (1967) also obtained an exponent of 1.5 when plotting log (density change) against log (time) for copper, he considered that this agreement with the Hull and Rimmer theory was 'fortuitous'. He explained the exponent of 1.5 by his own metallographic observation that the number of cavities present was proportional to $(\text{time})^{0.5}$ and the prediction of the Speight and Harris equation that the volume of an individual cavity should be proportional to time for large cavity spacings.

The research reviewed so far has been of those workers who favour the growth of cavities by stress directed diffusion of vacancies. The advocates of growth by grain boundary sliding place a different interpretation on the time exponents observed. Bowring, Davies and Wilshire (1968) obtained an exponent of 2.5 for Magnox AL80, agreeing with the work on magnesium, and an exponent of 1.5 for a nickel/0.1 at. pct palladium alloy, agreeing with the work on copper, when they plotted log (density change) against log (time). They also showed density change to be proportional

to strain after a certain amount of initial strain. The variation of this initial strain with material accounted for the different time exponents observed. Hence, cavity growth depended on strain and, therefore, on grain boundary sliding.

Much of the disagreement in the interpretation of results arises from the plotting of total crack volume per unit weight (V) against time (t) alone or strain (ε) alone. Since the relationship between time and strain in creep is complicated, it is difficult to extract the relative contributions of each to the total crack volume. Hence, research workers are now considering the variation of total crack volume with some combination of strain and time, so that strain and time may form a single parameter.

Greenwood (1969), having observed that the density measurements of Boettner and Robertson (1961) on copper were consistent with the relationship, $V \propto (\varepsilon \times t)$, derived an equation applicable to the primary and secondary stages of the creep curve :-

$$V \propto \varepsilon t \sigma^{2.5} f(n),$$

where σ is the applied stress and f(n) is a function which accounts for the influence of the size of cavities, in relation to their spacing, on their growth rate. Woodford (1969a) has produced a similar equation using Boettner and Robertson's results :-

$$V = \text{const.}\ \varepsilon t \sigma^{2.3} \exp.(-22500/RT),$$

where R is the gas constant and T the absolute temperature. Woodford (1969b) subsequently derived an equation for nickel :-

$$V = 1.52 \times 10^{-38} \varepsilon t \sigma^{7.5}$$

where V is in cm^3/g, t in hours and σ in lbf/in^2. This equation applies at a temperature of 525 Deg. C. and is valid

to the point of rupture. In these equations the direct dependence on time represents the diffusion controlled growth of individual cavities and direct dependence on strain reflects a continuous nucleation of cavities related to grain boundary sliding. Therefore, the above equations should only apply to the nucleation and growth of cavities at points along grain boundaries. Triple point cracks will immediately invalidate the form of the equation since they appear to grow by grain boundary sliding, mechanical tearing and only a small contribution from stress direct diffusion.

Before attempting to correlate the results of the present research with the theories of previous workers, the results themselves will be reported, illustrating their use in determining the growth of internal discontinuities and in comparing behaviour under different conditions of stress and temperature. Metallography was required, though, to determine the size, shape and distribution of the discontinuities. Attempts will then be made to correlate the data with the work already described. It must be pointed out, however, that since the material was shown earlier to exhibit triple point cracking at high strain rates and to exhibit grain boundary migration, the attempts may not be very successful. In the fourth section of this chapter, a comparison will be made between density measurements derived from constant strain rate tests (Chapter III) and from constant load creep tests. The purpose is to determine whether constant strain rate and constant load creep tests can be regarded as interchangeable with respect to the development of intergranular discontinuities.

8.2 Growth of Intergranular Discontinuities during Creep

The density changes in the gauge lengths of test pieces, stopped after various periods of creep under constant load conditions, were measured in the same way as previously described for constant strain rate tensile test pieces. The results are presented in Figures 8.1 to 8.6 for tests performed at 500 deg.C. and Table 8.1 for tests at 250 deg.C. As for tensile specimens, accuracy in the value for density change was $\pm$ 0.0004 g/cc ($\pm$ 0.015 pct) and repeated determinations on the same specimen confirmed this figure as the maximum error.

8.2.1 Results at 500 deg.C.

In Figures 8.1 to 8.6, fractional density decrease has been plotted against time for six of the stresses used in creep tests at 500 deg.C. The corresponding strain/time curves for most of the specimens have also been plotted on the same Figures. Examination of these figures shows that density decreases continuously from the beginning of creep. Therefore, in commercially pure aluminium at a temperature of 500 deg.C., growth of intergranular discontinuities takes place from the earliest stages of the deformation process.

However, metallography of the 'as received' material (section 2.4.2 of Tensile Testing) detected the presence of a few small grain boundary cavities. Hence, it was possible that the growth of internal discontinuities, detected by density change, from application of the creep stress, was due to existing cavities. To show that this was not the case, a test piece was annealed at 500 deg.C. for 24 hours prior to creep testing to sinter out any small grain boundary cavities. The annealing experiments of section 3.4 (Tensile Density Changes) had already shown that a total volume of intergranular discontinuities, corresponding to a density decrease of 0.3 pct, completely sintered out after 150 hours at 500 deg.C. The size and number of grain boundary cavities, corresponding to 0.3 pct density decrease, are such that

metallography can easily detect them (Figure 4.6). It was thought that 24 hours at 500 deg.C. would be sufficient to sinter out the small cavities in the grain boundaries of the 'as received' material. The annealed specimen was then strained by 0.9 pct at an initial stress of 1.38 N/mm^2 and a temperature of 500 deg.C. As shown in Figure 8.3, the strain/time curve (73) and the gauge length density decrease were consistent with the other tests under those conditions. Hence, it was concluded that growth of existing cavities in the material makes a negligible contribution to the total crack volume and that nucleation of intergranular discontinuities takes place from application of the creep stress.

Comparison of Figures 8.1 to 8.6 with one another was not feasible because of the different time scales involved. Comparison of density changes at the same strain is feasible but may be influenced by the scatter in the strain/time curves. Comparison of density changes at a strain of, say, 5 pct, shows that total crack volume reached a maximum at stresses in the region of 0.87 to 1.38 N/mm^2; for stresses larger or smaller, total crack volume was less. This behaviour was also observed in tensile tests at 500 deg.C., when a maximum density change was observed at a strain rate of 0.7 pct/h. The decrease in total crack volume with decreasing strain rate was explained by the increasing effect of grain boundary migration. As the stress decreased, nucleation of cavities was restricted and the growth of stable cavities hindered by boundary migration. The decrease in total crack volume with increasing strain rate, for the same strain, at strain rates greater than 0.7 pct/h was explained by the time-dependent growth of cavities.

The results suggest that there exists a limiting lower stress for which no cavity growth is possible. At this stress, grain boundary migration is able to annihilate all possible cavity nuclei and to cause the sintering out of existing cavities. The existence of this stress was confirmed by experiment. Creep tests at a stress of 0.35 N/mm^2 produced no significant density decreases.

Metallography

Some of the test pieces were sectioned, polished and etched to determine the nature of the internal discontinuities, causing the large decreases in density. At low stress, as shown by Figure 8.7, cavities develop and grow at points along the grain boundaries and at the triple point junctions of three grains. At small strains the cavities are individually identifiable, but grow with increasing strain and time to link up and form long cracks as shown in Figure 8.8. The large crack (in Figure 8.8) has a length of 0.72 mm. in the plane of the photograph. The ability of the material to accommodate such a large crack is undoubtedly due to the ease of plastic flow in the material at 500 deg.C. Hence, the length which a crack must achieve before propagation under the action of the stress concentration at the tip, alone, occurs, becomes very large.

Triple point cracking was more noticeable in sections of test pieces strained under large stresses. Figure 8.9 shows a wedge type crack revealed by polishing alone. The orientation of the wedge is in agreement with the method of nucleation by grain boundary sliding, proposed by Chang and Grant (1956). Evidence that large stresses and high strain rates favour triple point cracking has already been presented in previous chapters. However, in agreement with those earlier observations, grain boundary cavities were also found at large stresses (Figure 8.10).

8.2.2 Results at 250 deg.C.

Fewer tests were performed at the lower temperature, but some indication of behaviour was deduced. Most of the results, presented in Table 8.1, were derived from creep tests on the 'as received' material at 250 deg.C., without any intermediate heat treatment, save the soaking period at 250 deg.C. before application of the load. The last three results in the Table were derived from creep tests on the material after periods of annealing at 500 deg.C. The creep

properties of this annealed material at 250 deg.C. were slightly different from those of the 'as received' material and, hence, so were the measured density changes.

Only two results on the 'as received' material show a definite decrease in density to have occurred (the others were within the accuracy of the method of measurement). At stresses of 27.60 N/mm^2 and 17.91 N/mm^2 intergranular discontinuities developed by 2.9 pct strain or 1000 hours and 0.4 pct strain or 377 hours, respectively. Therefore, the intercrystalline fractures already noted in tests under constant strain rate and constant load conditions at this temperature, owe their origin to the development of intergranular discontinuities.

The tests on the annealed material at 27.60 N/mm^2 and 250 deg.C. illustrated that only a small volume of discontinuities was necessary to produce catastrophic failure. After 294 hours, in one test piece, the density decrease was only 0.086 pct, while rupture occurred in another test piece after only a further 24.5 hours. On sectioning, polishing and etching this latter test piece, grain boundary cavities and triple point cracks were found, both at and behind the fracture surface. Figures 8.11 and 8.12 show examples of these grain boundary fissures in the polished and then etched stages of preparation. It was noted in the section on metallography in Chapter II that caustic soda solution tended to attack the grains and to leave the boundaries untouched. Figure 8.12 confirms that intergranular cracks may still be clearly distinguished under these conditions. The existence of these discontinuities confirms the intercrystalline mode of failure of commercially pure aluminium under creep conditions at 250 deg.C.

8.2.3 Intergranular Cracks at High and Low Temperatures

The results, which have been described in the two preceding sections, illustrate that the ability of commercially pure aluminium to cope with intergranular discontinuities

depends on the conditions of stress and temperature. At a high temperature and a low stress, discontinuities were able to grow to a large size without causing sudden failure. In the sections describing fracture characteristics in Tensile Testing and in Uniaxial Creep Testing, it was shown that the material could easily sustain strains of 50 to 90 pct at low strain rates or low stresses at 500 deg.C. In Figure 8.8 a crack of 0.7 mm. has been found after only 24 pct elongation. Presumably, cracks of more than 1mm. are possible before complete failure occurs. At a lower temperature and a higher stress, fracture occurred after 15 pct strain, and the order of magnitude of the largest discontinuities found in a section behind the fracture surface was 0.1 mm. (Figure 8.12). What would the reaction of the material be to the low temperature/high stress creep conditions after a period under the high temperature/low stress conditions, in which discontinuities larger than 0.1 mm. had grown? The above results predict that immediate rupture should occur. Experiments to show the effects of different amounts of intergranular discontinuities on the creep properties of aluminium under different conditions of stress and temperature are described in the next chapter.

8.3 Correlation with Existing Theories of Rupture

In the review of the work of previous researchers, three principal methods of presenting density change data were noted. The three methods, logarithmic plots of density change with time, strain and the product (time x strain), have been used in Figures 8.13, 8.14 and 8.15, respectively, for the results on commercially pure aluminium at 500 deg.C. It should be noted that, in the present results, conditions of constant stress and constant structure were not obtained over the entire creep curve. Also, the mode of intergranular fracture changed with increase of stress from one of mainly grain boundary cavitation at low stresses to one of mainly triple point cracking at high stresses. The density measurements on copper, magnesium, Magnox AL80 and the nickel/0.1 at. pct palladium alloy were derived from creep tests performed at temperatures close to 0.5 Tm. Although the results on commercially pure aluminium are presented for 0.83 Tm, it is assumed that similar intergranular fracture processes operate at higher temperatures.

8.3.1 Time-Dependence of Density Decrease

In Figure 8.13 a linear relationship between log (density decrease) and log (time) was obtained at the two lowest stresses. Therefore, at these two stresses, $V \propto t^a$, where V is total crack volume, t is time, and a is a constant. At the lowest stress (0.61 N/mm^2) the time exponent is 1.5 and the behaviour of the material can be compared with that previously found for copper (Boettner and Robertson 1961, Gittins 1967) and for a nickel/0.1 at. pct palladium alloy (Bowring, Davies and Wilshire, 1968). At a slightly higher stress of 0.87 N/mm^2, the time exponent is 2.4 and behaviour can be compared with magnesium (Ratcliffe and Greenwood, 1965) and with Magnox AL80 (Bowring, Davies and Wilshire, 1968). Metallography has already shown that the intergranular fracture process in commercially pure aluminium at 500 deg.C. and low stress, consists of the nucleation and

growth of cavities at points along the grain boundaries. The cavities eventually coalesce to form long cracks. Figure 8.13 shows that $V \propto t^a$ holds for the entire process and, therefore, suggests that the same mechanism of growth was operative throughout. For stresses greater than 0.87 N/mm^2, the variation of V with t becomes more complicated and this is presumably due to the greater incidence of triple point cracking.

8.3.2 Strain-Dependence of Density Decrease

The plot of log (density change) against log (strain) in Figure 8.14 segregates the material behaviour into two distinct types, with respect to stress. For the stress range 0.61 to 2.26 N/mm^2, the results have produced a set of closely spaced, roughly parallel straight lines, one line for each stress. The gradient of the lines is approximately unity indicating that $V \propto \varepsilon$, where ε is strain, for this stress range. The intermixing of the experimental points on Figure 8.14 suggests that the growth of cracks is independent of stress for the range 0.61 to 2.26 N/mm^2.

For the larger stresses of 3.65 and 4.99 N/mm^2, log (density change) still has a linear relationship with log ε. The different slope is again explained by the greater incidence of triple point cracking at large stresses. The change in slope of the log (density change)/log ε plot for a stress of 3.65 N/mm^2 may be explained by the onset of localised necking at large strains. The test pieces strained by less than 10 pct at 3.65 and 4.99 N/mm^2 showed no sign of localised necking. Larger strains at 3.65 N/mm^2 did produce localised necking. With the onset of localised necking, mechanical tearing and the triaxial stress state within the neck will accelerate the growth of cracks.

Unlike the variation of V with time, the variation of V with strain does not agree with the results of Boettner and Robertson on copper. Their results suggest $V \propto \varepsilon^b$, where b has values of 2 to 3 depending on stress and strain.

However, Bowring, Davies and Wilshire found V to be proportional to strain (after some initial strain) for both Magnox A180 and a nickel/0.1 at. pct palladium alloy. For commercially pure aluminium at 500 deg.C., there was no primary creep stage in the ε/t curve, and so V was proportional to strain from the origin.

The results presented in Figures 8.13 and 8.14 have shown that comparison with previous density measurements is only feasible at the two smallest stresses, 0.61 and 0.87 N/mm^2. This is hardly surprising since the research reviewed in section 8.1 was applicable to the growth of grain boundary cavities, and metallography has shown that cavities are the principal intergranular fracture process in aluminium at low stresses. For larger stresses the growing incidence of triple point cracking upsets the simple relationships and, therefore, correlation was only possible for either V and t or V and ε, but not for both. The surprising feature of the results is that the relationships $V \propto t^a$ and $V \propto \varepsilon$, hold for the entire creep curve, even when the cavities have coalesced. It is not possible to say whether this is because of or inspite of the effects of varying stress and grain boundary migration.

8.3.3 Dependence of Density Change on the Product (ε x t)

Correlation of the results for commercially pure aluminium with the equations of Greenwood (1969) and Woodford (1969a,b) is illustrated by the plot of log (density decrease) against log (ε x t) in Figure 8.15. In their equations, $V \propto \varepsilon t$ and hence the plot of log (density change) against log (ε x t) should be linear with a gradient of 1. Figure 8.15 shows that this is only true for a stress of 0.87 N/mm^2. At the lower stress of 0.61 N/mm^2, $V \propto (\varepsilon t)^{0.7}$. The results for the four largest stresses (1.38, 2.26, 3.65 and 4.99 N/mm^2) appear to form a band with an approximate gradient of 0.7. Therefore, apart from the results at 0.87 N/mm^2, the relationship $V \propto (\varepsilon t)^{0.7}$ loosely holds for

commercially pure aluminium at a temperature of 500 deg.C. The analysis was not extended to include stress because of the uncertainty in the V, ε and t relationship.

Although correlation of the complete set of density measurements on commercially pure aluminium with existing equations for cavity growth has not been very successful, agreement has been achieved for particular values of stress. Thus, for stresses of 0.61 and 0.87 N/mm^2 in commercially pure aluminium at 500 deg.C., the results of density measurements have shown that the growth of intergranular cracks may be expressed by the relationship, $V \propto (\varepsilon t)^c$, where c has a value of 0.7 at 0.61 N/mm^2 and 1 at 0.87 N/mm^2. Metallography has shown that this relationship applies from the nucleation and growth of cavities at points along the grain boundaries to the growth of large cracks, formed after coalescence of the cavities.

8.4 Density Changes in Creep and Tensile Tests

In Chapter III, the variation of density decrease with strain and strain rate was described for constant strain rate tensile tests on commercially pure aluminium at temperatures of 250 deg.C. and 500 deg.C. For both temperatures, the variation of density change with strain was measured for four strain rates, viz. 0.1, 1, 10 and 100 pct/h. At the lower temperature, as shown by Table 3.2, the density changes recorded were within the accuracy of the method of measurement, except for those test pieces in which localised necking had occurred. The interpretation placed on these results was that, for the strain rates considered, small internal discontinuities develop in the material and fracture occurs when they coalesce or when one crack rapidly propagates across the load bearing area. The latter explanation seemed more likely since only a small density decrease was noted in necked test pieces. Owing to the small number of tests and the accuracy of the method of measurement, it was not possible to state when the internal discontinuities first stated to nucleate. That the failure was due to intergranular fissures was deduced from the appearance of the fracture surfaces, coupled with the small density decrease noted in necked specimens.

In the present chapter, density measurements have been presented for specimens creep tested under constant load conditions at a temperature of 250 deg.C. (Table 8.1). The three largest stresses employed corresponded to the maximum engineering stresses observed in constant strain rate tensile tests at 0.1, 1, and 10 pct/h (45.35, 61.50 and 76.65 N/mm^2, respectively). In agreement with the tensile tests, density changes recorded in creep test pieces, at these stresses and which had not necked, were within the accuracy of the method of measurement. Hence, although the fractures in creep rupture tests at this temperature were typically intercrystalline, it was not possible to state when the fissures nucleated. Additional creep tests were performed at lower stresses and the density measurements from these specimens

indicated the presence of internal discontinuities from early in the creep life. Metallography demonstrated that the discontinuities were intergranular in nature. It was further deduced that rupture had occurred after the development of only a small volume of intergranular discontinuities. Therefore, constant strain rate and constant load tests may only be compared in the respect that density changes indicated rupture to have occurred after the formation of only a small amount of intergranular discontinuities.

The density decreases, measured in test pieces which had been deformed under constant strain rate conditions at the higher temperature of 500 deg.C., were much larger. The results were plotted as density decrease against strain in Figure 3.3. Since strain and time should be linearly related in such tests, the two can be regarded as one parameter with stress as the other variable in the test. Figure 3.3 showed that density decrease and strain (or time) were linearly related for most of the curve at each strain rate. Hence, when the two quantities are plotted on a logarithmic basis, as in Figure 8.16, parallel lines, of slope equal to one, are obtained. Plotting log (density change) against log (time) would change the relative positions of the curves but not their slopes.

In sections 8.2 and 8.3, the density measurements recorded on specimens tested under constant load creep conditions at 500 deg.C. were described. Four of the stresses employed, 4.99, 3.65, 2.26 and 0.87 N/mm^2, corresponded to the maximum engineering stresses recorded in tensile tests at strain rates of 100, 10, 1 and 0.1 pct/h, respectively. Using these links as a basis for comparison, Figures 8.14 and 8.16 show that, the total crack volume in a tensile test at 1 pct/h has the same magnitude as that in a creep test at 2.26 N/mm^2, for the same strain. Therefore, as far as the intergranular fracture process is concerned, a constant load creep test at an initial stress of 2.26 N/mm^2 and a constant strain rate tensile test at 1 pct/h, in which

the maximum stress is 2.26 N/mm^2, are equivalent.

For the lowest strain rate, 0.1 pct/h, and its corresponding creep stress, 0.87 N/mm^2, the total crack volume was less in the tensile test piece, for the same strain. However, total crack volume was still proportional to strain for both. For the same strain rate of 10 pct/h and its corresponding creep stress, 3.65 N/mm^2, total crack volume was greater in the tensile test for the same strain. Since the plot of log (density change) against log (strain) for creep at this stress has two straight line segments, it is difficult to compare the gradients with that of the tensile results. For the highest strain rate, 100 pct/h, and its corresponding creep stress, 4.99 N/mm^2, the total crack volume appears to be much greater in tensile tests, although only a few creep tests at this stress were performed. Hence, although the comparison of density changes in tensile and creep tests showed that they were similar for 1 pct/h and 2.26 N/mm^2, this is not true at other strain rates and creep stresses. The difference in the volume of intergranular cracking for the same strain increases with increase of strain rate and creep stress. Since the times involved in tensile tests and creep tests at corresponding strain rates and stresses, respectively, were of the same order, these results show that short-time tensile tests do not produce equivalent behaviour to short-time creep tests.

8.5 Summary and Conclusions

Density change measurements on specimens of commercially pure aluminium, strained under constant load creep conditions at temperatures of 250 deg.C. and 500 deg.C., have proved useful in describing the growth of intergranular discontinuities in that material. With the additional aid of metallography, it was demonstrated that commercially pure aluminium at a temperature of 500 deg.C. may accommodate large internal cracks (1 mm. length) without fracture occurring. At the lower temperature of 250 deg.C., fracture occurred after the development of small intergranular discontinuities (0.1 mm. length) and with much smaller elongation at fracture. These results, which confirm the observations made in constant strain rate tensile tests, suggest that catastrophic failure would result in a specimen crept at the high temperature and small stress, so as to produce intergranular discontinuities larger than 0.1 mm., when that specimen was then subjected to the lower temperature and a larger stress.

Correlation of the results on commercially pure aluminium at 500 deg.C. with previous research on the growth of grain boundary cavities was attempted. Approximate agreement was obtained for low stresses where metallography had shown that the principal fracture process was the formation of cavities. At higher stresses, the greater incidence of triple point cracking upset the agreement in correlation. For the smallest stress (0.61 N/mm^2), the relationships, total crack volume proportional to $(time)^{1.5}$, to strain and to $(strain \times time)^{0.7}$ were found to hold. For the slightly larger stress of 0.87 N/mm^2, the relationships, total crack volume proportional to $(time)^{2.4}$, to strain and to (strain x time) were found to hold. These relationships were apparently valid for the entire intergranular fracture process – from the nucleation and growth of individual grain boundary cavities to the continued growth of large cracks, after the individual cavities had coalesced.

Comparison of density change measurements from specimens, strained under constant load creep and constant strain rate tensile conditions at a temperature of 500 deg.C., showed that the intergranular fracture processes were similar in both types of test. Although the total volume of cracking was the same for creep tests at a stress of 2.26 N/mm^2 and tensile tests at a strain rate of 1 pct/h, in which the maximum stress was 2.26 N/mm^2, this was not the case at other stresses and strain rates compared on similar terms. For large stresses or high strain rates, the volume of intergranular cracking in tensile tests was greater than in creep tests for similar testing times. The results illustrate the drawbacks in substituting short time tensile tests for creep tests. For the lower temperature of 250 deg.C., the few results obtained indicated that the intergranular fracture process was similar in both constant load creep and constant strain rate tensile tests.

Table 8.1

Temperature — 250 deg.C.

Stress N/mm^2	Strain pct	Time h	Density Change pct ($\pm$ 0.015)
76.65	0.38	0.12	—0.005
76.65	0.72	0.27	—0.006
61.50	0.30	1.75	0
61.50	0.74	4.00	—0.009
45.35	0.30	11.70	+0.005
45.35	0.63	27.67	—0.014
27.60	0.30	102.00	0
27.60	0.71	281.00	—0.006
27.60	2.85	1000.00	—0.070
17.91	0.26	265.00	—0.013
17.91	0.42	377.00	—0.026

Additional tests at 250 deg.C. on specimens annealed at 500 deg.C.

27.60	0.57	83.50	—0.030
27.60	6.56	294.00	—0.086
27.60	15.2	318.50	FRACTURE

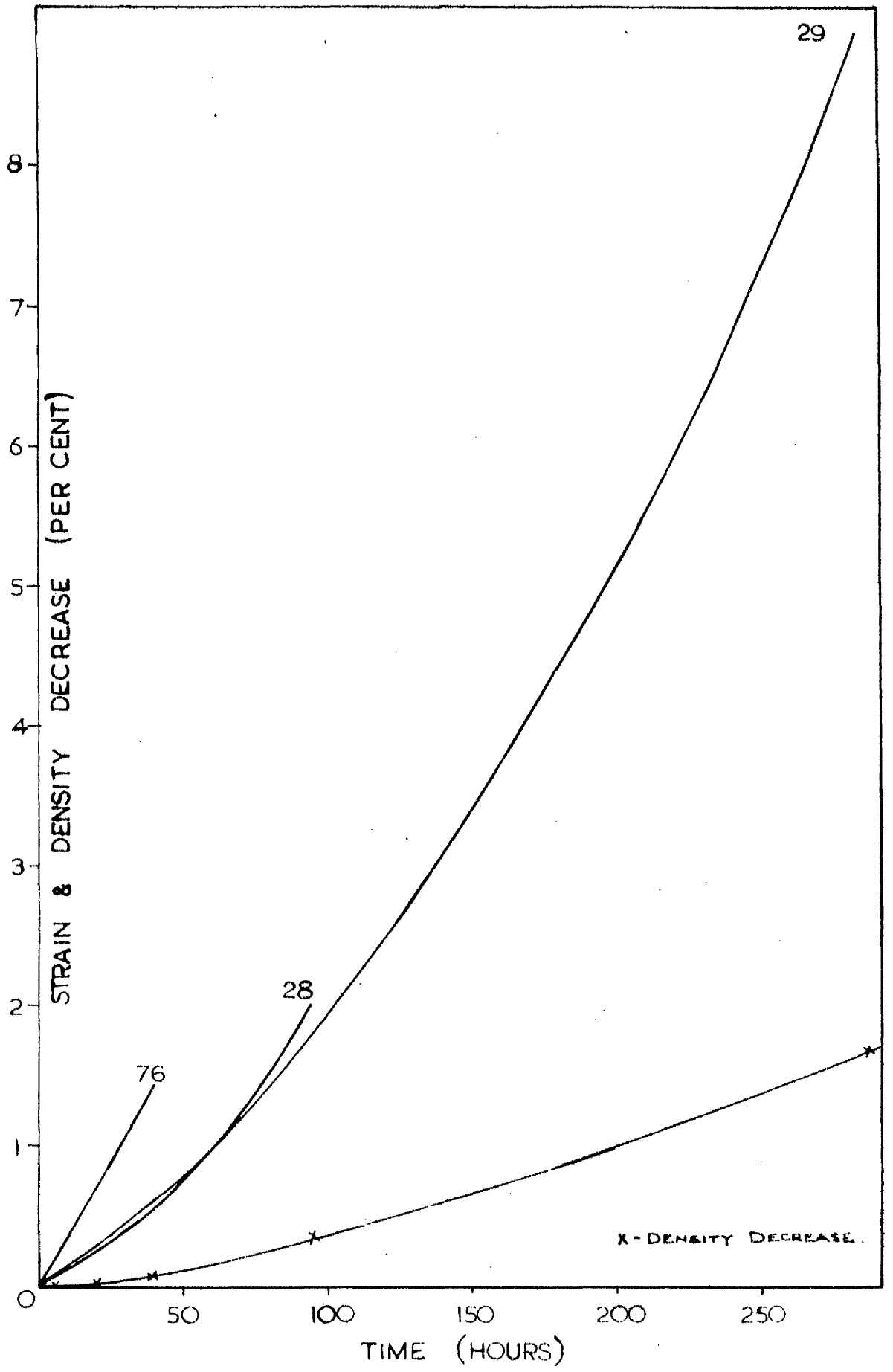

Figure 8.1. Constant load creep tests at 500 deg.C. and 0.61 N/mm^2; strain and density decrease against time

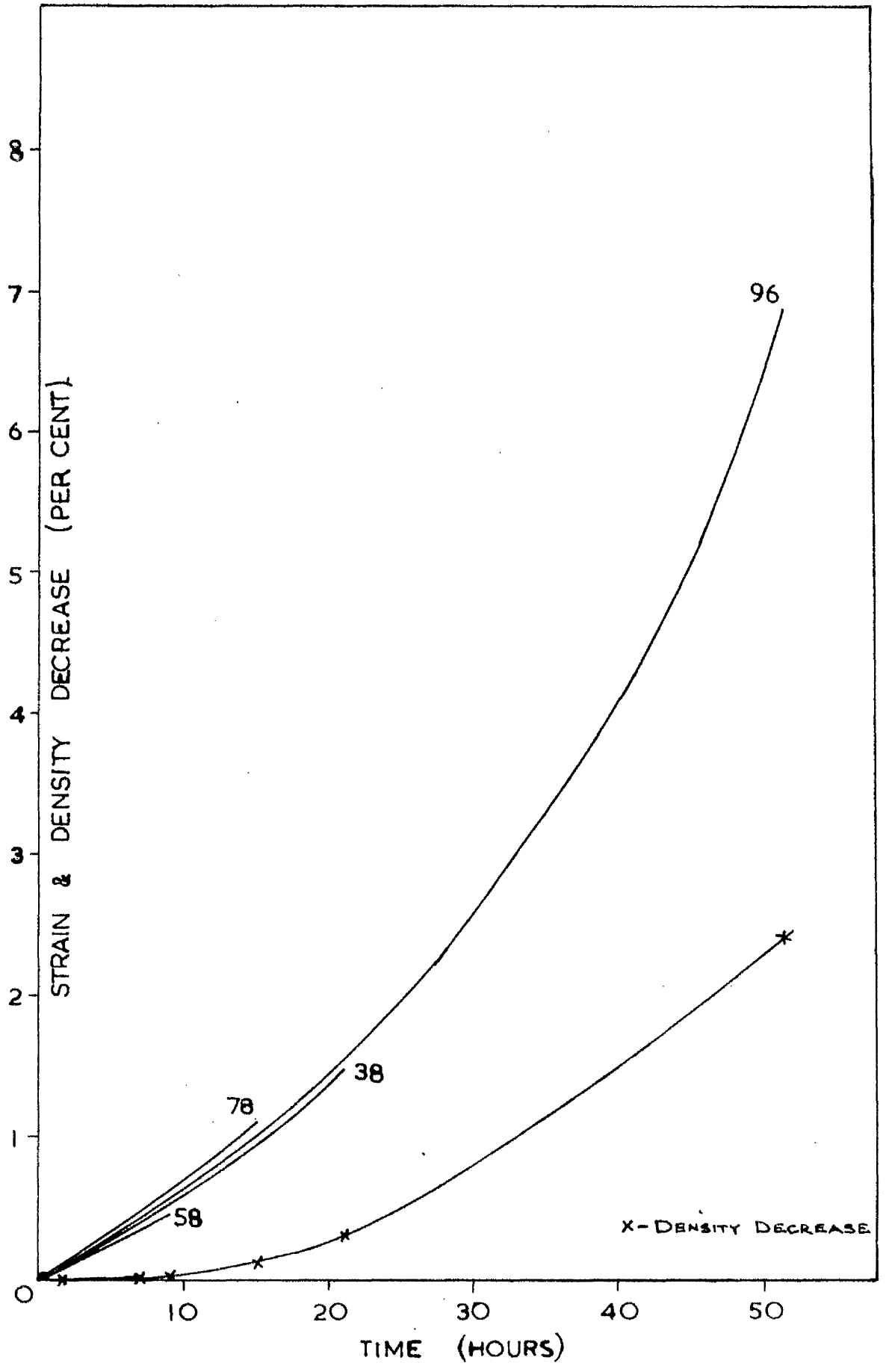

Figure 8.2 Constant load creep tests at 500 deg.C. and 0.87 N/mm^2; strain and density decrease against time

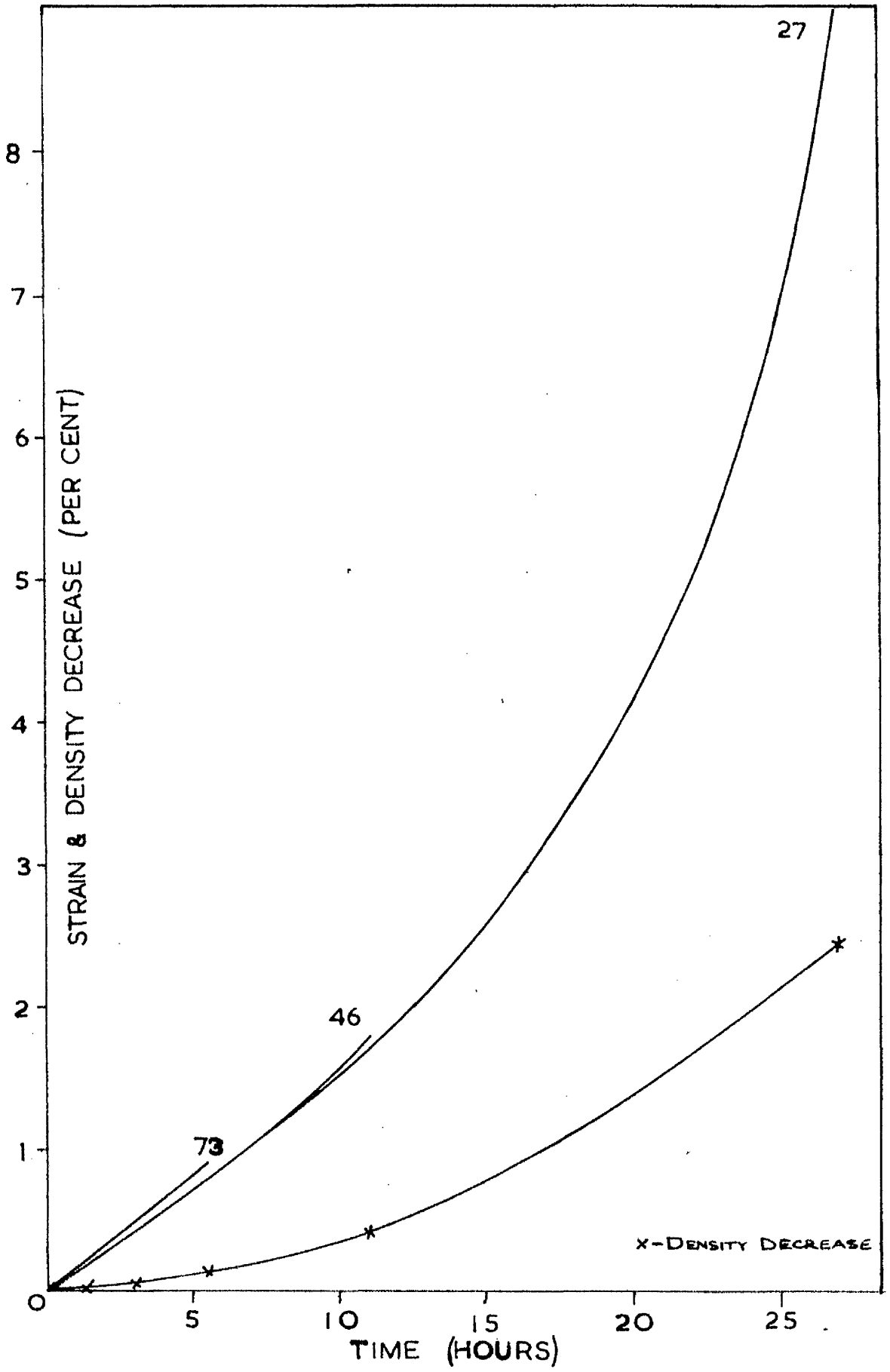

Figure 8.3 Constant load creep tests at 500 deg.C. and 1.38 N/mm^2; strain and density decrease against time

Figure 8.4 Constant load creep tests at 500 deg.C. and 2.26 N/mm^2; strain and density decrease against time

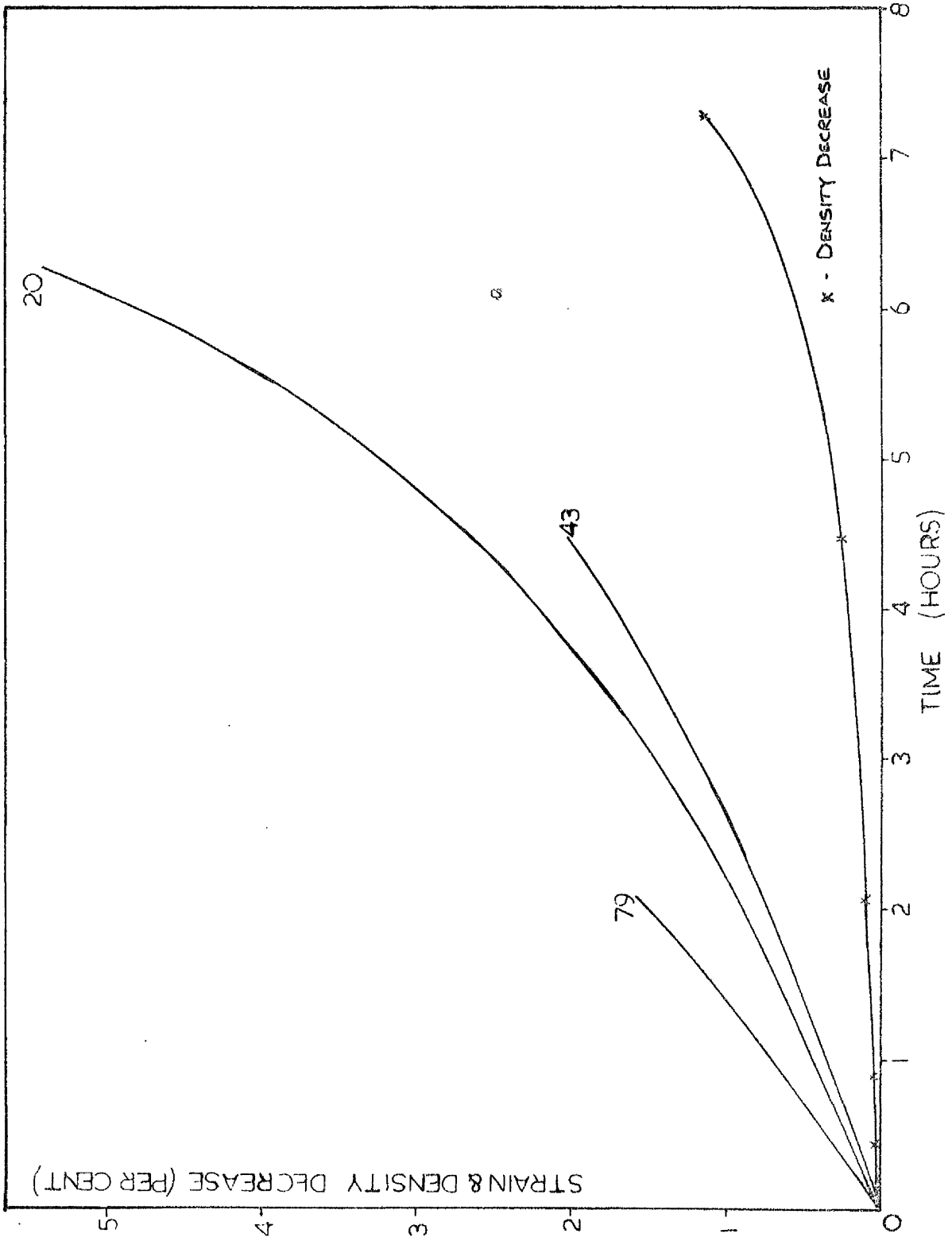

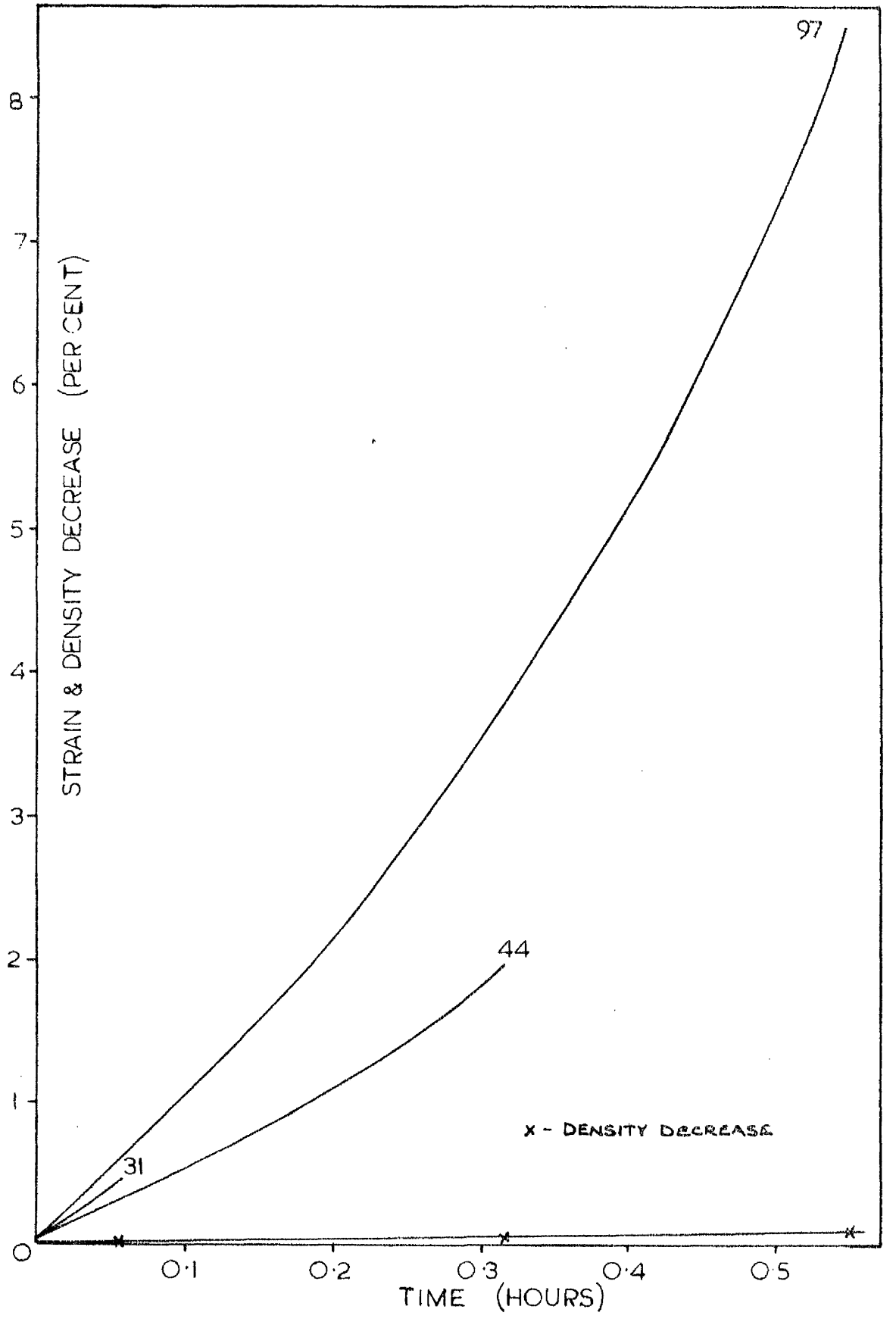

Figure 8.5 Constant load creep tests at 500 deg.C. and 3.65 N/mm^2; strain and density decrease against time

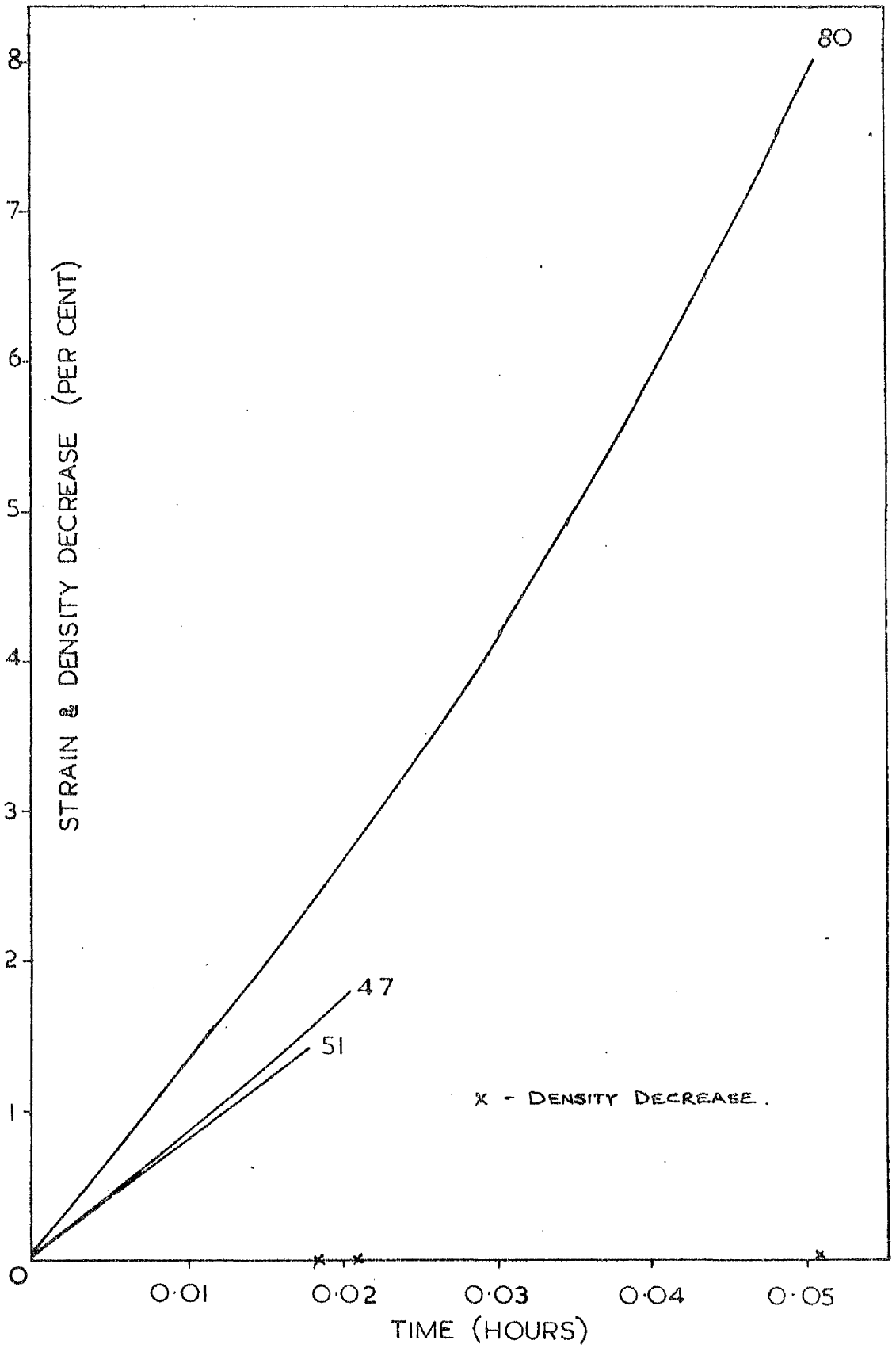

Figure 8.6 Constant load creep tests at 500 deg.C. and 4.99 N/mm^2; strain and density decrease against time

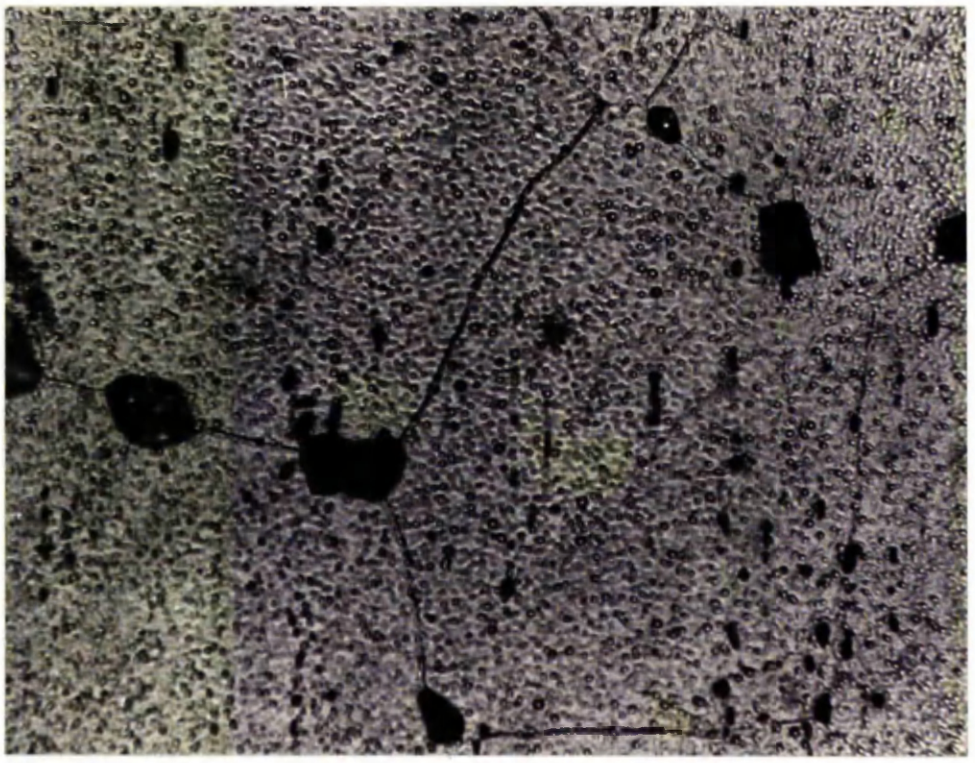

Figure 8.7 Grain boundary cavities. Creep, 500 deg.C., 0.61 N/mm^2 to 2 pct strain. Stress axis vertical. Magn. 630X.

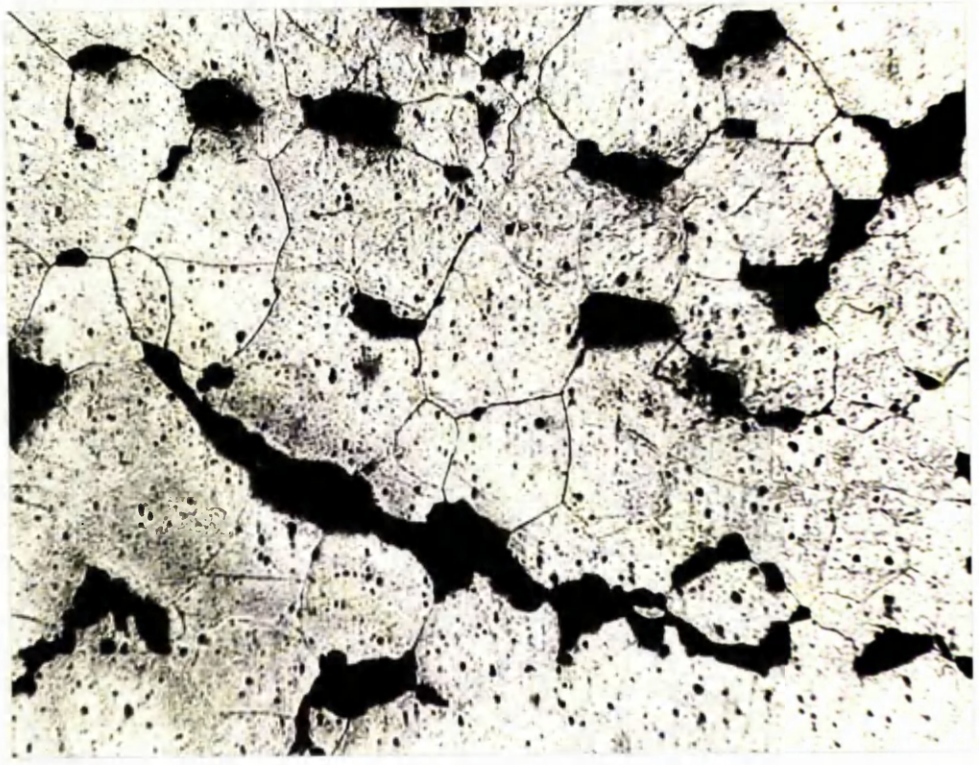

Figure 8.8 Formation of large cracks by linking of cavities. Creep, 500 deg.C., 0.87 N/mm^2 to 24.3 pct strain. Stress axis vertical. Magn. 125X.

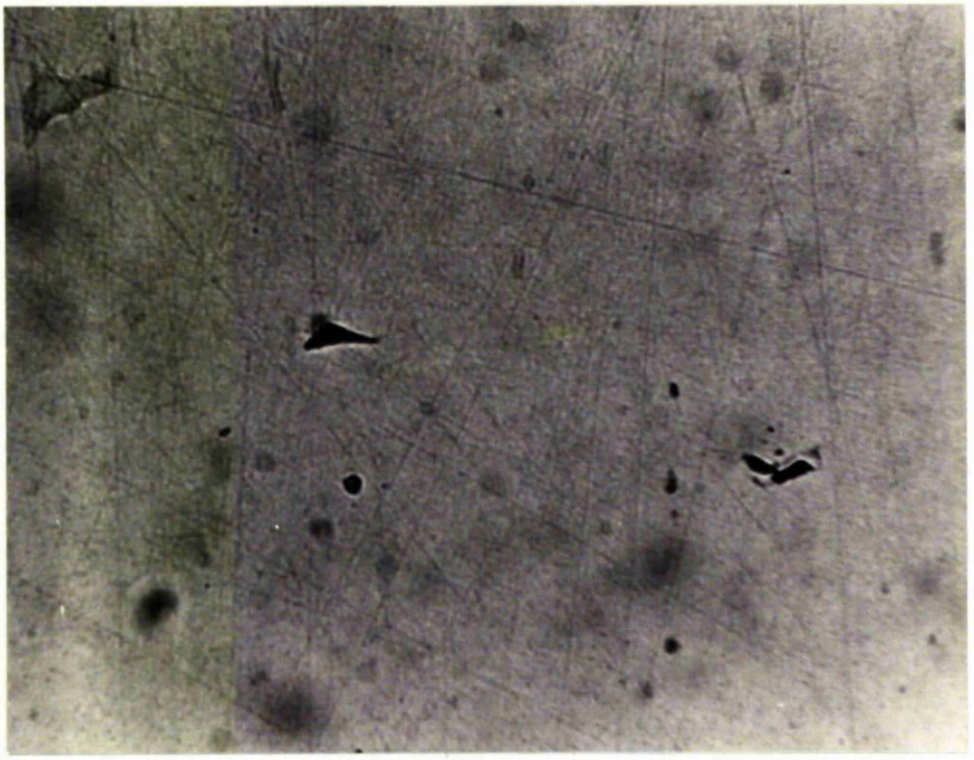

Figure 8.9 Triple point wedge crack. Creep, 500 deg.C., 3.65 N/mm^2 to 8.6 pct strain. Stress axis vertical. Magn. 630X.

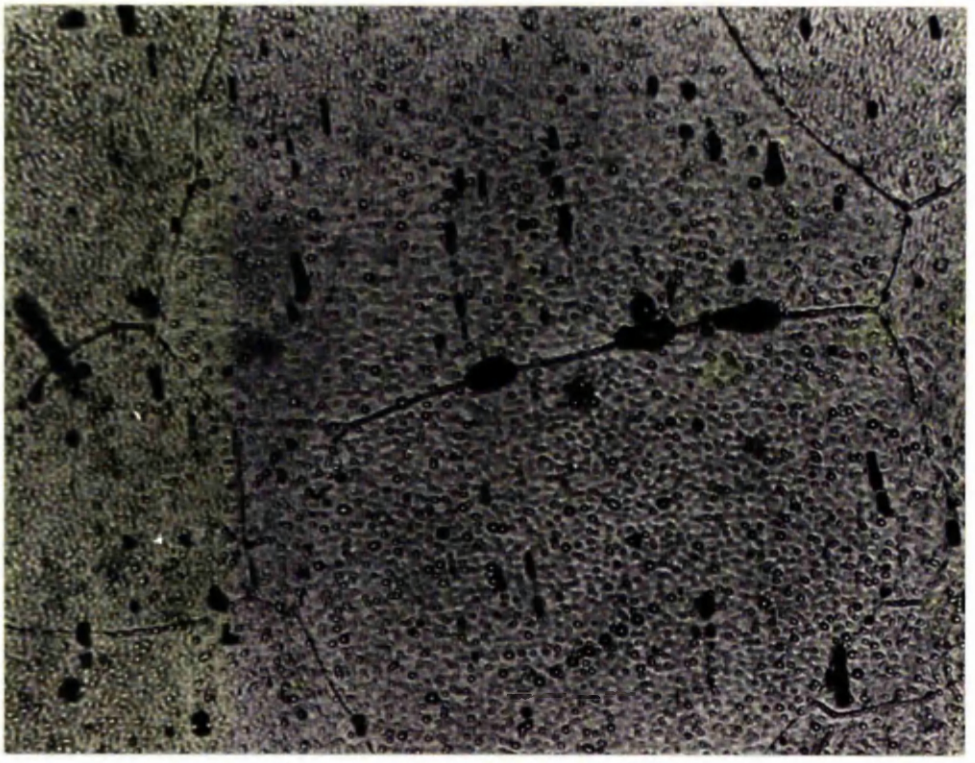

Figure 8.10 Grain boundary cavities. Creep, 500 deg.C., 3.65 N/mm^2 to 2.0 pct strain. Stress axis vertical. Magn. 630X.

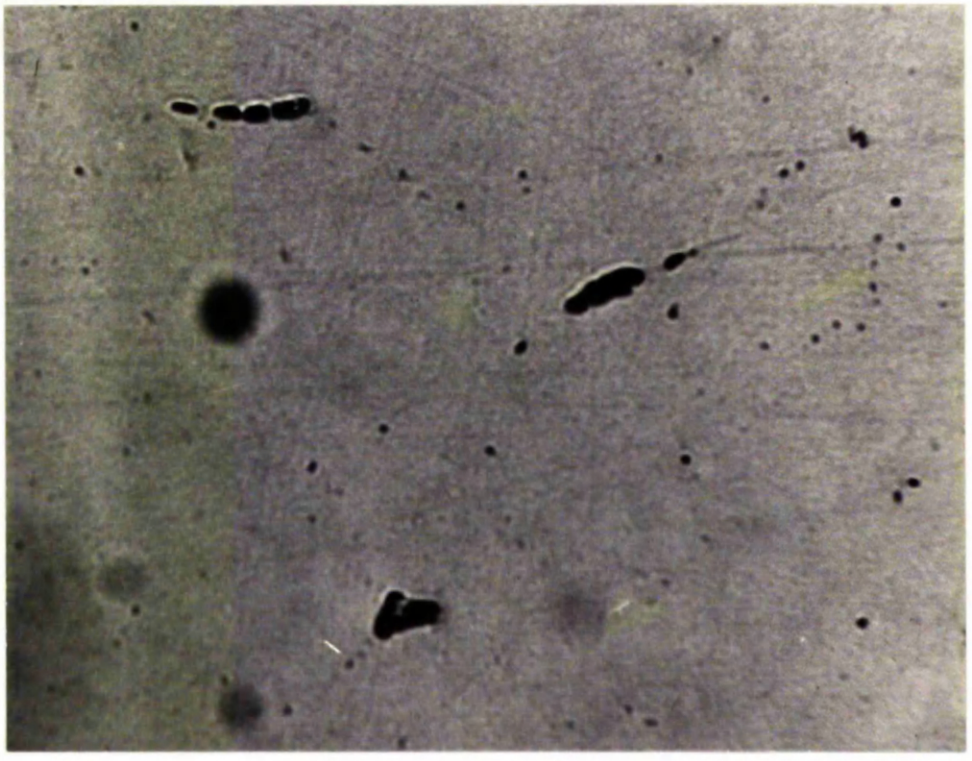

Figure 8.11 Wedge cracks and cavities. Creep, 250 deg.C., 27.60 N/mm^2 to 15.2 pct strain. Stress axis vertical. Magn. 250X.

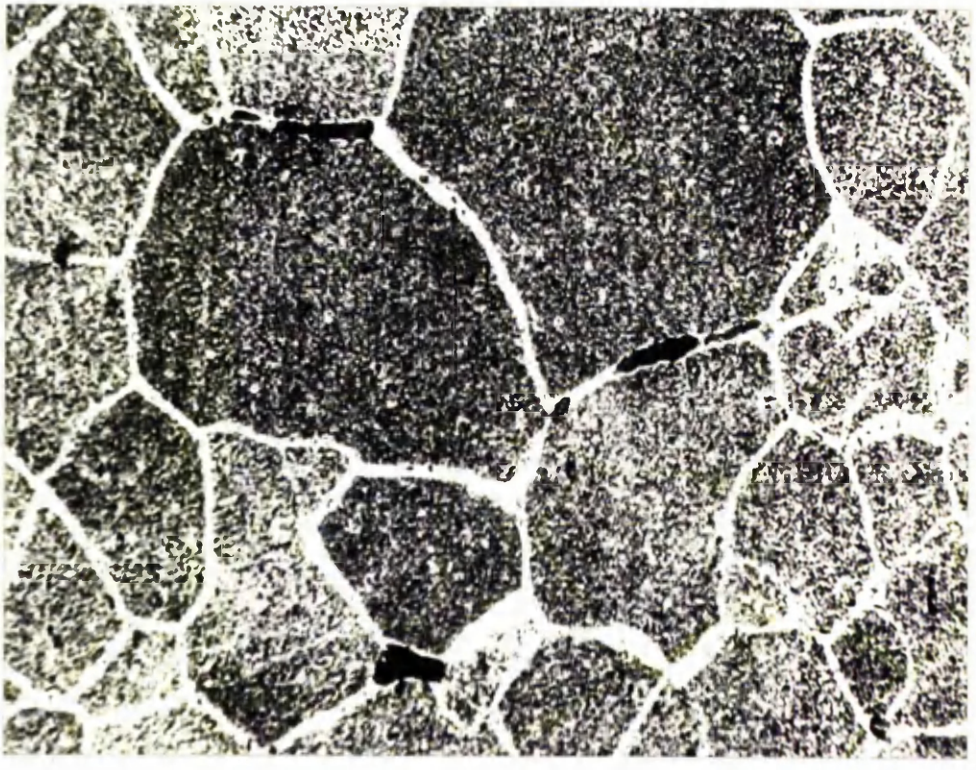

Figure 8.12 Same field of view as in Figure 8.11, after etching. Section was from 6 mm behind fracture surface. Magn. 250X.

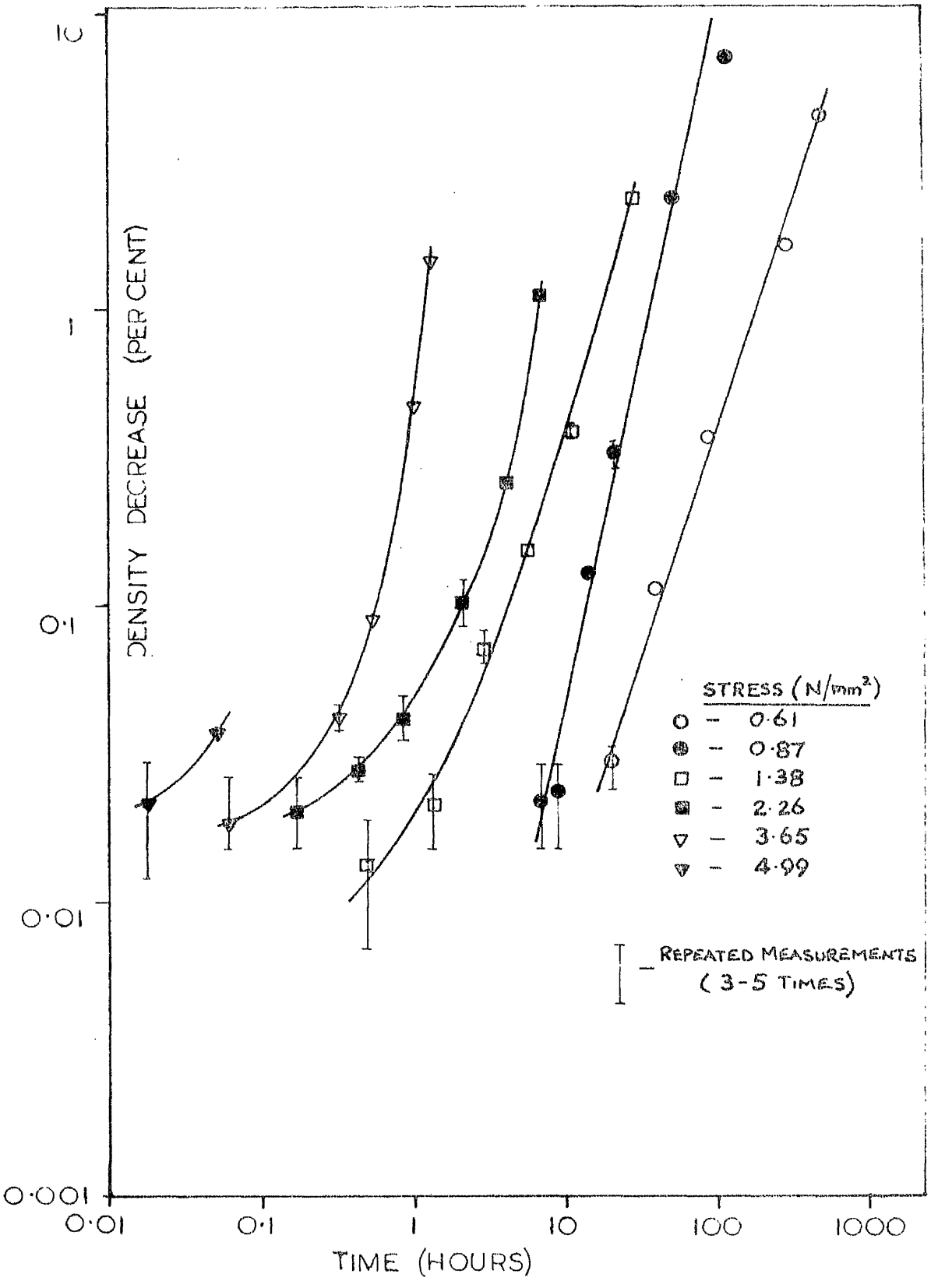

Figure 8.13 Constant load creep tests at 500 deg.C.; $\log_{10}$ (fractional density decrease) against $\log_{10}$ (time)

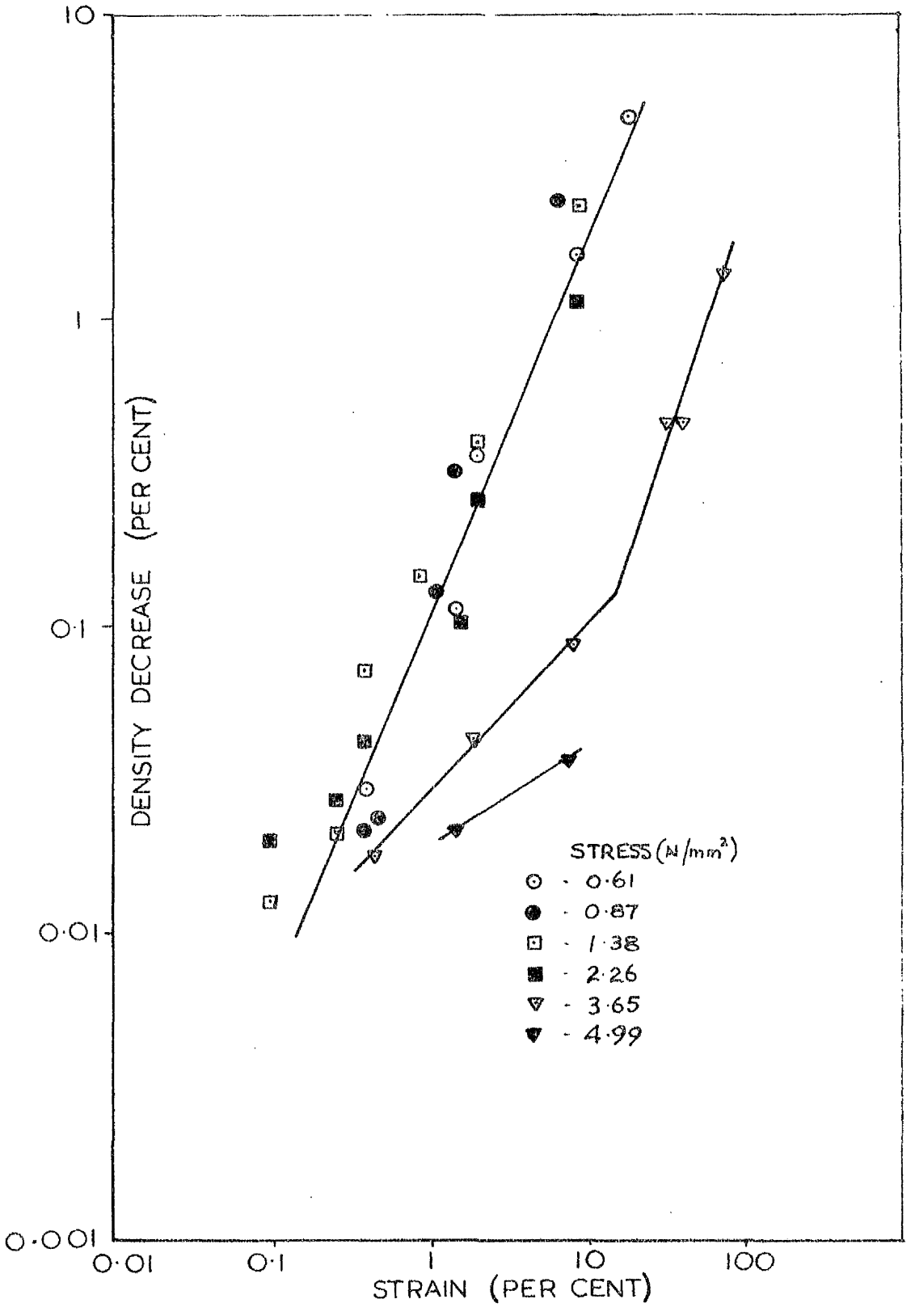

Figure 8.14 Constant load creep tests at 500 deg.C.; $\log_{10}$ (fractional density decrease) against $\log_{10}$ (strain)

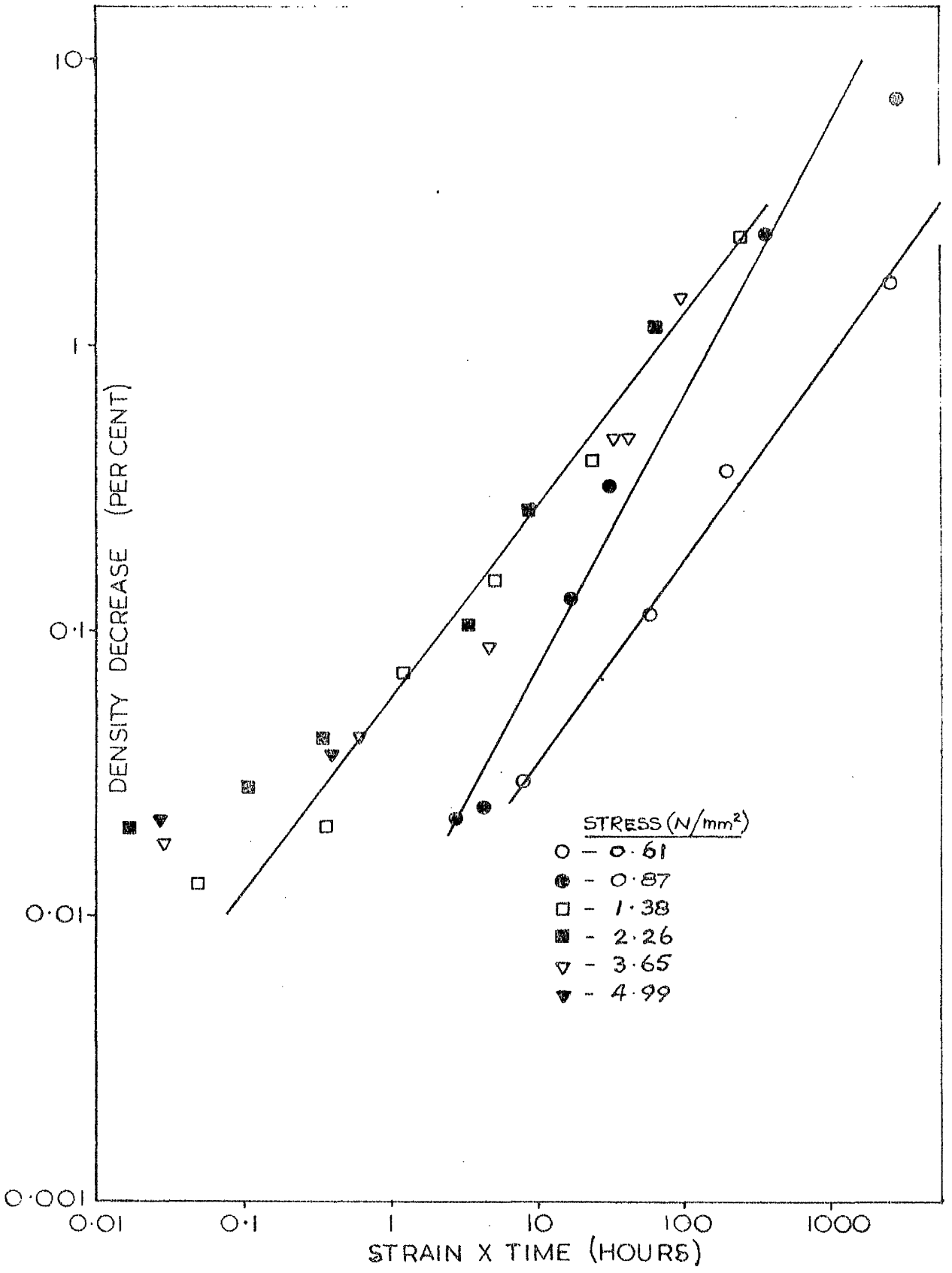

Figure 8.15 Constant load creep tests at 500 deg.C.; $\log_{10}$ (fractional density decrease) against $\log_{10}$ (strain x time)

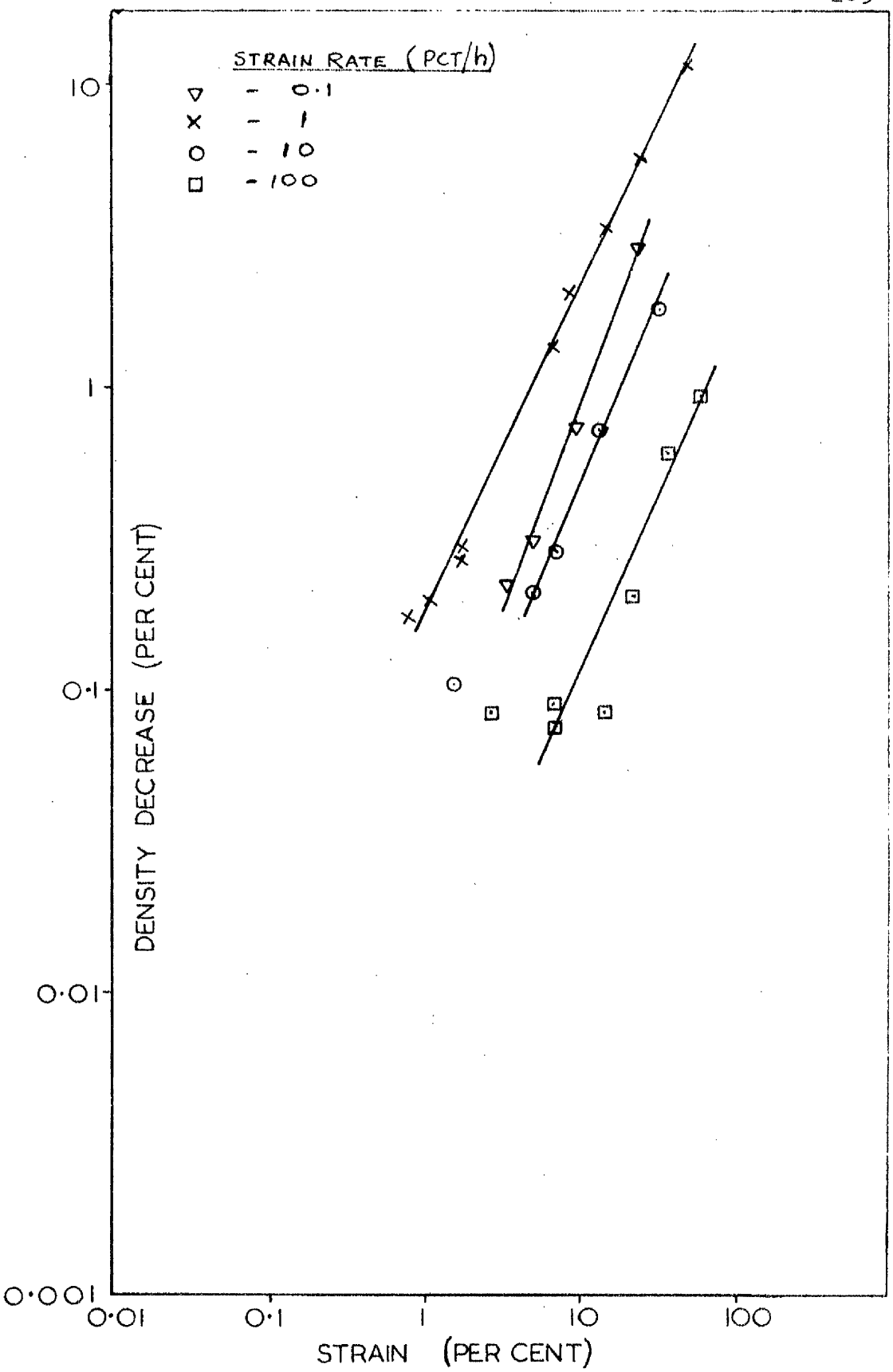

Figure 8.16 Constant strain rate tensile tests at 500 deg.C.; $\log_{10}$ (fractional density decrease) against $\log_{10}$ (strain)

CHAPTER IX

EFFECT OF INTERGRANULAR DISCONTINUITIES ON THE UNIAXIAL CREEP CURVE

9.1 Introduction

The work described in this Chapter brings together the techniques developed in Chapters II, III, and VI. In Chapter II a method was developed for producing test pieces of commercially pure aluminium with intergranular discontinuities by constant strain rate tensile testing at a temperature of 500 deg.C. Using a technique of high accuracy density measurements, a relationship between density decrease in a specimen and its strain was determined in Chapter III. Hence, test pieces could be produced with known amounts of intergranular discontinuities, the amount being determined, without destruction of the test piece, by way of the tensile strain. The Uniaxial Creep Testing of Chapter VI provided values of stress which produced low scatter strain/time curves at temperatures of 250 deg.C. and 500 deg.C. Creep tests, under those low scatter conditions of stress and temperature, were then performed on the prepared test pieces containing intergranular discontinuities. Comparison of the results with those on the material without initial discontinuities for the same temperature and stress would determine the effect of different amounts of discontinuities on the creep curves at 250 deg.C. and 27.60 N/mm^2 and at 500 deg.C. and 1.38 N/mm^2. Further comparison would be made to determine the effect of the same quantity of discontinuities under the different conditions of stress and temperature.

9.2 Experimental Procedure

The screw-grip test piece, already employed in uniaxial creep tests, was also suitable for use with the constant strain rate tensile testing equipment. Although the cross-head speed had to be adjusted to account for the longer gauge length, the same specimen grips, pull-rods and heating equipment were used. The test pieces were strained at a constant rate of 1 pct/h at a temperature of 500 deg.C., using the same experimental procedure described in Chapter II. After each test, the gauge diameter was carefully measured to ensure that no localised necking had occurred. Also, the stress/strain curve was compared with those of previous tensile tests to check that the deformation process was the same. Permanent strain was measured, as before, by the average of the three strains, measured on three pairs of points, 1.80 in. apart, at 120 degree intervals round the cylindrical surfaces of the extensometry protusions.

In general, the test pieces were deformed to one of four different strains and, therefore, the effects of four different amounts of intergranular discontinuities were determined. The largest strain was 7 pct, producing a density decrease, according to Figure 3.3, of 1.30 pct. This density decrease roughly corresponds to the size, shape and extent of intergranular cracking shown in Figure 4.5. In that figure, there are many long cracks extending along the grain boundaries of two or three grains. Since the major axis of each crack is roughly perpendicular to the stress axis, a maximum stress concentration will develop at the tip and should produce catastrophic failure in creep at 250 deg.C. The other strains employed were 3.5 pct, 1.7 pct, and 1.2 pct corresponding to density decreases of 0.57 pct, 0.24 pct and 0.17 pct, respectively. Some idea of the size, shape and number of grain boundary discontinuities for density decreases of 0.24 pct and 0.17 pct were given by Figures 2.8 and 2.11, respectively. In practice, these values of strain were not strictly adhered to and details of the value for each test piece are given later with the creep

data.

In section 2.2.2 of Tensile Testing, it was noted that, in the strain-hardening region of the stress/strain curve, the actual strain rate experienced by the test piece was as much as 100 times less than the strain rate at the maximum stress. Hence, as shown in section 3.3.2 and Figure 3.3 of Tensile Density Changes, the density decrease of a specimen strained by less than 1.4 pct at the nominal rate of 1 pct/h was larger than that predicted by extrapolating the curve produced by the other experimental points. The result was consistent with the specimen having experienced a strain rate of less than 1 pct/h. The discrepancy means that the values of density decrease assumed for the smallest strain (1.2 pct) are uncertain. In practice, the discrepancy was found to have little effect on the results, since the strain/time curves for specimens containing this smallest amount of discontinuities were consistent with the other strain/time curves from specimens containing larger amounts.

The error in the values of density decrease, measured from Figure 3.3, for the other three strains (1.7, 3.5, 7.0 pct) was considered to be less than $\pm$ 0.05 pct. This error was composed of $\pm$ 0.02 pct in the experimental points determining the density decrease/strain curve and $\pm$ 0.03 pct in the construction of the curve itself.

The next stage in the preparation of the test piece was the calculation of the loss in cross-sectional area due to intergranular discontinuities. The calculation assumed that the distribution of discontinuities along the gauge length was uniform so that the fraction of the cross-sectional area taken up by discontinuities was constant along the gauge length. The assumption was reasonable since the amounts of discontinuities were small. However, the error caused by the assumption increases with the size of the discontinuity, since the large cracks were caused by the coalescence of smaller ones. In addition, an error would

result from the temperature variation along the gauge length of the test piece during tensile straining. This error, however, was considered to be negligible.

The calculation of the cross-sectional area (A^1) of actual material of the test piece, ie. excluding the area of any discontinuities, was as follows :-

$$\text{Mass of gauge length} = \rho_1 A_1 L_1 = \rho_o A^1 L_1$$

where ρ_o was the original density of the material, ρ_1 its density after straining, L_1 was the strained gauge length, and A_1 was the measured cross-sectional area of the strained gauge length. Hence,

$$A^1 = \frac{\rho_1}{\rho_o} A_1 = (1 - \frac{\rho_o - \rho_1}{\rho_o}) A_1 \qquad (9.1)$$

The cross-sectional area of actual material may be calculated from equation 9.1 after measuring the cross-sectional area (A_1) of the strained gauge length and its fractional density decrease ($\frac{\rho_o - \rho_1}{\rho_o}$) from Figure 3.3. Then, knowing this value of area, the load necessary to produce a stress of 1.38 N/mm^2 or 27.60 N/mm^2 was calculated.

Creep tests on specimens containing discontinuities were performed in the same manner as described for creep tests on the virgin material. However, the gauge length of the test piece was now that length measured after tensile straining and creep strains were calculated from that value. Before the creep test was assembled, each prepared test piece was annealed for 1 hour at a temperature of 500 deg.C., so that it had received the same heat-treatment as the untreated test piece with which it was to be compared. From the evidence of the annealing/sintering experiments, described in section 3.4, the reduction in total crack volume, due to heating at 500 deg.C. for 1 hour, was considered negligible.

Some tests were taken to rupture but most were stopped before rupture occurred.

9.3 Results

9.3.1 Low Temperature : 250 deg.C.

Creep data for the annealed material, without any initial intergranular discontinuities, are presented in Table 9.1. The corresponding data for the annealed material, with various initial amounts of intergranular discontinuities, are presented in Table 9.2. Creep rupture data of tests which went to fracture are presented in Table 9.4. The results are illustrated graphically by the strain/time curves of Figures 9.1 and 9.2. The number associated with each curve corresponds to the Specimen Number in Tables 9.1, 9.2 and 9.4.

In Figure 9.1, the strain/time curves of test pieces, with and without initial discontinuities, are compared in the early stages of creep. For large amounts of initial discontinuities (tests 77 and 81), the strain/time curves diverge from those of the untreated material (tests 70 and 89) after application of the creep stress. However, for smaller amounts of initial discontinuities (tests 62, 65, 87), the strain/time curves are coincident with those of the untreated material during the primary stage and much of the secondary stage of the curves. The larger the initial amount of discontinuities, the earlier the strain/time curve diverges from that of the untreated material and goes into the tertiary stage. Comparison of values of minimum creep rates in Tables 9.1 and 9.2 confirms the above trend.

The results imply that small intergranular discontinuities do not affect the deformation processes in the early stages of creep of commercially pure aluminium at 250 deg.C. and 27.6 N/mm^2 : the material elongates as though the discontinuities were not present. Test 65 was stopped just as its strain/time curve was entering the tertiary stage. Density measurements on this test piece (Table 9.2) show that crack growth was almost negligible during the creep deformation, since the difference between the initial density

decrease (from Figure 3.3) and the final density decrease (after creep) was within the possible combined errors of measurement ($\pm$ 0.05 pct and $\pm$ 0.02 pct respectively). However, the same comparison applied to Test 62 (Figure 9.1 and Table 9.2) shows that significant growth occurs as the curve goes further into tertiary.

Comparison of density measurements from tests 62 and 70 shows that growth of discontinuities was more rapid when the material had some discontinuities before the start of creep. For the same creep strain, 62 increased its fractional density decrease by 0.13 pct while 70 reached a density decrease of 0.030 pct, starting from a condition of no intergranular holes. With increasing amount and size of initial discontinuities, the growth rate apparently increases and, as shown by test 87, the strain/time curve begins to diverge earlier in the creep life.

Presumably, intergranular discontinuities were growing in Tests 62 and 87 at the same small rate as in Test 70, for the period in which their strain/time curves were coincident. At first, the increase in volume of the initial discontinuities in 62 and 87 would be so insignificant (within the accuracy of the method of density change measurement, $\pm$ 0.015 pct) that the deformation process would remain unaffected. However, with the continued growth of discontinuities, it might be expected that deformation would become easier which would in turn create more cavity nuclei and again easier deformation. It would be expected, then, that the strain/time curves of the material, with and without initial discontinuities, would diverge eventually. For large amounts of initial discontinuities, such as in tests 77 and 81, the strain/time curve diverged from that of the untreated material right from the application of the creep stress, because the discontinuities were large enough either to cause easier deformation immediately or to propagate by mechanical tearing.

Figure 9.2 shows the entire strain/time curves for the four ruptured specimens at 250 deg.C. and 27.60 N/mm^2. Test

89, which, like 95, was on the annealed, untreated material, has been included to give an idea of scatter. Figure 9.2 and Table 9.4 demonstrate clearly the effect of different initial amounts of intergranular discontinuities on the creep rupture properties. As the initial amount of discontinuities increased, rupture life and ductility, as measured by elongation and reduction of area at fracture, rapidly decreased. Figure 9.3 shows the fractured specimens of tests 81, 87, 92 and 95. Although test 95 was an inter-crystalline failure, some necking did occur. However, with increasing initial amounts of discontinuities, the necking disappeared and test 81 exhibits a typical 'brittle' inter-crystalline fracture. The larger the amount of initial discontinuities, the more rapid will be the deformation process, since the local deformations around the cracks will be additive. The greater the size of individual cracks, the less they have to grow to reach the critical length capable of propagating across the entire load-bearing area. Hence, the deformation takes place in less time and fracture takes place with less total deformation.

9.3.2 High Temperature : 500 deg. C.

The results of creep tests on specimens with and without initial discontinuities, at 500 deg. C. and 1.38 N/mm^2 are presented in Table 9.3 and the rupture data in Table 9.4. The results are illustrated graphically in Figures 9.4 and 9.5 and, as before, the number on each curve corresponds to the test reference number in the tables. It was shown in section 6.6.3 that, although annealing at 500 deg.C. had an effect on the subsequent creep properties at 250 deg.C., it had no effect on creep at 500 deg.C. Hence, the strain/time curves from tests on specimens containing initial inter-granular discontinuities could be compared with those on specimens of the 'as received' material (27, 34, 46, 56, 60). Density decrease data for these five tests were plotted in Figure 8.3 alongside their strain/time curves.

In Figure 9.4, the strain/time curves of the material,

with and without initial discontinuities, are compared in the early stages of creep. For all tests at this temperature and stress, the strain/time relationship was linear for the first 1 pct of deformation. Figure 9.4 shows that the creep curve of the material containing initial discontinuities diverged from that of the untreated material right from the application of the creep stress, even for the smallest amount of discontinuities, (Test 90). The divergence increased with increasing initial amounts of discontinuities. Examination of the increases in the fractional density decreases of test pieces, containing initial discontinuities, during, provides some interesting observations. Table 9.5 compares this increase with that in the 'as received' material strained by the same amount under the same conditions of stress and temperature. Figure 8.3 was used to determine the density decrease in the 'as received' material.

Table 9.5

Test No.	Increase of fractional Density decrease (pct) (Column X minus Column Y in Table 9.3)	Creep Strain (pct)	Fractional density decrease (pct) of 'as received' material for the same strain, from Figure 8.3
83	0.16	0.74	0.11
71	0.47	0.87	0.13
85	0.30	1.01	0.17
82	1.01	2.04	0.53
86	1.21	3.74	1.21

Table 9.5 shows that, although initially the increase in total crack volume was greater for prepared test pieces, the untreated material 'catchs up' at larger strains. Hence, during the first 2 pct strain of the deformation, the presence of intergranular discontinuities greatly affects the deformation process. Presumably, the cavities in the grain

boundaries allow the deformation processes to continue more easily, thus creating more cavity nuclei and also more rapid cavity growth. That is, the presence of intergranular discontinuities allows for easier deformation and, in turn, easier deformation allows for easier cavity growth. Although this may be true for the first 2 pct of deformation, the results of test 86 suggest that, later on, the specimens containing initial discontinuities managed to 'catch up.'

Only two rupture tests were carried out at 500 deg.C. and 1.38 N/mm^2; but they were sufficient to show the trend in behaviour. Figure 9.5 shows the strain/time curves of the two tests (93, 94), with the curves of some other tests on specimens, with and without initial amounts of discontinuities, at 500 deg.C. and 1.38 N/mm^2. Tests 27 and 93 were on the untreated material and tests 88 and 94 had a large amount of initial discontinuities. Test 90 had a small amount of initial discontinuities. Figure 9.5 and Table 9.4 demonstrate that the large amount of initial discontinuities had little effect on the ductility of the material, as measured by elongation and reduction of area at fracture. Although the reductions of area were large, the values were constant along the gauge lengths of the fractured test pieces. Figure 9.6 shows the fractures in tests 93 and 94 to be typically intercrystalline with negligible localised necking having taken place. However, the word 'brittle' could not be applied to deformations of 70.0 pct or 85.5 pct. Both 93 and 94 had a large number of surface cracks uniformly distributed along the gauge length. The number and size of these cracks suggested that the whole specimen was riddled with cracks, confirming the earlier observations of metallography and density change measurements on crept specimens of the 'as received' material.

As shown by Figure 9.5, the strain/time curves of tests 94, 90 and 93, become parallel at about 10 pct strain and appear to remain so until fracture occurs. This suggests that the intergranular discontinuities in those three specimens were of the same size, shape and number for strains

greater than 10 pct. The similarity in the values of ductility for tests 93 and 94 supports this idea as do the appearance of the specimens, themselves, in Figure 9.6. The density measurements of Table 9.5 also suggested that this might occur, since test 86 showed the same increase in fractional density decrease during creep to what it would have shown, had it started without intergranular cracks. These observations suggest that the material becomes saturated with cracks and that the saturation strain is less than 10 pct. At low values of strain, test pieces with large amounts of initial discontinuities deform rapidly because the discontinuities make the deformation easier. However, at low values of strain in test pieces, with no initial discontinuities, the deformation process has to nucleate and then grow the cavities and hence the deformation is slower. When, at a strain less than 10 pct, the material becomes saturated with cracks, continued deformation will occur at the same rate in both types of test piece.

9.4 Effect of Discontinuities at High and Low Temperatures

The results described in the previous section show the effect of four different quantities of intergranular discontinuities on the creep properties of commercially pure aluminium at temperatures of 250 deg.C. and 500 deg.C. and at corresponding stresses of 27.60 N/mm^2 and 1.38 N/mm^2, respectively. An exact comparison of behaviour under the two extremes of temperature, for each quantity of initial discontinuities, is not possible since the stresses were chosen because of their low scatter strain/time curves. Hence, the comparison for the same minimum creep rates or the same rupture lives, of the annealed, untreated material at the two extremes of temperature, was sacrificed in order to determine clearly the difference in behaviour between specimens of the material, with and without initial discontinuities, at each of the temperatures. However, it may reasonably be expected that, in the absence of large-scale grain boundary migration, the behaviour at 500 deg.C. and 1.38 N/mm^2 would be similar to that at 500 deg.C. and a lower stress, which produced a minimum creep rate or rupture life equal to that of 250 deg.C. and 27.60 N/mm^2. Hence, comparison of behaviour at high and low temperatures may go ahead, if the value of each creep property is related proportionally to the corresponding value of the property for the material without initial discontinuities.

9.4.1 Minimum Creep Rates

Tables 9.1, 9.2 and 9.3 demonstrate that the same quantity of initial discontinuities had a greater effect on the minimum creep rate at 500 deg.C. than at 250 deg.C. For the largest amount of initial discontinuities (1.3 pct density decrease), tests 82 and 88 at 500 deg.C. showed a greater proportional increase in minimum creep rate than tests 77 and 81 at 250 deg.C. The minimum creep rates in tests 82 and 88 were approximately four times that of the untreated material while those of 77 and 81 were only two to three times greater. However, it must be pointed out that the proportional

increases in minimum creep rates of tests 71 and 94 at 500 deg.C. were also only two to three times greater.

For the three smaller initial amounts of discontinuities, increases in minimum creep rates at 250 deg.C. were negligible (Tests 92, 62, 65). At the higher temperature of 500 deg.C., the proportional increases in minimum creep rates were considerable (Tests 90, 85, 86). A possible explanation of this behaviour has, in effect, already been given in section 9.3. The larger rate of growth of discontinuities at the higher temperature presumably made the deformation process at that temperature easier than at the lower temperature, where the rate of growth was slow. Since the two processes of discontinuity growth and deformation are presumably complimentary, the high temperature strain/time curve diverges at the proportionately greater rate. However, as the initial amount of discontinuities in a test piece increases, the likelihood of mechanical tearing at low temperatures will also increase and, hence, tests 77 and 81, at 250 deg.C., were not as far behind tests 71, 82, 88 and 94, at 500 deg.C., as the corresponding tests with small amounts of initial discontinuities.

9.4.2 Rupture Life

When rupture data are used for comparison of the effects of similar initial amounts of discontinuities, the results show a very different trend from those of minimum creep rates. Table 9.4 and Figures 9.2 and 9.5 demonstrate clearly that, while initial discontinuities drastically reduced the ductility and rupture life at 250 deg.C., they had relatively little effect on those properties at the higher temperature of 500 deg.C. At 250 deg.C., the largest amount of discontinuities (1.3 pct density decrease, test 81) reduced rupture life by 90 pct, elongation to fracture by 87 pct, and reduction of area at fracture by 77 pct : the corresponding reductions at 500 deg.C. (Test 94) were 38 pct, 18 pct, and 5 pct, respectively. The initial discontinuities have provoked in Test 81, at 250 deg.C., the truly 'brittle'

intercrystalline failure, while in Test 94, at 500 deg.C., the material has easily accommodated them. Test 90 at 500 deg.C. and Test 92 at 250 deg.C. indicate a similar comparison for a small amount of discontinuities (0.15 pct density decrease), although Test 90 was not taken to rupture.

The different reactions, at high and low temperatures, to the same initial quantity of intergranular discontinuities, were undoubtedly due to the different maximum lengths of cracks which could be tolerated by the material under the different temperature conditions. At 250 deg.C., as surmised in section 8.2.3 of Uniaxial Creep Density Changes, the critical propagating length of a crack is of the order 0.1 mm. Cracks longer than 0.1 mm. were probably present in Test 81 before creep commenced (Figure 4.5). The deformation process at 250 deg.C. is such that some further deformation was necessary before fracture would occur. However, the further deformation was only 2 pct strain. At the higher temperature of 500 deg.C., the material has already been shown able to accommodate cracks of 0.7 mm. in length (Figure 8.8) at a low creep stress similar to 1.38 N/mm^2. Thus, the same initial amount of cracks has made little difference to the creep rupture properties of Test 94.

In the Introductory Chapter, the problem of predicting the behaviour of a metal or alloy, subjected to successive periods of different high temperature creep conditions was raised. When intergranular discontinuities develop readily at a high temperature (much greater than 0.5 Tm) and a small stress, and have little effect on the creep deformation under those conditions, it was postulated that subsequent behaviour at a lower temperature (about 0.5 Tm) and a large stress would become unpredictable. The rupture data, presented in Table 9.4 and Figures 9.2 and 9.5, confirm these statements, and show that prediction of behaviour would be impossible without accurate knowledge of the effects of different quantities of intergranular discontinuities on the creep properties at the lower temperature. Although the extremes of temperature used in the present research on aluminium are rarely, if ever, found in practice, the results adequately

demonstrate the dangers involved in extrapolating the creep data, available for a material under separate combinations of stress and temperature, to cases where several combinations of stress and temperature may be encountered. The extrapolation must endeavour to account for the difference in maximum size of cracks, which can be tolerated under different conditions, before the prediction of behaviour has any value.

The rupture data also provide an answer to the other question posed in the Introductory Chapter : does the appearance of holes in the grain boundaries constitute failure or does the material have additional reserves of strength? In commercially pure aluminium at 250 deg.C. and 27.60 N/mm^2, Tests 87 and 92 suggest that, when the intergranular discontinuities are small, the material has the ability to accommodate them and deforms, initially, as though they were not present. However, ultimately, rupture life and ductility are reduced. At the higher temperature of 500 deg.C., the same answer is derived from the reverse observations. Initially, even small amounts of intergranular discontinuities provoke faster deformation of the material. However, since the material has a greater ability to tolerate large cracks at the higher temperature, the initial cracks do not greatly reduce the rupture life or ductility. The conclusion is, therefore, that the appearance of intergranular discontinuities does not necessarily constitute failure. The criterion for failure has to be related to the size of the discontinuity which may be tolerated under the prevailing stress and temperature conditions. Thus, an amount of initial discontinuities, equivalent to a density decrease of 1.3 pct, does constitute failure at a temperature of 250 deg.C. and a stress of 27.60 N/mm^2, since the cracks are large enough to increase the overall rate of specimen deformation, resulting in a premature failure. In addition, the shape of the crack, also, will influence the criterion of failure since a discontinuity with sharp outlines will have a greater tendency to propagate than one with rounded contours.

9.5 Conclusions

Constant load creep tests have been described which demonstrate the reaction of commercially pure aluminium to four different quantities of initial intergranular discontinuities under different conditions of stress and temperature. At a temperature of 250 deg.C. and a stress of 27.60 N/mm^2, the rupture life and the ductility, as measured by elongation and reduction of area at fracture, rapidly decreased with increasing amounts of initial intergranular discontinuities. At a temperature of 500 deg.C. and 1.38 N/mm^2, the same quantities of initial discontinuities had little effect on ductility. Although not as much as at 250 deg.C., rupture life at the higher temperature was reduced, but this appeared to be due to the increase of minimum creep rate brought about by the presence of initial discontinuities. At 250 deg.C., small amounts of initial discontinuities had negligible effect on the early stages of the strain/time curves. However, for larger discontinuities, the likelihood of mechanical tearing caused a much faster rate of deformation.

The results showed that whether or not the appearance of intergranular discontinuities may be considered to constitute failure, depended on the size of the discontinuities and the stress and temperature conditions, to which they and the material were subjected. The results also illustrated the dangers of applying the separate creep data of a material under different conditions of stress and temperature to the behaviour of the material under a combination of stresses and temperatures. The effects of intergranular discontinuities may be small under one set of conditions but may cause catastrophic failure under another set.

Table 9.1

Creep data of annealed material containing no initial discontinuities at 250 deg.C. and 27.60 N/mm^2

Test No.	Anneal Period at 500 deg.C.	Creep Strain pct	Time hours	Minimum Creep Rate pct/h	Density Decrease pct from 2.6978 g/cc
74	24 h	0.32	44.5	0.0051	–
72	24 h	0.46	72.0	0.0049	–
75	12 h	0.46	72.0	0.0044	–
70	1 h	0.58	83.5	0.0051	0.030
89	1 h	6.56	294.0	0.0044	0.086
95	2 h	15.2 f	318.5	0.0044	–

f denotes fractured test piece.

Table 9.2

Creep data of annealed material containing initial discontinuities, at 250 deg.C. and 27.60 N/mm^2

Test No.	Pre-Strain pct	Density Decrease pct(from Fig 3.3)	Creep Strain pct	Time hours	Minimum Creep Rate pct/h	Density Decrease pct from 2.6978 g/cc
92	0.9	0.13	8.08 f	228.5	0.0047	–
62	1.8	0.25	0.55	69.0	0.0048	0.380
65	2.4	0.36	0.38	52.5	0.0052	0.413
87	3.6	0.60	3.62 f	107.8	0.0059	–
77	6.9	1.27	0.51	27.5	0.0103	1.489
81	7.0	1.30	2.04 f	28.3	0.0120	–

f denotes fractured test piece.

Table 9.3

Creep data of annealed material, with and without initial discontinuities, at 500 deg.C. and 1.38 N/mm^2

Test No.	Pre-Strain pct	Y Density Decrease pct (from Fig 3.3)	Creep Strain pct	Time hours	Minimum Creep Rate pct/h	X Density Decrease pct from 2.6978 g/cc
90	1.2	0.17	36.4	35.0	0.200	–
85	1.5	0.21	1.01	4.25	0.232	0.510
86	1.8	0.25	3.74	12.0	0.257	1.459
83	3.4	0.56	0.74	2.5	0.287	0.717
71	6.7	1.23	0.87	2.0	0.430	1.697
82	6.9	1.28	2.04	3.25	0.578	2.294
88	7.1	1.31	14.3	11.0	0.669	6.680
94	7.1	1.31	70.0 f	32.5	0.397	–
73	Annealed 500 deg.C. 24 h	0.89		5.5	0.156	0.150
93	Annealed 500 deg.C. 1 h	85.5 f		53.5	0.146	–

f denotes fractured test piece.

Table 9.4

Creep Rupture Data of annealed material, with and without initial discontinuities

Specimen No.	Pre-Strain pct	Density Decrease pct(from Fig 3.3)	Rupture Life h	Rupture Strain pct	Reduction of Area at Fracture pct
At 250 deg.C. and 27.60 N/mm^2					
95	0	0	318.5	15.2	52.60
92	0.9	0.13	228.5	8.08	29.05
87	3.6	0.60	107.8	3.62	16.64
81	7.0	1.30	28.3	2.04	11.93
At 500 deg.C. and 1.38 N/mm^2					
93	0	0	53.5	85.5	47.75
94	7.1	1.31	32.5	70.0	45.15

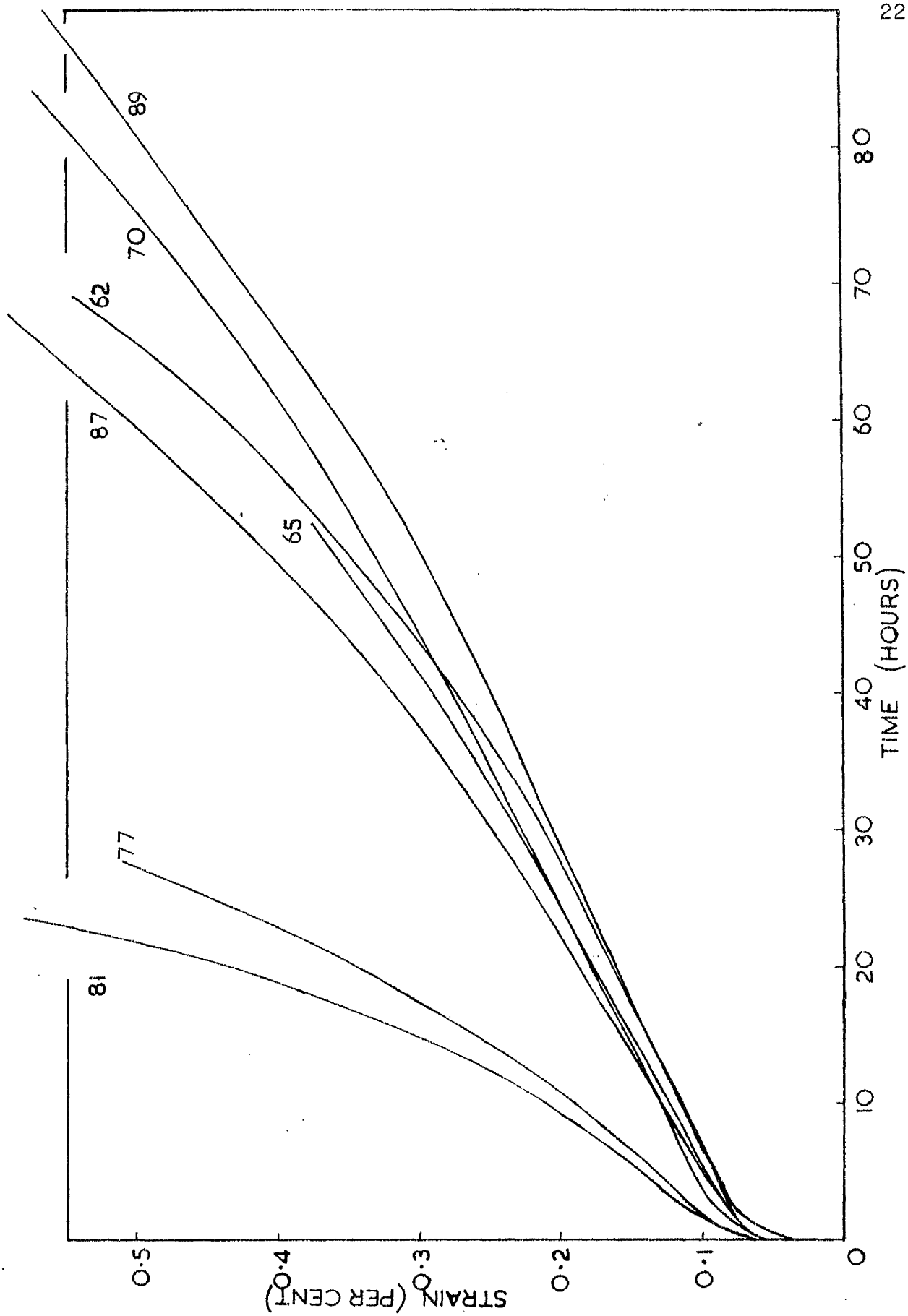

Figure 9.1 Constant load creep tests at 250 deg.C. and 27.60 N/mm^2 on test pieces with and without initial intergranular discontinuities.

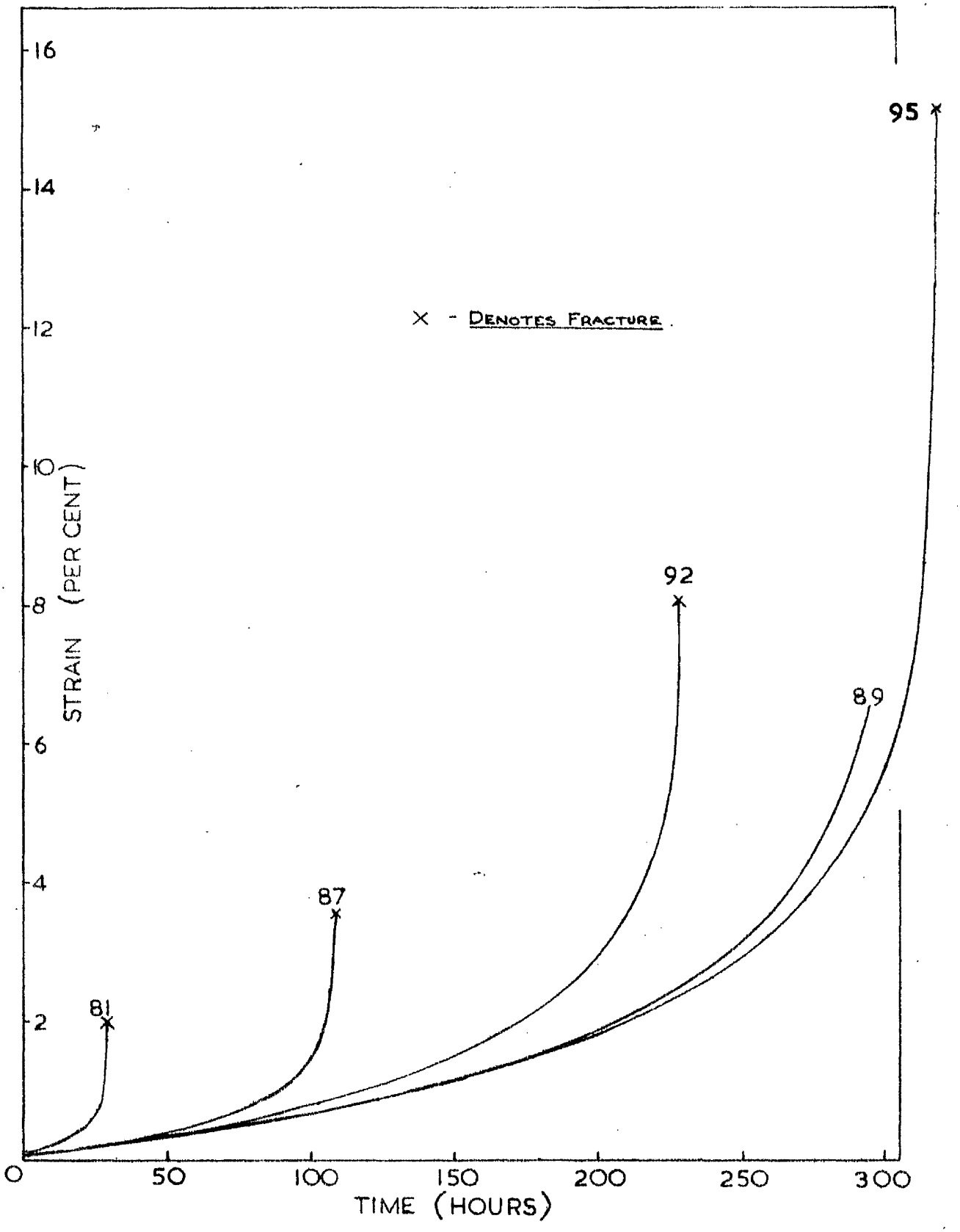

Figure 9.2 Constant load creep tests at 250 deg.C. and 27.60 N/mm^2 on test pieces with and without initial intergranular discontinuities

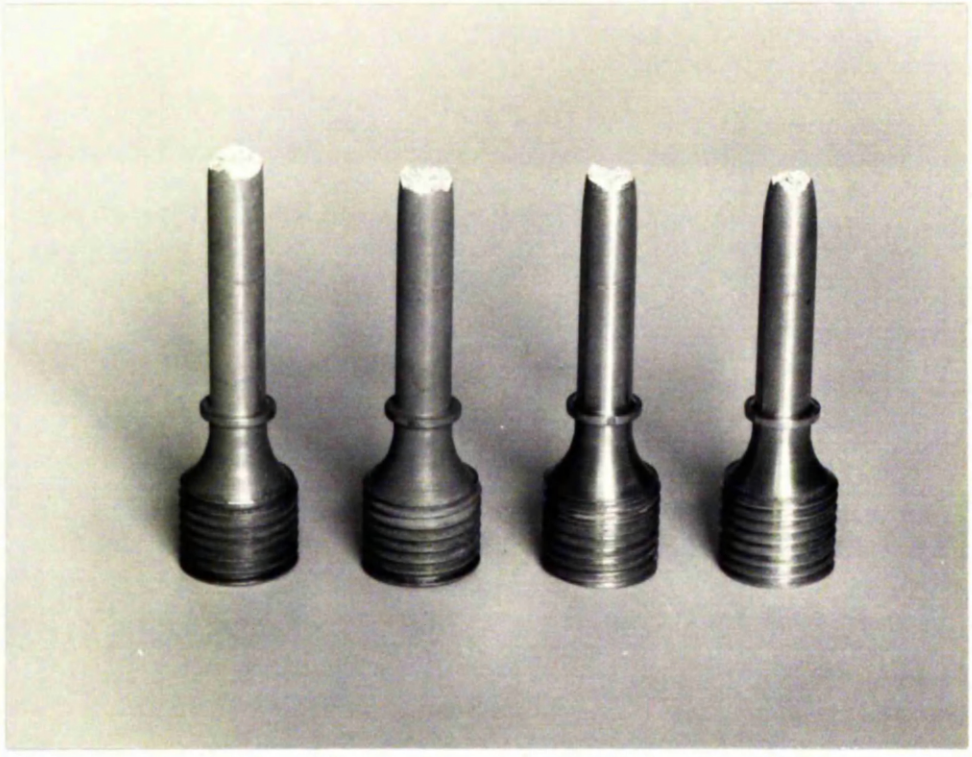

Figure 9.3 Creep, 250 deg.C. and 27.60 N/mm^2. From left to right, fracture profiles from Tests 81, 87, 92, 95 (see Table 9.4).

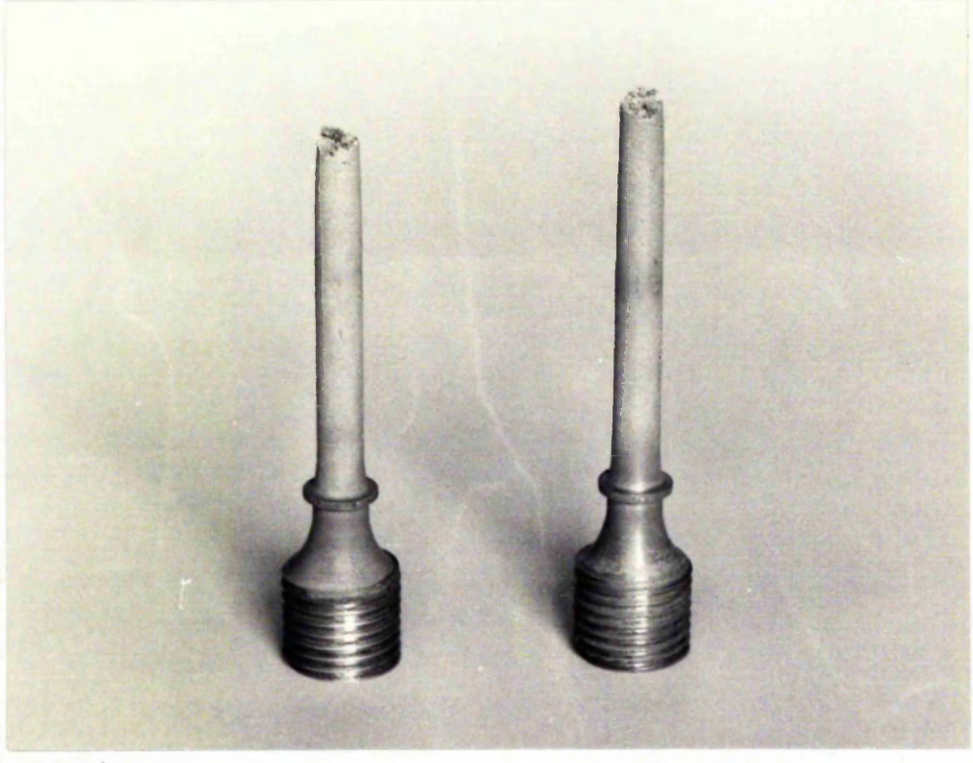

Figure 9.6 Creep, 500 deg.C. and 1.38 N/mm^2. Fracture profiles from Tests 93(right) and 94(left).

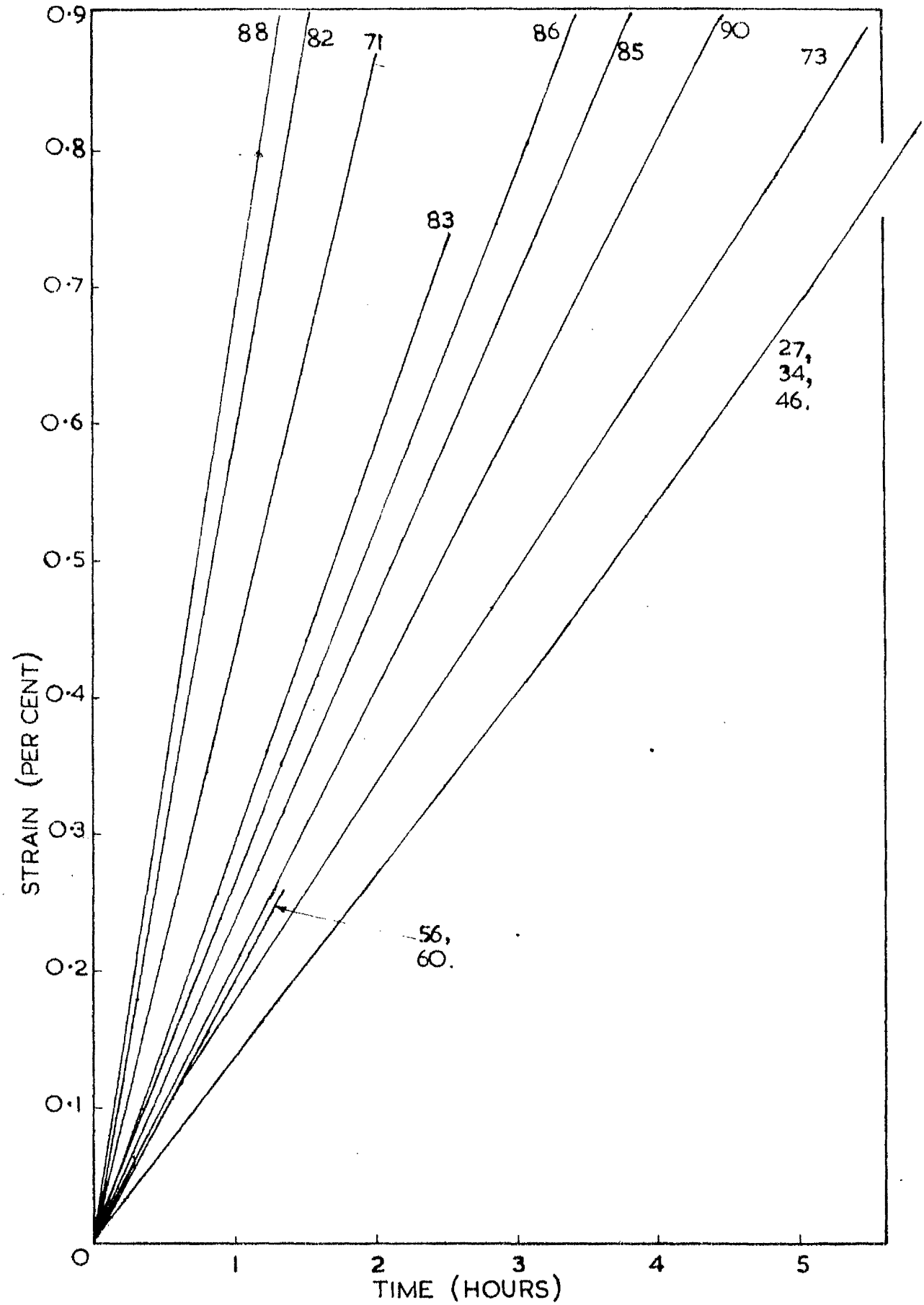

Figure 9.4 Constant load creep tests at 500 deg.C. and 1.38 N/mm^2 on test pieces with and without initial intergranular discontinuities

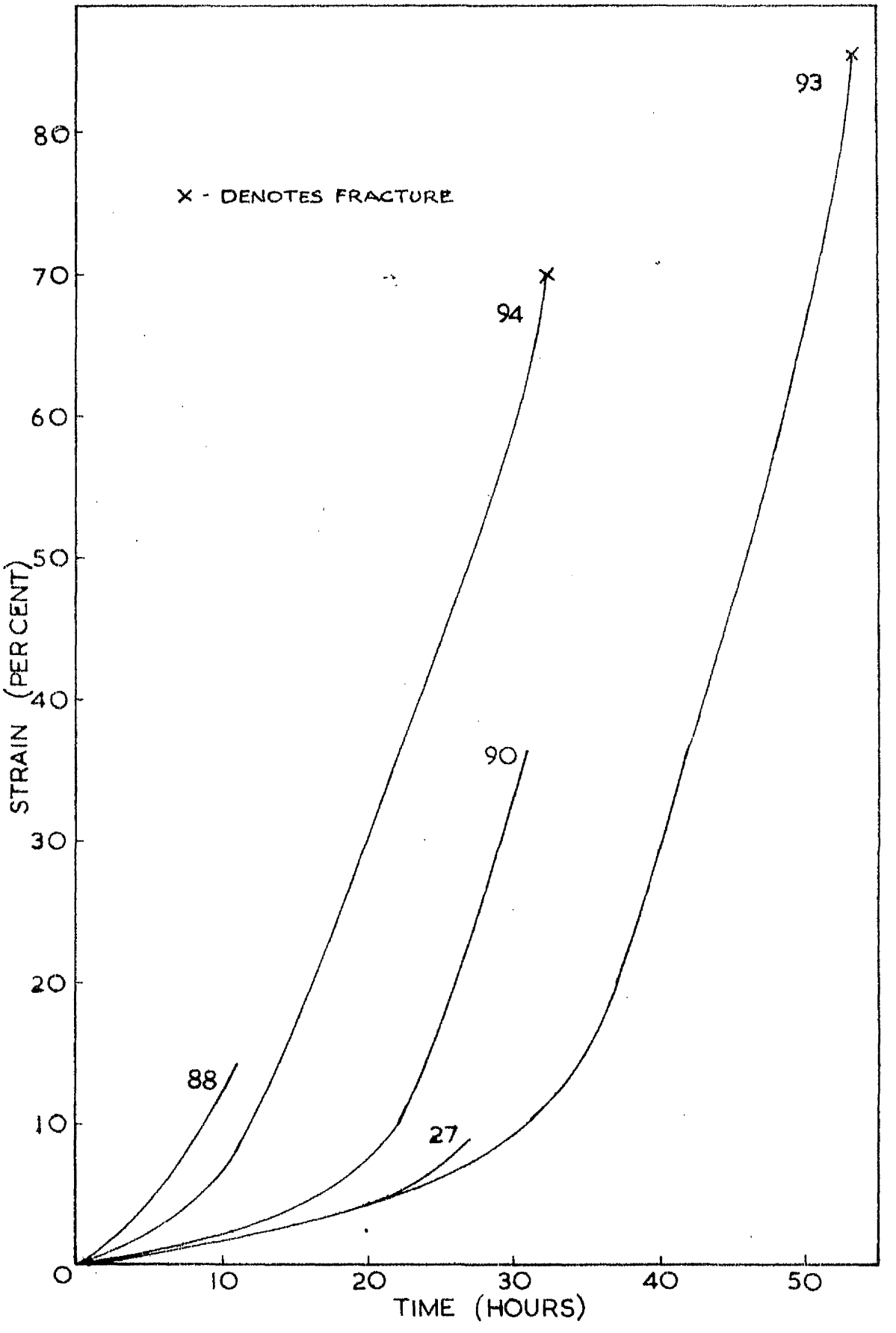

Figure 9.5 Constant load creep tests at 500 deg.C. and 1.38 N/mm^2 on test pieces with and without initial intergranular discontinuities

CHAPTER X

BIAXIAL STRESS CREEP TESTING

10.1 Introduction

In this chapter, a method of creep testing thin-wall tubular specimens of commercially pure aluminium under internal pressure at temperatures of 250 deg.C. and 500 deg. C. will be described. As pointed out in the Introductory Chapter, the objective of these tests was to show the effects of intergranular discontinuities on the creep properties of the material under a stress system other than the uniaxial stress state. With the thin-wall tube under internal pressure, a biaxial stress system is set up in the tube wall. The two principal stresses are tensile, and consist of a hoop or tangential stress σ_θ ($= \frac{PD}{2t}$) and an axial stress σ_L ($= \frac{PD}{4t}$) (P – internal pressure, D – internal diameter, t – wall thickness). Equations 1.3 and 1.10 defined the relationships between effective stress $\bar{\sigma}$ and the parameters P, D, and t, and between effective strain $\bar{\varepsilon}$ and the fractional change in diameter :–

$$\bar{\sigma} = \frac{\sqrt{3}}{4} \frac{PD}{t} \qquad (1.3)$$

$$\bar{\varepsilon} = \frac{2}{\sqrt{3}} \frac{\delta D}{D} \qquad (1.10)$$

These relations were derived for an isotropic material in which the principal strain axes do not rotate. These conditions have been assumed to apply to the present batch of commercially pure aluminium. In addition, the validity of the equations depends on the maintaining of a constant

ratio between hoop and axial stresses. While the tube retains its cylindrical shape the ratio will be constant, but, when localised bulging of the tube occurs, the equations will no longer apply. The present tests were carried out at constant pressure and, therefore, the effective stress increased as the tube deformed. Hence, the tests may be regarded as analagous to the constant load uniaxial creep tests. The assumption was also made that the elastic strains in the tube wall were negligible in comparison to the plastic strains.

The tube testing equipment, therefore, required the accurate control and measurement of pressure P and some means of measuring the change in diameter of the tube as it deformed. Since the deformation was to take place at temperatures of 250 deg.C. and 500 deg.C., some difficulty was expected in obtaining an accurate measurement of change in diameter. The design and development of the apparatus are described in the next section.

At first, it was intended to carry out biaxial stress creep tests at temperatures of 250 deg.C. and 500 deg.C. and at effective stresses corresponding to each of the tensile stresses used in the uniaxial creep tests, described in Chapter VI. It was further intended to perform similar tests to those described in Chapter IX, but under biaxial stress conditions. Tube test pieces with different amounts of intergranular discontinuities would be creep tested under internal pressure such that the effective stress at 250 deg. C. would be 27.60 N/mm^2 and at 500 deg.C. it would be 1.38 N/mm^2. As well as obtaining creep data, it was also intended that density measurements would be made on deformed specimens. Hence, the tube testing equipment was designed and built to accommodate the full range of stresses at the two test temperatures.

Owing to lack of time, this programme of testing could not be carried out and tests had to be restricted to one stress at 500 deg.C. and one at 250 deg.C. Another problem was the method of preparation of tube test pieces with a

known, controlled amount of intergranular discontinuities. To carry out a proper comparison with uniaxial tests, the discontinuities would have to be put into the tube specimens in the same way that they had been put into the uniaxial specimens, ie. by constant strain rate tensile testing at 500 deg.C. and 1 pct/h. Although it was possible to prepare tube test pieces with intergranular discontinuities by that method, subsequent machining operations to produce a pressure tight specimen, suitable for biaxial stress creep testing, were very difficult, due to the softness of the material after being heated to 500 deg.C. Alternatively, it could be argued that the discontinuities should be put in by deforming the tube under internal pressure at 500 deg.C. such that the effective strain rate was 1 pct/h. Apart from the difficult technical feat of controlling the increase of internal pressure such that the effective strain rate would be 1 pct/h, this method would probably not produce the same amount of intergranular discontinuities. The method adopted was creep testing under internal pressure at 500 deg.C., such that the effective stress was 2.26 N/mm^2 (the maximum stress in tensile tests at 500 deg.C. and 1 pct/h). Hence, tube tests at 500 deg.C. were conducted at an effective stress of 2.26 N/mm^2 and some of the deformed specimens were then creep tested at 250 deg.C. under internal pressure such that the effective stress was 27.60 N/mm^2. Biaxial stress creep tests at 250 deg.C. and 27.60 N/mm^2 effective stress were also performed on tube test pieces previously annealed at a temperature of 500 deg.C. and containing no initial discontinuities.

Thus, biaxial stress creep tests, by thin-wall tubes under internal pressure, were performed on commercially pure aluminium at 250 deg.C. and an effective stress of 27.60 N/mm^2 and at 500 deg.C. and an effective stress of 2.26 N/mm^2. These tests could be compared with the corresponding uniaxial creep tests. Further biaxial stress creep tests were performed at 250 deg.C. and 27.60 N/mm^2 effective stress on some of the tube test pieces previously deformed at 500 deg.C. The results of these biaxial tests could then be

compared with the corresponding uniaxial tests described in Chapter IX, with the reservation that the intergranular discontinuities had been put into the material in different ways.

10.2 Tube Testing Equipment

The dimensions of the tube test piece would dictate the design of the rest of the apparatus and hence it was important to determine the dimensions before proceeding further. The commercially pure aluminium was obtained in the form of 1 in. diameter extruded rod. Uniaxial tensile and creep specimens of 0.357 in. (9.07 mm.) diameter were machined from the rod so that the axes of test piece and original rod were coincident. Ideally, tube test pieces should be machined in similar fashion with the same overall diameter so that the same material would be used for both uniaxial and biaxial tests. However, a thin-wall tube of that overall diameter would have been difficult to machine and measurement of the increase in diameter during a creep test even more difficult. For the latter reason, as large an overall diameter as possible was desirable. Metallography of the 'as received' rod showed the grain size to be reasonably constant across the entire 1 in. diameter. Radial and longitudinal sections also showed the grain structure to be equiaxed. It was considered valid, therefore, to use a tube test piece of $\frac{3}{4}$ in. overall diameter and $\frac{1}{32}$ in. wall thickness. The diameter/wall thickness ratio was then comfortably greater than the ratio 10:1 normally regarded as the limit for considering a tube to be thin-wall.

Using the above tube dimensions, the constant strain rate tensile data and the concept of effective stress as the link between uniaxial and multiaxial stresses, calculations showed that internal pressures of 10 – 60 lbf/in^2 (0.07 – 0.40 N/mm^2) would be required at a temperature of 500 deg.C., pressures of up to 1000 lbf/in^2 (7 N/mm^2) at a temperature of 250 deg.C., and pressures of the order 1500 lbf/in^2 (10 N/mm^2) at room temperature to deform the tube specimen. Cylinders of gas were commercially available with pressures of 2500 lbf/in^2 (17 N/mm^2). Hence, it was decided to use argon gas from a commercially available cylinder as the means of producing an internal pressure in the tube specimens. Argon was selected to avoid complications of gas reaction

with the material during testing. The pressure control and measurement system was designed to cater for argon gas pressures of 10 – 1500 lbf/in^2 with supply of gas from an argon cylinder at 2500 lbf/in^2 initial pressure.

In all experimental investigations on thin-wall tubes subjected to internal pressure, it is necessary to reduce the end effects to a minimum. It is usually recommended that the parallel portion of the tube should be at least four times the outside diameter of the tube (Mellor, 1962). In the present test piece, a parallel length of 4 in. was chosen providing a length/diameter ratio of 5:1. In the subsequent design of a suitable furnace to heat the test piece to 250 deg.C. or 500 deg.C., a constant temperature length of 4 in. was aimed for.

10.2.1 Pressure Control and Measurement

A schematic diagram of the Pressure Control and Measurement system is shown in Figure 10.1. All of the equipment used in this system was available commercially, being employed mainly in the field of hydraulics. Pressure lines were of steel tubing – $\frac{1}{4}$ in. O.D., $\frac{1}{8}$ in. wall thickness. The pressure regulator was of the spring loaded diaphram type and fitted directly on to the argon cylinder. Two regulators were used : the first had a delivery range of 0 – 100 psig. and was suitable for tests at a temperature of 500 deg.C. ; the second had a delivery range of 0 – 3000 psig. and was suitable for tests at a temperature of 250 deg.C. (and room temperature if required). The delivery pressure from the regulators was measured approximately by Pressure Gauge 1, which registered pressure to $\pm$ 10 psig.

Two of the major problems in the pressure testing of tubes arise when the tube ruptures. One is the destructive force of the pressure supply and the other is the total loss of that supply. These two problems were overcome in the present apparatus by employing a surge check valve (Kooistra et al. 1952) to shut off the gas supply when the tube

ruptured and by making the total volume of the pressure system as small as possible. During a creep test, shut-off valve 3 (Figure 10.1) remained closed and the surge check valve allowed passage of the small flow of gas necessary to maintain constant pressure in the system. When the tube test piece ruptured, the large pressure difference across the valve caused a poppet to rise against a seating, shutting off the flow of gas. The poppet was held in this position by the pressure difference until pressures were again equalised.

Accurate measurement of pressure, over the wide range of anticipated internal pressures, required the use of three separate gauges. All three were of the Bourdon tube type and had an accuracy of $\frac{1}{4}$ pct of full scale reading. Thus, pressure gauge 2 measured pressure to $\pm \frac{3}{4}$ psig, pressure gauge 3 to $\pm$ 5 psig and pressure gauge 4 to $\pm 1\frac{1}{2}$ psig. Shut-off valves 6 and 7 (Figure 10.1) allowed the use of the appropriate pressure range without damage to a gauge whose maximum was less than that range.

Shut-off valve 5 (Figure 10.1) was a needle type valve so that initial pressurising of the tube test piece could take place at a controlled rate. With this valve, and valves 1 and 4, closed, the pressure system was tested before use with a tube specimen. The low pressure regulator was found to be capable of maintaining, for long periods, a specified initial pressure to within the $\pm \frac{3}{4}$ psig accuracy of gauge 2. The high pressure regulator was found to be insensitive to pressure changes of less than 5 psig. Thus, setting of the initial pressure was only possible to approximately $\pm$ 5 psig of the desired value. A further consequence of this insensitivity was the inability of the regulator to correct the small pressure losses due to leaks in the closed system. These losses amounted to a decrease of pressure of approximately 5 psig at 400 psig for the first 2 – 3 hours. Thereafter, the setting of the regulator accounted for the small pressure losses and the pressure reading on Gauge 4 fluctuated by $\pm$(2 – 3)psig. Although attempts were made to eliminate the leaks and hence reduce the pressure loss, a

completely closed system was never achieved.

Another test applied to the closed system was a check on the accuracy of the pressure gauges by comparison of readings. The readings on gauges 2 and 4 agreed (to within the accuracy of each scale) over the entire pressure range of the lower pressure gauge. It was concluded that these two gauges were accurate, as stated by the manufacturer. Pressure gauge 3, however, had to be re-calibrated against the other gauges. The re-calibration was irrelevant since in the tube tests performed the internal pressures employed were capable of measurement by gauges 2 and 4.

10.2.2 Specimen Design and Strain Measurement

The basic dimensions to the tube test piece have already been outlined – $\frac{3}{4}$ in. overall diameter, $\frac{1}{32}$ in. wall thickness, 4 in. parallel length. Besides the creation of a test piece, pressure tight at temperatures of up to 500 deg.C., the design process also involved the creation of a suitable method of suspending the specimen in the furnace and at the same time allowing an unrestricted flow of gas to it. The specimen also required to be accurately aligned in the furnace to facilitate measurement of the change in diameter during a test. The test piece is shown in Figure 10.2, the method of suspension and alignment in Figure 10.3, and details of the pressure coupling in Figure 10.4.

The tube test piece (Figure 10.2) was machined from the 1 in. diameter rod by drilling and reaming of the $\frac{11}{16}$ in. diameter central hole and then turning down of the 4 in. length to the required diameter of $\frac{3}{4}$ in. The tube had a plug, machined from the same batch of aluminium inserted into it from the left hand end. This plug reduced the internal volume of the tube and thus helped to attenuate the release of energy on rupture. The space between plug and tube wall was $\frac{1}{32}$ in. The test piece was made pressure tight at the left hand end by an argon arc weld along the join of plug and tube.

The tube specimen was suspended in the furnace by means of an aluminium alloy tube ($\frac{1}{2}$ in. O.D. x $\frac{1}{4}$ in. I.D.). This tube was placed over a spigot at the end of the test piece (Figure 10.2) and was then welded in position to produce a pressure tight joint. This tube also provided the means of supplying pressure to the test piece. The other end of the alloy tube was welded to a similar spigot on the aluminium end piece forming one part of the pressure coupling (Figure 10.4). Thus, each test piece consisted of the above three parts welded together. The pressure coupling consisted of a brass cap with a conical nose which was pressed into the conical seating of the aluminium end piece, by means of the split flange assembly, as shown in Figure 10.4. A steel banjo coupling then made the connection between brass cap and the $\frac{1}{4}$ in. O.D. steel tubing leading to shut-off valve 5 (Figure 10.1). Since the aluminium end piece, welded to the alloy tube, was not re-used, the conical brass nose was allowed to deform the conical seating to produce a sealed joint.

The problem of aligning the test piece in the furnace was overcome by placing the test piece inside an 18/8 stainless steel tube (Figure 10.3). This tube remained permanently in a central position in the furnace, alignment being maintained by the asbestos ring at the top end of the furnace and the hole in the asbestos end-plate at the lower end of the furnace. A split ring, clamped to the alloy tube, positions the specimen at the correct height and prevents undue stress on the weld between alloy tube and test piece by eliminating possible bending moments. The stainless steel tube also helped to maintain a constant temperature along the parallel length of the test tube by the increased heat conduction it brought about from centre of furnace towards the ends. The tube had one further purpose in maintaining axiality of the test specimen during an internal pressure creep test. Bending of the tube can occur due to anisotropy of the material or when a localised bulge forms in the tube wall. Kallstrom (1969) overcame this problem in the pressure testing of Zircaloy canning tubes by placing

a telescopic rod inside the tube to prevent the tube from bending, without restricting its change in length. However, with the present batch of commercially pure aluminium, it was considered that, by allowing enough clearance between specimen and stainless steel tube, to account for the differential expansion between the materials, the stainless steel tube would be sufficient to counteract any tendency of the specimen to bend. After each test, the specimen was easily removed from the stainless steel tube and it was concluded that very little bending had occurred during testing.

The stainless steel tube had an internal diameter of 1 in. Since the thin-wall tube specimen had a test diameter of $\frac{3}{4}$ in., the maximum, uniform, tangential or hoop strain which the system could accommodate was of the order 30 pct. However, this limiting strain was never achieved in any of the tests and even tubes which ruptured with the formation of a localised bulge did so before the inside surface of the stainless steel tube was reached. The above maximum limit on hoop strain could have been increased by, firstly, removing the section of the stainless steel tube covering the thin-wall length of the test piece and, then, replacing it with a larger diameter stainless steel tube. The overall diameter of the original tube was $1\frac{1}{4}$ in. and, hence, a tube of $1\frac{1}{4}$ in. internal diameter could have formed a sleeve over it. This procedure would have increased the maximum hoop strain to 60 - 70 pct. It was considered that some form of covering was necessary for the thin-wall tube to prevent the cold stream of gas, occurring on rupture, from impinging on the hot furnace tube wall.

Strain Measurement

Monitoring of the change in diameter along the entire parallel length of the tube during a test was impracticable. Instead, the change in diameter of the specimen at the mid-point was measured. Holes were machined in the stainless steel tube, furnace tube and furnace casing to accommodate four alumina tubes, such that their axes were perpendicular

to the longitudinal axis of the test piece and with the tubes distributed at 90 degree intervals round the circumference of the test piece at its mid-point. The tubes were 8 mm. O.D. x 5 mm. I.D. and had 4.76 mm. ($\frac{3}{16}$ in.) diameter alumina rods free to slide inside them. The ends of the rods rested against the surface of the test tube at its mid-point and the average movement of the four rods was considered to be an accurate measure of the increase in radius of the tube during deformation.

At first, it was intended that the movement of each rod would be measured by linear displacement transducers (described in Chapter VI) and provision was made in the design for that method. However, this system of measurement was not employed because of lack of transducers. Instead, dial gauges, with a range of 12 mm. and 0.01 mm. divisions, were used to measure the movement of the rods and readings had to be performed manually. The return spring in the dial gauge held the rod against the tube surface. The dial gauges were supported in position by way of clamps attached to magnetic bases. The magnetic bases secured themselves to steel plates on the base of the test rig. The test rig is shown in Figure 10.5.

Although the dial gauges could be read to $\pm$ 0.001 mm., the accuracy of measurement of rod movement was probably only $\pm$ 0.01 mm., due to the slight lateral movement of the alumina rod. The overall diameter of the test piece was measured along a length 1 in. on either side of the mid-point, before and after testing. The measurement was performed with a micrometer and readings were taken at $\frac{1}{4}$ in. intervals along the 2 in. length. Two readings were taken at each interval such that the diameters were perpendicular to each other. Diameters of test pieces over the 2 in. length were found to vary by as much as $\pm$ 0.01 mm. from the specified diameter of 19.05 mm. ($\frac{3}{4}$ in.). The size of the tubular specimen prevented measurement of the tube wall thickness with sufficient accuracy to determine if the thickness was uniform round the circumference. It was assumed, therefore, that the

wall thickness was uniform.

10.2.3 Furnace Design and Temperature Control

The cylindrical furnace used to heat the test piece has already been illustrated in Figures 10.3 and 10.5. The design of the furnace was formulated, like that for the uniaxial creep furnace, with the aid of formulae from the paper by Laubitz (1959). The furnace was 17 in. long x $8\frac{1}{2}$ in. overall diameter. The furnace tube, which had an internal diameter of $1\frac{3}{4}$ in., was of 'Purox' alumina. The single winding was resistance wound using 'Brightray C' wire of 21 S.W.G. The winding density varied according to the formula of Laubitz with a gradual increase in the number of turns per inch from the mid-point to the ends of its 13 in. length. The insulation of 'Triton Kaowool' ceramic fibre was contained by the aluminium alloy sheeting and the asbestos end plates, the latter also forming the support for the furnace tube. During construction of the furnace, care had to be exercised in ensuring that the holes for the strain measuring system were in proper alignment.

Temperature control of the furnace was accomplished with a three term (proportional, derivative and integral) instrument with a thyristor drive output. The thyristor unit (silicon controlled rectifiers), controlling the load current to the furnace winding, was mounted at the rear of the instrument. The sensing element of the controller was an Alumel/Chromel thermocouple enclosed in a stainless steel sheath. The sheath, like the alumina tubes (strain measurement), passed through a hole in the furnace at its mid-point and perpendicular to the axis of the furnace. The tip of the sheath rested against the stainless steel tube used to align the aluminium tube test piece. The setting accuracy of the instrument was $\pm$ 1 deg.C. Stability of the controller was such that temperature rose by 0.5 deg.C. over a 10 hour period.

Before embarking on the programme of internal pressure

tests, it was necessary to determine the temperature distribution over the parallel length of the thin-wall tube. Seven Chromel/Alumel thermocouples were secured by wire to the surface of a test piece at intervals along the parallel length of the thin-wall tube. Grooves were machined in the 1 in. diameter shoulder of the test piece to allow passage of the thermocouple wires along the inside of the stainless steel tube to their exit through holes in the brass split ring (Figure 10.3). During this temperature distribution test, a small pressure of approximately 10 psig was applied to the test tube to simulate, as closely as possible, actual test conditions. The temperature distribution observed on heating the specimen to approximately 500 deg.C. was as shown in Table 10.1. Measurement of thermocouple output e.m.f. was performed with a slidewire potentiometer to $\pm$ 0.1 deg.C.

Table 10.1

Position of thermocouple w.r.t. mid-pt. of tube	$1\frac{1}{2}$in. above	1in. above	$\frac{1}{2}$in. above	Mid-Point	$\frac{1}{2}$in. below	1in. below	$1\frac{1}{2}$in. below
Temperature (deg.C.)	494.4	498.0	498.7	499.0	498.4	498.2	493.4

This distribution was achieved after experimenting with different lengths of aluminium rod, pushed into the lower end of the stainless steel tube (Figure 10.3). Without the rod, insufficient heat conduction took place from the lower end of the furnace and temperatures below mid-point were greater than the temperature at the mid-point.

From Table 10.1, it was concluded that the portion of the parallel length of the tube, 1 in. on either side of the mid-point, was suitable for measurement of diameter before and after testing. Since the change in diameter was to be

measured only at the mid-point during a test, the required test temperature was aimed for at that point. The remainder of the 2 in. gauge length could be regarded as being within - 1 deg.C. of the test temperature.

The measurement of tube wall temperature during an internal pressure test at first presented some difficulty. Thermocouples could not be attached by wire to the tube, as in uniaxial creep tests, since the diameter of the tube increased during an internal pressure test. Spot welding of the thermocouples to the tube surface was considered, but the pressure required to weld the thermocouple bead to the surface would, undoubtedly, have caused serious deformation. The method adopted made use of the strain measuring system. The alumina tubes used in that system were not truly circular in cross-section. They had an oval cross-section such that there was sufficient clearance across the major diameter of the oval for the accommodation of two bare thermocouple wires as well as the alumina rod, measuring the movement of the tube wall. The bead of the thermocouple was held against the tube surface by the end of the alumina rod. Before attempting to use this system in a creep test, the reading of the latter thermocouple was compared with the reading of the thermocouple attached by wire to the tube surface during a temperature distribution test at 500 deg.C. The readings differed by 0.6 deg.C. with the wire attached thermocouple the lower of the two. It was concluded, therefore, that, during an internal pressure test, the temperature controller should be adjusted to produce a recorded temperature 0.6 deg.C. above the required value. The actual temperature at the mid-point would then be the required test temperature.

10.3 Experimental Procedure

After manufacture, each welded assembly of tubular test piece, alloy suspension tube and pressure coupling end piece, was tested at room temperature to a pressure of 40 psig in order to detect possible leaks. The test piece was then cleaned with alcohol to remove oil and dirt from the manufacturing process. A pencil line grid was then marked on the surface of the tube as a reference for diameter measurements. Two perpendicular diameters were measured at $\frac{1}{4}$ in. intervals for 1 in. on either side of the mid-point. The test piece was then assembled with the pressure coupling, as shown in Figures 10.3 and 10.5. An argon pressure of approximately 50 psig was then applied to check the pressure coupling for leaks. The strain measuring system and thermo-couple were then assembled.

Heating of the test piece to temperature took 30 minutes with an overshoot of approximately 3 deg.C. A further $1\frac{1}{4}$ hours were allowed for stabilisation of temp-erature to the required value. During this period, argon gas was allowed to flow through the system, venting through valve 4 (Figure 10.1). The intention was to dilute, as far as possible, the small amount of air contained by test piece and pressure measuring system. Before the end of the temp-erature soaking period, valves 4 and 5 were closed and the regulator adjusted to produce the required value of internal pressure. The latter value was calculated with the aid of equation 1.3,

$$\bar{\sigma} = \frac{\sqrt{3}}{4} \frac{PD}{t} \qquad (1.3)$$

The value of effective stress ($\bar{\sigma}$) was 4000 lbf/in^2 (27.60 N/mm^2) for tests at 250 deg.C. and 327.3 lbf/in^2 (2.26 N/mm^2) for tests at 500 deg.C. Thickness (t) was assumed to be $\frac{1}{32}$ in. The value of internal diameter (D) was calculated by subtracting $\frac{1}{16}$ in. (2t) from the average value of outside diameter measured previously over the 2 in. central length.

Argon gas at the specified pressure was then introduced to the test tube by opening valve 5 (Figure 10.1). Readings of the four dial gauges were taken before opening valve 5 and at suitable time intervals after opening valve 5. Internal pressure and specimen temperature were also measured at regular time intervals. Some tests were taken to rupture but most were stopped before rupture occurred. Pressure was released from the test piece by opening valve 4 and simultaneously closing valve 2. After removing the test piece from the furnace, the diameters were again measured at the reference marks.

10.4 Results

The programme of testing has already been outlined in section 10.1. In this section, the results of the biaxial stress creep tests will be described in three parts, noting in each one similarities to and differences from the corresponding uniaxial behaviour. In the first part, results of tube tests at a temperature of 500 deg.C. and an effective stress of 2.26 N/mm^2 will be described. In the second part, results of tube tests at a temperature of 250 deg.C. and an effective stress of 27.60 N/mm^2 will be described. In the third part, the results of tube tests at a temperature of 250 deg.C. and an effective stress of 27.60 N/mm^2, on two of the specimens, previously deformed at a temperature of 500 deg.C. and an effective stress of 2.26 N/mm^2, will be described.

The results are presented in Tables 10.2, 10.3 and 10.4, and in Figures 10.6 and 10.9. The values of strain have been quoted in the Tables as effective ($\bar{\varepsilon}$) and tangential (ε_ϑ). Since elastic strains have been assumed negligible, the values of strain represent both plastic and total strains. Values of effective strain were calculated using equation 1.9 :-

$$\varepsilon_\vartheta = \frac{\sqrt{3}}{2}\,\bar{\varepsilon} \qquad (1.9)$$

and ε_ϑ was taken to be equal to the fractional change of outside diameter of the tube. The values of strain in all three Tables were the final values, when the internal pressure was released from the tube. In Figures 10.6 and 10.9, only effective strain has been plotted against time in order to compare the results with the corresponding uniaxial tests. However, values of tangential strain at any time may be obtained by multiplying the effective strain by 0.866.

In Appendix 10.1 estimations of the errors in the values of applied stress and measured strain have been made.

Although it was not possible to measure the wall thickness before testing, measurements of wall thickness after testing indicated that the average wall thickness before testing was as much as 0.00120 in. less than the specified value of 0.03125 in. An error of $\pm$ 0.0012 in. was, therefore, assumed in the initial value of wall thickness. The above calculation used the relation that strain through the thickness and tangential strain were equal in magnitude but opposite in sign. From Appendix 10.1, the error in the initial values of effective, axial and tangential stresses was $\pm$ 1.52 N/mm^2 for the tests at a temperature of 250 deg. C. and 27.60 N/mm^2 effective stress. At 500 deg.C. and 2.26 N/mm^2 effective stress, the error was $\pm$ 0.18 N/mm^2. The error in the value of strain measured by dial gauges was $\pm$ 0.05 pct, and in the value measured by micrometer it was $\pm$ 0.01 pct.

10.4.1 Temperature 500 deg.C., Effective Stress 2.26 N/mm^2

The results of creep tests, under the above conditions, on thin-wall tubes of commercially pure aluminium, are presented in Table 10.2 and Figure 10.6.

In the first tube test at 500 deg.C. (No. 2, Table 10.2), some difficulty was encountered with the strain measuring system. The return springs of each dial gauge were exerting a force on the alumina rod equivalent to that exerted by the tube wall as it moved outwards under the applied internal pressure. Consequently, dimples formed on the tube wall at the points of contact with the ends of the rods. As shown in Table 10.2, the strain measured by the dial gauges was much less than the strain measured by the micrometer readings. Although the tube was restrained at the points of contact with the alumina rods, the deformation of the rest of the tube apparently continued unhindered. The problem was alleviated by removing one of the return springs from each dial gauge. This is shown, in Table 10.2, by the results of Tests 3 and 9, when the strain recorded by the dial gauges is compared with the strain at the mid-point

recorded by the micrometer. Test No. 5 was performed without the strain measuring system in operation, to determine if the forces from the alumina rods produced any general restraint on the central 2 in. length of the tube. The test lasted for the same time as No. 3 and Table 10.2 shows the effect of any restraint to be small, since the values of strain in Test 5 are only slightly greater than the corresponding values in Test 3.

Although Tests 2 and 5 did not provide strain/time curves, they both provided other useful information, which will be described in due course. The values of strain for Tests 3, 5 and 9 (Table 10.2) show that, under the high temperature test conditions, the results were reasonably repeatable. In addition, the values of strain were uniform along the central 2 in. portion of each of the three tubes. Therefore, for Tests 3 and 9, the effective strain/time curves, shown in Figure 10.6, represent the deformation of the central portion as well as the deformation at the midpoint. Although the strain/time curves for these two tests coincided at 4 pct effective strain, the minimum creep rates were in the ratio 2:1 (Table 10.2). Apparently the initial deformation does not greatly influence the subsequent behaviour of the material.

In Figure 10.6, uniaxial and biaxial effective strain/time curves have been plotted for comparison. Initially, the effective strain rate of the tube under internal pressure was smaller than that of the material under uniaxial conditions. However, the effective strain rate of the tube increased more rapidly than that of the uniaxial specimen after approximately 0.2 – 0.3 pct strain. The density decrease in the central portion of specimen No. 9 was 0.207 pct. As shown by Figure 10.6, this value of density decrease lies very close to the density decrease/time curve for uniaxial creep at the same effective stress and temperature. After the measurement of density, two sections of the tube, one perpendicular to the tube axis and the other along the tube axis, were polished and etched as described in section 2.4 of Tensile Testing.

Figures 10.7 and 10.8 show micrographs of the etched sections. The internal discontinuities, detected by the density measurement, were a mixture of triple point cracks and grain boundary cavities, similar to those already observed under uniaxial conditions. Therefore, although the same quantity of intergranular discontinuities developed under the equivalent uniaxial and biaxial conditions, the effect of them on the biaxial strain/time curve was apparently greater than on the uniaxial strain/time curve. The density decrease recorded on tube specimen 2 (0.877 pct) does not lie close to the uniaxial density decrease curve (Figure 10.6). However, the density decrease of specimen 2 compares more favourably with the uniaxial density measurements when the comparison takes place at the same effective strains.

In Figure 10.7, the section of tube perpendicular to the axis, the tangential stress axis is horizontal, and the longitudinal stress axis is perpendicular to the plane of the micrograph. The micrograph shows that the discontinuities develop mainly on grain boundaries perpendicular or almost perpendicular to the tangential stress axis. In Figure 10.8, the section of the tube along the axis, the longitudinal stress axis is horizontal, and the tangential stress axis is perpendicular to the plane of the micrograph. In this section, the discontinuities do not appear to have a preferred grain boundary orientation. These observations imply that it is the maximum principal tensile stress (tangential stress) which governs the formation and growth of intergranular discontinuities, since, in uniaxial creep tests also, the discontinuities were observed to form mainly on grain boundaries perpendicular or nearly perpendicular to the axis of the maximum principal stress (the uniaxial tensile stress). It follows, therefore, that comparison of uniaxial and multiaxial behaviour, regarding the growth of intergranular discontinuities, should be carried out at the same maximum principal stress. Since the deformation process was apparently influenced by the growth of intergranular discontinuities, it may be more appropriate to compare uniaxial and multiaxial creep data at the same maximum

principal stress, when it is known that intergranular discontinuities develop under the stress and temperature conditions considered.

10.4.2 Temperature 250 deg.C., Effective Stress 27.60 N/mm^2

The results of tube tests, under the above creep conditions, are presented in Table 10.3 and Figure 10.9. Each tube was annealed for 1 hour at a temperature of 500 deg. C. prior to testing at 250 deg.C.

The data from Test 1 had to be discarded because premature failure appeared to have occurred due to a local blemish in the tube wall. Around the point of rupture, severe plastic deformation had taken place and a small bulge had formed. Test 6 was the repeat of Test 1. In this test, rupture occurred, after 19 hours, close to the mid-point of the parallel length of the thin-wall tube. The force of the burst pushed the strain measuring system out of alignment and, hence, dial gauge readings at rupture point were not obtained. Although the average effective strain on the central 2 in. length was 7 pct, the value at the point of rupture was 12 pct. This latter value was less than the elongation at fracture of the corresponding uniaxial creep test. The latter, as shown by Test 95 of Table 9.3, had an elongation at fracture of 15.2 pct. The two values, however, are reasonably close when compared to the relative differences in rupture life and minimum creep rate. Rupture lives of tube and uniaxial test piece were in the ratio 1:16 and minimum creep rates in the ratio 9:1.

Tube Test 8 was stopped before rupture took place in order to obtain a density measurement for the 250 deg.C. creep condition. Final strains at the mid-point measured by dial gauges and micrometer showed reasonable agreement (Table 10.3). In addition, deformation was fairly uniform along the central 2 in. length of the thin-wall tube. Therefore, the effective strain/time curve of Figure 10.9 represents the deformation of the central portion as well as

that of the mid-point. Figure 10.9 shows that the test was stopped at a point when the strain/time curve was well into the tertiary stage. The observation of uniform strain along the central portion indicates that localised 'necking' was not responsible. In a thin-wall tube, localised 'necking' would occur as a localised thinning of the tube wall creating a bulge. The density decrease of 0.098 pct (Table 10.3) was similar to that which occurred in the corresponding uniaxial creep test for the same effective strains (Test 89, Table 9.3). However, tube and uniaxial testing times were in the ratio 1:34 and minimum creep rates in the ratio 18:1. Metallographic examination of sections of the tube wall showed the internal discontinuities, detected by the density measurement, to be a mixture of triple point cracks and grain boundary cavities.

The strain/time curves of the annealed material, under the corresponding uniaxial creep conditions (250 deg.C., 27.60 N/mm^2), were shown in Figure 6.19 of Uniaxial Creep Testing. The creep data of those tests were presented in Table 9.3. Scatter was small under those conditions and, hence, the strain/time curve of CT70 in Figure 10.9 may represent all of the above tests. The effective strain/time curves of Tube Tests 6 and 8, also plotted in Figure 10.9, show that, in addition to shorter rupture lives and larger minimum creep rates, scatter in the results was greater under the multiaxial creep conditions, when comparison takes place at the same effective stress.

10.4.3 Effect of Intergranular Discontinuities

The tube tests (3, 5 and 9) described in sub-section 10.4.1, produced three similarly strained, thin-wall tubes in which deformation was uniform along the central 2 in. length. The central portion of Specimen 9 was removed and density measurements showed a decrease of 0.2 pct in density. Metallography of sections of the tube wall showed the presence of triple point cracks and grain boundary cavities, similar to those already observed in uniaxial specimens,

tested under equivalent conditions. Since Tests 3 and 5 achieved similar strains to Test 9 in similar times, it appeared reasonable to assume that they each contained a similar quantity of intergranular discontinuities to Specimen 9. In Chapter IX, the results of uniaxial creep tests on specimens containing a known, controlled amount of intergranular discontinuities were described. In an analogous way, biaxial stress creep tests were performed on the strained tube specimens, 3 and 5, containing a known amount of intergranular discontinuities. The two tests were performed at a temperature of 250 deg.C. and an effective stress of 27.60 N/mm^2. The results are presented in Table 10.4 and in Figure 10.9. Both specimens were annealed for 1 hour at a temperature of 500 deg.C. prior to testing at 250 deg.C. The same heat treatment had been applied to the specimens used for Tests 6 and 8.

To produce the same value of effective stress, a lower value of internal pressure had to be used. Outside diameter could be measured directly, but the thickness of the tube wall after the 500 deg.C. deformation had to be estimated using equation 1.9 :-

$$\varepsilon_\vartheta = -\varepsilon_t$$

that is, the tangential strain ε_ϑ and the strain through the thickness ε_t were equal in magnitude but opposite in sign. An allowance for the reduction of cross-sectional area of tube wall due to internal discontinuities was difficult to formulate. In the uniaxial case, the fractional reduction in load, to allow for the presence of internal discontinuites, was equivalent to the fractional density decrease in the material due to the discontinuities. It seemed reasonable, therefore, to reduce the applied internal pressure in the same way for tube tests. However, the reduction of 0.2 pct in an internal pressure of approximately 400 psig was only 0.8 psig, which was within the $\pm$ 1.5 psig accuracy of the pressure measuring gauge. The allowance, therefore, for

intergranular discontinuities, was negligible.

In Table 10.4, the final strains measured by dial gauges and micrometer show reasonable agreement. Since the deformation was fairly uniform along the central 2 in. length of each tube, the effective strain/time curves of Tests 4 and 7, in Figure 10.9, represent the deformation of the central portion as well as that of the mid-point. The two sets of curves, 4 and 7, 6 and 8, cannot be compared too closely since extensive scatter was indicated by the strain/time curves of each set. With this reservation in mind, comparison of the two sets of curves indicates that the presence of an initial amount of intergranular discontinuities in specimens 4 and 7 has accelerated the deformation process in those two specimens. However, confirmation that the pattern of deformation in Tests 4 and 7 was different from that in Tests 6 and 8 was given by density measurements (Tables 10.3 and 10.4). Assuming that specimens 4 and 7 initially contained an amount of intergranular discontinuities corresponding to 0.2 pct fractional density decrease, the fractional density decrease increased during the creep tests by 0.4 pct and 0.45 pct, respectively. However, specimen 8 (Table 10.3), with no initial discontinuities, showed a density decrease of 0.1 pct after testing under the same creep conditions for a longer time and to a larger strain. It is rather surprising that the larger rate of growth of discontinuities in Test 4 and 7 has not caused a greater divergence of the strain/time curves.

A uniaxial specimen which had a similar density decrease, before creep testing at a temperature of 250 deg. C. and a stress of 27.60 N/mm^2, was that of Test 62 (Table 9.2). Its strain/time curve has been plotted in Figure 10.9 (CT62) and, for the strain and time scales employed, the curve is coincident with the curve of CT70, which was of a specimen with no initial intergranular discontinuities. With the previously mentioned reservations about the increased scatter in tube tests, and the different ways in which intergranular discontinuities were put into uniaxial and biaxial

specimens, in mind, the strain/time curves of Figure 10.9 suggest that the effect of the same quantity of initial intergranular discontinuities on the creep properties has been greater under the biaxial stress creep conditions than under the uniaxial stress creep conditions.

10.4.4 Fracture Behaviour

In Figure 10.10, the sections of the thin-wall tubes of Tests 2 and 6 containing the fracture surfaces are shown. Data for these two tests have already been presented in Tables 10.2 and 10.3, respectively. Figure 10.10 shows that rupture occurred, at both temperatures, by the formation of a crack whose major axis was parallel to the tube axis. This crack orientation implies that the tangential stress (the maximum principal tensile stress) was responsible for the failure. These observations are consistent with the metallographic evidence of Figure 10.7 where intergranular discontinuities were found to develop mainly on grain boundaries, perpendicular or nearly perpendicular to the axis of the tangential stress. Continued growth of the discontinuities over the above boundaries would produce cracks whose major axes would be perpendicular to the axis of the tangential stress. Rupture would take place when one of the cracks attained a length suitable for rapid propagation under the stress concentration around the tips. This process of rupture would produce the observed fracture profiles on the tube wall. The creep rupture data of thin-wall tubes under internal pressure and uniaxial test pieces should, therefore, be compared at the same values of maximum principal tensile stress since, in uniaxial specimens also, discontinuities developed on grain boundaries perpendicular or almost perpendicular to the axis of the tensile stress.

In Table 10.5, the creep rupture data of the tube tests and the relevant uniaxial tests have been presented for comparison. The values of the maximum principal tensile stresses, and the strains in the same direction, have been quoted in addition to the values of effective stress and

strain.

At both temperatures, comparison of data, on the basis of effective stress and effective strain, shows that the biaxial stress system has reduced both rupture life and strain at fracture. At the higher temperature of 500 deg.C., the reduction of rupture life was approximately 40 pct (TT2 and CT98) and of strain at fracture approximately 70 pct. Although the use of maximum principal tensile stress as the rupture criterion would provide a better correlation between the rupture lives, it would not do the same for strains at fracture. In the two uniaxial tests at higher and lower stresses (CT16 and CT93) the strain at fracture was much larger than at 2.26 N/mm^2. Therefore, the biaxial stress system has certainly restricted the amount of possible deformation in the material. At the lower temperature of 250 deg.C., the reduction of rupture life was approximately 94 pct and strain at fracture approximately 20 pct. Uniaxial creep tests at this temperature were performed at other stresses on the 'as received' material but not on the material which had been annealed at a temperature of 500 deg. C. Therefore, it is not possible to state what effect the use of the maximum principal tensile stress criterion would have on the correlation of rupture data. However it does seem unlikely that it would account for the very large difference in rupture lives. Also, under uniaxial stress creep conditions, the elongation to fracture generally increases with increase of applied stress when intercrystalline failure is known to be the fracture mode. This was shown to be the case for the 'as received' commercially pure aluminium at 250 deg.C. Hence, correlation of rupture strains on the basis of maximum principal tensile stress would create an even larger difference between the values obtained from uniaxial and tube tests. Therefore, the biaxial stress system appears to restrict the amount of possible deformation at both temperatures.

10.5 Comparison of Uniaxial and Biaxial Creep Behaviour

In section 10.4, the results of creep tests on thin-wall tubes under internal pressure were described, attempting, as far as possible, to compare the biaxial stress behaviour with that observed in the relevant uniaxial creep tests. The tube tests were planned using the concept of effective stress ($\bar{\sigma}$) as the correlation between uniaxial and multiaxial data. The corresponding link between uniaxial and multiaxial strains was effective strain ($\bar{\varepsilon}$). However, the effective strain/time curves derived from the biaxial stress creep tests have shown to be inadequate in providing a reasonable correlation with the existing strain/time curves of uniaxial tests. The results at 250 deg.C. show that prediction of thin-wall tube behaviour from uniaxial behaviour using effective stress and effective strain as the correlation would be dangerous. Such predictions would seriously underestimate creep rate, and overestimate rupture life and rupture strain, even allowing for the extensive scatter in tube results indicated by the strain/time curves. At the higher temperature of 500 deg.C., the use of effective stress and effective strain provided a fairly reasonable correlation for the initial stages of the strain/time curves. However, the agreement soon broke down as the deformation continued, and rupture life and rupture strain were again ~~underestimated~~ overestimated.

The density measurements performed on sections of strained tubes, and metallography of those sections, showed that, as in the uniaxial case, grain boundary cavities and triple point wedge cracks developed in the material under biaxial stress creep conditions at both temperatures. At 250 deg.C., the density decrease in the tube section (No. 6, Table 10.3) was similar to that in a uniaxial creep specimen which had been strained by a similar amount at the same effective stress. However, the tube achieved this density decrease in $\frac{1}{34}$ of the time taken by the uniaxial specimen. At 500 deg.C., one density decrease (No. 9, Table 10.2) agreed with the uniaxial density measurements on a time basis while the other (No. 2, Table 10.2) showed some agreement on

the basis of equal effective strains. Although there were insufficient density measurements for a conclusive study of the growth of intergranular discontinuities under biaxial stress creep conditions, the above three results indicate that the increased rate of deformation found under biaxial conditions was accompanied by an increased rate of growth of the discontinuities.

Metallography of sections of the tube strained at 500 deg.C. indicated that discontinuities formed preferentially on grain boundaries, perpendicular or nearly perpendicular to the axis of the tangential stress. The same preferred distribution, however, was less apparent in sections of tubes strained at a temperature of 250 deg.C. The tangential stress was the maximum principal tensile stress and the above observations suggested that this stress governed the formation of intergranular discontinuities since, in uniaxial creep tests also, discontinuities developed mainly on grain boundaries perpendicular or nearly perpendicular to the applied tensile stress. The shape of the fracture profiles of ruptured tubes (Figure 10.10) was a further indication that the tangential stress had been responsible for the failure. These observations suggested that creep rupture data of the thin-wall tubes under internal pressure and of the uniaxial tensile specimens would correlate better at the same maximum principal tensile stresses. The results presented in Table 10.5, however, indicated that adoption of the maximum principal tensile stress as the criterion for rupture would provide slightly better correlation of rupture lives (especially at 500 deg.C.) but not of rupture strains whether as tangential or effective strain. These observations illustrate the inability of simple criteria, such as effective stress or maximum principal tensile stress, to correlate multiaxial creep rupture data with uniaxial creep rupture data of commercially pure aluminium at temperatures of 250 deg.C. and 500 deg.C.

In the preceding paragraphs, the results discussed have all been from tube tests on specimens which contained no

initial intergranular discontinuities. The results showed that correlation of the deformation with uniaxial creep data on the basis of effective stress and strain was not feasible. In general, the effective strain/time curve under biaxial stress conditions indicated much faster rates of deformation than under uniaxial conditions at the same effective stress. Similar quantities of intergranular discontinuities were found to develop under the two stress systems. Therefore, it was possible that the different rates of deformation were caused by the reaction of the discontinuities to the different stress systems. It has already been shown that, under uniaxial conditions, even small amounts of intergranular discontinuities greatly affect the deformation of commercially pure aluminium at temperatures of 250 deg.C. and 500 deg.C. (Chapter IX). Under the influence of a biaxial stress system, the effect of discontinuities might have been greater. The results, described in sub-section 10.4.3, of biaxial stress creep tests on tubes containing initial amounts of intergranular discontinuities indicated that the different stress system was at least one factor causing the lack of correlation in effective strain/time curves. The results of those tests, within the limitations stated in sub-section 10.4.3, showed the same quantity of intergranular discontinuities to cause a greater divergence of the effective strain/time curves under biaxial stress conditions than under uniaxial stress conditions, for the same effective stress at a temperature of 250 deg.C. Under uniaxial conditions, a quantity of intergranular discontinuities, corresponding to 0.2 pct density decrease, had negligible effect on the initial stages of the strain/time curve. Under biaxial conditions, the effective strain/time curves of the material, with and without the above quantity of intergranular discontinuities, diverged from application of the creep stress. Hence, it appears that the influence which the intergranular discontinuities exert on the overall deformation of the material varies with the type of stress system imposed on the test piece of that material.

Kinky for commas.

10.6 Summary and Conclusions

A method has been described for the creep testing of thin-wall tubes of commercially pure aluminium under internal gas pressure at temperatures of 250 deg.C. and 500 deg.C. The apparatus designed and built to test the thin-wall tubes was able to measure the tangential strain directly during the creep test and, hence, strain/time curves of the deformation could be obtained as well as the rupture life and rupture strain. The results of the biaxial stress creep tests performed showed the use of effective stress and effective strain to be inadequate in correlating the uniaxial and biaxial creep properties. Prediction of the multiaxial creep behaviour of commercially pure aluminium at a temperature of 250 deg.C., using the concepts of effective stress and effective strain, seriously ~~underestimated~~ overestimates rupture life and rupture strain, ~~and~~ but underestimates minimum creep rate. At a temperature of 500 deg.C., only rupture life and rupture strain were underestimated. The use of maximum principal tensile stress, as the rupture criterion, improved correlation of rupture lives but not of rupture strains. There appears to be no simple criterion for prediction of the creep properties of commercially pure aluminium at temperatures of 250 deg.C. and 500 deg.C. under biaxial stress conditions.

At both temperatures, intergranular discontinuities were found to develop. The discontinuities were first detected by the accompanying decrease in density of the material and confirmation was given by metallography. The latter showed the discontinuities to be a mixture of triple point wedge cracks and grain boundary cavities occurring mainly on grain boundaries perpendicular or nearly perpendicular to the tangential stress (maximum principal tensile stress). It was also shown that rupture occurred, in the tube creep tests, by the formation of a crack in the tube wall parallel to the tube axis. Both of these observations pointed to the tangential stress as being responsible for the failure.

ZONKED ON COMMAS

The inability of effective stress and effective strain

to produce a correlation between the strain/time curves, under the uniaxial and biaxial stress creep conditions, was accounted for by the influence of the stress system on the interaction between the deformation process and the growth of intergranular discontinuities. It was shown that, when similar quantities of intergranular discontinuities were put into uniaxial and biaxial test pieces, prior to creep testing at the same effective stress and temperature, the effect on the strain/time curve resulting from testing under biaxial stress conditions was greater than that on the strain/time curve resulting from the uniaxial conditions. It was concluded that stress system does alter the effect that intergranular discontinuities have on the creep deformation process.

APPENDIX 10.1

1) Estimation of Error in Effective Stress ($\bar{\sigma}$)

From equation 1.3,

$$\bar{\sigma} = \frac{\sqrt{3}}{4} \frac{PD}{t}$$

where P is internal pressure, D is internal diameter, t is thickness.

Applying the same analysis as in Appendix 2.1,

$$\frac{\delta\bar{\sigma}}{\bar{\sigma}} = \frac{\delta P}{P} + \frac{\delta D}{D} + \frac{\delta t}{t}$$

where prefix δ denotes error in measured quantity.

At $\bar{\sigma}$ = 4000 lbf/in^2 (27.60 N/mm^2),

internal pressure = 400 ± 5 psig.

At $\bar{\sigma}$ = 327.3 lbf/in^2 (2.26 N/mm^2),

internal pressure = 34 ± 1 psig.

Initial Wall Thickness (t) = 0.0313 ± 0.0012 in.

Since internal diameter, D = $D_o - 2t$, where D_o is the measured outside diameter,

Error in internal diameter, $\delta D = \delta D_o + 2\delta t$

$= 0.01 + 0.061$

$= \pm 0.071$ mm.

Hence, at $\bar{\sigma}$ = 4000 lbf/in^2 (27.60 N/mm^2),

$$\frac{\delta\bar{\sigma}}{\bar{\sigma}} = \frac{5}{400} + \frac{0.0012}{0.0313} + \frac{0.071}{19.050} = 5.5 \text{ pct.}$$

and at $\bar{\sigma}$ = 327.3 lbf/in^2 (2.26 N/mm^2),

$$\frac{\delta\bar{\sigma}}{\bar{\sigma}} = 7.2 \text{ pct.}$$

Therefore, error in applied effective stress was $\pm$ 220 lbf/in^2 ($\pm$ 1.52 N/mm^2) at 4000 lbf/in^2 (27.60 N/mm^2) and $\pm$ 24 lbf/in^2 ($\pm$ 0.18 N/mm^2) at 327.3 lbf/in^2 (2.26 N/mm^2). The calculated values of error also apply to the tangential and axial stresses.

2) Estimation of Error in Strain Measured by Micrometer

$$\text{Tangential Strain, } \varepsilon_\vartheta = \frac{D_F - D_o}{D_o}$$

where D_o is the initial value of outside diameter and D_F is final value of outside diameter.

Hence,

$$\frac{\delta\varepsilon_\vartheta}{\varepsilon_\vartheta} = \frac{\delta D_F + \delta D_o}{D_F - D_o} + \frac{\delta D_o}{D_o}$$

$$\text{and } \delta\varepsilon_\vartheta = \frac{\delta D_F + \delta D_o}{D_o} + \varepsilon_\vartheta \frac{\delta D_o}{D_o}$$

Initial outside diameter = 19.050 $\pm$ 0.001 mm.

Final outside diameter measured to $\pm$ 0.001 mm.

Therefore,

$$\delta\varepsilon_\vartheta = 0.00010 + 0.00005\,\varepsilon_\vartheta$$
$$= \pm 0.0001 \text{ for } \varepsilon < 0.8$$

Error in measured value of tangential strain was $\pm$ 0.0001 for values less than 0.8.

3) Estimation of Error in Strain Measurement by Dial Gauges

$$\text{Tangential Strain, } \varepsilon_{\vartheta} = \frac{2\mu}{D_o}$$

where D_o is the initial value of outside diameter and μ is the average alumina rod movement.

Hence,

$$\delta\varepsilon_{\vartheta} = \frac{\delta\mu}{D_o} + \varepsilon \frac{\delta D_o}{D_o}$$

Error in value of $\mu = \pm 0.01$ mm.

Initial value of outside diameter $D_o = 19.050 \pm 0.001$ mm.

Therefore,

$$\delta\varepsilon_{\vartheta} = 0.0005 + 0.00005\ \varepsilon$$

For tangential strains less than 1 error in measured strain is ± 0.0005.

Table 10.2

Temperature 500 deg.C., Internal Pressure 34.2 psig., Effective Stress ($\bar{\sigma}$) 327.3 lbf/in^2 (2.26 N/mm^2), Tangential Stress (σ_ϑ) 378 lbf/in^2 (2.60 N/mm^2), Effective Plastic Strain ($\bar{\varepsilon}$), Tangential Plastic Strain (ε_ϑ)

Test No.	Time (hours)	Strains (pct) at mid-point				Average Strain (pct) on central 2 in. length		Density Decrease (pct) in central 2 in. length	Minimum Creep Rate (pct/h)	
		Dial Gauges		Micrometer						
		ε_ϑ	$\bar{\varepsilon}$	ε_ϑ	$\bar{\varepsilon}$	ε_ϑ	$\bar{\varepsilon}$		$\dot{\varepsilon}_\vartheta$	$\dot{\bar{\varepsilon}}$
2 (a)	5.25	2.26	2.60	5.85	6.75	7.61	8.80	0.877	–	–
3	3.58	3.50	4.05	3.31	3.85	3.34	3.86	–	0.288	0.332
5	3.58	–	–	3.50	4.05	3.52	4.06	–	–	–
9	3.50	3.32	3.84	3.12	3.60	3.13	3.62	0.207	0.151	0.174

Notes :– (a) Rupture occurred $1\frac{1}{8}$ in. above mid-point

ε_ϑ = 13.86 pct

$\bar{\varepsilon}$ = 16.02 pct

Table 10.3

Temperature 250 deg.C., Internal Pressure 418 psig., Effective Stress ($\bar{\sigma}$) 4000 lbf/in^2 (27.60 N/mm^2), Tangential Stress (σ_ϑ) 4620 lbf/in^2 (31.80 N/mm^2), Effective Plastic Strain ($\bar{\varepsilon}$), Tangential Plastic Strain (ε_ϑ)

Test No.	Time (hours)	Strains (pct) at mid-point				Average Strain (pct) on central 2 in. length		Density Decrease (pct) in central 2 in. length	Minimum Creep Rate (pct/h)	
		Dial Gauges		Micrometer						
		ε_ϑ	$\bar{\varepsilon}$	ε_ϑ	$\bar{\varepsilon}$	ε_ϑ	$\bar{\varepsilon}$		$\dot{\varepsilon}_\vartheta$	$\dot{\bar{\varepsilon}}$
1 (a)	0.75	0.06	0.07	0.05	0.06	0.05	0.06	–	–	–
6 (b)	19.00	–	–	–	–	6.03	6.96	–	0.032	0.037
8	8.75	5.16	5.96	5.45	6.30	5.32	6.15	0.098	0.064	0.074

Notes :– (a) Rupture occurred $1\frac{5}{8}$ in. below mid-point, ε_ϑ = 3.52 pct, $\bar{\varepsilon}$ = 4.06 pct.

(b) Rupture occurred $\frac{1}{8}$ in. below mid-point, ε_ϑ = 10.67 pct, $\bar{\varepsilon}$ = 12.31 pct.

Table 10.4

Temperature 250 deg.C., Internal Pressure 391 psig., Effective Stress ($\bar{\sigma}$) 4000 lbf/in^2 (27.60 N/mm^2), Tangential Stress (σ_θ) 4620 lbf/in^2 (31.80 N/mm^2), Effective Plastic Strain ($\bar{\varepsilon}$), Tangential Plastic Strain (ε_θ)

Test No.	Time (hours)	Strains (pct) at mid-point				Average Strain (pct) on central 2 in. length		Density Decrease (pct) in central 2 in. length		Minimum Creep Rate (pct/h)	
		Dial Gauges		Micrometer							
		ε_θ	$\bar{\varepsilon}$	ε_θ	$\bar{\varepsilon}$	ε_θ	$\bar{\varepsilon}$	before	after	$\dot{\varepsilon}_\theta$	$\dot{\bar{\varepsilon}}$
4	4.00	1.85	2.14	2.22	2.56	1.86	2.15	0.2	0.593	0.236	0.272
7	3.33	3.71	4.29	3.84	4.44	3.96	4.57	0.2	0.625	0.548	0.633

Notes :- Test No. 4 used the strained specimen of Test No. 3 (Table 10.2).

Test No. 7 used the strained specimen of Test No. 5 (Table 10.2).

Table 10.5

Test No.	Temperature (deg.C.)	Effective Stress (N/mm^2)	Maximum Principal Tensile Stress (N/mm^2)	Rupture Life (hours)	Effective Strain (pct)	Strain in direction of Maximum Principal Tensile Stress (pct)
TT2	500	2.26	2.60	5.25	16.0	13.9
CT98	500	2.26	2.26	8.40	51.0	51.0
CT16	500	3.65	3.65	1.17	77.5	77.5
CT93	500	1.38	1.38	53.50	85.5	85.5
TT6	250	27.60	31.80	19.00	12.3	10.7
CT95	250	27.60	27.60	318.50	15.2	15.2

TT – Thin-wall tube under internal pressure

CT – Uniaxial creep test

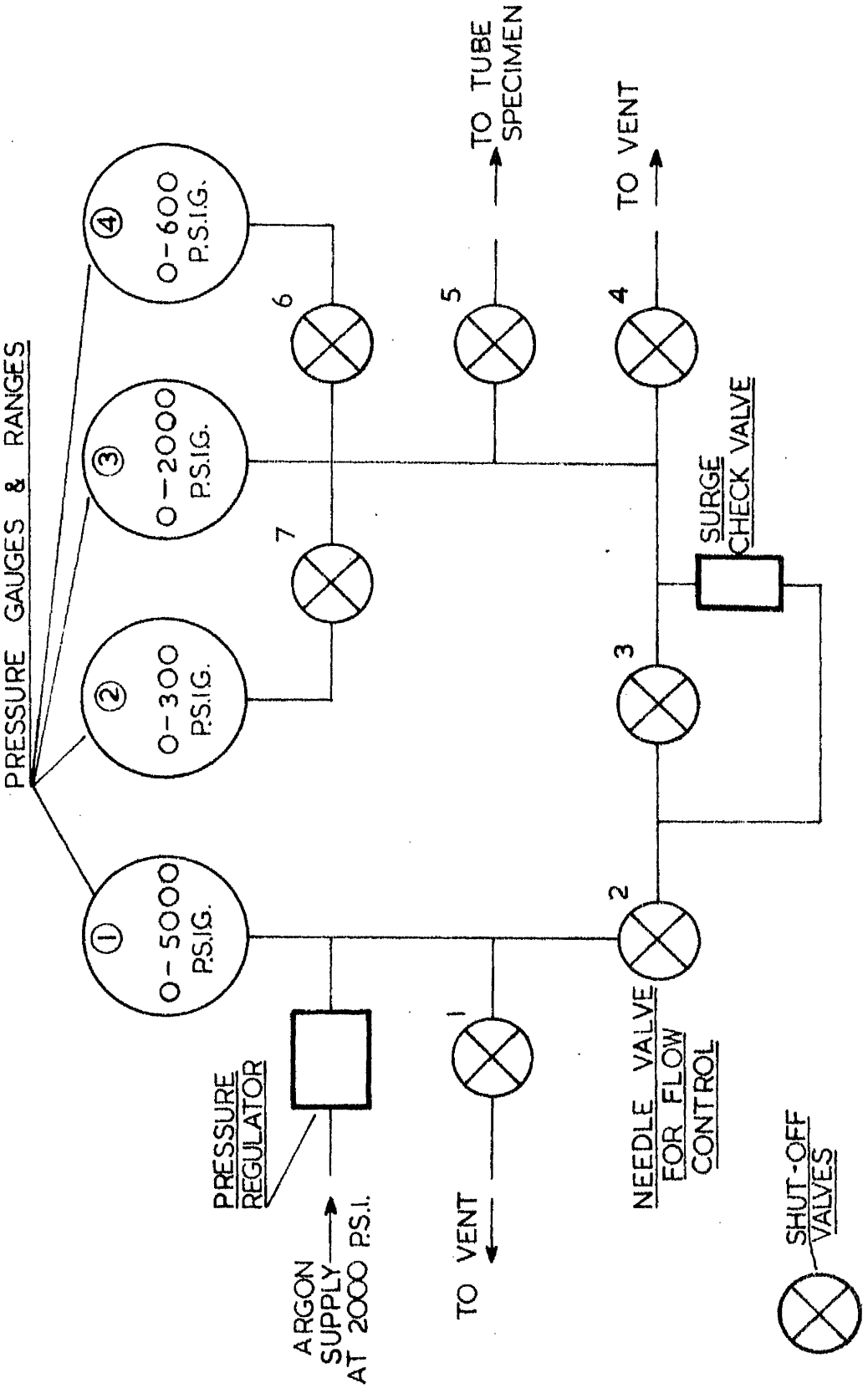

Figure 10.1 Schematic Diagram of Pressure Control and Measurement System

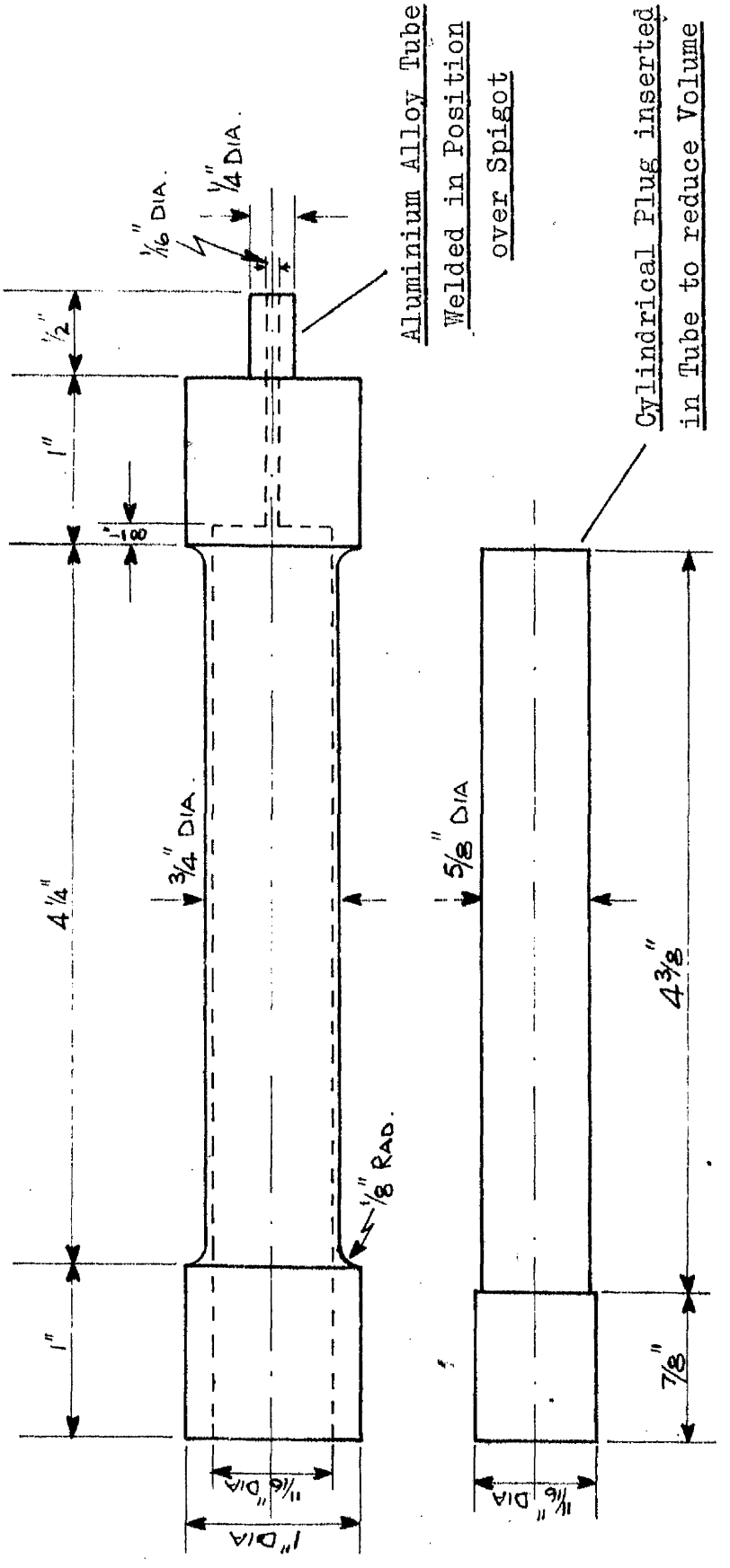

Figure 10.2 Tube Test Piece and Plug (To reduce volume under pressure)

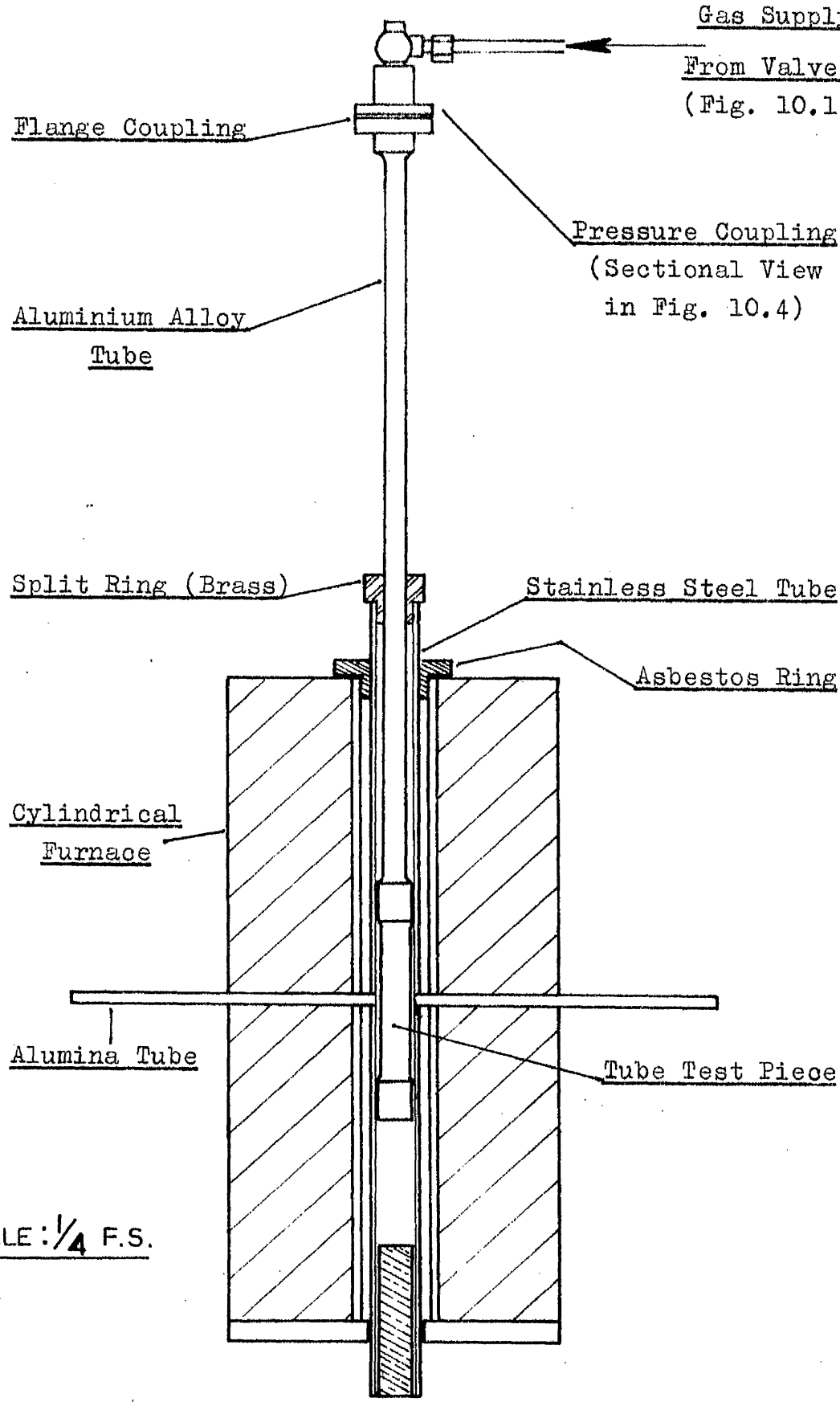

Figure 10.3 Assembly of Test Piece and Furnace showing Method of Suspension, Pressure Coupling and Strain Measurement

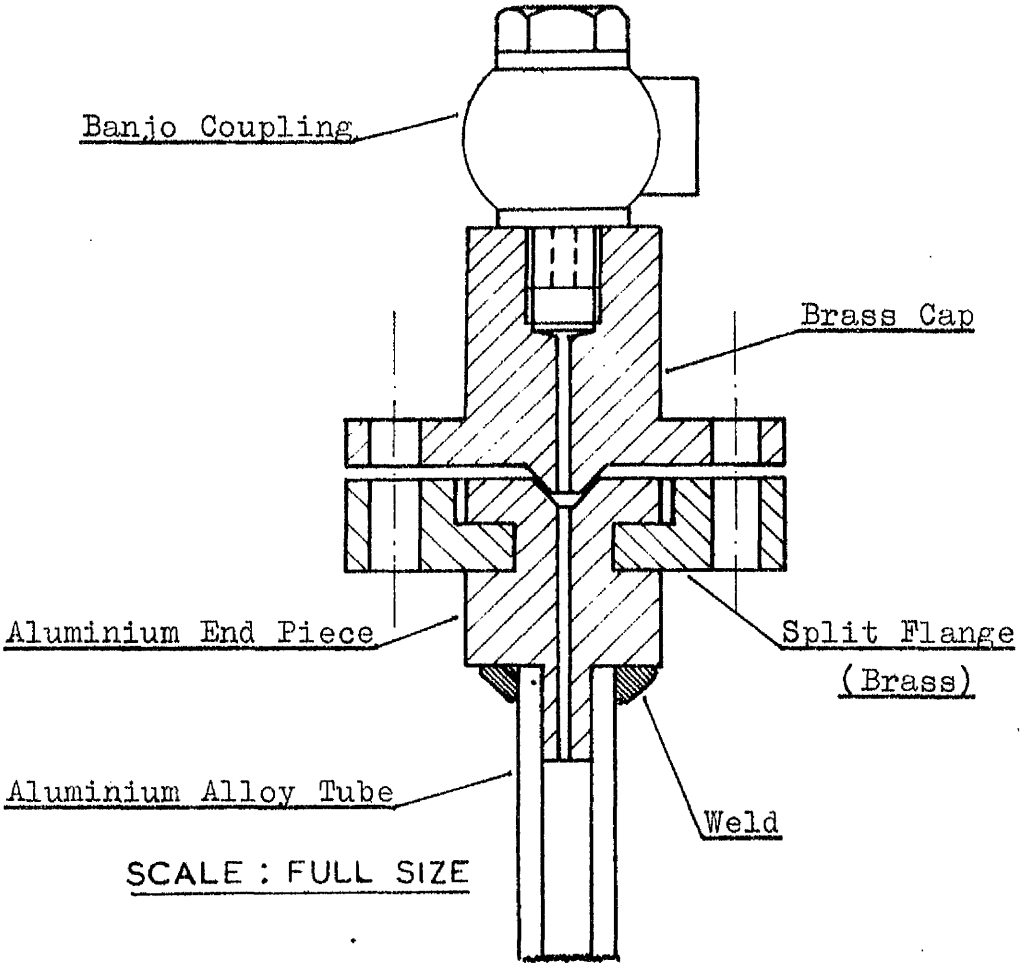

Figure 10.4 Sectional View of Pressure Coupling

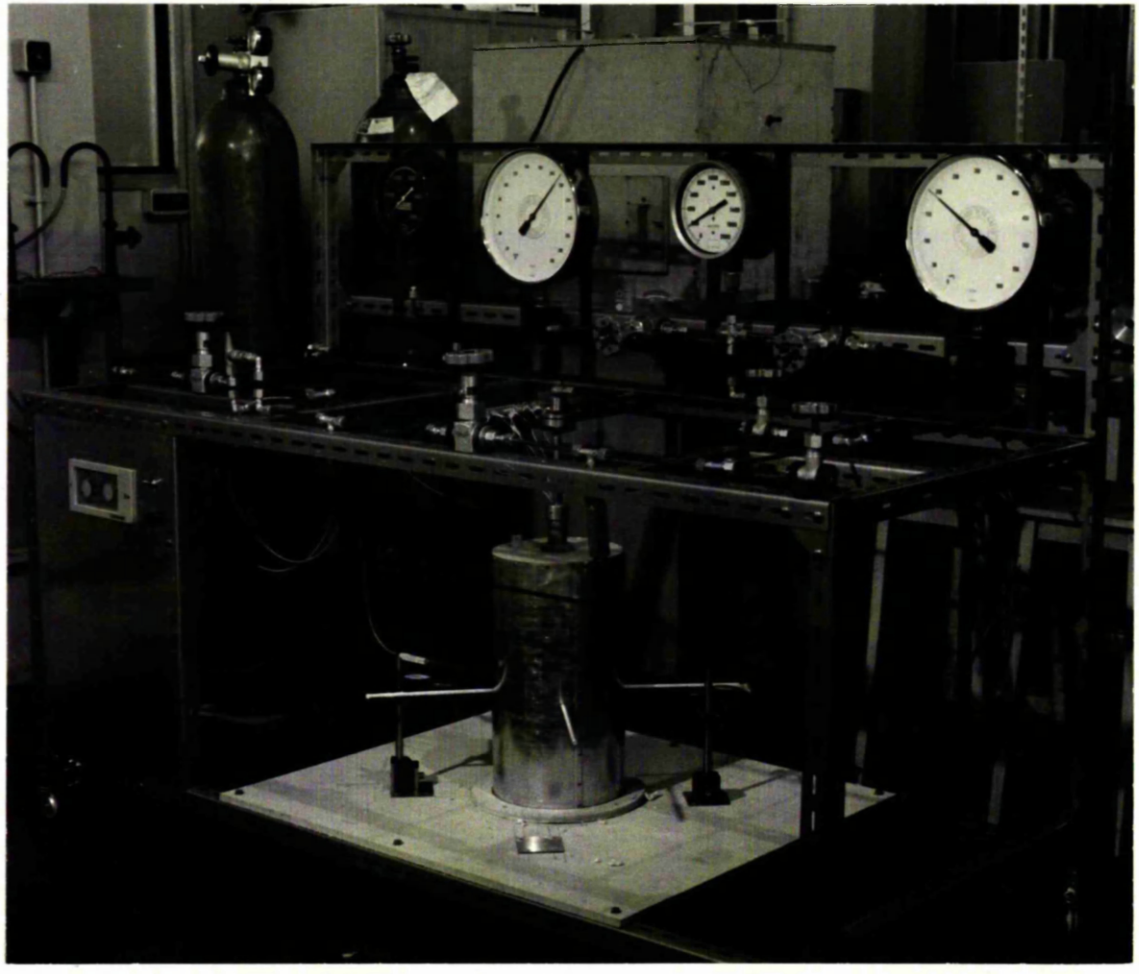

Figure 10.5 Apparatus for creep testing thin-wall tubes at high temperatures under internal gas pressure.

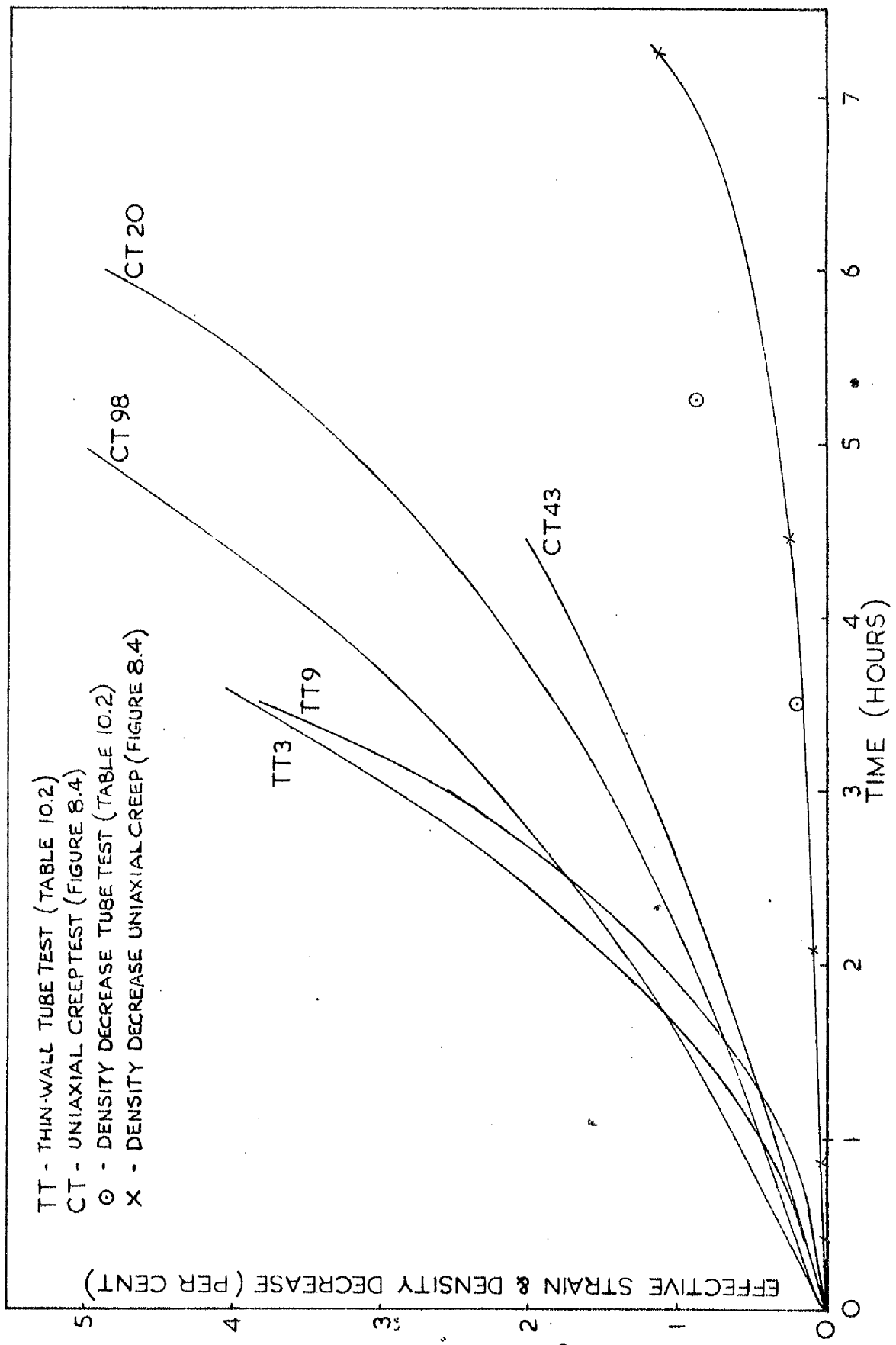

Figure 10.6 500 deg.C. and 2.26 N/mm^2 effective stress; comparison of uniaxial and biaxial stress creep tests

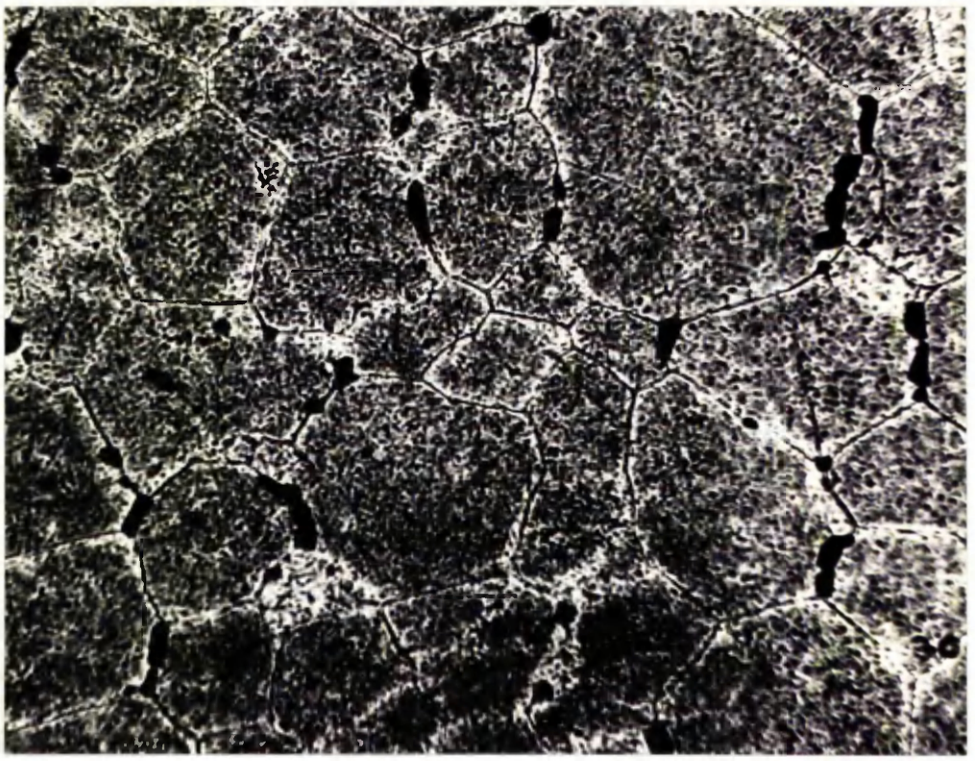

Figure 10.7 Section of tube wall perpendicular to axis after creep at 500 deg.C. and 2.26 N/mm^2 effective stress. Magn. 250X.

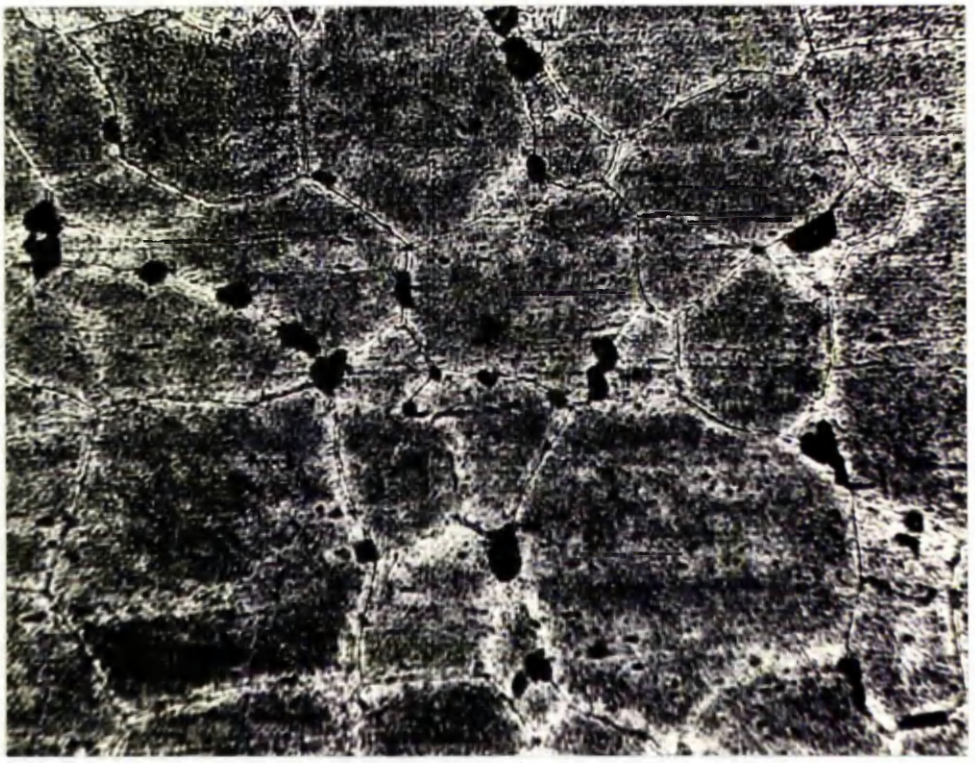

Figure 10.8 Section of tube wall along the axis after creep at 500 deg.C. and 2.26 N/mm^2 effective stress. Magn. 250X.

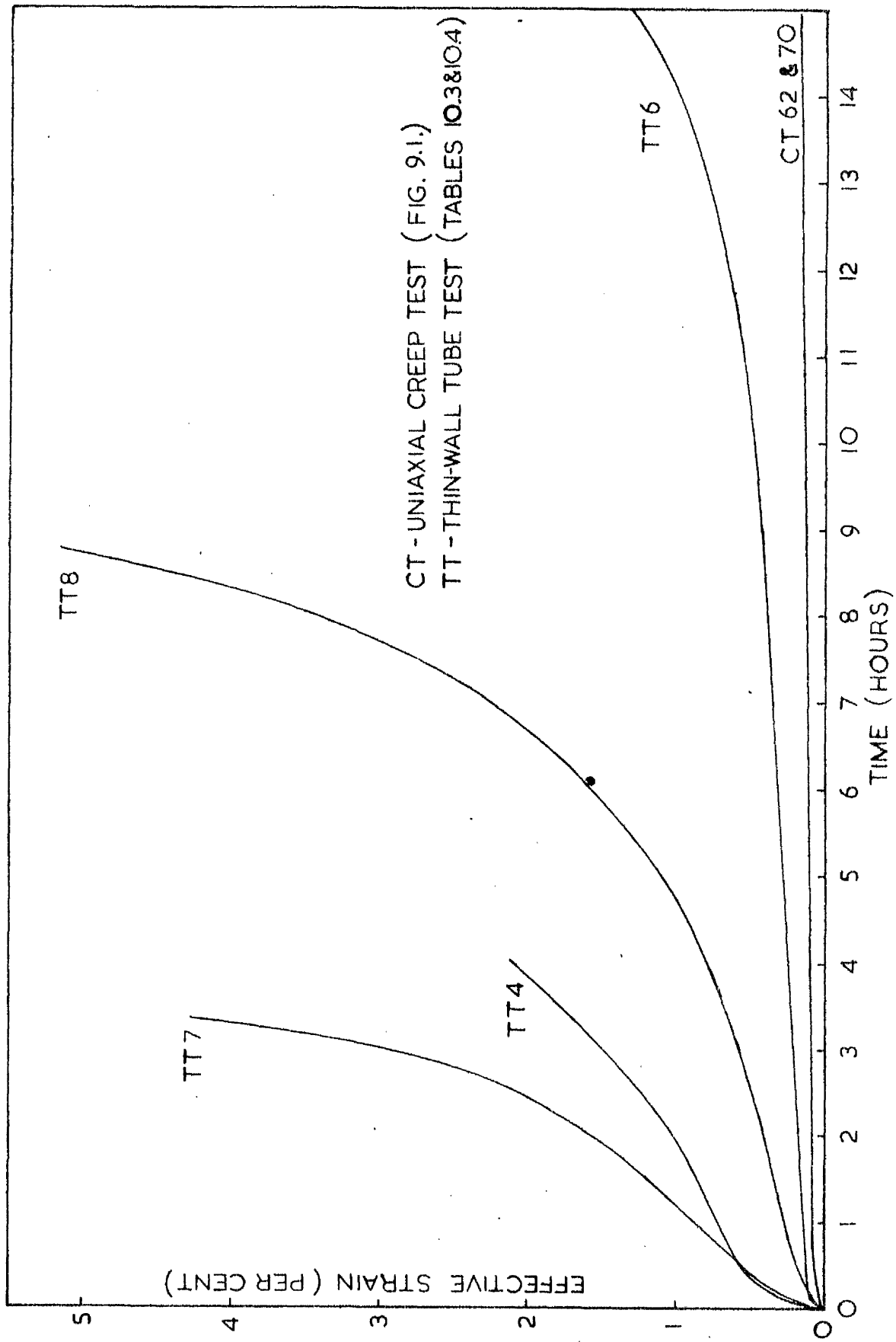

Figure 10.9 250 deg.C. and 27.60 N/mm^2 effective stress; comparison of uniaxial and biaxial stress creep tests

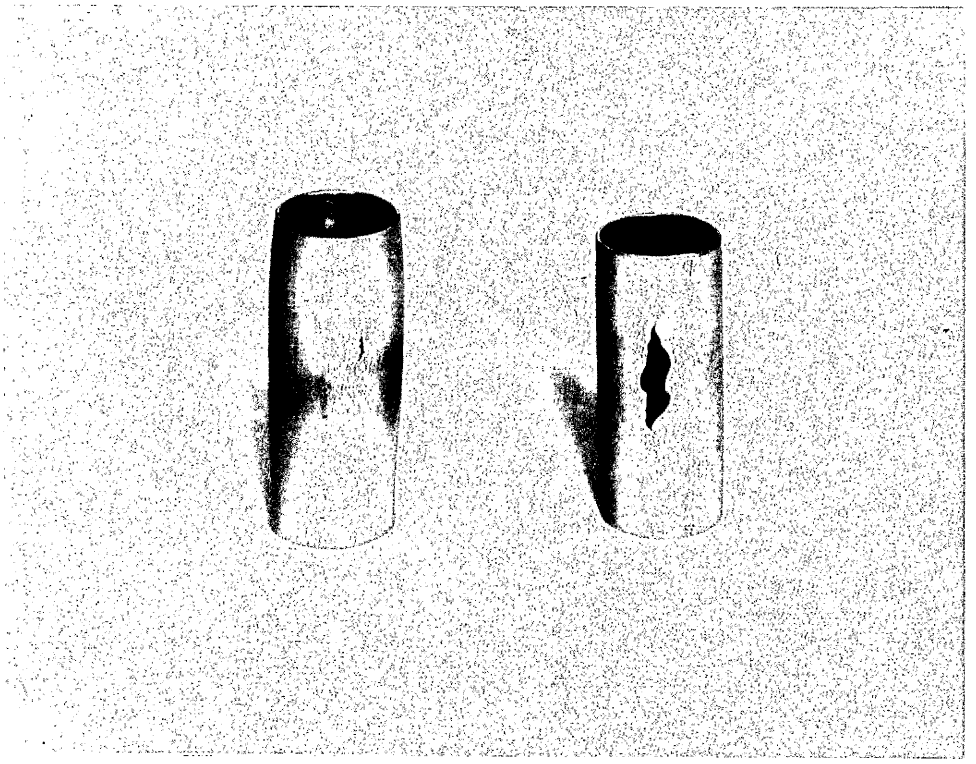

Figure 10.10 Fracture behaviour under biaxial stress creep conditions ; left, 500 deg.C. and 2.26 N/mm^2 effective stress; right, 250 deg.C. and 27.60 N/mm^2 effective stress.

REFERENCES

ALEXANDER, B.H., and BALLUFFI, R.W., 1957, Acta Met., 5, 666.

BEERE, W.B., and GREENWOOD, G.W., 1971, Metal Sci. J., 5, 107.

BEGHI, C., GEEL, C., and PIATTI, G., 1970, J. of Materials Sci., 5, 331.

BELL, G.A., 1958, Australian J. Appl. Sci., 9, 236.

BLEAKNEY, H.H., 1952, Canadian J. of Technology, 30, 340.

BOETTNER, R.C., and ROBERTSON, W.D., 1961, Trans Met. Soc. AIME, 221, 613.

CHANG, H.C., and GRANT, N.J., 1952, Trans AIME, J. of Metals, 619.

CHANG, H.C., and GRANT, N.J., 1953, Trans AIME, J. of Metals, 305.

CHANG, H.C., and GRANT, N.J., 1956, Trans AIME, 206, 544.

CHEN, C.W., and MACHLIN, E.S., 1956, Acta Met., 4, 655.

CHEN, C.W., and MACHLIN, E.S., 1957, Trans AIME, J. of Metals, 829.

CHEN, C.W., and MACHLIN, E.S., 1960, Trans Met. Soc. AIME, 218, 177.

DAVIES, P.W., and DENNISON, J.P., 1958–59, J. Inst. Metals, 87, 119.

DAVIES, P.W., BOWRING, P., and WILSHIRE, B., 1968, Metal Sci. J., 2, 168.

DAVIES, P.W., and WILLIAMS, K.R., 1969, Metal Sci. J., 3, 220.

EVANS, H.E., and WADDINGTON, J.S., 1969, Phil. Mag., 20, 1075.

EVANS, H.E., and WALKER, G.K., 1970, Metal Sci. J., 4, 210.

FINNIE, I., and HELLER, W.R., 1959, Creep of Engineering Materials, McGraw-Hill.

GAROFALO, F., 1963, Trans Met. Soc. AIME, 227, 351.

GAROFALO, F., 1965, Fundamentals of Creep and Creep-Rupture in Metals, Macmillan Co., New York.

GIBBS, G.B., 1967-68, Mater. Sci. Eng., 2, 269.

GIFKINS, R.C., 1956, Acta Met., 4, 98.

GIFKINS, R.C., 1959, Fracture (Ed. Averbach et al.), The Technology Press of M.I.T. and J. Wiley and Sons Inc.

GIFKINS, R.C., 1963, Proc. First Tewkesbury Symposium, Melbourne.

GITTINS, A., 1967, Metal Sci. J., 1, 214.

GITTINS, A., and WILLIAMS, H.D., 1967, Phil. Mag., 16, 849.

GITTINS, A., and WILLIAMS, H.D., 1969, Metal Sci. J., 3, 226.

GRANT, N.J., 1959, Fracture (Ed. Averbach et al.), J. Wiley, New York.

GREENWOOD, G.W., 1963, Phil. Mag., 8, 707.

GREENWOOD, G.W., 1969, Phil. Mag., 19, 423.

GREENWOOD, G.W., and HARRIS, J.E., 1965, Acta Met., 13, 936.

GREENWOOD, J.N., MILLER, D.R., and SUITER, J.W., 1954, Acta Met., 2, 250.

GUARD, R.W., KEELER, J.H., and REITER, S.F., 1954, Trans AIME, J. of Metals, 226.

HAMSTAD, M.A., and GILLIS, P.P., 1966, Materials Research and Standards, 11, 569.

HANSON, D., and WHEELER, M.A., 1931, J. Inst. Metals, 45, 229.

HARRIS, J.E., 1965, Trans Met. Soc. AIME, 233, 1509.

HULL, D., and RIMMER, D.E., 1959, Phil. Mag., 4, 673.

HULT, J.A.H., 1966, Creep in Engineering Structures, Blaisdell Publishing Co., Waltham, Massachusetts.

INTRATER, J., and MACHLIN, E.S., 1959, Acta Met., 7, 140.

ISHIDA, Y., and McLEAN, D., 1967, Metal Sci. J., 1, 171.

ISHIDA, Y., MULLENDORE, A.W., and GRANT, N.J., 1965, Trans Met. Soc. AIME, 233, 204.

KÄLLSTRÖM, O.K., 1969, J. of Nuclear Materials, 31, 111.

KENNEDY, C.R., HARRIS, W.O., and DOUGLAS, D.A., 1959, Trans ASME, J. of Basic Engineering, 599.

KOOISTRA, L.F., BLASER, R.U., and TUCKER, J.T., 1952, Trans ASME, 74, 783.

KRAMER, D., and MACHLIN, E.S., 1959, Trans Met. Soc. AIME, 215, 110.

LAUBITZ, M.J., 1959, Canadian J. Phys., 37, 1114.

LUBAHN, J.D., and FELGAR, R.P., 1961, Plasticity and Creep of Metals, J. Wiley, New York.

MACHLIN, E.S., 1956, Trans AIME, J. of Metals, 106.

McKEOWN, J., EBORALL, R., and LUSHEY, R.D.S., 1954, Metallurgia, 13.

McLEAN, D., 1956–57, J. Inst. Metals, 85, 468.

McLEAN, D., 1957, Grain Boundaries in Metals, O.U.P.

McLEAN, D., 1966, Rep. Progress in Physics, 29, 1.

MELLOR, P.B., 1962, J. Mech. Engineering Sci., 4, 251.

NADAI, A., and MANJOINE, M.J., 1941, J. of Appl. Mech., 8, A77.

NEMY, A.S., and RHINES, F.N., 1959, Trans Met. Soc. AIME, 215, 992.

NIELD, B.J., and QUARRELL, A.G., 1956–57, J. Inst. Metals, 85, 480.

PENNY, R.K., ELLISON, E.G., and WEBSTER, G.A., 1966, Materials Research and Standards, 6, 76.

PENNY, R.K., and LECKIE, F.A., 1968, Int. J. Mech. Sci., 10, 265.

PRESLAND, A.E.B., and HUTCHINSON, R.I., 1963–64, J. Inst. Metals, 92, 264.

RACHINGER, W.A., 1952–53, J. Inst. Metals, 81, 33.

RACHINGER, W.A., 1959, Acta Met., 7, 374.

RATCLIFFE, R.T., 1965, Brit. J. Appl. Phys., 16, 1193.

RATCLIFFE, R.T., and GREENWOOD, G.W., 1965, Phil. Mag., 12, 59.

SCAIFE, E.C., and JAMES, P.L., 1968, Metal Sci. J., 2, 217.

SERVI, I.S., and GRANT, N.J., 1951(a), Trans AIME, J. of Metals, 909.

SERVI, I.S., and GRANT, N.J., 1951(b), Trans AIME, J. of Metals, 917.

SHERBY, O.D., FRENKEL, R., NADEAU, J., and DORN, J.E., 1954, Trans AIME, J. of Metals, 275.

SLOCOMBE, T.A., and BEYNON, W.G., 1963, J.R.N.S.S., 18, 6.

SPARK, I.J., 1969, Scripta Met., 3, 747.

SPEIGHT, M.V., and HARRIS, J.E., 1967, Metal Sci. J., 1, 83.

STEVENS, R.N., 1966, Metallurgical Reviews, 11, 129.

STICHA, E.A., 1969, Trans ASME, J. Basic Engineering, 590.

TAPLIN, D.M.R., 1970, Metals Engineering Quarterly, 10, 31.

VON MISES, R., 1928, Ztschr. f. angew. Math. und Mech., 8, 161.

WEERTMAN, J., 1955, J. Appl. Phys., 26, 1213.

WEERTMAN, J., 1956, J. Mech. Phys. Solids, 4, 230.

WILLIAMS, J.A., 1969, Phil. Mag., 20, 635.

WILMS, G.R., 1954, Trans AIME, J. of Metals, 1291.

WOOD, W.A. et al. 1951–52, J. Inst. Metals, 80, 501.

WOODFORD, D.A., 1969(a), Metal Sci. J., 3, 50.

WOODFORD, D.A., 1969(b), Metal Sci. J., 3, 234.

ZENER, C., 1948, Elasticity and Anelasticity of Metals, Univ. of Chicago Press, Chicago.

CREEP FAILURE OF ALUMINIUM ALLOYS AT HIGH TEMPERATURES

ALEXANDER McLURE B.Sc.

SUMMARY

The majority of polycrystalline metals and alloys, when subjected to certain conditions of stress at temperatures > 0.5 Tm (Tm - melting temperature), display an intercrystalline mode of failure. In general, this type of fracture occurs under creep conditions when the applied stress system produces low strain rates and long rupture lives. Low ductility, as measured by elongation and reduction of area at fracture, characterises the failure. Research has established that the failure is initiated by the nucleation and subsequent growth of sub-microscopic fissures in the grain boundaries.

Although it is to be expected that the development of discontinuities in the grain boundaries should adversely affect the creep properties of a metal or alloy, it is not clear how the effect might vary with temperature and/or stress system. The existence of discontinuities in a stressed material produces local stress concentrations around those discontinuities. However, since ease of plastic flow varies with both temperature and stress system, the effect of the discontinuities on creep properties can also be expected to vary with temperature and stress system. In addition, the question arises as to whether the appearance of discontinuities in the grain boundaries necessarily constitutes failure.

The main objective of this research was, therefore, to determine the effects that intergranular discontinuities have on the creep properties of a metal or alloy under different conditions of stress and temperature and under different stress systems. Commercially pure aluminium (99.0 + pct) was chosen for the study. Specimens of the material were strained at constant rate and a temperature of 500 deg. C. in a standard tensile testing machine (Hounsfield Tensometer). Metallography of control specimens determined the size, shape and distribution of the discontinuities which were found in the grain boundaries of the strained material. A hydrostatic weighing technique was employed to determine the density decrease and, hence, the total volume of internal discontinuities in control specimens. Creep tests were then performed at temperatures of 250 deg. C. and 500 deg. C., using lever loading machines, on test pieces with and without quantities of initial intergranular discontinuities. It was observed that the same quantity of discontinuities resulted in much greater reductions of rupture life, strain to fracture and reduction of cross-sectional area at fracture, in creep tests at 250 deg. C. than in the corresponding tests at the higher temperature of 500 deg. C. However, the same quantity of discontinuities resulted in greater minimum creep rates at the higher temperature than at the lower temperature. Both metallography and density change established that the material was able to tolerate much larger intergranular discontinuities at 500 deg. C. than at 250 deg. C. before complete failure would occur.

Biaxial stress creep tests, at temperatures of 250 deg. C. and 500 deg. C., were performed on the material by the use of apparatus designed to blow up thin-wall tubes under internal gas pressure. The concepts of effective stress and effective strain were found inadequate in correlating uniaxial and biaxial results. However, it was observed that a quantity of initial discontinuities corresponding to 0.2 pct density decrease had a much greater effect on the effective strain/time curve under biaxial stress creep conditions than the same quantity had had under equivalent uniaxial stress creep conditions.

The experimental work involved in the project also provided results for two other topics. The density measurements on creep and tensile specimens produced information on the nucleation and growth of intergranular discontinuities, the interpretation of which was complicated by the presence of both grain boundary cavities and triple point wedge cracks in most specimens. The measurement of strain rates and stresses in tensile and creep tests showed that, under some conditions, tensile and creep data can be regarded as interchangeable. The same results showed that the Power Creep Law was only valid over a lower range of stress and that at high stresses it seriously underestimated actual creep rates.

The influence of environment on the nucleation and growth of intergranular discontinuities was also studied. Density measurements performed on specimens, which had been strained at constant rate and a temperature of 500 deg. C. in air and in argon, showed that the intergranular fracture process was accelerated by the presence of air in the test atmosphere.

m

$T_m = 650 + 273$

$= 923\,^{\circ}K$

3. 210 =